Investigation of batch and continuous crystallisation processes using non-invasive Raman and acoustic emission spectrometries

Laura Palmer

A thesis submitted to the Department of Pure and Applied Chemistry, University of Strathclyde, Glasgow, in fulfilment of the requirements for the degree of Doctor of Philosophy.

2013

This thesis is the result of the author's original research. It has been composed by the author and has not been previously submitted for examination which has led to the award of a degree.

Signed: Date:

For my family, *Illa res es sent*
experior nos…….. quod they operor

Acknowledgements

Firstly, I would like to thank my supervisor, Professor David Littlejohn for all his help and support throughout the duration of this project. Thanks also to Dr Alison Nordon for her assistance in many areas, especially MATLAB and for always having her door open to me for a natter. Other thanks go to members of CMAC including Lihua Zhao and Vishal Ravel for their technical support in the lab, Neil Hodgson for his help fixing and altering glassware and Natalie Kerr for her invaluable help with lots of matters.

I also acknowledge the University of Strathclyde and the Scottish funding council SPIRIT scheme for the funding to make this project possible. Special thanks to all the people who made my placement visits possible which made my PhD experience so much more interesting and varied. These include Professor Allan Myerson, Steven Ferguson and Chris Lai at MIT and Paul Sharratt, Chew Wee, Alvin Yeoh and Martin Hermanto at ICES, Singapore.

I'd also like to thank members of the analytical and CMAC research groups for keeping me sane and others, not so sane, especially David Wilsdon, Peter Hamilton, Melissa Black, Allyson McIntyre, Jaclyn Dunn and Naomi Briggs - "special" friends who will last far beyond my PhD days. Finally, the biggest thanks go to my family and close friends who have always been there for me throughout my time at university and beyond to offer gentle (and not so gentle) encouragement and support.

Abstract

Crystallisation of L-glutamic acid (LGA) and D-mannitol were studied in batch and continuous reactors using non-invasive, wide area illumination Raman spectrometry to identify the nucleation point, monitor crystal growth and identify the polymorphs formed. Non-invasive broadband acoustic emission (AE) spectrometry was also investigated as a means to monitor the crystallisation profile (by integrating the AE intensity over specific frequency ranges) and changes in particle size (by ratioing the intensities at high and low frequency regions).

A design of experiments approach evaluated the effects of solution concentration, oscillation frequency and amplitude, and final temperature on crystal formation and polymorph transformation for batch and continuous oscillatory baffled reactors. For both compounds, concentration had the biggest impact on the particle properties while the main interaction was between the oscillation frequency and amplitude. Comparisons were made with results from crystallisations in batch stirred tank and continuous mixed suspension, mixed product removal (MSMPR) reactors.

Metastable α-LGA was more easily obtained in both continuous reactors than conventional batch reactors. Narrower size distributions (e.g. spans of 1.5 – 2 and 4 – 8, respectively) and lower yields (e.g. 20 – 50% and 30 – 70%, respectively) were obtained in the continuous OBR than the MSMPR. The continuous OBR exhibited limited operating conditions, outside of which poor nucleation or blocking of the reactor occurred. The MSMPR reactor was more versatile and could be operated for up to 70 hours compared to several hours for the continuous OBR.

The study of D-mannitol in stirred tank and batch OBR explained how different operating conditions (especially oscillation frequency and amplitude) affected the polymorph formed, the rate of crystal formation, particle size range, and the degree of polymorph conversion. The metastable α- and the stable γ-forms were the predominant polymorphs obtained; higher solution concentration and mixing intensity gave more alpha and vice versa for the gamma form.

Table of contents

Acknowledgements **iv**
Abstract **v**
Table of contents **vi**
List of abbreviations **xi**
1 Introduction **1**
1.1 Crystallisation 1
1.1.1 Crystal formation process 2
1.1.1.1 Supersaturation 2
1.1.1.2 Nucleation 7
1.1.1.3 Crystal Growth 8
1.2 Crystallisation reactor technology 9
1.2.1 Continuous reactors 12
1.2.2 Oscillatory baffled reactors 15
1.3 Drivers for adoption of continuous manufacturing in the pharmaceutical industry 19
1.4 In-situ techniques for the monitoring and control of crystallisation 21
1.4.1 Spectroscopic methods 23
1.4.1.1 Mid-infrared 23
1.4.1.2 Near-infrared 24
1.4.1.3 Raman 26
1.4.1.4 UV-Visible 28
1.4.2 Non-spectroscopic methods 28
1.4.2.1 Particle sizing 29
1.5 Conclusions 31
1.6 Aims 32
1.7 References 34
2 Theory of instrumental and experimental techniques **38**
2.1 Crystallisation 38
2.1.1 Nucleation and Crystal Growth 38
2.1.1.1 Meta-stable zone width 41
2.1.1.2 Induction period 41
2.1.1.3 Crystal Growth 42
2.1.2 Polymorphism 43
2.1.3 Population balance model 44

2.2 Theory of vibrational spectroscopy 46
2.2.1 Raman spectrometry 49
2.2.1.1 Classical Theory 53
2.2.1.2 Intensity and fluorescence 55
2.3 Acoustic emission spectrometry 56
2.3.1 Signal analysis 59
2.4 Particle size analysis 60
2.4.1 Laser diffraction 62
2.4.2 Focused beam reflectance measurement 66
2.5 X-ray diffraction 68
2.6 Design of experiments 70
2.7 Data analysis 72
2.7.1 1st derivative transformation 72
2.7.2 Principal components analysis 73
2.8 References 74
3 Experimental 79
3.1 Introduction 79
3.2 Materials 79
3.3 Crystallisation reactors 81
3.3.1 Batch stirred tank reactor 81
3.3.2 Batch oscillatory baffled reactor 82
3.3.3 Continuous oscillatory baffled reactor 84
3.3.4 Mixed suspension, mixed product removal reactor 87
3.4 Instrumentation 90
3.4.1 Kaiser RxN1 spectrometer 90
3.4.1.1 Pre-filter stage 91
3.4.1.2 Axial transmission spectrograph 91
3.4.1.3 Charge couple device 92
3.4.1.4 PhAT probe 92
3.4.2 Acoustic emission instrumentation 95
3.4.3 Malvern mastersizer 98
3.4.4 Focused beam reflectance measurement 100
3.4.5 X-ray powder diffraction 101
3.5 References 103
4 Effect of operating conditions on particle properties in batch oscillatory baffled and stirred tank reactors 105

4.1 Introduction 105
4.2 Experimental 110
4.2.1 Materials 110
4.2.2 Batch STR conditions 110
4.2.3 Batch OBR conditions 111
4.2.4 Raman instrumentation-Kaiser RxN1 112
4.2.5 Laser diffraction 113
4.2.6 X-ray diffraction 113
4.3 Results and Discussion 114
4.3.1 Batch OBR DoE 114
4.3.2 Effect of operating conditions on polymorphic form and particle size 129
4.3.2.1 Effect of final temperature 130
4.3.2.2 Effect of oscillation frequency on particle properties 130
4.3.2.3 Effect of oscillation amplitude on particle properties 134
4.3.2.4 Effect of oscillation concentration on particle properties 136
4.3.3 Comparison of OBR and STR 139
4.4 Conclusions 151
4.5 References 153
5 Crystallisation of L-glutamic acid in continuous oscillatory baffled reactors 156
5.1 Introduction 156
5.2 Experimental 159
5.2.1 Materials 159
5.2.2 Continuous OBR conditions 159
5.2.3 Raman instrumentation-Kaiser RxN1 spectrometer 160
5.2.4 Laser diffraction 161
5.2.5 X-ray diffraction 161
5.3 Results and Discussion 162
5.3.1 Preliminary COBR experiments 162
5.3.2 Effect of particle size on Raman measurements 166
5.3.3 Effect of operating conditions on particle properties in the continuous OBR 168
5.3.4 Continuous OBR DoE 173
5.3.4.1 Effect of oscillation frequency on particle properties 174
5.3.4.2 Effect of oscillation amplitude 182

5.3.4.3 Effect of solution concentration 190
5.3.5 Comparison of batch and continuous OBR 193
5.4 Conclusions 198
5.5 References 201
6 Mixed suspension, mixed product removal (MSMPR) as an alternative continuous reactor in the preferential crystallisation of L-glutamic acid polymorphs **203**
6.1 Introduction 203
6.2 Experimental 210
6.2.1 Materials 210
6.2.2 Batch STR conditions 210
6.2.3 Continuous MSMPR conditions 210
6.2.4 Raman instrumentation-Kaiser RxN2 spectrometer 212
6.2.5 Laser diffraction 213
6.2.6 X-ray diffraction 213
6.3 Results and Discussion 213
6.3.1 Batch STR 213
6.3.2 MSMPR unseeded experiments 218
6.3.3 MSMPR seeded experiments 230
6.3.4 Comparison of continuous oscillatory baffled and mixed suspension, mixed product removal technology 241
6.4 Conclusions 242
6.5 References 245
7 Non-invasive monitoring of the batch crystallisation of D-mannitol using Raman and acoustic emission spectrometries **247**
7.1 Introduction 247
7.2 Experimental 253
7.2.1 Materials 253
7.2.2 Batch STR conditions 253
7.2.3 Batch OBR conditions 254
7.2.4 Raman instrumentation-Kaiser RxN1 255
7.2.5 Acoustic emission monitoring 255
7.2.6 Focused beam reflectance measurement 256
7.2.7 X-ray diffraction 256
7.3 Results and Discussion 256
7.3.1 Batch STR 256
7.3.1.1 Effect of scale in the batch STR 265

7.3.1.2 Acoustic emission monitoring of batch STR crystallisation of D-mannitol 271
7.3.2 Batch OBR: Non-invasive Raman monitoring 278
7.3.2.1 Effect of oscillation frequency and amplitude 282
7.3.2.2 Effect of solution concentration 286
7.3.2.3 Effect of scale of operation 289
7.3.3 Acoustic emission monitoring in the batch OBR 292
7.4 Conclusions 316
7.5 References 319
8 Conclusions and suggestions for future work 322
8.1 Conclusions 322
8.1.1 Evaluation of non-invasive measurement techniques 322
8.1.2 Evaluation of crystallisation reactor technology 326
8.1.2.1 Batch 326
8.1.2.2 Continuous 327
8.1.3 Additional knowledge of L-glutamic acid and D-mannitol 329
8.2 Future work 330
8.3 References 333

Abbreviation List

AES	Acoustic emission spectrometry
API	Active pharmaceutical ingredient
ATR	Attenuated total reflectance
CCD	Charge couple device
CLD	Chord length distribution
COBR	Continuous oscillatory baffled reactor
CPACT	Centre for process analytics and control technology
CSTR	Continuous stirred tank reactor
CSV	Comma separated variable
DIA	Dynamic image analysis
DLS	Dynamic light scattering
DoE	Design of experiments
FBRM	Focused beam reflectance measurement
FTIR	Fourier transform infrared
GMP	Good manufacturing practice
LD	Laser diffraction
LGA	L-glutamic acid
Mid-IR	Mid-infrared
MIT	Massachusetts institute of technology
MSMPR	Mixed suspension mixed product removal
MSZW	Metastable zone width
Near-IR	Near-infrared
OBR	Oscillatory baffled reactor
PC	Principal component
PCA	Principal components analysis
PLS	Partial least squares
PSD	Particle size distribution
PTFE	Polytetrafluoroethylene
PVM	Particle vision measurement
RMS	Root mean square
STR	Stirred tank reactor
UV-VIS	Ultra violet-visible
XRD	X-ray diffraction

1 Introduction

1.1 Crystallisation

Crystallisation is an operation performed in many industries including food and fine chemicals, however, this operation is especially important in the pharmaceutical industry as over 90 % of all pharmaceutical products contain a drug in a particulate or crystalline form.[1] It is not a new concept and has been used for hundreds of years as a cheap and effective way to remove impurities from final products. In the pharmaceutical industry crystallisation is used as a technique to separate, purify, produce and recover solid material.[2] The aim of industrial crystallisation is to consistently produce a product with the desired properties for the lowest cost possible. However, historically the crystallisation process was thought of as more of an art and left to a certain degree down to chance which often resulted in particles of widely varied properties. Despite advances in the last 30-40 years, this process is still poorly understood and the root of many manufacturing problems.[3] This lack of knowledge results in the production of active pharmaceutical ingredients (APIs) of poor product quality. In fact, a great number of problems encountered in the formulation of drug compounds is often attributable to the crystallisation process. Although conventional equipment such as stirred tank reactors appears simple, control of the process is complicated.

The crystallisation process is also not particularly well researched, especially crystallisation kinetics which are vital for understanding and attempting to control the process. This results in a trial and error approach being adopted meaning the quality of the end product cannot be guaranteed.[4] This is due to pharmaceutical companies not investigating important information on the fundamentals of crystallisation most often due to complexity, cost and resource constraints. Also there is a lack of sufficient measurement techniques available to obtain this information which is vital for optimising the process.[4, 5] The quality of the end product is of the upmost importance especially for pharmaceuticals where the consumer is potentially at risk. The purity of the drug must be high and of the correct form to reduce possible side effects.[3] Some of

the challenges for industrial crystallisation are due to the current reactor technology being dated and the necessity for new, novel equipment to be developed to move crystallisation forward at the rate of emerging industrial needs.[4] If the crystallisation process is not optimised sufficiently to produce particles of certain properties this will have a knock on effect on subsequent unit operations and increase overall production costs.[6]

The physical properties of solid particles produced during crystallisation are of great significance as they determine the end product quality and efficacy. There are several crystal properties which must be explored prior to a new drug application. These include particle size, morphology, particle size distribution and polymorphism, and all can impact the final product. They can affect the appearance of the product, its free flowing nature (affecting downstream processing) and determine the effect of the drug, e.g. the absorption in the body.[7] The polymorphic form of a compound impacts the end product properties such as the solubility, as well as downstream processing. Polymorphism is the ability of a compound to exist as more than one crystal structure and is apparent in approximately 80% of pharmaceuticals on the market. Therefore, it is vital to be able to control the formation of polymorphs during crystallisation and beyond.[5]

1.1.1 Crystal formation process

1.1.1.1 Supersaturation

The crystallisation process comprises two main steps: nucleation and crystal growth. Supersaturation is the driving force and is a requirement for both steps to occur.[2] The solubility is the maximum amount of solute that can exist at equilibrium under given conditions and this usually increases with temperature (shown by the solubility curve).[8] A saturated solution contains the maximum amount of solute which can be dissolved in a certain amount of solvent at a given temperature. Therefore, in a supersaturated solution, the solute concentration is greater than the equilibrium solute concentration at a certain temperature so that the solution contains more dissolved solid than represented

by the equilibrium saturation.[3] The chemical potential (μ) is defined by the standard potential (μ_o) and activity (a):

$$\boldsymbol{\mu = \mu_0 + RTlna} \quad \textbf{(1-1)}$$

R = gas constant (8.314 J mol^{-1} K^{-1})

T = temperature (K)

The driving force for crystallisation can also be described as the difference between the chemical potentials of the substance in the solution and crystalline states.[2] When a solution is at equilibrium, the chemical potentials, μ, of the solute in solution and the crystalline phase are equal, such that Δμ is zero.

$$\boldsymbol{\Delta\mu = \mu_{solution} - \mu_{solid}} \quad \textbf{(1-2)}$$

When Δμ is positive, the solution is supersaturated which means nucleation and crystal growth can take place. The supersaturation at a given temperature is defined by equation 1-3.

$$\boldsymbol{\Delta C = C - C^*} \quad \textbf{(1-3)}$$

$\boldsymbol{C}$ **= solute concentration**

$\boldsymbol{C^*}$ **=equilibrium solute concentration**

The supersaturation can also be expressed as the supersaturation ratio:

$$\boldsymbol{S = \frac{C}{C^*}} \quad \textbf{(1-4)}$$

S=greater than 1 for a supersaturated solution

The relative supersaturation is described by the equation:

$$\boldsymbol{\sigma = \frac{C - C^*}{C^*}} \quad \textbf{(1-5)}$$

A supersaturated solution displays a meta-stable zone (Figure 1-1), which is one of the most important factors in determining crystal properties as it shows the allowed level of supersaturation for the process.[9] A solution will have a certain level of supersaturation it can tolerate before it becomes unstable. The metastable zone occurs between this unstable level (the super-solubility curve) and the solubility curve.[10] The position of the super-solubility curve and hence the width of the metastable zone is affected by factors such as the rate of generating supersaturation, the type and intensity of mixing and the presence of impurities. The width of the meta-stable zone impacts product properties such as crystal size, crystal size distribution and polymorphic form due to the strong impact it has on nucleation.[11]

In industrial crystallisation, the desired supersaturation for nucleation and eventually crystal growth is approximately half the width of the metastable zone (shown by the arrow in Figure 1-1) since this is the best compromise between productivity and crystals of an adequate quality. A high supersaturation results in increased levels of crystal fines due to an excessive initial nucleation rate which means there are a larger number of nuclei which grow to a smaller size.[10] A low level of supersaturation results in a decrease in the production rate due to slower nucleation rates which means there are fewer crystals produced which grow to a larger ultimate size. However, changes in operating conditions such as mixing intensity can alter the size of the metastable zone so this level of supersaturation is not always easy to achieve. An understanding of the crystallisation process including the phase diagram for individual compounds is essential with respect to polymorphs as the operating conditions can favour one polymorph over another.[7]

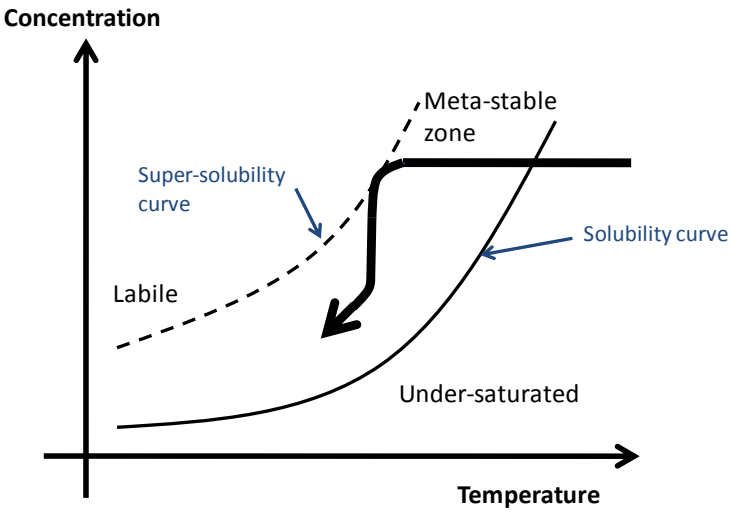

Figure 1-1: Solubility diagram showing a typical solution crystallisation process[12]

The arrow in Figure 1-1 of the solubility diagram describes the path of a cooling crystallisation and shows the following process: an under-saturated solution is cooled, and it crosses the solubility curve to become supersaturated. When it is cooled further it enters the metastable zone which induces nucleation when seeding is employed. Seeds are small solid bodies present in solution, which act as centres of crystallisation.[2] Further cooling allows spontaneous nucleation to occur in most cases.[13] It can be seen that once certain conditions are reached, crystallisation can be encouraged by seeding or through spontaneous processes. The likelihood of crystallisation occurring increases as the labile zone is entered, however above a certain point the solution may become increasingly viscous and this can prevent crystallisation.[2] The solubility diagram is important in deciding which crystallisation method to use and is also beneficial as it can be used to estimate the conditions required to promote crystallisation at a certain temperature.[6] The main methods to create supersaturation and, therefore, promote crystallisation are:

- Temperature change of which cooling is the most common. The solubility generally decreases as the temperature is lowered causing the supersaturation to increase leading to crystallisation.

- Evaporation which is ideal for solvents with high vapour pressure. The solvent evaporates which causes the solute concentration to increase, creating supersaturation and inducing crystallisation.
- Chemical reaction where two soluble materials are mixed in solution causing them to react to give a product with low solubility.
- Varying the solvent composition by the mixing of solvents can change the solubility of a solute. The additional solvent(s) are known as antisolvents and can be added to an undersaturated solution to create supersaturation.[6] This is ideal for solvents which are not volatile enough for evaporation or for compounds which are temperature sensitive and cannot be heated to dissolve the material in solution.[3]

Desupersaturation is the process which follows supersaturation occurring, when nucleation and crystal growth have taken place, and describes the concentration of the compound in solution decreasing through crystallisation.[14]

In industrial crystallisers the main methods to create supersaturation are cooling, anti-solvent addition, evaporation or a combination of these.[8] Cooling the solvent causes conditions to move towards the supersolubility curve and then into the labile zone resulting in spontaneous crystallisation. With evaporation, some of the solvent is removed from the solute, which can also encourage crystallisation. However the conditions do not fully reflect those of the labile zone as the surface which has been evaporated is more supersaturated than the bulk solution. Crystals on this surface disperse into the solution and seed it before ideal conditions for crystallisation are reached in the bulk solution. Therefore, the use of both cooling and evaporation often results in improved crystallisation.[2] This is not always ideal, especially for pharmaceutical compounds many of which are stable only over a limited temperature range. This limits the methods available to generate supersaturation.[15]

1.1.1.2 Nucleation

As supersaturated solutions are not at equilibrium, the solution crystallises in order to become more stabilised. Nucleation is the start of production of the solid phase through the initial formation of crystals. Molecules begin to cluster in a supersaturated solution and when this cluster is large enough it will continue to grow rather than dissolve.[8] Due to the fact a certain (critical) sized cluster is required before nucleation can take place in a supersaturated solution, the solution is described as being metastable, however, as the supersaturation is increased the minimum cluster size necessary for nucleation decreases.[3] Nucleation can occur via two methods; primary or secondary.

Primary nucleation is evident in systems where no other crystalline material is present (i.e. unseeded). This can be further divided into homogeneous and heterogeneous nucleation. Homogeneous nucleation is spontaneous and occurs in clear, supersaturated solutions. Heterogeneous nucleation is induced by impurities, for example foreign particles such as dust. These impurities reduce the energy required for nucleation and so this will happen at lower supersaturation levels than those required for primary homogeneous nucleation.

Secondary nucleation involves existing crystals in solution (parent crystals) inducing the formation of smaller particles. This enhances the nucleation rate which means secondary nucleation can also occur at lower supersaturation levels. In industrial crystallisers primary homogeneous nucleation does not occur due to impurities always being present, even in very small levels e.g. in crevices on the walls of the reactor. Primary heterogeneous nucleation is possible, but usually only in conditions of relatively high supersaturation and this method of nucleation is undesirable as it is practically impossible to control due to the random nature of this mechanism of nucleation. In addition, at high supersaturation, the nucleation rate increases significantly and results in high levels of particle fines which is undesirable for processing. Therefore, secondary nucleation is the main process for nucleation in industry; however the mechanisms are not well understood. It is important to be able to control the process or excessive

nucleation can be an issue. This most often occurs through contact nucleation, where crystals can impact walls, stirrers, and each other, and break up creating additional secondary nucleation sites. Measures can be taken to limit this, for example using padded stirrers or more commonly by attempting to control secondary nucleation by seeding the process to give crystals of the desired particle size.[2, 3, 8] As described above, it is a combination of both nucleation and crystal growth which determines the physical properties of the particles produced including the particle size and the distribution.

The starting point of unseeded nucleation is dependent on the cooling rate. As the cooling rate is increased, the metastable zone width enlarges which affects the position of the optimum supersaturation level. Therefore, it is important to choose the best possible cooling profile for the process. A parabolic cooling profile results in constant crystal growth, but this is often difficult to achieve. A natural profile is often achieved by keeping the temperature of the reactor jacket constant and allowing the temperature of the solution to decrease to this fixed temperature. This is not ideal as it often leads to rapid, uncontrolled growth. Therefore, in practice a linear cooling profile is most often used as a compromise.[11]

1.1.1.3 Crystal Growth

The second step in the crystallisation process is crystal growth, which determines the ultimate size of the crystals. Although the exact mechanism of crystal growth is not known and there are many theories, it is thought the main steps are as follows: solute molecules diffuse through the liquid phase to approach the crystal face where they need to first become organised before being adsorbed. This results in layer-by-layer growth of the crystal.[3] The main steps in crystal growth are believed to be mass transport of solute by diffusion from solution to the crystal face, and surface integration of the material into the crystal lattice. The second process can be divided into several steps. The first involves the molecule being adsorbed onto the crystal surface where it loses part of its solvation shell. It is then either added into the lattice where it loses the rest of its shell or

returned back to solution.[8] If these steps (adsorption and addition to the lattice) take place in parallel, the mechanism giving faster growth determines the rate. If, however, they take place in series, the slower mechanism will determine the rate.[8] Different crystal faces can also have different growth rates even under identical conditions. This leads to a variation in the shape of the crystal with the slowest growing face describing the habit. This also means that crystals of the same original size under identical conditions can grow at different rates.[8]

1.2 Crystallisation reactor technology

The crystallisation process has been used in manufacturing for hundreds of years but in this time little advancement has been made in reactor technology. Conventionally batch reactors have been used and until recently there has been no real alternative. One of the most commonly used reactors in the pharmaceutical industry is the stirred tank reactor (STR) (Figure 1-2). This consists of a vessel with a mounted impeller which helps to create a suspension of crystals. By creating agitation within the vessel, issues with heat transfer and temperature and concentration gradients can be reduced to an extent. This results in reduced batch time and a more uniform product than that obtained with an unstirred vessel.[8] However, stirred tank reactors are still problematic since addition of reactants can have a different effect depending on the location they are added. Reactant addition to a poorly mixed area like the liquids surface will lead to an area of high local supersaturation which intensifies with an increase in the reactant concentration. Adding reactant near the impeller, which is a more efficiently mixed area of the vessel, means that conditions will be more uniform. It is important, if possible, that no areas of local supersaturation are present in the vessel since this can have an impact on properties including the polymorphic composition of the crystals by encouraging nucleation to occur at a higher temperature than desired.[7]

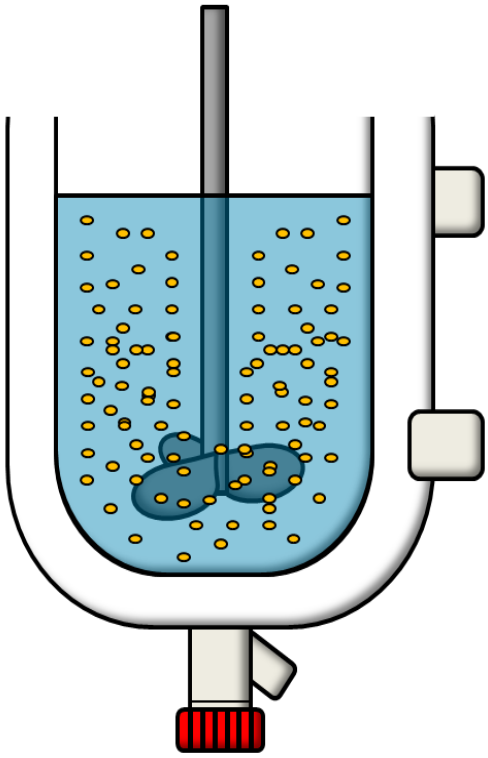

Figure 1-2: Diagram of a batch stirred tank reactor

One of the major disadvantages of current batch reactor technology is the issues encountered when scaling up from laboratory to industrial scale. There are many parameters to take into account such as impeller speed, dimensions of impeller in comparison to vessel, etc. and the scale up of these in stirred tank reactors is complex. In addition, there are no set guidelines as to which conditions should be kept constant during scale up. This leads to difficulties at industrial scale resulting in inconsistent products.[13] Even when optimum operating conditions have been established at lab scale through time-consuming experimental work, often they will not be the ideal conditions for industrial scale and the experiments will need to be repeated.[16] Mixing is an operating parameter which is problematic to scale up since it is possible to obtain adequate mixing at lab scale, but inconsistencies in mixing become more apparent as the scale is increased. An increase in scale leads to improved mixing surrounding the impeller but increasingly poorer mixing towards the sides of the vessel. This results in

mixing gradients and, therefore, temperature and concentration gradients within the reactor which have an effect on factors such as supersaturation.

Heat transfer is another parameter which causes difficulties during scale up. Effective heat transfer is necessary for successful cooling crystallisation; however, heat transfer effects decrease in STRs as the scale is increased due to the reduced relative volume of solution in contact with the heat transfer surface as the total reactor volume increases. Both mixing gradients and heat transfer affect cooling profiles in industrial stirred tank reactors.[14] It would be extremely beneficial to develop a crystalliser which could be linearly scaled up as this would avoid the problems which are encountered with traditional batch reactors in the scale up of operational parameters.

Although batch reactors are still widely used (being the core reactor of choice for pharmaceutical crystallisation) and have generally been successful in achieving the end product, there are opportunities to improve manufacturing processes due to advancements in technology. Batch crystallisers are relatively simple to operate, require low maintenance, and are ideal for containment of more difficult materials e.g. toxic compounds.[3] They are appropriate for crystallisations requiring wide cooling ranges and for relatively small scale production of multiple products. In addition, it is possible to investigate numerous process parameters within a short space of time with batch technology.[3] They also have the advantage that if the process is not optimised correctly only one batch is at risk. However, batch processes are not particularly efficient, or consistent, for example the product crystal size can vary significantly from batch to batch and despite the fact various researchers have investigated improving current batch manufacturing, optimisation of these processes has typically led to less than a 5 % improvement.[17]

1.2.1 Continuous reactors

There have been modifications made to the basic batch reactor in order to improve product properties and adapt to different needs in industrial crystallisation, for example by facilitating continuous operation. However, these continuous reactors are not commonplace in the pharmaceutical industry. These modified crystallisers include Swenson forced circulation, Oslo fluidised-bed, and draft-tube and baffled reactors. The draft-tube and baffled crystalliser (Figure 1-3) contains an impeller within a draft tube which circulates growing crystals from the base of the reactor to a boiling surface where it becomes similar to a magma. This hot suspension is surrounded by an annular baffle zone where fine crystals are separated from growing crystals. The mother liquor containing the fines is then removed and diverted to a separate tank to be destroyed by e.g. heating before returning the mother liquor to the circulator. These adaptations mean the liquor flow is drawn upwards while the crystals fall to the bottom of the vessel where they are collected. This reactor is best for compounds with normal or flat solubility profiles and is ideal for creating large particles with crystals produced typically in the size range 500-1200 μm.[2, 3]

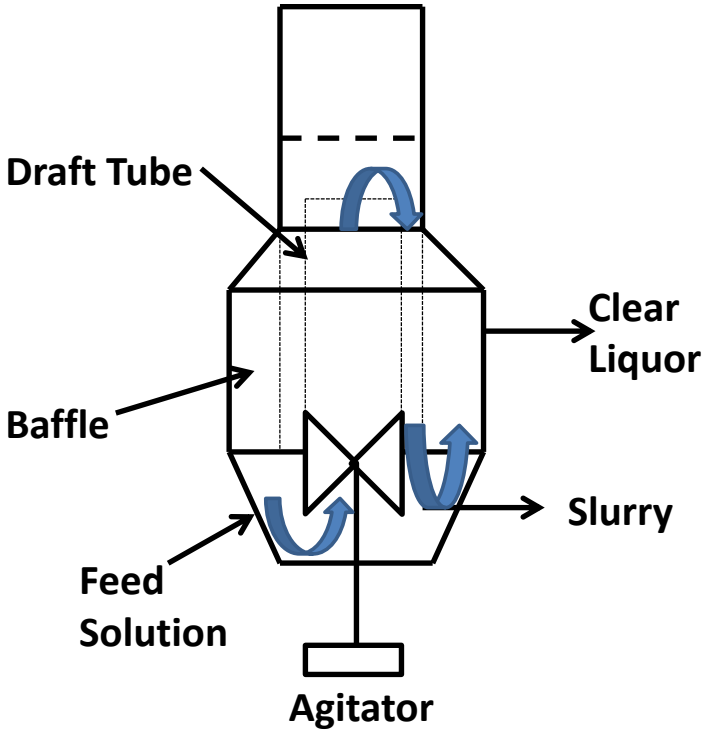

Figure 1-3: Diagram of the draft-tube and baffled crystalliser[18]

The Oslo fluidised-bed crystalliser (Figure 1-4) has separate areas for generating supersaturation and, for the crystal suspension, where growth takes place. Supersaturation is created externally by cooling or evaporation and the liquor is pumped into the main vessel where crystals are suspended in the vessel by an upward stream of supersaturated liquor. This reactor is also suitable for compounds with a normal or flat solubility profile and the slurry collected continuously at the base of the vessel contains crystals greater than 1000 μm in size.[3, 8]

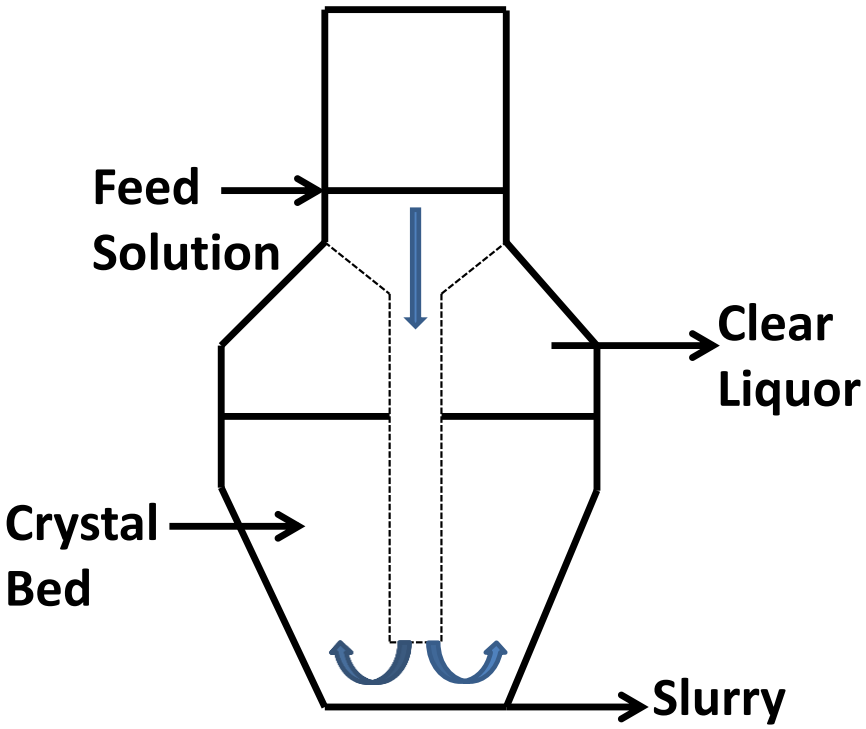

Figure 1-4: Diagram of Oslo fluidised-bed crystalliser[18]

The most commonly used continuous reactor is the forced-circulation crystalliser also known as the mixed suspension, mixed product removal crystalliser (MSMPR) which will be described in more detail in a later section. It is most often used for evaporative crystallisation processes in industry and is the least expensive reactor to operate. The important features of this reactor are; the volume chosen, as this determines the residence time of the material, and the agitation (recirculation) applied as this governs the supersaturation of the solution.[18] It is likely that the continuous reactor technology described in this section has not been adopted by the pharmaceutical industry due to the properties of the particles which are produced in these crystallisers. In all three reactors described, the particle sizes obtained are significantly larger than that required for pharmaceutical products. In addition, a wide range of particle sizes is also obtained in these reactors and currently a narrower particle size distribution is acquired when

crystallisations are carried out in batch stirred tank reactors so there is no motivation to convert manufacturing to continuous operating with the current technology available.

1.2.2 Oscillatory baffled reactors

A more recent development in technology with potential in pharmaceutical crystallisation is the oscillatory baffled reactor (OBR) which can be applied to both batch and continuous modes of operation (Figure 1-5 and Figure 1-7). Mixing is obtained by oscillating the fluid leading to the creation of eddies which are vortices generated when the flow and baffles interact.[19] This oscillatory mixing is more efficient than external mixing (e.g. with impellers) and consequently products manufactured in a batch OBR have been found to be of a better quality and consistency in terms of particle properties than with conventional batch operation.[20, 21] Furthermore, by changing the operating conditions, different crystal characteristics are obtained.

Figure 1-5: Diagram of the batch oscillatory baffled reactor

Two important parameters influence mixing in an OBR. The Reynolds number is used to describe the intensity of the mixing applied to the column and is described by the following equation:[8, 12]

$$Re_o = \frac{2\pi f x_o \rho D}{\mu} \quad \textbf{(1-6)}$$

D=column diameter (m)
ρ=fluid density (kg m^{-3})
μ=fluid viscosity (kg m^{-1} s^{-1})
x_o=oscillation amplitude (m)
f=oscillation frequency (Hz)

The Strouhal number (St) describes the ratio of column diameter to stroke length, which explains the generation of eddies in the reactor and is determined by the equation:[12]

$$St = \frac{D}{4\pi x_o} \quad \textbf{(1-7)}$$

Uniform mixing within a crystalliser can be difficult to achieve and causes the majority of problems with scale up. A way to overcome the problem of inconsistent mixing is to develop a plug flow crystalliser. There are two ways to achieve plug flow: through a series of (continuous) stirred tank reactors (CSTR) or through a tubular reactor. Flow within a tubular reactor can be described as laminar, turbulent or plug (Figure 1-6):

- Laminar flow has a parabolic profile due to the velocity at the centre of the tube being equal to that of the incoming flow, whilst the velocity at the walls of the tube is as low as zero depending on the viscosity of the fluid. This means the flow at the centre of the tube will exit first resulting in a velocity gradient and a difference in residence time along the tube.
- Turbulent flow also has a parabolic profile, however it is flattened and less obvious as the velocity gradient is not as great as with laminar flow.

- Plug flow has a flat profile as it has no difference in velocity to the incoming flow across the tube so has the same residence time and shows mixing taking place across the entire tube. There is complete mixing in the radial but not axial direction. Plug flow can only be achieved in continuous systems using tubular components and a net flow. As there is no net flow in batch systems, plug flow conditions cannot be achieved.[13, 21]

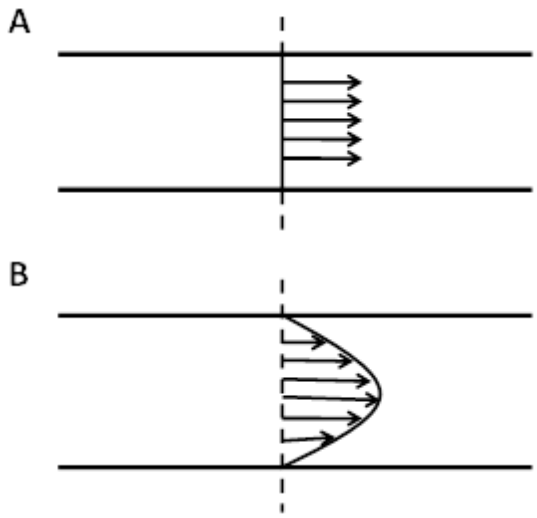

Figure 1-6: Diagram comparing plug flow (A) with laminar flow (B)[22]

A CSTR in practice requires five to ten reactors in series, drastically increasing the equipment required and increasing the expense; despite this a CSTR will still not achieve true plug flow conditions.[14] Plug flow can normally only be created in tubular reactors using very high flow rates which requires long lengths of tubing even for crystallisation over a short timescale.[13] A continuous oscillatory baffled reactor (COBR) is an alternative reactor which approaches plug flow conditions under certain operating parameters using laminar flow, as each cell acts as a STR.[14, 23] A COBR is a tubular crystalliser containing orifice baffles at fixed periods along the length of the reactor. There is complete mixing in the radial but not axial direction, which reduces the likelihood of forward and back mixing meaning the conditions in each cell (between baffles) are more uniform.[24] Mixing is independent of the net flow and can be controlled quite precisely by varying from soft to intense mixing depending on the requirements. In addition, residence times can be much longer than in turbulent systems.[21] The

temperature can also be controlled along the length of the reactor to obtain the required heat transfer and temperature profiles.[13]

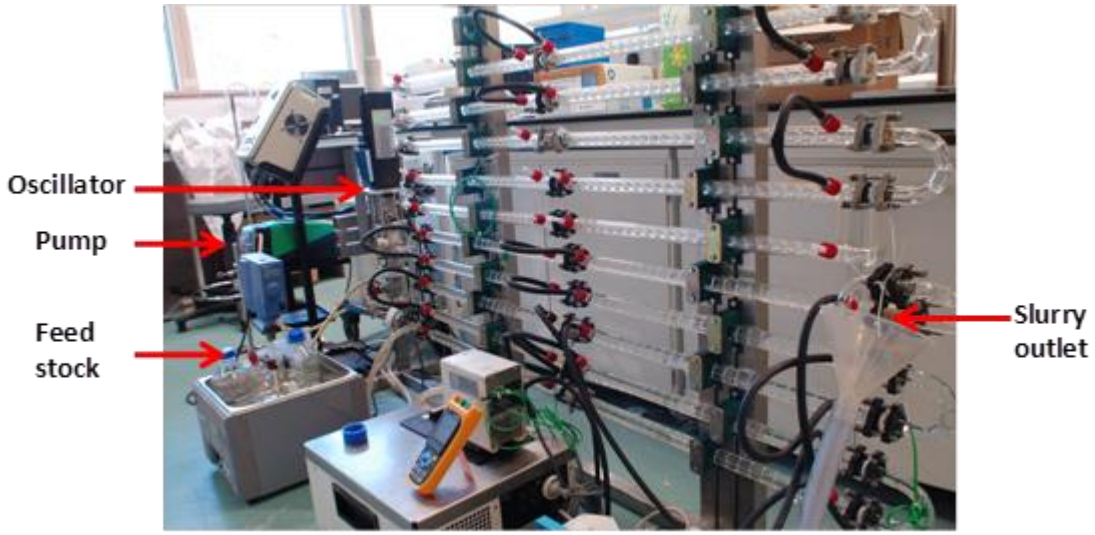

Figure 1-7: Set-up of continuous oscillatory baffled reactor

The potential advantages of batch and continuous OBR technology over conventional batch reactors are consistent product quality including crystal morphology, size and size distribution, as solid material in the column is evenly suspended and distributed due to the uniform mixing. Plug flow crystallisers are known to provide products with a narrower particle size distribution than alternative reactors.[25] In addition, the crystallisation time, space and energy used are all reduced. Downstream processes such as filtration are improved due to the crystal properties being more consistent. For example, a product which has a narrow range of particle sizes and the same morphology will require less time and will be easier to filter. One of the most important factors is that OBR technology can be linearly scaled up owing to more control over the process than with traditional batch methods and so the move from laboratory to industrial scale is less problematic.[14] Also, cooling profiles (linear, step, non-linear) can be optimised for different processes to produce particles of the required characteristics. A further advantage is that *in situ* analytical techniques proven to be useful in laboratory reactors can be used in COBR cells as measurements in different cells will be representative due to uniform mixing within the reactor.[13]

1.3 Drivers for adoption of continuous manufacturing in the pharmaceutical industry

Continuous crystallisation has been identified as a way forward in manufacturing and several industries already have continuous manufacturing processes in place (e.g. foods and chemicals) as a way to move to more time- and cost-efficient processing. However, the pharmaceutical industry continues to use batch manufacturing as in the past it has not had the same need to reduce costs due to the high value (and hence profit) of the products manufactured. Additionally, there has been scepticism from the pharmaceutical industry about switching to continuous manufacturing. Many believe that batch technology has an advantage over continuous if the product being manufactured is changed regularly and also that the product quality would not be sufficient with continuous reactors.[26] There are also regulatory bodies to convince since they need to approve a move from approved batch methods to alternative continuous manufacturing processes.[16] Many companies simply do not want to make the change to continuous technology as it is not economically viable due to their current batch process being adequate for their needs. It can be expensive initially to change from batch to continuous processing, and the best time to do this is prior to commencing the manufacture of a new product, at a time when money is already being invested into the process.[17] By doing this, approval can be sought from regulatory bodies to initiate manufacture in a continuous manner from the outset and this avoids the issues involved with transferring a current batch process. However, implementing batch OBR technology over stirred tank reactors still offers advantages even if transferring to continuous crystallisation is not deemed necessary (chapter 4).

Recently, companies have started to assess the use of continuous technology to manufacture their products for a number of reasons. When increasing the scale of production using batch processes, larger reactors or several in parallel are required utilising a great deal of space and expense.[16] However, by operating a COBR or similar continuous crystalliser constantly for extended periods of time, increased amounts of

material can be produced without the need for multiple batches or larger reactors, which is often a much more efficient way of large scale production.[27] On average, a continuous plant is predicted to cost around 40% less than a batch plant due to the reduced size and running costs.[17] By implementing continuous technology it is possible to develop new and novel products which were not possible with current batch methods. For example, it has been shown that it is possible to form certain polymorphs of a compound which are more troublesome to obtain in batch stirred tank reactors. (Section 4.3). The ultimate goal is to integrate all unit operations into a single, continuous process as conventionally, different stages of manufacture can take place at different locations, which adds to the timescale of the entire process. Continuous processing removes the need for sample transport between reaction vessels on plant, or even manufacturing sites in some cases. This increases sample throughput and leads to a reduction in process cycle times. A typical timescale for a batch process can be up to 300 days from start to finish while a similar fully continuous process is predicted to be reduced to less than 30 days.[17]

The pharmaceutical company Novartis is currently working in collaboration with the Massachusetts Institute of Technology (MIT) to trial a continuous process where the product, from start to finish, will be manufactured continuously in one facility. This "Integrated Drug Substance and Drug Product Manufacturing" process will have a continuous line for manufacturing e.g. crystallisation, drying, blending and tablet production. The initial stage of the project will be carried out at lab scale before being transferred to Novartis to develop it into an industrial scale project using one of its own pharmaceutical products.[28] It is anticipated that manufacture using one continuous line will reduce operational costs, capital expenditure, and active ingredient and product development/manufacturing times significantly whilst improving time to market.[29] There are a wide range of continuous reactors available, one of which is the continuous mixed suspension, mixed product removal crystalliser (MSMPR) which is currently also being studied at MIT.[8] Although continuous crystallisation offers many advantages over

current batch methods, it is still in the relatively early stages and much more research needs to be carried out in order to encourage industry to make the transition.

However, transferring to continuous manufacturing does not necessarily mean that a certain process will instantly be problem free and produce products with the desired characteristics. As with batch processing, a certain amount of investigation is required to identify the kinetics of the process in order to be able to design the experiment. The main difference between batch and continuous processing is that with continuous, the aim is to build quality into the product throughout the process whilst in batch it has most often been tested for in the final product.[30] For this to be possible, the process must be monitored and controlled throughout to obtain the desired product and quality.

1.4 *In-situ* techniques for the monitoring and control of crystallisation

Process control within industry has become of increasing importance in recent times spanning the entire manufacturing process, from the identification of raw materials right through to the end product. Efficient control and optimisation of the process relies on the implementation of on-line and/ or *in situ* analytical techniques at each unit operation of a manufacturing process which identify any variations in the system as early as possible meaning corrective measures can be taken. Traditional off-line techniques usually have a substantial time lag between sampling and the results of analysis, which means if any problems are highlighted it is often too late to rectify them. Despite this, the pharmaceutical industry has often been unwilling to apply new analytical techniques due to the fact they are often expensive and can be challenging to retrofit into existing processes. There are also time-consuming procedures to follow for the approval of new techniques to comply with regulatory bodies and satisfy good manufacturing practice (GMP) guidelines. However, the problems encountered with control of manufacturing processes including the crystallisation operation, and product quality, requires the development and implementation of sufficient measurement techniques.

Batch processing has conventionally been coupled with off-line techniques, which has made control of the process and properties of the product difficult. With present quality control measures in batch processes, a material cannot progress to the next unit operation until confirmation of the quality is assured. The testing is often time consuming and may be destructive. In addition, each batch needs to be sampled then tested and if the quality of the material is not satisfactory, the entire batch will be discarded or reprocessed costing time and money.[31] However, if on-line and in situ techniques replaced or supplemented current off-line analysis, real-time information about the process is possible which means any fluctuations in the system can be identified and corrected for before they affect the properties and, therefore, the quality of the product. A great deal of money is lost in discarded batches due to investigations which are necessary to determine the cause and resolution of the rejected batches. Even though this occurrence is common place, the likelihood of having to reject batches was accepted, as the pharmaceutical industry had a high profit margin to rely on. However, this is no longer the case and the industry is now having to look for ways to save money.[31]

Continuous crystallisation involves reactants being added and products removed continuously whilst keeping the volume at a constant level. The product quality depends on the ability to control the crystallisation conditions which affect formation and growth. For this to be possible, on/in-line techniques are required for the process which means crystallisation is monitored in real-time and any fluctuations in the system can quickly be corrected. This would result in a decrease in wasted product, by approximately 85 % (compared to batch coupled with off-line analysis) since the problems associated with quality are dramatically reduced.[31] *In-situ* techniques are commonly used in laboratory scale and have shown encouraging results, however they are not widely used in industry due to the harsh conditions and scale of operation. Nevertheless, it is important to be able to incorporate these techniques into both existing batch and continuous manufacturing processes as it would provide the ability to control and monitor the process in real-time, which means the crystallisation can be optimised more effectively.

The following section provides an overview of current *in-situ* techniques which have been applied to crystallisation monitoring.

1.4.1 Spectroscopic methods

There are many analytical techniques which can be utilised in crystallisation processes and the majority that are already in use or show potential to measure properties in crystallisation are spectroscopic. These techniques include mid infrared (mid-IR) and near infrared (near-IR) absorption, Raman scattering and UV-visible (UV-Vis) absorption spectroscopies, although most have only been used at the lab scale or in batch processes. These techniques have shown promise for the measurement of the most important variables to be able to control the process including supersaturation, crystal size, polymorphic form and solute concentration.[32]

1.4.1.1 Mid-infrared

Mid-IR measurements can be applied to crystallisation processes through the use of *in-situ* probes. The main types of probe available are reflectance and attenuated total reflectance (ATR), which is the most commonly used probe in process analysis for mid-IR measurements, and in particular for solute concentration measurements in crystallisation processes.[33] This is due to the fact it can be used to measure the liquid phase in the presence of solid particles since it has a short pathlength and only measurements of the liquid sample in contact with the ATR crystal are recorded. There are several advantages to the use of *in-situ* ATR-Fourier transform infrared (FTIR) spectroscopy. The measurements are relatively quick, the analysis is non-destructive and usually no sample preparation is required.[34] In addition, the probes can be composed of different materials depending on the nature of the process stream. Inert materials such as stainless steel can be used which can be immersed into harsh sample conditions.[33] However, the ATR crystal is the weak point of the probe as it can degrade over time e.g. from scratching. A further disadvantage is probe fouling where solid material adheres to the crystal hindering liquid phase measurements. The ATR crystal can also act as a

nucleation site, especially scratched crystals, which can hold seed particles that promote nucleation. This can usually be prevented by ensuring the probe is cleaned thoroughly between and in some instances during crystallisation experiments.

Mid-IR spectroscopy has found application in crystallisation monitoring through solute concentration measurements. The solute concentration is an important parameter since it can be related to the supersaturation of the solution, which in turn impacts the nucleation and growth of the crystals. Therefore, by controlling the supersaturation, the desired crystal properties can be obtained.[35] Firstly, calibration data (taking into account effects of temperature on spectra, etc.) is collected off-line and along with the use of chemometrics this information is used to estimate the solute concentration from the measurements recorded in-situ.[36] This method has been found to be particularly accurate in predicting the solute concentration during crystallisation.[6, 32, 34-36] By monitoring the process, a decrease in the solution concentration can be related to the initiation of crystallisation and the subsequent crystal growth.

1.4.1.2 Near-infrared

Near-IR spectroscopy has not been investigated as thoroughly as mid-IR with respect to crystallisation processes, although it has been used widely in other areas including reaction and environmental monitoring. Traditionally, near-IR absorption was used to measure raw materials in the pharmaceutical industry but due to advances in instrumentation such as fibre optics and spectrometers it has more recently been investigated as a real-time technique, which could be used for the monitoring and control of certain parameters in crystallisation processes. It has been shown to be particularly beneficial in the analysis of polymorphs and polymorph transformations which is an important outcome to control in pharmaceutical manufacturing.[37-39] Near-IR has been difficult to implement as a crystallisation monitoring technique as conventionally it was applied to liquid phase measurements and the solid material in slurries was found to interfere with instrumentation and cause distortion of the spectra.[38]

In addition, until recently there has been a lack of robust probes which can be applied to industrial processes. However, it was discovered that near-IR spectra could in fact provide valuable information on particles in solution meaning that the near-IR spectra obtained could give information on both the liquid and solid phase including particle size, solid and liquid concentration, and polymorphic composition. This has been achieved using a single transflectance probe[38] and additionally by implementing multiple probes into the process information on the solid phase was obtained using a diffuse reflectance probe and liquid phase measurements were obtained using a transflectance probe.[37] However, these variables cause different effects on the near-IR spectra obtained. For example, the chemical information determines the absorption pattern of the spectrum obtained. On the other hand, the particle size and solid concentration information is contained within the spectral baseline where a decrease in the particle size results in an increase in the baseline observed and an increase in the solid concentration causes a corresponding increase in the baseline offset.[38, 40] Therefore, the absorption and scattering effects need to be separated from the spectral data obtained using chemometric methods such as principal component analysis[40] and multiplicative scatter correction.[41]

Near-IR, like mid-IR can make use of *in-situ* probes to make measurements and there are a range available depending on the application e.g. transmission, diffusive reflectance and transflectance. The wide range of probes available mean that almost any sample type can be analysed and non-invasive measurements are possible with reflectance measurements through some types of sample container.[37] Like mid-IR, the probes are connected to the spectrometer via optical fibres which means several probes can be located at different positions in the system and connected to a spectrometer which is isolated from the process. An advantage of near-IR over mid-IR is the use of silica fibres which means the spectrometer can be located much further away from the process with lengths in excess of 1000 m possible. Conversely, mid-IR spectrometers are restricted to distances of up to 15 m from the process.[33] This feature of near-IR facilitates greater safety measures protecting staff and the spectrometer itself from

potentially dangerous processes (e.g. explosive hazards). However, also like mid-IR, probe fouling can be an issue especially with transmission probes with small pathlengths where the window can become blocked with particles. Along with alternative process analysis techniques, near-IR would be a useful technique for industrial crystallisation as the results are obtained rapidly meaning that fluctuations are identified quickly, the analysis is non-destructive and both qualitative and quantitative information is obtained.[38] However, unlike Mid-IR where the spectra can be directly interpreted, near-IR spectra are much more complex and require more complex chemometric methods to aid with interpretation.[42] In addition, time consuming calibration procedures are required prior to analysis.

1.4.1.3 Raman

Raman spectroscopy is an extremely promising technique for industrial crystallisation as it is possible to obtain information on both the solid and liquid phase but in particular for the monitoring of polymorphs and any transformations occurring during the process. Raman has been used off-line for the identification of polymorphs in pharmaceutical products however, there is the potential to use *in-situ* or non-invasive measurements to determine the concentration of one or multiple polymorphs. As with the other techniques, calibration data must first be collected in order to predict the concentrations of the polymorphs from in-situ measurements.[43] In addition, by monitoring the polymorphic transitions taking place the optimum crystallisation conditions such as temperature can be chosen in order to give a product of the desired polymorph.[5] However, during a cooling crystallisation, the temperature and particle size also have an effect on the spectral data so these effects either need to be included in the calibration model (further complicating the model) or removed using alternative methods. *Chen et al* applied a multiplicative effects correction (MEC) technique in order to remove the effects of physical properties (*i.e.* particle size) from crystallisation data to improve the prediction of the solid concentration carried out using a partial least squares (PLS) method.[44] Furthermore, additional work by the same author has shown the use of

advanced chemometric methods such as loading space standardisation (LSS) to remove temperature effects in slurry samples meaning the variation caused by temperature can be removed and more accurate predictions of polymorphic mixtures are possible.[45]

Raman has the advantage over near-IR for monitoring polymorphs in aqueous solutions. Water has a strong OH absorption in near-IR spectra, which can mask peaks in that region whereas water is a weak Raman scatterer and has a relatively minor effect on the spectrum. Raman spectra are usually less problematic to interpret as the relationship between a certain variable and the peak height is often more obvious than alternative analysis techniques which means the use of chemometric analysis is not always required.[5] Real-time monitoring is possible as the analysis is rapid and no sample preparation is required. It is also useful for the analysis of inhomogeneous samples and for certain samples where only a few milligrams of material is present, for example during nucleation and the early stages of crystal growth in crystallisation processes.[46]

Fluorescence from components in a sample or materials of construction can be an issue in Raman spectrometry and is discussed further in section 2.2.1.2. Issues can also arise with certain pharmaceutical compounds of low solubility which generate a low concentration in solution meaning the Raman spectrum will be very weak or non-existent due to the low sensitivity of this technique. This limited sensitivity is due to the low probability of Raman scattering occurring and the restricted collection of Raman scattered photons by the instrument (since scattering occurs in all directions). If these measurements are collected non-invasively, through glass for example, the spectra can be further weakened from the contribution of the glass which results in a significant background signal onto which the analyte signal is superimposed, meaning a sufficient spectrum of the sample may not be obtained. In addition, if the solvent used is not water and it has scattering properties, the signal from the compound and the solvent can be difficult to separate.[5]

1.4.1.4 UV-Visible (UV-Vis)

UV-Vis fibre spectroscopy has shown potential on-line, for the determination of solute concentration as demonstrated by *Zhang et al.*[47] ATR-UV spectroscopy has also been used as an alternative to ATR-FTIR for the determination of solute concentration, however to gain useful information from the spectra multivariate data analysis is required as UV spectra are relatively indistinctive compared to ATR-FTIR. It is necessary for the target molecule to contain a chromophore which results in high UV absorption in order to make sensitive measurements. In addition, the UV absorption of the solvent can in some cases mask the absorption of the solute in question.[48]

1.4.2 Non-spectroscopic methods

There are many other techniques which have been investigated for their use in monitoring crystallisation. The use of ultrasound measurements to determine particle size and concentration is a relatively recent development which has been discussed by *Mougin et al.*[49-51] A change in the solid and liquid phase occurs as a sound wave interacts with suspended particles. A change in this wave is also observed which is related to the particle size and concentration. However to gain accurate information, knowledge of seven physical properties of the particulate phase including density and shear rigidity and seven properties of the continuous phase including sound speed and attenuation are required, which is often not always available and can therefore affect the accuracy of the data. The technique is useful over a wide range of particle sizes and also at high concentrations.[49]

Turbidity measurements are also commonly used in crystallisation monitoring to provide kinetic information on nucleation and are based on the solution transmittance being inversely proportional to the concentration of crystals within the solution. These measurements have been used to determine the metastable zone width (MSZW)[12] and the particle size, particle size distribution and solid concentration.[52]

X-ray diffraction (XRD) has been explored for the in-situ monitoring of polymorphic transformations during the crystallisation of L-glutamic acid (LGA) whereas traditionally it has been used as an off-line technique to identify polymorphs.[53] This is partly due to slurry samples absorbing X-rays which results in a reduction in the intensity of diffracted X-rays detected. This means only peaks of higher intensity are detected. The variation in X-ray diffraction spectra obtained from different polymorphs is due to the differences in the crystal structure of the different forms. An in-situ XRD method would also have the potential to monitor the effect of variations in the system meaning that optimum conditions can be established to obtain the desired polymorph.

1.4.2.1 Particle sizing

There has been advancement in recent years with the development of techniques which are much more efficient and effective at measuring the size and range of particles. Focused beam reflectance measurement (FBRM) can be used in-situ to give information on the particle properties including the particle size distribution and is often used alongside in-situ microscopy to provide complementary images of the particles.[54] An alternative method for monitoring the formation of particles is dynamic light scattering (DLS). DLS can detect significantly smaller nuclei and crystals than is possible with optical microscopy so it is possible to monitor the early stages of crystallisation. This means there is potential to intervene and change conditions at the most important stage of crystallisation, if required. This technique can be used non-invasively and can discriminate between very small differences in particle sizes (>1 nm).[55]

Dynamic image analysis (DIA) can provide rapid information on both the size and shape of particles down to 1 μm. It has the advantage that the data provided covers a large number of particles, giving a wider picture of the sample characteristics and reducing the error associated.[56] This technique is particularly useful for fast moving particles such as in a process stream making it particularly well-suited to continuous processes. In

addition, the improvements in this technology mean on-line analysis is possible when an appropriate sampler is connected.

1.5 Conclusions

The literature review conducted has highlighted several points with respect to the monitoring of crystallisation.

- Crystallisation is an important unit operation in many industries and especially the pharmaceutical industry, however, inadequate process control has often resulted in poor quality products being obtained.
- The pharmaceutical industry is starting to investigate on-line and in-line analytical techniques for the monitoring and control of crystallisation and other processes in order to provide real time information.
- In addition, new procedures such as continuous manufacturing are emerging as an alternative to traditional batch processing due to the increased benefits such as reductions in wasted materials and cost.
- There are many examples in the literature of on-line and in-line analytical techniques being explored to monitor crystallisation in real time, however, the majority of these are applied to batch reactor technology at laboratory scale.
- The most common techniques used in crystallisation monitoring are spectroscopic and include Raman scattering for identification and quantification of polymorphs, mid-IR absorption for solute concentration measurements and near-IR spectroscopies for changes in particle size and in some cases, polymorphic form. Focused beam reflectance measurement (FBRM) is also frequently used to provide information on the particle size distribution.

1.6 Aims

The proposal for the following PhD project was to perform an evaluation of non-invasive spectroscopic methods, in particular, Raman spectroscopy, to establish whether or not they would provide valuable information that could be used in the monitoring and control of crystallisation processes. Non-invasive measurements have the advantage of avoiding probe fouling issues that are prevalent with the insertion probes that have typically been used in crystallisation studies. An initial model compound was identified with the aim of moving on to an alternative compound which was important in pharmaceutical crystallisation.

L-glutamic acid (LGA) was chosen as the model compound as it is well defined in the literature, however, the majority of results have been achieved with the use of stirred tank reactors. The purpose of the initial study was to gain experience in the use of batch and continuous OBR reactors, evaluate analytical techniques, recreate previous results and develop process understanding. These objectives were explored in chapters 4 and 5 of the thesis. The next stage of work focused on the main alternative continuous crystalliser available; the mixed suspension, mixed product removal reactor. L-glutamic acid was studied once more in order to be able to make comparisons and draw conclusions between these two presently available continuous reactor types. These results are discussed in chapter 6.

The secondary compound selected for this study was D-Mannitol, which is used in the pharmaceutical industry in the treatment of many conditions including renal failure and cystic fibrosis as well as an excipient in many tablet formulations. Mannitol has three reported polymorphs; however, it is less well studied in comparison with L-glutamic acid with respect to the crystallisation process and has not been reported in the literature in association with oscillatory baffled reactor technology. During this section of work, as discussed in chapter 7, the potential of a second non-invasive measurement technique,

acoustic emission spectroscopy, was explored for its applicability to crystallisation monitoring as a complementary technique to Raman spectroscopy.

In the following report, results are presented from non-invasive Raman monitoring of crystallisations of LGA in both batch STR and OBRs, and continuous OBR and MSMPRs, which has not been previously reported in the literature. Raman spectroscopy with a probe that delivered optically broadened illumination was employed to identify the two polymorphs of LGA and monitor any polymorphic transformations taking place during the crystallisation process. The knowledge acquired from the initial stage of work using the model compound was then transferred to a secondary compound, Mannitol which was investigated for its compatibility with OBR technology. Acoustic emission spectroscopy was employed at this stage as a complementary non-invasive monitoring technique with the goal of obtaining information including particle size and solids concentration. The overall aim of the project was to gain an understanding of the crystallisation processes taking place, investigate and optimise the OBR and other reactor technology, and establish which non-invasive and in situ techniques should be combined to monitor and control crystallisation through the provision of real-time information on the process. Furthermore, data analysis methods were explored to interpret the spectral data obtained and extract additional information to enable increased understanding of the crystallisation process.

1.7 References

1. B. Y. Shekunov and P. York, Crystallization processes in pharmaceutical technology and drug delivery design, *Journal of Crystal Growth*, 2000, **211**, 122-136.
2. J. W. Mullin, Crystallization, 4th edn., Elsevier Butterworth-Heinemann, Oxford, 2001.
3. A. S. Myerson, Handbook of industrial crystallization, 2nd edn., Butterworth-Heinemann, Woburn, 2001.
4. J. Ulrich and M. J. Jones, Industrial Crystallization: Developments in Research and Technology, *Chemical Engineering Research and Design*, 2004, **82**, 1567-1570.
5. G. Févotte, In Situ Raman Spectroscopy for In-Line Control of Pharmaceutical Crystallization and Solids Elaboration Processes: A Review, *Chemical Engineering Research and Design*, 2007, **85**, 906-920.
6. J. Dunn, Monitoring a crystallisation reaction using in-situ mid-infrared spectrometry, University of Strathclyde, 2009.
7. H. Qu, H. Alatalo, H. Hatakka, J. Kohonen, M. Louhi-Kultanen, S. Reinikainen and J. Kallas, Raman and ATR FTIR spectroscopy in reactive crystallization: Simultaneous monitoring of solute concentration and polymorphic state of the crystals, *Journal of Crystal Growth*, 2009, **311**, 3466-3475.
8. A. G. Jones, Crystallisation Process Systems, Elsevier Butterworth-Heinemann, 2002.
9. K. Sangwal, Recent developments in understanding of the metastable zone width of different solute−solvent systems, *Journal of Crystal Growth*, 2011, **318**, 103-109.
10. W. Omar and J. Ulrich, Application of Ultrasonics in the On-line Determination of Supersaturation, *Crystal Research and Technology*, 1999, **34**, 379-389.
11. J. Ulrich and C. Strege, Some aspects of the importance of metastable zone width and nucleation in industrial crystallizers, *Journal of Crystal Growth*, 2002, **237**, 2130-2135.
12. X. Ni and A. Liao, Effects of mixing, seeding, material of baffles and final temperature on solution crystallization of l-glutamic acid in an oscillatory baffled crystallizer, *Chemical Engineering Journal*, 2010, **156**, 226-233.
13. X. Ni, Bridging the gap, March 2011. http://www.nitechsolutions.co.uk/Uploads/crystallisation-TCE.pdf.
14. S. Lawton, G. Steele, P. Shering, L. Zhao, I. Laird and X. Ni, Continuous Crystallization of Pharmaceuticals Using a Continuous Oscillatory Baffled Crystallizer, *Organic Process Research & Development*, 2009, **13**, 1357-1363.
15. Z. K. Nagy, M. Fujiwara, J. W. Chew and R. D. Braatz, First-principles and direct design approaches next term for the previous term control of pharmaceutical crystallization, *Journal of Process Control*, 2005, **15**, 493-504.
16. C. Vervaet and J. P. Remon, Continuous granulation in the pharmaceutical industry, *Chemical Engineering Science*, 2005, **60**, 3949-3957.

17. A. Pellek and P. V. Arnum, Continuous Processing: Moving with or against the Manufacturing Flow, *Pharmaceutical Technology*, 2008, **9**, 5258.
18. GEA Process Engineering Inc, May 2013. http://www.Near-IRoinc.com/evaporators_crystallizers/forced_circulation_crystallizer. asp.
19. P. Stonestreet and P. M. J. Van Der Veeken, The Effects of Oscillatory Flow and Bulk Flow Components on Residence Time Distribution in Baffled Tube Reactors, *Chemical Engineering Research and Design*, 1999, **77**, 671-684.
20. R. I. Ristic, Oscillatory Mixing for Crystallization of High Crystal Perfection Pharmaceuticals, *Chemical Engineering Research and Design*, 2007, **85**, 937-944.
21. X. Ni, Continuous Oscillatory Baffled Reactor Technology, March 2013. http://www.nitechsolutions.co.uk/Uploads/InnovationinPharmaTech.pdf.
22. E. M. Haacke and Y. C. N. Cheng, Phase Dependence on Motion: Current Protocols in Magnetic Resonance Imaging, Wiley, 2005.
23. X. Ni, M. R. Mackley, A. P. Harvey, P. Stonestreet, M. H. I. Baird and N. V. Rama Rao, Mixing Through Oscillations and Pulsations—A Guide to Achieving Process Enhancements in the Chemical and Process Industries, *Chemical Engineering Research and Design*, 2003, **81**, 373-383.
24. O. Levenspiel, Chemical Reaction Engineering, 3rd edn., John Wiley & Sons, Inc., 1999.
25. H. Gros, T. Kilpiö and J. Nurmi, Continuous cooling crystallization from solution, *Powder Technology*, 2001, **121**, 106-115.
26. K. Plumb, Continuous Processing in the Pharmaceutical Industry: Changing the Mind Set, *Chemical Engineering Research and Design*, 2005, **83**, 730-738.
27. J. Chen, B. Sarma, J. M. B. Evans and A. S. Myerson, Pharmaceutical Crystallization, *Crystal Growth & Design*, 2011, **11**, 887-895.
28. P. Richards, MIT and Novartis in new partnership aimed at transforming pharmaceutical manufacturing, May 2012. http://web.mit.edu/newsoffice/2007/novartis-0928.html.
29. A. S. Myerson, Nucleation of Organic Molecular Crystals: Evidence for the Two Step Nucleation Model, Heriot-Watt University, 2011.
30. B. Swichtenberg, Moving Beyond the Batch, October 2013. http://www.pharmamanufacturing.com/articles/2008/010.html?page=1.
31. T. Crosby, Designing For the Future of Continuous Processing, May 2012. http://www.pharmpro.com/Archives/2006/01/Designing-For-the-Future-of-Continuous-Processing/.
32. L. X. Yu, R. A. Lionberger, A. S. Raw, R. D'Costa, H. Wu and A. S. Hussain, Applications of process analytical technology to crystallization processes, *Advanced Drug Delivery Review*, 2004, **56**, 349-369.
33. J. Andrews and P. Dallin, Getting to grips with the process: extractive and remote "sampling", *Spectroscopy Europe*, 2003, **15**, 27-30.
34. S. Wartewiga and R. H. H. Neubert, Pharmaceutical applications of Mid-IR and Raman spectroscopy, *Advanced Drug Delivery Review*, 2005, **57**, 1144-1170.

35. H. Grön, A. Borissova and K. J. Roberts, In-Process ATR-FTIR Spectroscopy for Closed-Loop Supersaturation Control of a Batch Crystallizer Producing Monosodium Glutamate Crystals of Defined Size, *Industrial & Engineering Chemistry Research*, 2003, **42**, 198-206.
36. Z. Chen, J. Morris, A. Borissova, S. Khan, T. Mahmud, R. Penchevc and K. J. Roberts, On-line monitoring of batch cooling crystallization of organic compounds using ATR-FTIR spectroscopy coupled with an advanced calibration method, *Chemometrics and Intelligent Laboratory Systems*, 2009, **96**, 49-58.
37. G. Févotte, J. Calas, F. Puel and C. Hoff, Applications of NEAR-IR spectroscopy to monitoring and analyzing the solid state during industrial crystallization processes, *International Journal of Pharmaceutics*, 2004, **273**, 159-169.
38. S. B. Abebea, X. Z. Wang, R. Lia, K. J. Roberts and X. Lai, The information content in NEAR-IR spectral data for slurries of organic crystals, *Powder Technology*, 2008, **179**, 176-183.
39. C. Y. Ma and X. Z. Wang, Simultaneous characterization of multiple properties of solid and liquid phases in crystallization processes using NEAR-IR, *Particuology*, 2011, **9**, 589-597.
40. M. Otsuka, Comparative particle size determination of phenacetin bulk powder by using Kubelka–Munk theory and principal component regression analysis based on near-infrared spectroscopy, *Powder Technology*, 2004, **141**, 244-250.
41. Y.-C. Chen and S. N. Thennadil, Insights into information contained in multiplicative scatter correction parameters and the potential for estimating particle size from these parameters, *Analytica Chimica Acta*, 2012, **746**, 37-46.
42. Y. Roggo, P. Chalus, L. Maurer, C. Lema-Martinez, A. Edmond and N. Jent, A review of near infrared spectroscopy and chemometrics in pharmaceutical technologies, *Journal of Pharmaceutical and Biomedical Analysis*, 2007, **44**, 683-700.
43. T. Ono, J. H. Horst and P. J. Jansens, Quantitative Measurement of the Polymorphic Transformation of l-Glutamic Acid Using In-Situ Raman Spectroscopy, *Crystal Growth & Design*, 2004, **4**, 465-469.
44. Z.-P. Chen, G. Fevotte, A. Caillet, D. Littlejohn and J. Morris, Advanced Calibration Strategy for in Situ Quantitative Monitoring of Phase Transition Processes in Suspensions Using FT-Raman Spectroscopy, *Analytical Chemistry*, 2008, **80**, 6658-6665.
45. Z.-P. Chen and J. Morris, Improving the linearity of spectroscopic data subjected to fluctuations in external variables by the extended loading space standardization, *Analyst*, 2008, **133**, 914-922.
46. T. Vankeirsbilck, A. Vercauteren, W. Baeyens, G. Van der Weken, F. Verpoort, G. Vergote and J. P. Remon, Applications of Raman spectroscopy in pharmaceutical analysis, *Trends in Analytical Chemistry*, 2002, **12**, 869-877.
47. Y. Zhang, Y. Jiang, D. Zhang, K. Li and Y. Qian, On-line concentration measurement for anti-solvent crystallization of β-artemether using UV–vis fiber spectroscopy, *Journal of Crystal Growth*, 2011, **314**.

48. D. R. Thompson, E. Kougoulos, A. G. Jones and M. W. Wood-Kaczmar, Solute concentration measurement of an important organic compound using ATR-UV spectroscopy, *Journal of Crystal Growth*, 2005, **276**, 230-236.
49. P. Mougin, D. Wilkinson, K. J. Roberts, R. Jack and P. Kippax, Sensitivity of particle sizing by ultrasonic attenuation spectroscopy to material properties, *Powder Technology*, 2003, **134**, 243-248.
50. P. Mougin, D. Wilkinson, K. J. Roberts and R. Tweedie, Characterization of particle size and its distribution during the crystallization of organic fine chemical products as measured in situ using ultrasonic attenuation spectroscopy, *The Journal of the Acoustical Society of America*, 2001, **109**, 274-282.
51. P. Mougin, D. Wilkinson and K. J. Roberts, In Situ Ultrasonic Attenuation Spectroscopic Study of the Dynamic Evolution of Particle Size during Solution-Phase Crystallization of Urea, *Crystal Growth & Design*, 2002, **3**, 67-72.
52. M. Moscosa-Santillán, O. Bals, H. Fauduet, C. Porte and A. Delacroix, Study of batch crystallization and determination of an alternative temperature-time profile by on-line turbidity analysis -- application to glycine crystallization, *Chemical Engineering Journal*, 2000, **55**, 3759-3770.
53. R. B. Hammond, X. Lai and K. J. Roberts, Application of In-Process X-ray Powder Diffraction for the Identification of Polymorphic Forms during Batch Crystallization Reactions, *Crystal Growth & Design*, 2004, **4**, 943-948.
54. M. Kempkes, J. Eggers and M. Mazzotti, Measurement of particle size and shape by FBRM and in situ microscopy, *Chemical Engineering Journal*, 2008, **63**, 4656-4675.
55. N. E. Chayen, Methods for separating nucleation and growth in protein crystallisation, *Progress in Biophysics and Molecular Biology*, 2005, **88**, 329-337.
56. W. Witt, U. Köhler and J. List, Current limits of particle size and shape analysis with high speed image analysis, August 2013. http://www.sympatec.com/docs/ImageAnalysis/publications/IA_2007_CurrentPossibilitiesofIA_E_1.0.pdf.

2 Theory of instrumental and experimental techniques

2.1 Crystallisation

2.1.1 Nucleation and Crystal Growth

As explained in the previous chapter, crystallisation is an important operation in industry, in particular the pharmaceutical industry. It is known that the nucleation and crystal growth processes during crystallisation are very much dependent on the supersaturation of the solution, the theory of which has already been discussed in section 1.1.1. Nucleation and crystal growth are relatively complex processes which are still not fully understood. As explained in section 1.1.1, nucleation can either take place in a primary (further sub-divided into homogeneous and heterogeneous) or secondary manner. In order for homogeneous nucleation to take place, there needs to be a clustering of the molecules resulting in a nucleus above a certain critical size which will continue to grow rather than dissolve. Figure 2-1 shows the free energy diagram for homogeneous nucleation and the equation for the value of the critical nucleus.

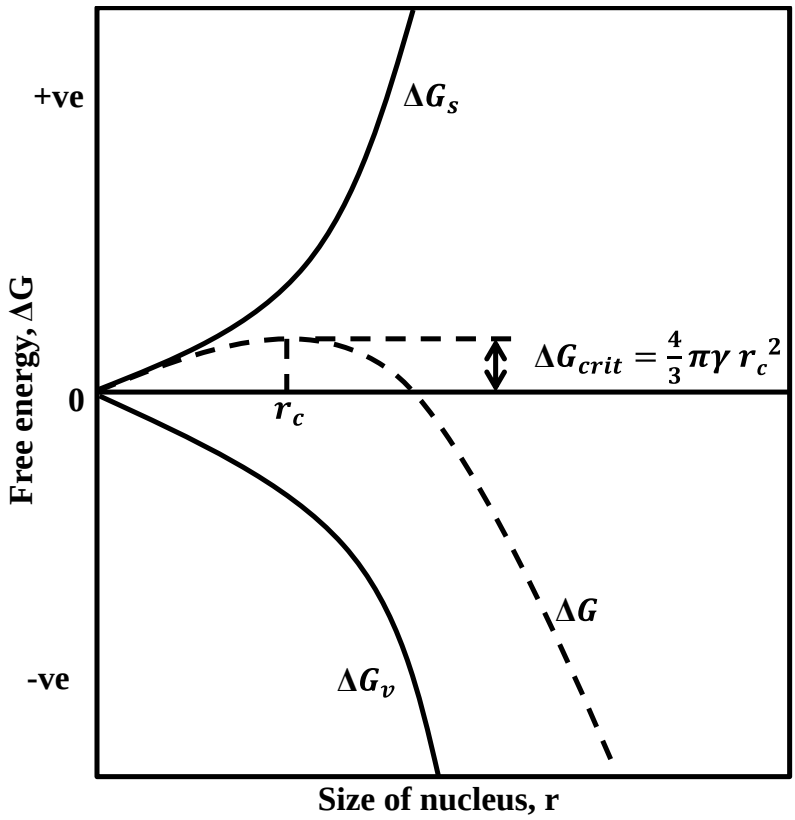

Figure 2-1: Diagram showing the energy requirements for formation of the critical nucleus in homogeneous nucleation[1]

Figure 2-1 shows that particles of a size smaller than the critical size ($\boldsymbol{r_c}$) will dissolve in order to reduce its free energy. On the other hand, a particle larger than the critical size will continue to grow.[1] Equation 2-1 shows the value for the maximum free energy of formation ($\Delta \boldsymbol{G_{crit}}$) which is related to the critical nucleus size ($\boldsymbol{r_c}$).

$$\Delta \boldsymbol{G_{crit}} = \frac{16\pi\gamma^3}{3(\Delta G_v)^2} = \frac{4\pi\gamma r_c^2}{3} \qquad \textbf{(2-1)}$$

ΔG_v = volume excess free energy

γ = interfacial tension

The nucleation rate (determined from equation 2-2) is known to be affected by a number of factors including the temperature and supersaturation. There is a critical

supersaturation value above which almost instantaneous nucleation will occur. At values below this, nucleation will occur but just on a longer timescale of hours, days or years.[1]

$$J = Aexp\left[\frac{16\pi\gamma^3 v^2}{3k^3T^3(lnS)^2}\right] \quad \textbf{(2-2)}$$

J = nucleation rate

k = Boltzmann constant

S = supersaturation ratio

v = molecular volume

T = temperature

Figure 2-2 shows the effect of supersaturation on the nucleation rate both theoretically (determined from equation 2-2), and as observed experimentally. It can be seen that equation 2-2 suggests that the nucleation rate will continue to increase once a certain critical supersaturation value has been reached. However, in practice, there is a temperature and supersaturation range over which the nucleation rate will be enhanced. This is due to the size of the critical nucleus increasing with an increase in the temperature making nucleation less likely.

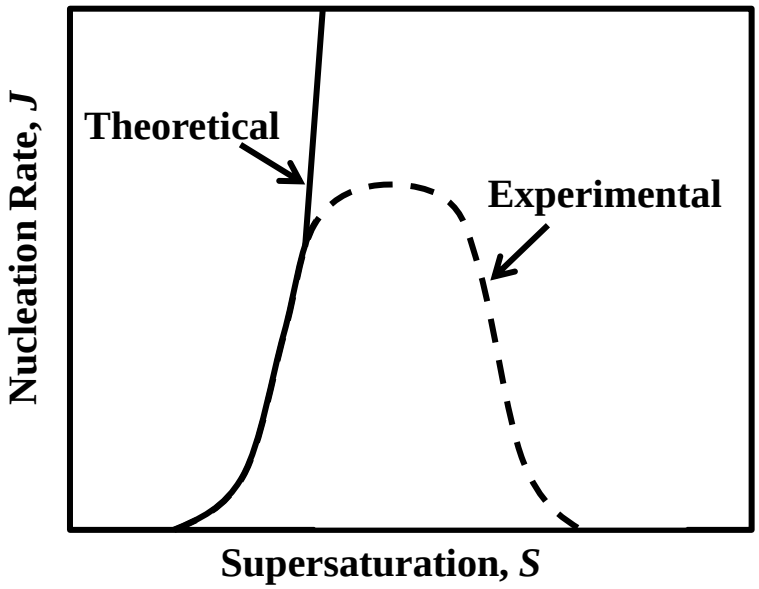

Figure 2-2: Diagram showing the effect of supersaturation on the nucleation rate[1]

Impurities can be problematic in industrial crystallisation as in some cases they induce nucleation whilst an alternative impurity can act as an inhibitor. Heterogeneous nucleation occurs when foreign particles present seed the solution and encourage nucleation to take place earlier than spontaneous nucleation. Therefore, the energy required to form the critical nucleus is lower than homogeneous nucleation.[2] When existing particles of the solute are present, nucleation occurs at a lower supersaturation value than in homogeneous or heterogeneous primary nucleation. Secondary nucleation can arise due to a number of reasons and can be intentional due to seeding or unintentional due to contact nucleation (between particles or impellers) or attrition.[2]

2.1.1.1 Meta-stable zone width

The metastable zone width is known to be an important parameter in industrial crystallisation (discussed further in section 1.1.1.) and therefore several different methods have been investigated to characterize it including turbidity, mid-infrared spectrometry and ultrasound.[3-6] Once a solution reaches supersaturation, nucleation will not always immediately occur as there is an allowable (meta-stable) level of supersaturation where particles will not form. The maximum allowable supersaturation, or the meta-stable zone width (ΔC^{n}_{max}) is related to the nucleation rate (J) in the following equation:[1]

$$J = k_n \Delta c^{n}_{max} \qquad \textbf{(2-3)}$$

k_n = nucleation rate constant

2.1.1.2 Induction period

The induction time is the period between reaching supersaturation and nucleation first taking place. This was particularly evident in the results obtained with D-mannitol in chapter 7. This value can be important in calculating crystallisation kinetics of a given compound and can be affected by the level of supersaturation, agitation and impurities present.[2, 7] Figure 2-3 shows the processes that take place during the initial stages of nucleation and subsequent crystal growth.

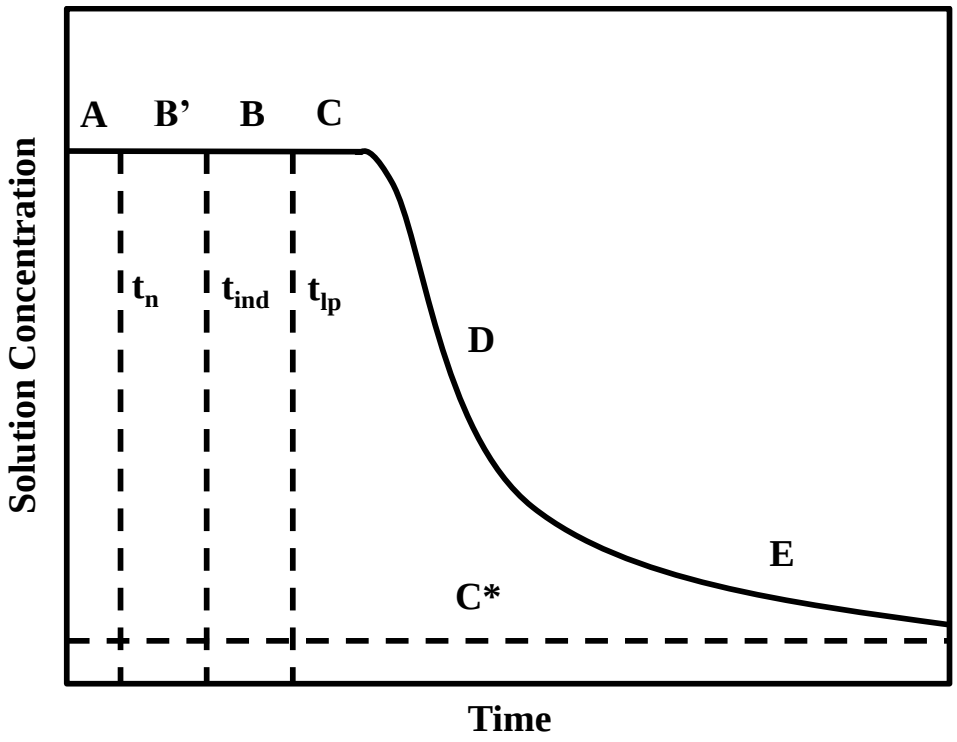

Figure 2-3: Diagram showing a desupersaturation curve during crystallisation[1]

Figure 2-3 shows that at time point A, (t=zero) supersaturation is created; however, there is a delay between supersaturation being generated and the nucleation event (B). During the period from point A to B, the first nucleus above a critical size is formed (t_n), which then requires a certain time period (known as the induction period) to grow to a size large enough to be detected (t_{ind}). During the period from point B to C, there is little change in the solution concentration following the detection of the initial nuclei (known as the latent period (t_{lp})), until a rapid decrease in the solution concentration (desupersaturation) is observed during time period D. This is the region where crystal growth is the dominant process. The final stage of the process, point E, shows the crystallisation beginning to reach equilibrium.[1]

2.1.1.3 Crystal Growth

There have been many mechanisms proposed for crystal growth which will not be discussed in detail; however, it has still not been determined exactly how crystals grow

following nucleation. It is widely thought that crystal growth takes place through an initial diffusion step, followed by integration into the crystal lattice.[1, 2] Firstly, the solute molecules diffuse through the liquid phase to reach the crystal surface. Secondly, the molecules are integrated into the crystal lattice which takes place in a number of stages. The growth unit is first adsorbed onto the crystal surface where it releases part of its solvation shell and is subsequently incorporated into the lattice or returned back to solution. If the growth unit is retained it will lose the rest of its solvation shell to be fully incorporated into the lattice.[2] The difference in growth rates between alternate crystal faces will result in the production of crystals of differing habit (prismatic, needle, etc.). The overall growth rate is given by the following equation.[8]

$$\boldsymbol{G = A\, exp(\frac{-E_G}{RT})\Delta C} \qquad \textbf{(2-4)}$$

$\boldsymbol{A}$ **= constant**

$\boldsymbol{E_G}$ **= activation energy**

$\boldsymbol{\Delta C}$ **= supersaturation**

2.1.2 Polymorphism

Polymorphs are different crystal structures of the same compound and identifying and characterising all possible polymorphs is of the upmost importance in industry (explained further in chapter 1.1). Ostwald's rule of stages states that *an unstable system does not necessarily transform directly into the most stable state, but into one which most closely resembles its own, i.e. into another transient state whose formation from the original is accompanied by the smallest loss of free energy*.[1] However, it has been found that there are many exceptions to this rule and that in these cases it may be kinetics (nucleation and crystal growth rates) that determine the polymorphic outcome rather than thermodynamics. If a meta-stable polymorph nucleates initially, it is possible that it may begin to transform immediately to the thermodynamically stable form or it may remain for a prolonged period of time depending on its stability. Transformations from a metastable to a thermodynamically stable form are non-reversible in monotropic

systems, however transformations in enantiotropic compounds can be reversed. Figure 2-4 shows an example of solubility curves for a monotropic and enantiotropic system.

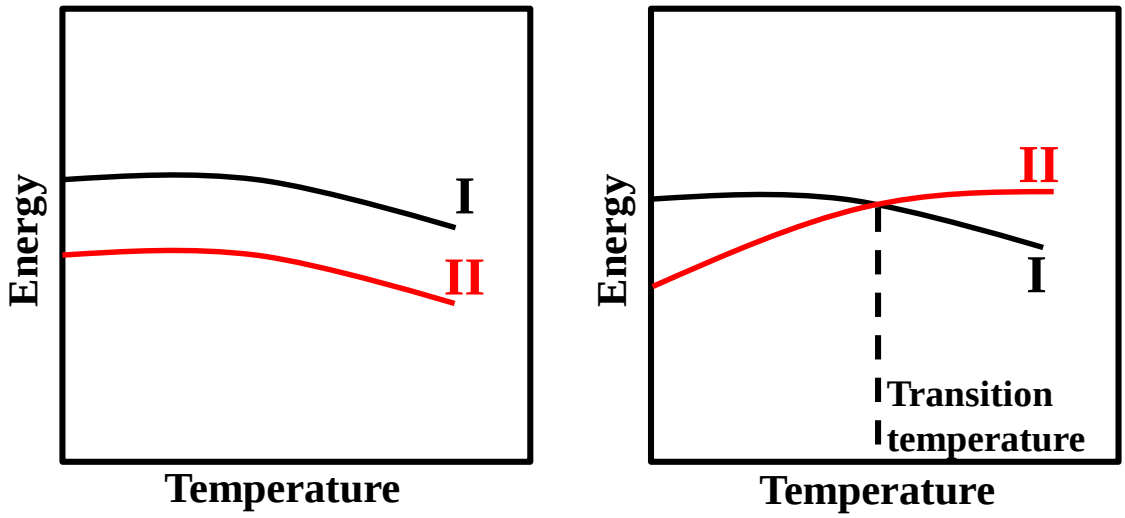

Figure 2-4: Solubility curves showing a monotropic system (left) and enantiotropic system (right)[1]

Under certain conditions (*e.g.* temperature and pressure) only one polymorph will be thermodynamically stable and therefore, all others which form will be metastable and can potentially transform to the stable form which has the lower free energy. The stable form will also be the least soluble so in the monotropic system in Figure 2-4 polymorph II is the most stable, while in the enantiotropic system, form II is stable at temperatures below the transition temperature while above this temperature, polymorph I is stable.[1]

2.1.3 Population balance model

The population balance model was developed to predict the performance and kinetics in both batch and continuous crystallisers at steady and unsteady state. It has most often been applied to continuous MSMPR reactors which are studied in chapter 6 using L-glutamic acid. The population balance connects the crystallisation kinetics, particle size distribution and residence time in the following equation:[2, 8]

$$\boldsymbol{n(L) = n^0 \exp\left(\frac{-L}{G\tau}\right)} \qquad \textbf{(2-5)}$$

$n\ (L)$ = **population density**

n^0 = **nuclei population density**

L = **crystal size**

G = **growth rate**

τ = **mean residence time**

Figure 2-5 shows the method for calculating the crystal size distribution from data obtained during a crystallisation in a MSMPR. The growth rate (***G***) is determined from the slope and from this the nucleation rate (***B***) can be calculated.

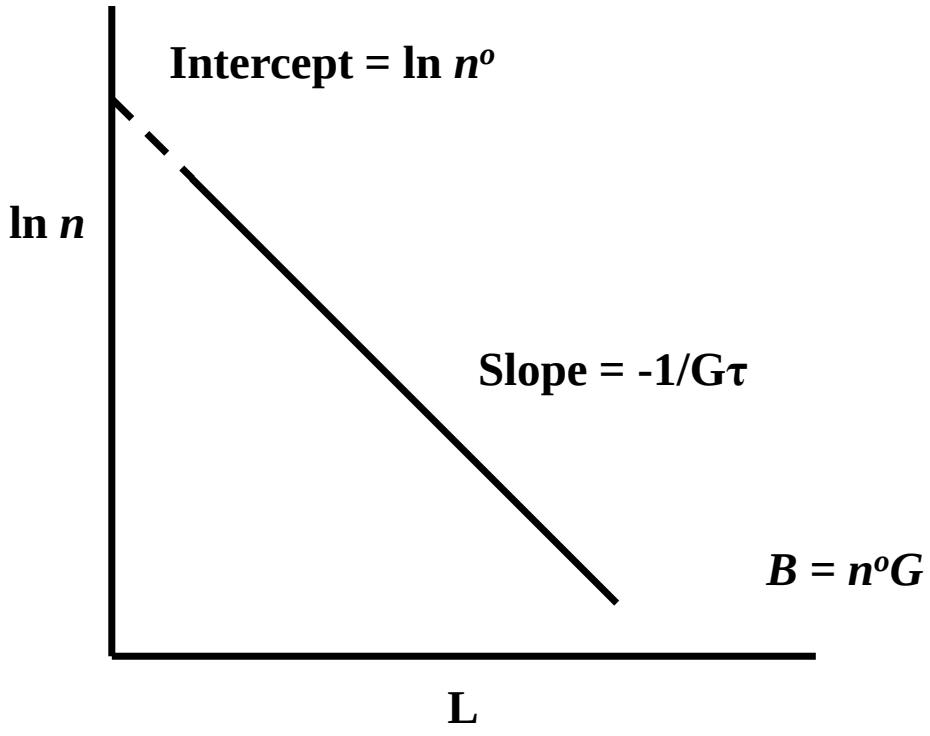

Figure 2-5: Crystal population distribution from an MSMPR reactor[2]

2.2 Theory of Vibrational Spectroscopy

The bond vibrations in a molecule can be thought of in terms of a diatomic molecule (harmonic oscillator) - two atoms, m_1 and m_2, connected by a spring which stretches and contracts. This can be represented mathematically in the following equation.[9]

$$\boldsymbol{F = -kx} \qquad \textbf{(2-6)}$$

$\boldsymbol{F}$ **= force applied**

$\boldsymbol{k}$ **= force constant**

$\boldsymbol{x}$ **= displacement of spring from equilibrium position**

The total energy in a harmonic oscillator will remain constant whilst it is moving assuming there are no friction losses as a result of interactions. This is illustrated in Figure 2-6 and by equation 2-7.

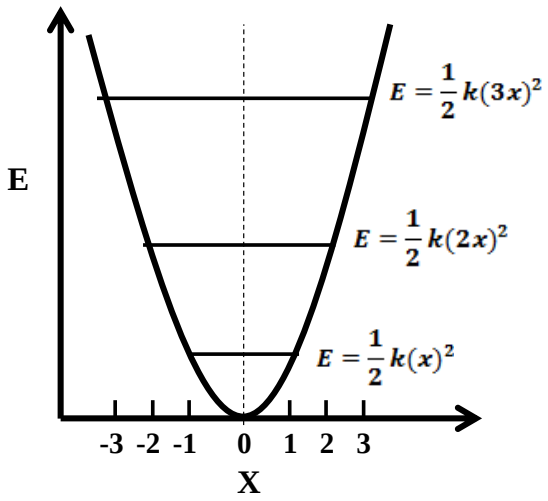

Figure 2-6: Potential energy for a harmonic oscillator[9]

$$\boldsymbol{E = \frac{1}{2}k(x)^2} \qquad \textbf{(2-7)}$$

Figure 2-6 shows that during oscillation the distance ($\boldsymbol{x}$) between the two atoms, m_1 and m_2, will vary. However, when the distance between $\boldsymbol{m_1}$ and $\boldsymbol{m_2}$ is $\boldsymbol{x_o}$, the potential energy will be zero.

The frequency of the oscillation in a harmonic oscillator can also be derived from Hooke's law.[9]

$$\boldsymbol{v = \frac{1}{2\pi}\sqrt{\frac{k}{\mu}}} \qquad \textbf{(2-8)}$$

μ = reduced mass which is determined from the equation below

$$\boldsymbol{\mu = \frac{m_1 m_2}{m_1 + m_2}} \qquad \textbf{(2-9)}$$

In order to use directly the wavenumber values of bond frequencies, equation 2-10 is used.[10]

$$\boldsymbol{\overline{v} = \frac{1}{2\pi c}\sqrt{\frac{k}{\mu}}} \qquad \textbf{(2-10)}$$

c = speed of light

However, the majority of diatomic molecules cannot be described as harmonic oscillators due to the fact Hooke's law relates the frequency of the bond vibration to the distance the bond stretches or contracts meaning a molecule could absorb energy of any wavelength. As in reality a particular bond will only absorb energy of a certain frequency, the term anharmonic is used. The potential energy curve for these oscillators is shown in Figure 2-7 which describes the fact that in reality a bond cannot be compressed beyond a certain point and can be stretched to a maximum distance before the bond breaks.

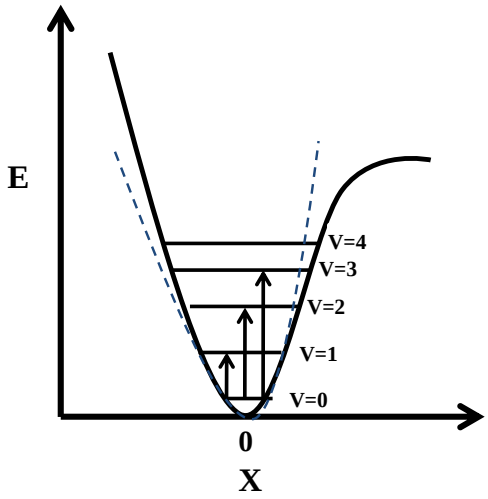

Figure 2-7: Potential energy curve for an anharmonic oscillator[9]

As can be seen in Figure 2-7, the lower energy levels agree relatively well with the harmonic energy parabola (Figure 2-6). However the higher energy levels which become more populated as the temperature is increased, are best described by an alternative equation.[9]

$$\boldsymbol{E = hv[\left(v + \frac{1}{2}\right) - x(v + \frac{1}{2})^2]} \qquad \textbf{(2-11)}$$

$\boldsymbol{x}$ **= anharmonicity constant**

The energy between levels is now explained by equation 2-12.

$$\boldsymbol{E_n - E_{n-1} = \Delta E = hv(1 - 2vx), v = 1, 2, 3} \ldots \qquad \textbf{(2-12)}$$

Figure 2-8 illustrates the vibrational modes for CH_2.

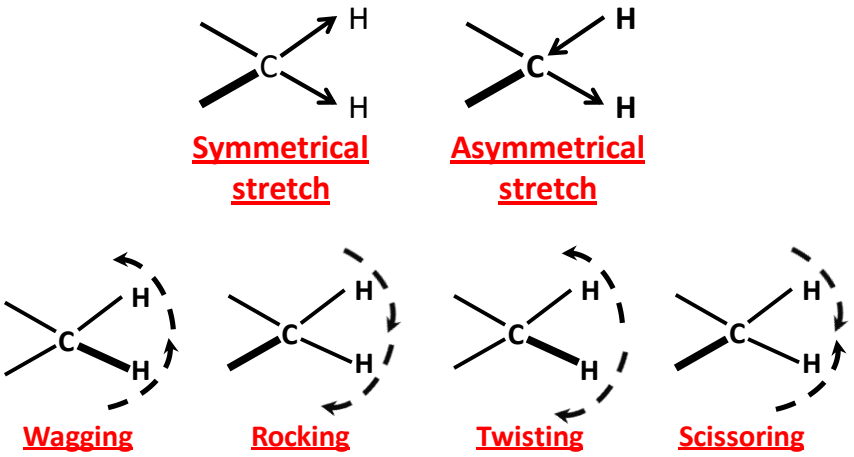

Figure 2-8: Vibrational modes of CH_2[11]

Symmetrical stretches produce the most intense bands in Raman scattering as the polarisability changes during the vibration, however these vibrations are IR inactive as the 2 hydrogens (in the case of Figure 2-8) are moving equal distances from the carbon atom and so there is no change in the dipole moment. On the other hand a change in the dipole moment is observed with asymmetric stretches as the centres of highest positive (H) and negative charge (C) move, resulting in an IR active vibration. The bending vibrations above are more easily envisaged if a plane is imagined cutting through the carbon and hydrogen atoms. Therefore, the hydrogen atoms are either moving in the same direction or different directions within the plane.

2.2.1 Raman Spectrometry

Raman spectrometry was traditionally not used as extensively as alternative spectroscopic techniques, for example infrared spectrometry, due to Raman scattering being a relatively weak effect with only every 1 in 10^6-10^8 photons being Raman scattered.[12] However, recent advances in instrumentation including laser sources, notch filters and fibre optics have meant there has been an increase in interest in this technique

especially in the pharmaceutical industry regarding the transition from off-line to in-line analysis.[13-15] Both Raman and infrared spectroscopies provide information on the vibrational states of a molecule and the transitions taking place when molecules and light (electromagnetic radiation) interact. However, Raman spectrometry involves measuring the scattering of photons while infrared involves the absorption of photons. Infrared spectrometry will not be discussed any further in this work, nevertheless, Figure 2-10 shows a comparison of the spectroscopic transitions involved in these two processes. Spectroscopic techniques involve the measurement of the interaction of radiation with molecules and are most often described in terms of frequency or wavenumber. Electromagnetic radiation comprises electrical and magnetic components and can also be thought of in terms of photons. The photons can be depicted as an electromagnetic wave (Figure 2-9), the energy of which is determined from the equation below.

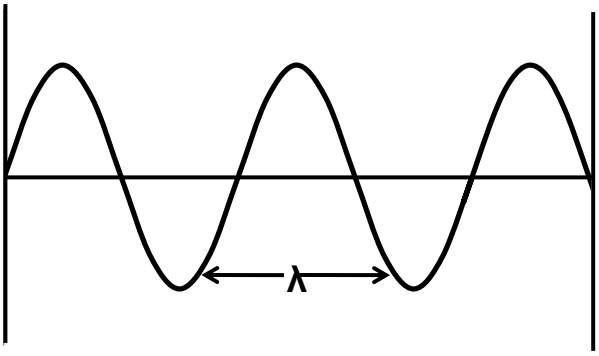

Figure 2-9: Diagram describing electromagnetic wave

$$\boldsymbol{E = h\nu = \frac{hc}{\lambda}} \qquad \textbf{(2-13)}$$

$\boldsymbol{E}$ **= energy of photon**

$\boldsymbol{h}$ **= Planck's constant**

$\boldsymbol{\nu}$ **= frequency (no.of waves that pass fixed point P in a certain time)**

$\boldsymbol{\lambda}$ **= wavelength of radiation**

When light interacts with matter, photons can either be absorbed, scattered or not interact at all. In the case of Raman spectrometry, scattered photons are detected which was a phenomenon first discovered by Raman and Krishnan in 1928.[16] An incident laser beam of a single frequency of radiation is focussed onto a sample (solid, liquid or gas) causing it to interact with a molecule. This results in distortion of the electron cloud surrounding the nuclei causing it to be unstable and resulting in a photon being scattered. When the laser interacts with the molecule and electron cloud distortion occurs (polarization), a virtual state is created (from which the photon is scattered), the energy of which is determined by the frequency of the light source. The resulting spectrum is a plot of the scattered intensity against the wavenumber shift from the exciting line (usually in the visible or near-infrared region).

There are two possible scattering processes which can occur. Elastic scattering (Rayleigh scattering) is the dominant process and involves no change in frequency of the emitted photon to that of the incident photon. In Raman scattering (inelastic scattering) either energy is transferred from the incident photon to the molecule or from the molecule to the scattered photon. There is an energy difference between the scattered photon and the incident photon corresponding to the energy of the excited vibrational state.

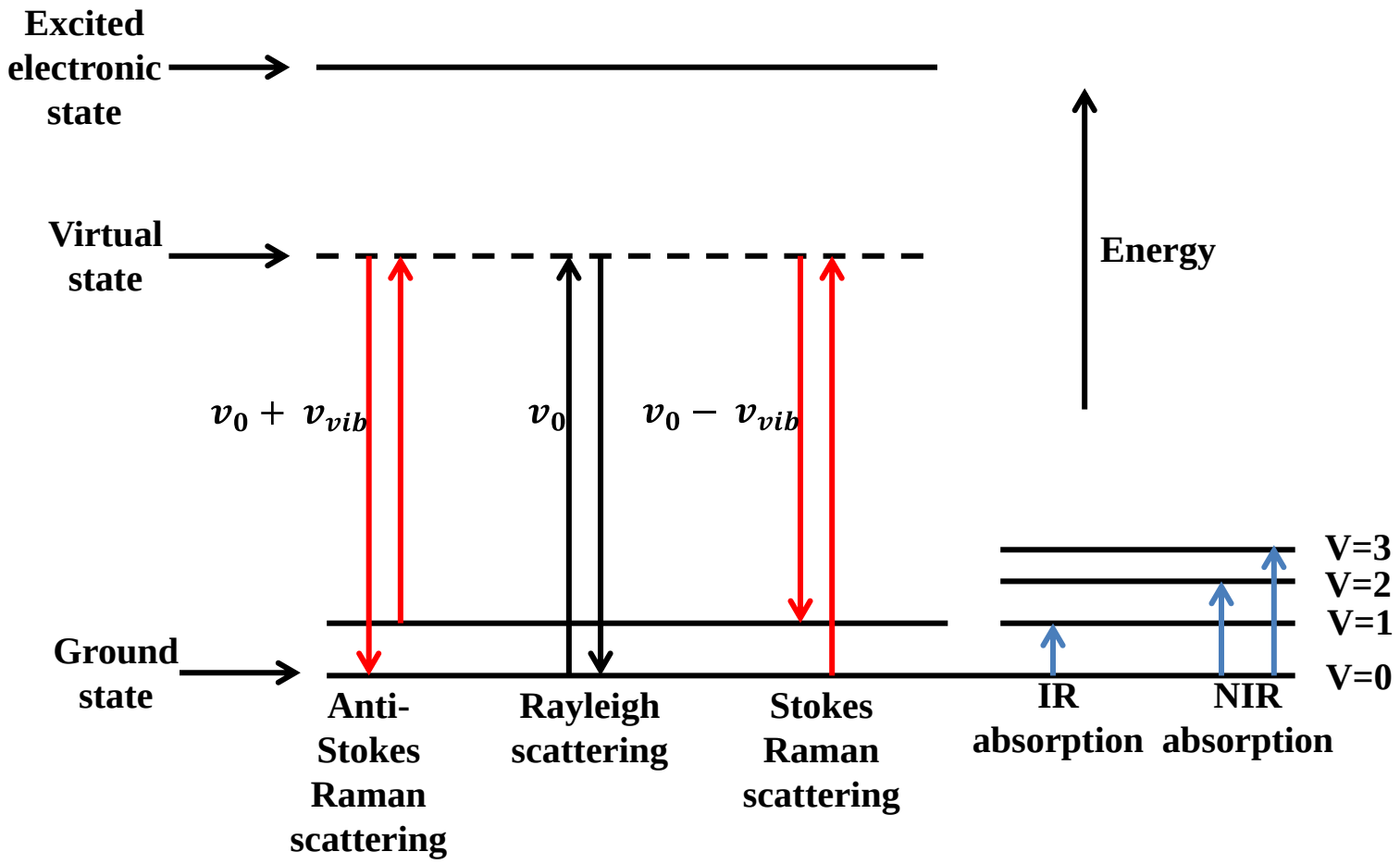

Figure 2-10: Diagram showing the spectroscopic transitions which occur during Raman scattering and mid- and near-infrared absorption[17]

As Figure 2-10 illustrates, the Rayleigh process involves no energy change and is also the most intense process. Raman scattering can be divided into Stokes and anti-Stokes. Anti-Stokes Raman scattering involves molecules in an excited vibrational state returning to the ground vibrational state from the virtual state by transferring energy to a photon. This scattering produces photons at higher energy than the incident laser beam. Stokes Raman scattering involves loss of energy to the molecule as the relaxation from the virtual state is to an excited vibrational state. At room temperature, Stokes scattering is more intense as most molecules will be in the ground state. As the temperature increases, the intensity of anti-Stokes scattering will increase while Stokes scattering will decrease as the population of the excited state will increase. Generally, Stokes scattering is preferred unless molecular fluorescence is a problem, overlapping the Stokes Raman spectrum; then anti-Stokes may be a better option depending on the sensitivity involved. The population of the energy levels (ground state or first vibrational state) can be determined from the Boltzmann distribution given in equation 2-14.[10]

$$\frac{N_1}{N_0} = \frac{g_1}{g_0} exp\left[\frac{-(E_1 - E_0)}{kT}\right] \quad \textbf{(2-14)}$$

N_1 & N_0 = number of molecules in the excited and ground vibrational states

g_1 & g_0 = degeneracy levels of the energy states

k = Boltzmann constant (1.38×10^{-23} J K^{-1})

T = temperature (Kelvin)

2.2.1.1 Classical Theory

Raman scattering is a two-photon event (incident and scattered) which makes the theory more complex in comparison with infrared which involves a single photon. Classical Raman theory is based on the effect of molecular vibrations on the polarizability. Equation 2-15 describes how the incident electric field (E) affects the strength of the induced polarization (P).[17, 18]

$$P = \alpha E \quad \textbf{(2-15)}$$

α = polarizability

The oscillating electric field ($\boldsymbol{E}$) created when electromagnetic radiation of a certain frequency ($\boldsymbol{v_o}$) is given in the following equation:

$$\boldsymbol{E = E_o cos 2\pi v_0 t} \quad \textbf{(2-16)}$$

$\boldsymbol{t}$ **= time**

$\boldsymbol{E_0}$ **= maximum electric field strength**

This causes the polarization to become:

$$\boldsymbol{P = \alpha E_o cos 2\pi v_0 t} \quad \textbf{(2-17)}$$

If the polarized molecule is vibrating at a certain frequency ($\boldsymbol{v_{vib}}$), the resulting distortion from its equilibrium position (**q**) will be given by:

$$\boldsymbol{q = q_0 cos(2\pi v_{vib} t)} \quad \textbf{(2-18)}$$

$\boldsymbol{q_0}$ **= maximum possible distortion**

For a molecule to be Raman active, a change in the polarisability must occur as the bond vibrates. The polarisability of the distorting molecule is given in equation 2-19.

$$\boldsymbol{\alpha = \alpha_0 + \left(\frac{\delta_\alpha}{\delta_q}\right) q} \quad \textbf{(2-19)}$$

$\boldsymbol{\alpha_0}$ **= polarisability of the molecule at equilibrium**

$\boldsymbol{\left(\frac{\delta_\alpha}{\delta_q}\right)}$ **= rate of change of polarisability around the equilibrium structure**

The polarisability consists of two parts; the polarisability when the atoms of the molecule are at their equilibrium position and the sum of the polarisabilities of the molecule due to the rotational and vibrational motions. Therefore, by combining equations 2-18 and 2-19:

$$\boldsymbol{\alpha = \alpha_0 + \left(\frac{\delta_\alpha}{\delta_q}\right) q_0 cos(2\pi v_{vib} t)} \quad \textbf{(2-20)}$$

Combining equations 2-17 and 2-20 gives:

$$\boldsymbol{P = \alpha E_o cos 2\pi v_0 t + \left(\frac{\delta_\alpha}{\delta_q}\right) q_0 cos(2\pi v_{vib} t) \cos(2\pi v_0 t)} \quad \textbf{(2-21)}$$

Finally, as cosαcosb = [cos(a + b) + cos(a - b)]/2;

$$\boldsymbol{P = \alpha E_o cos 2\pi v_0 t + \frac{E_0}{2}\left(\frac{\delta_\alpha}{\delta_q}\right) q_0 cos[2\pi(v_0 - v_{vib})t]}$$

$$\boldsymbol{+ \frac{E_0}{2}\left(\frac{\delta_\alpha}{\delta_q}\right) q_0 cos[2\pi(v_0 + v_{vib})t]} \quad \textbf{(2-22)}$$

Equation 2-22 contains two different terms which describe the scattering events which occur during Raman measurements. The first term, which is the most intense, describes the incident radiation and so represents Rayleigh scattering. The second term describes the Stokes ($\boldsymbol{v_0 - v_{vib}}$) and Anti-stokes ($\boldsymbol{v_0 + v_{vib}}$) processes and the resulting Raman bands.[11]

2.2.1.2 Intensity and Fluorescence

The intensity of Raman scattering is related to the power of the laser ($\boldsymbol{I_L}$), the square of the polarizability ($\boldsymbol{\alpha}$) and the fourth power of the laser frequency ($\boldsymbol{v}$).[12]

$$\boldsymbol{I = K I_L \alpha^2 v^4} \quad \textbf{(2-23)}$$

Therefore, according to the above equation an increase in frequency should result in an improvement in the sensitivity. The highest possible frequency (lowest excitation wavelength) which can be used in Raman is the ultraviolet (UV) region. Using a laser source in this frequency range can be problematic as many samples absorb UV radiation which can lead to sample degradation. However, the chance of fluorescence occurring in this region is reduced compared to using a laser in the visible region. Fluorescence is a process which interferes with Stokes Raman scattering as it also occurs at a lower energy than the excitation energy and is a much stronger effect than Raman scattering. Therefore a compromise needs to be made with the choice of laser source so that degradation or burning of the sample does not occur and that any fluorescence is minimised. A 785 nm laser source is a popular choice as fluorescence is reduced

compared to a laser in the visible range and sample degradation is not as much of an issue as it is with the use of laser sources in the UV region.

2.3 Acoustic emission spectrometry

Acoustic emission spectrometry (AES) involves the measurement of sound and vibrations within gases, liquids or solids or a mixture of these *e.g.* slurries. Whereas with active acoustics, where the effect of the process on a transmitted wave is studied, AES is described as passive and measures the acoustic emission created by the process itself.[19] The sensor (transducer) attached to the process vessel detects the elastic energy of acoustic waves propagating from the physical source of acoustic emission and therefore changes occurring in the process can be identified.[20] These include phase changes, for example the generation of a solid phase during a crystallisation process. The acoustic waves which are generated and propagate through the liquid phase prior to nucleation will be different to those detected once nucleation and crystal growth have occurred. This is due to additional processes which take place once solid material is present in the process vessel which cause further acoustic emission signals. Particle collisions can be a significant source of acoustic emission which occurs with components of the process vessel such as impellers and walls and also between the particles themselves. In the case of particulate processes, many properties can affect the acoustic emission signal obtained such as particle size, shape and density as well as operating parameters such as mixing speed.[20] However, as explained in section 7.1, acoustic emission can also be generated from alternative sources which are not necessarily of interest such as heater-chiller units and impeller agitation. Therefore, it is important to be able to identify the areas of interest in the AE spectrum and be able to extract and separate this information. An acoustic wave can be characterized by its speed ($\boldsymbol{c}$), frequency ($\boldsymbol{f}$) and wavelength ($\boldsymbol{\lambda}$) which are related in the following equation:[21, 22]

$$\boldsymbol{c = \lambda f} \qquad \textbf{(2-24)}$$

The velocity of the acoustic wave is a characteristic property of a material as different materials will cause different propagation of the acoustic wave. For example, less dense

materials will result in an increasingly propagated acoustic wave. However, the elasticity of the material has the greater effect on the acoustic signal than the density resulting in a greater wave velocity in solids than liquids and gases. This is a useful characteristic for monitoring crystallisation where a phase change from liquid to solid is observed.[21] The effect of the physical properties of the material on the speed of the acoustic wave is given in equation 2-25.[19]

$$\boldsymbol{c = \sqrt{\frac{B}{\rho'}}} \qquad \textbf{(2-25)}$$

B = elasticity of the material

ρ = density of the material

As a wave passes through a material, attenuation occurs leading to a reduction in the amplitude (Figure 2-11). Attenuation mainly occurs due to adsorption and scattering processes. Adsorption is evident in both homogeneous and heterogeneous materials and results in the conversion of the acoustic energy to an alternative form such as heat. Scattering occurs in heterogeneous materials and results in the acoustic wave being scattered in directions other than the incident wave when it encounters a 'discontinuity' such as a particle. The size of this particle and the frequency of the incident wave will influence the extent of scattering.[19] As the AE monitoring carried out during this study involved a heterogeneous process (crystallisation resulting in a solute and solid particles), attenuation of the wave would be expected which would mean the signal reaching the transducer could potentially be relatively weak. Therefore, the use of a pre-amplifier was important which was included for the purpose of filtering background noise and enhancing the signal. The attenuation coefficient is determined from equation 2-26.

$$\boldsymbol{A = A_0 e^{ax}} \qquad \textbf{(2-26)}$$

A_0 = initial amplitude of the wave

x = distance wave has travelled through the material

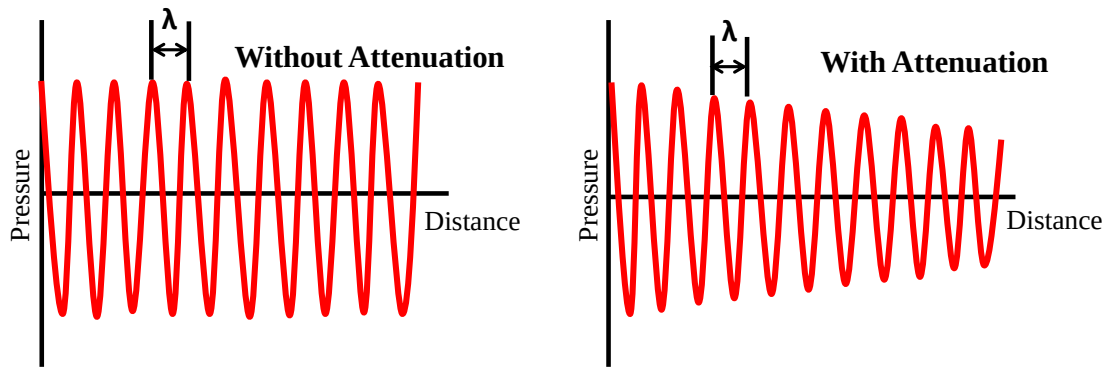

Figure 2-11: Sound wave propagation from a source with and without attenuation[19]

The acoustic impedance of different materials (*e.g.* in relation to this work the solute and particles) affects the transmission and reflection of an acoustic wave. Materials of similar acoustic impedance will reflect only a small proportion of the acoustic wave, however, when an acoustic wave encounters two different materials with significantly different impedance, a large proportion of the wave will be reflected. Figure 2-12 shows the process which occurs when a wave encounters a boundary between two materials and equation 2-27 gives the specific acoustic impedance ($\boldsymbol{Z}$) of a material.

$$\boldsymbol{Z = \frac{P}{U} = \frac{\omega\rho}{k}} \qquad \textbf{(2-27)}$$

$\boldsymbol{P}$ **= acoustic excess pressure**

$\boldsymbol{U}$ **= particle velocity**

$\boldsymbol{\omega}$ **= angular frequency**

$\boldsymbol{\rho}$ **= density**

$\boldsymbol{k}$ **= complex wave number**

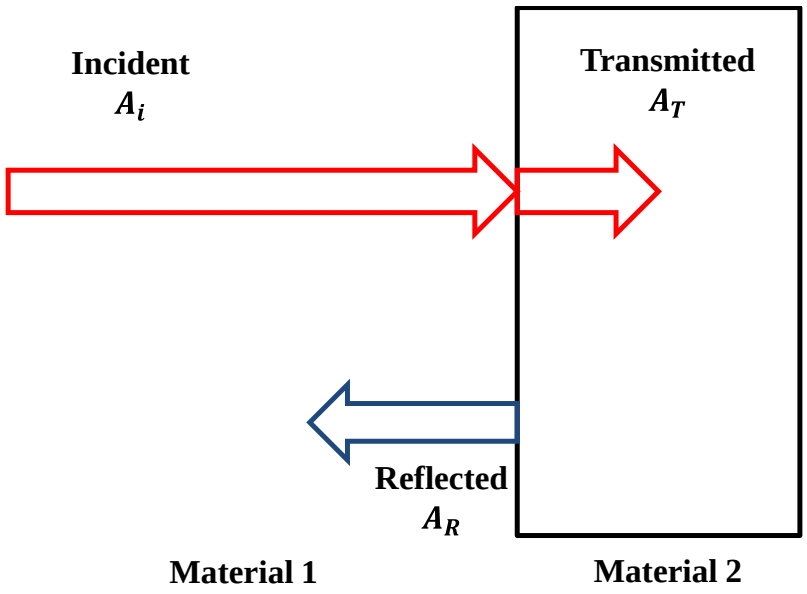

Figure 2-12: Diagram showing the transmission and reflection of an acoustic wave when it reaches the boundary between two different materials[21]

2.3.1 Signal Analysis

Acoustic emission measurements were obtained in this study using a broadband transducer attached to the process vessel which contains piezoelectric crystals. This allows for a wide range of frequency ranges to be detected to produce a full spectrum providing both frequency and amplitude information. It was anticipated that this would allow for information to be obtained and extracted on both solid concentration and particle size. These crystals produce small electrical voltages when changes in the acoustic wave are detected. Different transducers have a characteristic response over a range of frequencies and can be more sensitive to certain regions than others.[16] The signal obtained during acoustic emission measurements is displayed as changes in voltage with time. The root mean square value (RMS) provides an indication of the strength of the signal when it is in the time domain given in equation 2-28. The energy of the sound wave can then be obtained from the square of the RMS value.[22]

$$\bar{P}rms = \sqrt{\frac{1}{t_2 - t_1}\int_{t_1}^{t_2} p(t)^2 dt} \qquad \textbf{(2-28)}$$

$p(t)$ = **pressure magnitude of a continuous acoustic wave between times t_1 and t_2**

The amplitude is defined as the maximal voltage of the acoustic emission signal divide by the reference voltage of the sensor given in equation 2-29 while the average frequency of the signal is obtained by equation 2-30.[20]

$$A_{DB} = 20\ log\ (\frac{u_{max}}{u_{ref}}) \quad \textbf{(2-29)}$$

u_{max} **= maximal voltage of the acoustic emission signal**

u_{ref} **= reference voltage of the sensor equal to 1 µV**

$$\bar{f} = \frac{n}{d} \quad \textbf{(2-30)}$$

n **= number of counts**

d **= duration of the burst**

The acoustic signal obtained in the time domain can be converted to obtain the frequencies constituting the wave by performing a Fourier transform. This calculation is performed using Fourier transform algorithms which produce a spectrum which can be used to identify frequency regions of interest.

2.4 Particle size analysis

Determining the particle size of an end product is an essential procedure in any industrial process; however, as discussed in section 1.1, this physical property of the product is of the upmost importance in the pharmaceutical industry since it can affect the influence the drug has on the consumer. There are many different values used to report the particle size and in most of the techniques currently available the particle size becomes increasingly more challenging to assess as the shape moves further away from spherical. Additionally, different techniques measure different characteristic properties of a particle and will therefore produce a different answer. A number of these methods to describe the particle size and population will be outlined. The mean, mode and median are important values which are widely used in particle size analysis techniques. The mean is an average of the data obtained and can be calculated in a number of

different ways including the D[4,3] and the D[3,2] (equation 2-31 and 2-32). The median value divides the particle population into two equal halves; 50% below and 50% above this value. The mode is the most common value of the frequency distribution and describes the highest point of the frequency curve. Figure 2-13 shows how in one case these values can all be at the same position of the distribution and in another case they can be completely different.[23]

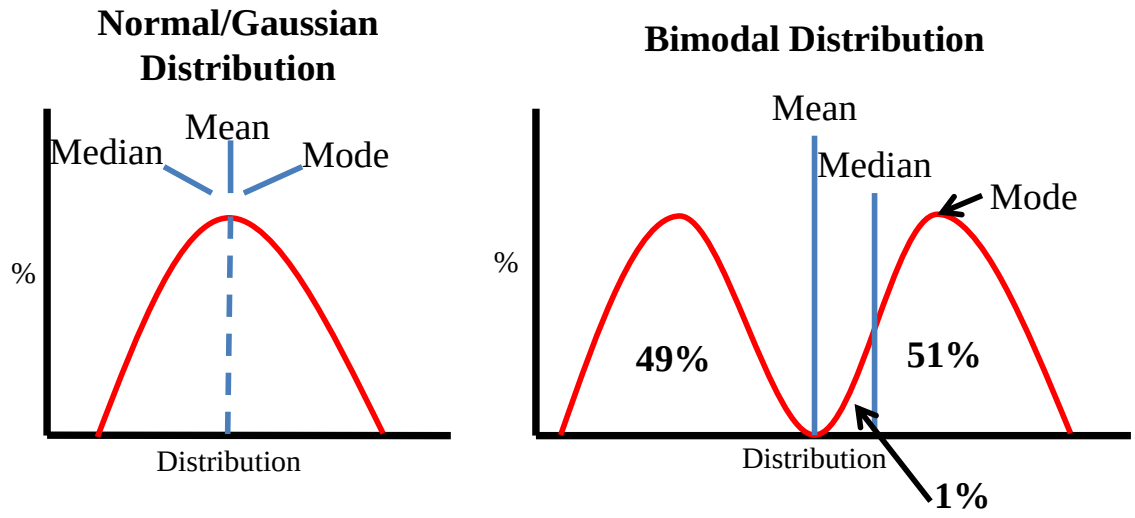

Figure 2-13: Diagram showing the values of the mean, median and mode in a Gaussian and Bimodal distribution[23]

The D[4,3] value is described as the volume or mass moment mean while the D[3,2] value is the surface area moment mean and are given in the following equations (if three spheres of sizes 1, 2 and 3 µm are considered).[23]

$$\boldsymbol{D(3,2) = \frac{1^3+2^3+3^3}{1^2+2^2+3^2} = 2.72\mu m} \qquad \textbf{(2-31)}$$

$$\boldsymbol{D(4,3) = \frac{1^4+2^4+3^4}{1^3+2^3+3^3} = 2.57\mu m} \qquad \textbf{(2-32)}$$

The two methods for particle size analysis used in this project were laser diffraction (LD) and focused beam reflectance measurement (FBRM); the theory behind the techniques will be discussed in the following sections.

2.4.1 Laser diffraction

Laser diffraction is a widely used technique for particle size analysis in industry due to the instrumentation being relatively cheap and the analysis rapid. Laser diffraction relates the diffraction angle to being inversely proportional to the particle size during measurements. A diffraction pattern is obtained when a particle is illuminated with an incident light source of a fixed wavelength and the properties of this pattern can be used to infer a particle size. For example, the intensity and distance between diffraction rings differs with particle size. Larger particles will result in more intense, clearly separated diffraction patterns due to scattering occurring at a narrower angle to the incident beam in comparison to smaller particles (Figure 2-14).[24] The distance r_o of the first minimum to the centre is dependent on the particle size.[25] The detector and intensity distribution plotted as a function of the distance from the centre of the lens is shown in Figure 2-15.

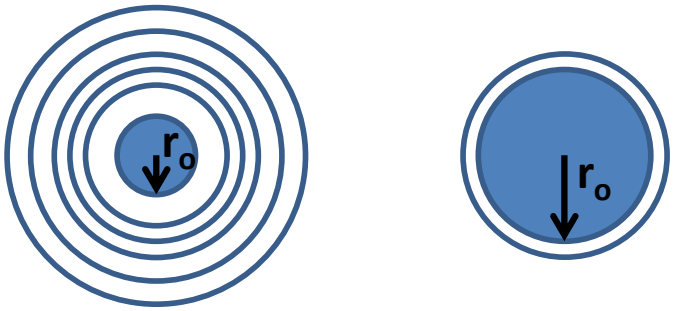

Figure 2-14: Typical diffraction pattern obtained from a large particle (left) and a smaller particle (right)[24, 25]

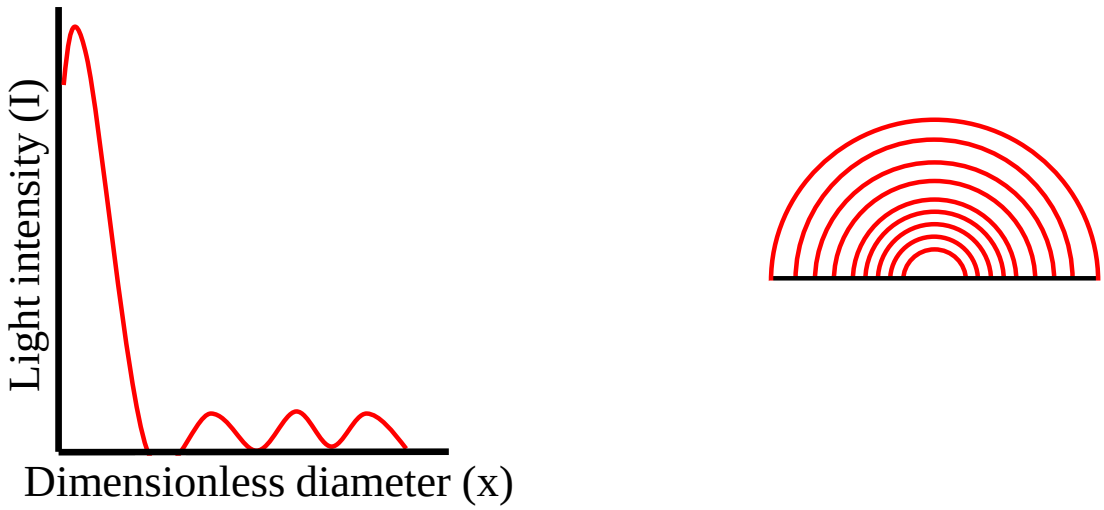

Figure 2-15: Intensity distribution of light against radial distance from centre of focal plane of lens for a typical particle (left) and schematic of detector containing a series of photosensitive rings (right)[26]

Laser diffraction uses a combination of Mie and Fraunhofer theories in order to convert the scattering patterns obtained into particle size distribution data. Fraunhofer scattering occurs if the particle size is greater than 5 or 6 times the wavelength of incident light, whereas Mie scattering occurs when the D/λ ratio (D= particle diameter) is approximately 1.[24] Both theories are relatively complex and also have the limitation in that an approximation is made based on the particles being spherical. This causes an error in the resulting particle size distribution with particles that are not spherical in shape and many reports have investigated the extent of this error in comparison to alternative methods such as microscopy.[27-30] Fraunhofer theory is valid if the following requirements are met: i) the wavelength of the illuminating light is much smaller than the diffracting particle, ii) the illuminating light corresponds to planar wave front (laser light) and the diffraction pattern is observed in the focal plane of the lens, iii) the intensity distribution of the illuminating light is homogeneous over the particle, iv) the refractive index of the particle differs sufficiently from the surrounding medium.[31] From Figure 2-15, the dimensionless diameter (***x***) for a single particle described by Fraunhofer theory is given in equation 2-33.[32]

$$x = \frac{2\pi rs}{\lambda F} \quad \textbf{(2-33)}$$

r = particle radius

s = radial distance in the detection place measured from the optical axis

λ = wavelength of light

F = focal length of the lens

The diffraction intensity of the scattering ring pattern obtained when a spherical particle is illuminated with incident light is given by:[20]

$$I(\theta, x) = I_o \frac{A^2}{\lambda^2 f^2}\left[\frac{2J_1(\frac{kxsin\theta}{2})}{kxsin\theta/2}\right]^2 \quad \textbf{(2-34)}$$

A = area of projected sphere

x = diameter

θ = scattering angle

For more than a single particle, the diffraction pattern is more complicated as different particles scatter light at different angles and so the total light energy distribution for a suspension containing a collection of particles can be expressed in the form of a matrix.[33]

$$L(j) = W(i).T(i,j) \quad \textbf{(2-35)}$$

$L(j)$ = light energy falling on the ring

$W(i)$ = weight fraction of the particles in the size range i

$T(i,j)$ = scattering matrix for spherical particles containing the coefficients which define the light energy distribution for each particle size range

It is common for the weight distribution to be quoted rather than the distribution based on the number of particles. This weight distribution is given by:[26]

$$W_i = \frac{4}{3}\pi r_i^3 \rho N_i \quad \textbf{(2-36)}$$

N **=number of particles**

r **= radius**

Mie theory requires the refractive index of both the solution and the particles to be measured to be known as well as the coefficient of light absorptivity of the particles in the suspension. The values obtained are a function of both the particle size and relative refractive index and takes into account the reflected, refracted and diffracted components of the light.[33] Mie's theory was first developed in 1908 and the simplified version is given in the following equation:[24]

$$I(\theta) = E\{k^2 D^4 [JI]^2 \theta^1 + [k_1 \theta]^1 + [k_2 \theta]^3 + [k_3 \theta]^5 + K^4 D^6 (m-1)^2 \theta^6 / 8\pi\} \quad \textbf{(2-37)}$$

I **= scattered light intensity**

E **= flux of incident light per unit area**

k & K **= constants**

D **= diameter of particles**

$J1$ **= Bessel function**

θ **= scattering angle**

m **= complex refractive index**

2.4.2 Focused Beam Reflectance Measurement (FBRM)

FBRM is a commonly used particle size technique in the pharmaceutical industry and is more often used for *in situ* measurements.[34-36] The measurements obtained are reported in terms of the chord length distribution which consists of thousands of individual chord lengths recorded with each measurement to provide an indication of changes in particle dimension and particle count.[37] Figure 2-16 shows a representation of the measurement of a particle and the subsequent signal processing.

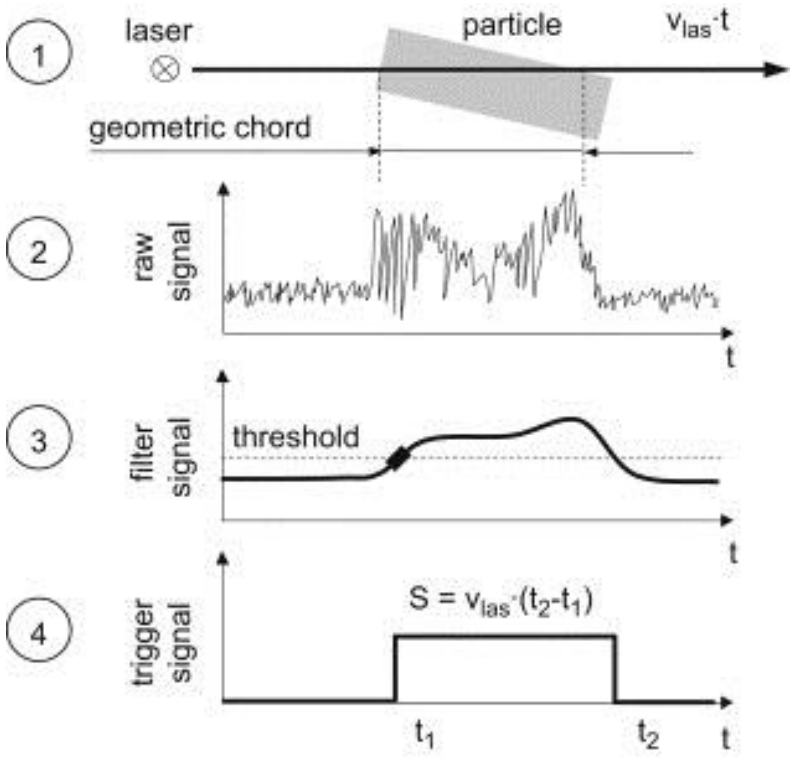

Figure 2-16: Visualisation of the signal processing and chord discrimination of an FBRM system[38]

FBRM measurements are made when light scattering occurs after the laser light interacts with a particle. From Figure 2-16, the particle moves into the plane of the laser beam (step 1) where this causes varying light scattering intensity due to spot light reflections on the particles surface (step 2). The signal is then low-pass filtered in order to minimise the surface effects (step 3) whereby a mean scattering signal and subsequent threshold

scattering intensity are set. Finally, when the filtered signal passes the trigger threshold, a trigger signal is set (step 4). The trigger is reset once the signal passes below the threshold once more. The time difference ($\Delta t = t_2 - t_1$) between the two trigger events is recorded and multiplied by the laser velocity which gives a value for the path length. The path length can then be related to the chord length of the particle.[16, 19]

However, FBRM also has limitations as a particle size analysis technique. Firstly, it does not directly give the value of the particle size, this has to be determined mathematically and the chord length related to the particle size distribution.[38, 39] Although FBRM measures the chord length independent of the particles shape, like LD, there are also issues when attempting to gain values for non-spherical particles. This is due to the position and orientation of the particles impacting the measurement, for example, particles with a high aspect ratio such as needles may in some cases have the width of the particle measured and in other cases the length measured when passing through the laser beam.[40] The position of the probe in the vessel will also affect the measurements obtained and a position should be selected where the material is suspended and presented to the probe window sufficiently.[41] Additionally, it is more difficult to compare particle size information obtained from a LD and FBRM instrument and they are often found to give significantly different responses in terms of the particle size distribution.[42] Weighting factors need to be applied to FBRM data in order to be able to directly compare the measurements with those obtained using a laser diffraction instrument, an example of which is shown in equation 2-38.[41]

$$p_k(R) = \frac{R^k n(R)}{\int_0^\infty R^k n(R) dR} \qquad \textbf{(2-38)}$$

$p_k(R)$ = particle distribution frequency
R = particle size
$n(R)$ = size distribution
$n(R)dR$ = number of particles in size range R to R+dR
k = weighting factor

The weighting factor is 0 for non-weighted distributions, 1 for length-weighted distributions, 2 for surface-weighted distributions and 3 for volume-weighted. As the weighting is increased it becomes more heavily weighted towards large particles.

2.5 X-ray powder diffraction

X-ray diffraction (XRD) is a widely used technique in the pharmaceutical industry to determine the identity and polymorphic composition of a sample. It is most often used as an off-line technique to determine the polymorphic form of an end product but in recent years there has been studies carried out showing the potential for on-line analysis whereby real-time information on polymorphic transformations taking place during a process could be monitored.[43, 44] The X-ray diffraction pattern obtained from a powder sample is determined by the geometry and structure of the crystalline solid. Although polymorphs of the same compound have the same chemical structure, they can be identified using XRD as the difference in crystal structure results in a distinctive diffraction pattern between polymorphs.[45] X-ray diffraction involves the inelastic interaction of radiation with matter. An incoming X-ray beam will be scattered if its wavelength is of a similar size order to the interatomic distance present in the material. The photons are scattered in what is known as a series of Debye cones which are registered by the detector (Figure 2-17).

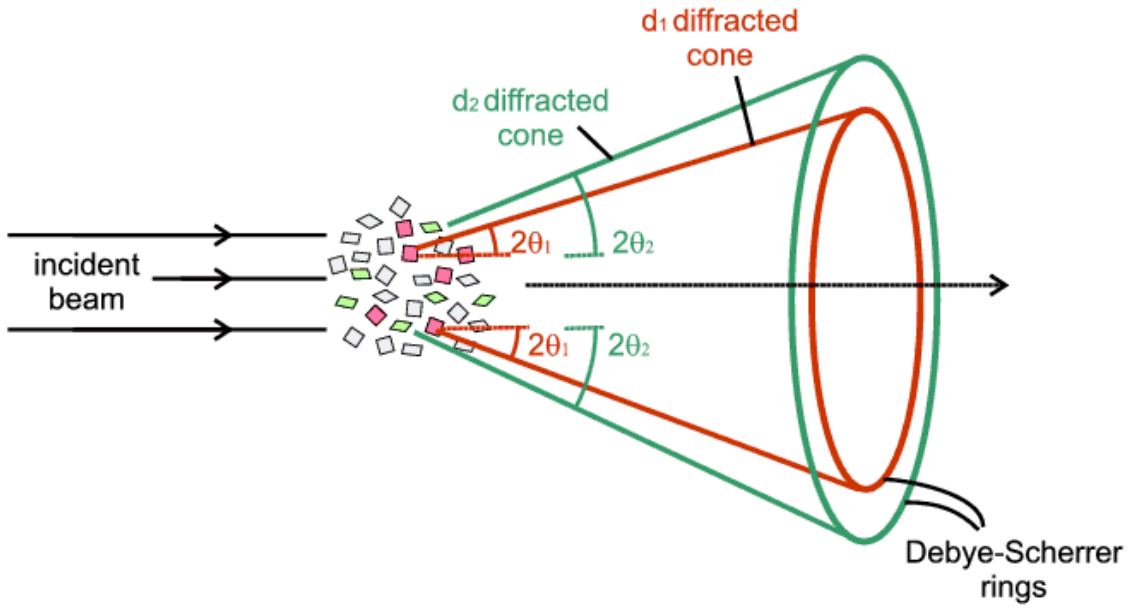

Figure 2-17: Diagram showing two different crystallites satisfying Bragg's law to produce the resulting Debye cones[46]

The oscillating electric vector of the electromagnetic radiation interacts with the electrons causing scattering of the X-rays with the same wavelength and frequency as the initial beam. In most directions, destructive interference causes extinction of the waves. However, in a few directions constructive interference will occur due to the regular arrangement of the atoms in the crystal lattice.[47, 48] Bragg's law (Figure 2-18) details the conditions required for constructive interference to take place:[47]

$$2dsin\theta = n\lambda \qquad \textbf{(2-39)}$$

$\boldsymbol{d}$ **= distance between identical planes in crystal structure**

$\boldsymbol{\theta}$ **= angle between incident beam and lattice planes**

$\boldsymbol{n\lambda}$ **= nth order of the wavelength of radiation**

According to Bragg's law, constructive interference only takes place when the difference in path length of reflected beams is equal to an integral number of wavelengths. The interatomic distance of the lattice planes in the structure result in a

reflection at a specific incident angle 2θ and the intensity of the reflection is determined by the type of atoms arranged in the plane.[48]

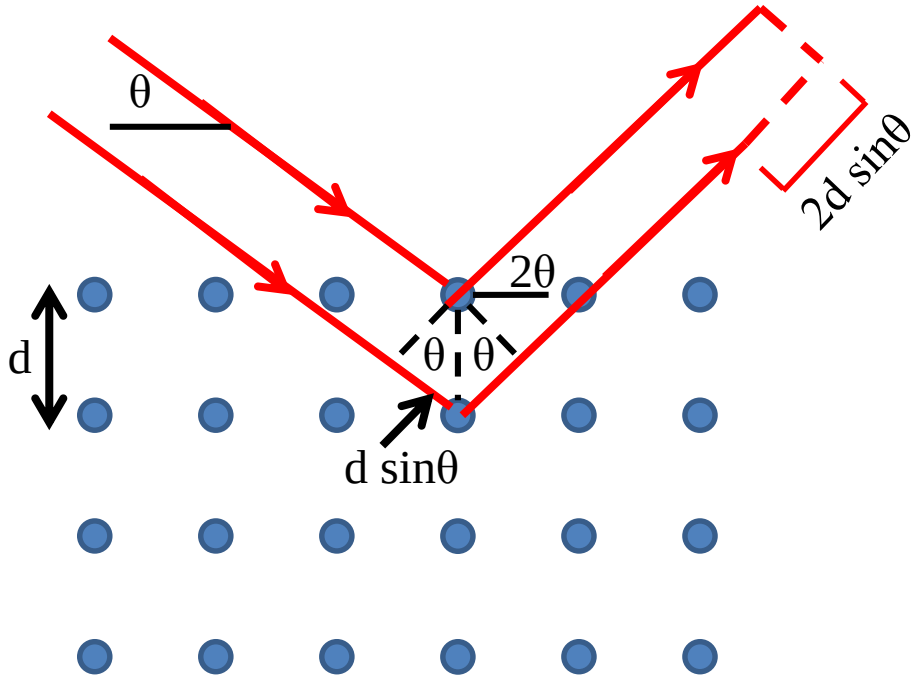

Figure 2-18: Diagram showing the interaction of the incoming beam with the crystal lattice to produce scattering[49]

2.6 Design of Experiments

During this work both fractional and full factorial design of experiments was undertaken. Design of experiments is a technique employed to obtain the maximum amount of information from a certain process or experimental apparatus with the minimum amount of analyses, cost and time. A set of experiments are devised to identify the input variables to be modified, how the modification will be made and the output variables that will be measured to observe these effects.[50, 51] The main reasons for conducting a design of experiments are for the development of new products or processes or enhancement and optimisation of existing products/processes. Additionally it can be used as a preliminary screening technique for the identification of important factors which affect a certain process. The three main areas addressed with a design of experiments are screening, optimisation and robustness testing. Firstly, the factors which

are deemed most important to the outcome of the process are identified along with the operating range of each variable. Secondly, the optimum operating conditions are identified in regard to a certain output(s) or response. Finally, robustness testing is carried out to investigate the effect of small fluctuations in the operating conditions which could be expected in for example, a production process.[52] In the completion of this study, both a 2-level, 3-factor (2^3) full factorial and 2-level, 4^{-1} factor (2^{4-1}) fractional design of experiments were carried out. For each factor a high and a low level are selected within the appropriate range identified and a number of experiments (depending on the number of factors and levels) are formulated with varying values for the variables resulting in a design space. Figure 2-19 shows the design space for a 2^3 and 2^{3-1} design.

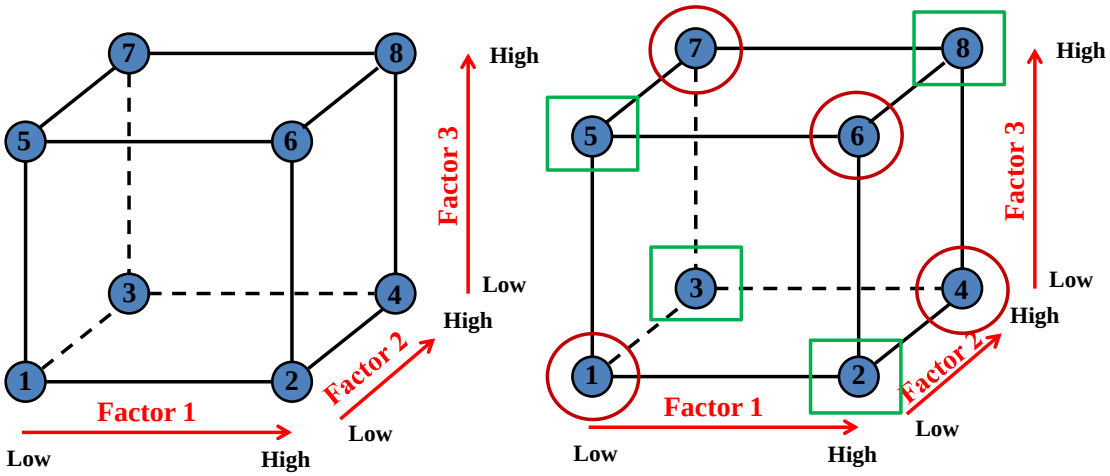

Figure 2-19: Diagram showing a 2-level, 3-factor full factorial design (left) and a 2-level, 3-factor fractional design (right) showing the two possible experimental selections using the experiment numbers in squares or circles[52]

As can be seen in Figure 2-19, only half of the possible experiments are performed in the fractional design and there are two different designs which can be adopted, however, in both cases only four experiments are undertaken which include all three factors. Once the experimental design has been carried out, the response values (*e.g.* in the case of crystallisation particle size, polymorph, *etc*. are important outputs) are used to determine the main effect and main interaction of the factors. The factor which is determined to be

the main effect will have the most significant influence on the process for the experiments conducted. The main interaction between two factors is defined as that which affects the optimum value most significantly. A 2^3 design can be used to determine the main effect from the three selected factors (1, 2 and 3 in the case of Figure 2-19), the most important from three, two-term interactions (1-2, 2-3 and 1-3) and the effect of one, three term interaction (1-2-3). Once the main effects and interactions have been determined, the factors which have little or no effect on the process can also be identified which helps to reduce the number of unnecessary experiments conducted to optimise a process.

2.7 Data Analysis

2.7.1 1st derivative transformation

Throughout this study, spectral data obtained were interpreted once a 1st derivative transformation had been applied. Derivatives are applied in order to remove offset and background slope variations between samples. With spectroscopic data, a 1st derivative transformation removes the baseline offset variation between spectra while a 2nd derivative is applied to data in order to remove both the baseline offset differences and differences in baseline slopes between spectra.[53] In this work, the 1st derivative transformation was applied to Raman data in an attempt to remove the baseline offset and separate overlapping peaks from solute and polymorph spectra of the same compound. Figure 2-20 shows an example of a 1st and 2nd derivative transformation of a spectral peak.

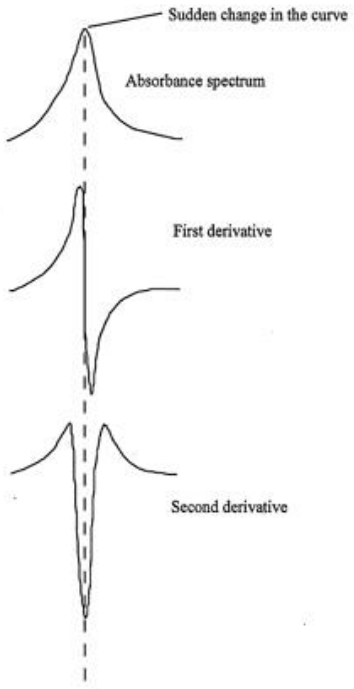

Figure 2-20: Example of a 1st and 2nd derivative transformation of a spectral peak[54]

2.7.2 Principal Components Analysis

Principal components analysis (PCA) is often a starting point for multivariate data analysis and is a data compression technique which reduces a data set to provide a simpler visual representation. A data matrix (*X*) consisting of *N* rows (samples) and *K* columns (variables) is reduced to a much smaller number of compressed variables known as principal components.[53, 55] This technique can be used to illustrate observations, trends and outliers in a certain data set. However, it is important that the underlying structure of the data is retained in terms of the relationship between the different samples and measurement variables. A data matrix can be thought of as being composed of two components; the underlying structure of the data (***M***) and random fluctuations or noise (***E***) due to the measurement process, sampling, *etc*. Due to the fact both ***M*** and ***E*** matrices contain *N* x *K* dimensions, a successful PCA outcome will reduce the model matrix to two smaller matrices:[53]

$$\boldsymbol{X = M + E \xrightarrow{PCA} X = TP + E} \quad \textbf{(2-40)}$$

The $\boldsymbol{T}$ value is known as the scores matrix and illustrates any sample patterns in the data while the $\boldsymbol{P}$ value is the loadings matrix and describes any relationships between individual measurement variables. As the $\boldsymbol{E}$ matrix should only contain 'noise' in the data, the scores and loadings matrices will describe the underlying structure of the data in a fewer number of latent variables than original variables. Prior to PCA being carried out on a data set, mean centering is often undertaken which removes the absolute intensity information from each of the variables and allows the focus to be on the variation between the spectra. During mean centering the mean response of a certain variable over all samples is subtracted from each individual variables response which is represented in the following equation:[53]

$$\boldsymbol{X_{mc} = X - 1_N * \bar{x}} \quad \textbf{(2-41)}$$

$\bar{x}$ = vector containing mean response values for each of the *K* variables

1_N = vector of ones that is *N*-elements long

The techniques described in this section were all applied to crystallisation processes (batch and continuous) of the model compound L-glutamic acid and the secondary compound D-mannitol. Non-invasive Raman spectrometry was used to monitor the crystallisation process to provide information on solids concentration and polymorphic composition and transformations. Off-line analysis in the form of LD, FBRM and XRD was invaluable in obtaining supplementary information on this process. A design of experiments approach was adopted in the batch and continuous OBR studies for both L-glutamic acid and D-mannitol to include parameters important to crystallisation and determine their effect on the properties of the end product including the polymorphic form and particle size. Principal components analysis was applied to the Raman data obtained using the model compound L-glutamic acid to extract additional information that was not observed during the univariate analysis. The materials, equipment, and instrumentation used in this study are described in chapter 3.

2.8 References

1. J. W. Mullin, *Crystallization*, 4th edn., Elsevier Butterworth-Heinemann, Oxford, 2001.
2. A. G. Jones, *Crystallisation Process Systems*, Elsevier Butterworth-Heinemann, 2002.
3. X. Ni and A. Liao, *Effects of Cooling Rate and Solution Concentration on Solution Crystallization of l-Glutamic Acid in an Oscillatory Baffled Crystallizer*, *Crystal Growth & Design*, 2008, **8**, 2875-2881.
4. M. Fujiwara, P. S. Chow, D. L. Ma and R. D. Braatz, *Paracetamol Crystallization Using Laser Backscattering and ATR-FTIR Spectroscopy: Metastability, Agglomeration, and Control*, *Crystal Growth & Design*, 2002, **2**, 363-370.
5. W. Omar and J. Ulrich, *Application of Ultrasonics in the On-line Determination of Supersaturation*, *Crystal Research and Technology*, 1999, **34**, 379-389.
6. Z. K. Nagy, M. Fujiwara, X. Y. Woo and R. D. Braatz, *Determination of the Kinetic Parameters for the Crystallization of Paracetamol from Water Using Metastable Zone Width Experiments*, *Industrial & Engineering Chemistry Research*, 2008, **47**, 1245-1252.
7. J. Garside, R. J. Davey and A. G. Jones, *Advances in Industrial Crystallisation*, Butterworth Heninemann, Oxford, 1991.
8. A. S. Myerson, ed., *Handbook of industrial crystallization*, 2nd edn., Butterworth-Heinemann, Woburn, 2001.
9. J. H. van der Maas, *Basic Infrared Spectroscopy*, Heyden & Son Ltd, London, 1972.
10. B. Stuart and D. J. Ando, *Biological Applications of Infrared Spectroscopy*, John Wiley & Sons Ltd, Chichester, 1997.
11. H. H. Willard, L. L. Merritt Jr, J. A. Dean and F. A. Settle Jr, *Instrumental Methods of Analysis*, 7th edn.
12. E. Smith and G. Dent, *Modern Raman Spectroscopy A Practical Approach*, John Wiley & Sons Ltd, Chichester, 2005.
13. G. Févotte, *In Situ Raman Spectroscopy for In-Line Control of Pharmaceutical Crystallization and Solids Elaboration Processes: A Review*, *Chemical Engineering Research and Design*, 2007, **85**, 906-920.
14. T. De Beer, A. Burggraeve, M. Fonteyne, L. Saerens, J. P. Remon and C. Vervaet, *Near infrared and Raman spectroscopy for the in-process monitoring of pharmaceutical production processes*, *International Journal of Pharmaceutics*, 2011, **417**, 32-47.
15. S. Wartewiga and R. H. H. Neubert, *Pharmaceutical applications of Mid-IR and Raman spectroscopy Advanced Drug Delivery Review*, 2005, **57**, 1144-1170.
16. C. V. Raman and K. S. Krishnana, *A new type of secondary radiation*, *Nature*, 1928, **121**, 501-502.

17. R. L. McCreery, *Raman spectroscopy for chemical analysis*, John Wiley & Sons, Inc., Canada, 2000.
18. I. R. Lewis and H. G. M. Edwards, *Handbook of Raman Spectrosocpy*, Marcel Dekker, Inc., New York, 2001.
19. J. W.R. Boyd and J. Varley, *The uses of passive measurement of acoustic emissions from chemical engineering processes*, *Chemical Engineering Science*, 2001, **56**, 1749-1767.
20. N. Gherras, E. Serris and G. Fevotte, *Monitoring industrial pharmaceutical crystallization processes using acoustic emission in pure and impure media*, *International Journal of Pharmaceutics*, 2012, **439**, 109-119.
21. D. J. McClements, *Ultrasonic Characterisation of Foods and Drinks: Principles, Methods, and Applications*, *Critical Reviews in Food Science and Nutrition*, 1997, **37**, 1-46.
22. L. E. Kinsler, A. R. Frey, A. B. Coppens and J. V. Sanders, *Fundamentals of Acoustics*, 4th edn., John Wiley & Sons, Inc., 2000.
23. A. Rawle, *Basic Principles of Particle Size Analysis*, Malvern Instruments Limited.
24. Z. Stojanovic and S. Markovic, *Determination of particle size distributions by Laser Diffraction*, *Technics-New Materials*, 2012, **21**, 11-20.
25. Sympatec GMBH, Laser Diffraction, http://www.sympatec.com/EN/LaserDiffraction/LaserDiffraction.html.
26. G. B. J. deBoer, C. deWeerd, D. Thoenes and H. W. J. Goossens, *Laser diffraction spectrometry: Fraunhofer diffraction versus Mie scattering*, *Particle Characterization*, 1987, **4**, 14-19.
27. N. Stevens, J. Shrimpton, M. Palmer, D. Prime and B. Johal, *Accuracy assessments for laser diffraction measurements of pharmaceutical lactose*, *Measurement Science Technology*, 2007, **18**, 3697-3706.
28. A. H. de Boer, D. Gjaltema, P. Hagedoorn and H. W. Frijlink, *Characterization of inhalation aerosols: a critical evaluation of cascade impactor analysis and laser diffraction technique*, *International Journal of Pharmaceutics*, 2002, **249**, 219-231.
29. M. Naito, O. Hayakawa, K. Nakahira, H. Mori and J. Tsubaki, *Effect of particle shape on the particle size distribution measured with commercial equipment*, *Powder Technology*, 1998, **100**, 52-60.
30. Z. Ma, H. G. Merkus, J. G. A. E. de Smet, C. Heffels and B. Scarlett, *New developments in particle characterization by laser diffraction: size and shape*, *Powder Technology*, 2000, **111**, 66-78.
31. H. Mühlenweg and E. D. Hirleman, *Laser Diffraction Spectroscopy: Influence of Particle Shape and a Shape Adaptation Technique*, *Particle & Particle Systems Characterization*, 1998, **15**, 163-169.
32. G. B. J. de Boer, C. de Weerd, D. Thoenes and H. W. J. Goossens, *Laser Diffraction Spectrometry: Fraunhofer Diffraction Versus Mie Scattering*, *Particle & Particle Systems Characterization*, 1987, **4**, 14-19.

33. N. Gabas, N. Hiquily and C. Laguerie, *Response of Laser diffraction particle sizer to anisometric particles*, *Particle & Particle Systems Characterization*, 1994, **11**, 121-126.
34. M. Kempkes, J. Eggers and M. Mazzotti, *Measurement of particle size and shape by FBRM and in situ microscopy*, *Chemical Engineering Journal*, 2008, **63**, 4656-4675.
35. A. N. Saleemi, C. D. Rielly and Z. K. Nagy, *Monitoring of the combined cooling and antisolvent crystallisation of mixtures of aminobenzoic acid isomers using ATR-UV/vis spectroscopy and FBRM*, *Chemical Engineering Science*, 2012, **77**, 122-129.
36. D. Greaves, J. Boxall, J. Mulligan, A. Montesi, J. Creek, E. Dendy Sloan and C. A. Koh, *Measuring the particle size of a known distribution using the focused beam reflectance measurement technique*, *Chemical Engineering Science*, 2008, **63**, 5410-5419.
37. Mettler Toledo, FBRM (Focused Beam Reflectance Measurement) Technology, http://us.mt.com/us/en/home/supportive_content/specials/Lasentec-FBRM-Method-of-Measurement.html.
38. N. Kail, W. Marquardt and H. Briesen, *Estimation of particle size distributions from focused beam reflectance measurements based on an optical model*, *Chemical Engineering Science*, 2009, **64**, 984-1000.
39. M. Li and D. Wilkinson, *Determination of non-spherical particle size distribution from chord length measurements. Part 1: Theoretical analysis*, *Chemical Engineering Science*, 2005, **60**, 3251-3265.
40. P. Barrett and B. Glennon, *In-line FBRM Monitoring of Particle Size in Dilute Agitated Suspensions*, *Particle & Particle Systems Characterization*, 1999, **16**, 207-211.
41. W. Yu and K. Erickson, *Chord length characterization using focused beam reflectance measurement probe - methodologies and pitfalls*, *Powder Technology*, 2008, **185**, 24-30.
42. A. Ruf, J. Worlitschek and M. Mazzotti, *Modeling and Experimental Analysis of PSD Measurements through FBRM*, *Particle & Particle Systems Characterization*, 2000, **17**, 167-179.
43. R. B. Hammond, X. Lai and K. J. Roberts, *Application of In-Process X-ray Powder Diffraction for the Identification of Polymorphic Forms during Batch Crystallization Reactions*, *Crystal Growth & Design*, 2004, **4**, 943-948.
44. S. D. MacMillan, K. J. Roberts, A. Rossi, M. A. Wells, M. C. Polgreen and I. H. Smith, *In Situ Small Angle X-ray Scattering (SAXS) Studies of Polymorphism with the Associated Crystallization of Cocoa Butter Fat Using Shearing Conditions*, *Crystal Growth & Design*, 2002, **2**, 221-226.
45. B. B. He, *Two-dimensional X-ray diffraction*, John Wiley & Sons, 2009.
46. P. Barnes, S. Jacques and M. Vickers, Powder diffraction, http://pd.chem.ucl.ac.uk/pdnn/diff2/kinemat2.htm.

47. L. Brügemann and E. K. E. Gerndt, *Detectors for X-ray diffraction and scattering: a user's overview*, *Nuclear Instruments and Methods in Physics Research Section A: Accelerators, Spectrometers, Detectors and Associated Equipment*, 2004, **531**, 292-301.
48. H. Dittrich and A. Bieniok, in *Encyclopedia of Electrochemical Power Sources*, ed. G. Editor-in-Chief: Jürgen, Elsevier, Amsterdam, 2009, pp. 718-737.
49. A. Agrawal and A. R. Barron, Wide Angle X-ray diffraction studies of liquid crystals, http://cnx.org/content/m46154/1.2/, 26 April 2013.
50. G. Franceschini and S. Macchietto, *Model-based design of experiments for parameter precision: State of the art*, *Chemical Engineering Science*, 2008, **63**, 4846-4872.
51. A. Collins, in *International Encyclopedia of Education (Third Edition)*, eds. P. Editors-in-Chief: Penelope, B. Eva, E. B. Barry McGawA2 - Editors-in-Chief: Penelope Peterson and M. Barry, Elsevier, Oxford, 2010, pp. 367-372.
52. L. Eriksson, E. Johansson, N. Kettaneh-Wold, C. Wikstrom and S. Wold, *Design of Experiments Priciples and Applications*, Third edn., Umetrics Academy, 2008.
53. K. A. Bakeev, *Process Analytical Technology*, Blackwell Publishing, 2005.
54. ASD Inc, What is a derivative spectrum?, http://www.asdi.com/resource-center/faqs/what-is-a-derivative-spectrum.
55. L. Eriksson, E. Johansson, N. Kettaneh-Wold, J. Trygg, C. Wikstrom and S. Wold, *Multi- and Megavariate Data Analysis Part 1 Basic Principles and Applications*, Second edn., Umetrics Academy, 2006.

3 Experimental

3.1 Introduction

This study focused on the implementation of *in situ* spectroscopic techniques to the monitoring of both batch and continuous crystallisation processes in a number of different types of reactor. In particular, Raman spectrometry and passive acoustic emission spectrometry were concentrated on for their applicability in providing information on particle properties important to industrial crystallisation. In addition, off-line analysis was carried out using X-ray diffraction, laser diffraction and focused beam reflectance measurement to provide supplementary information to the *in situ* measurements obtained. The following sections outline the equipment and materials used to carry out the experimental work during the project.

3.2 Materials

In this work, L-glutamic acid (beta polymorph ≥ 98.5%, Sigma-Aldrich) and D-Mannitol (Gamma polymorph ≥ 98%, Sigma-Aldrich) were studied (Figure 3-1) and distilled water was used for all the cooling crystallisation experiments. LGA is a white powder which has two known polymorphs, a meta-stable α-form, which has prismatic crystals, and a thermodynamically stable β-form (commercially available), which has needle-shaped crystals. Figure 3-2 shows the solubility of alpha and beta LGA.

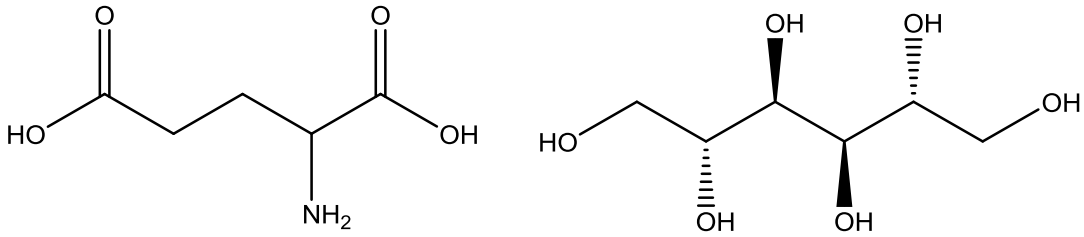

Figure 3-1: Structures of L-glutamic acid (left) and D-mannitol (right)[1, 2]

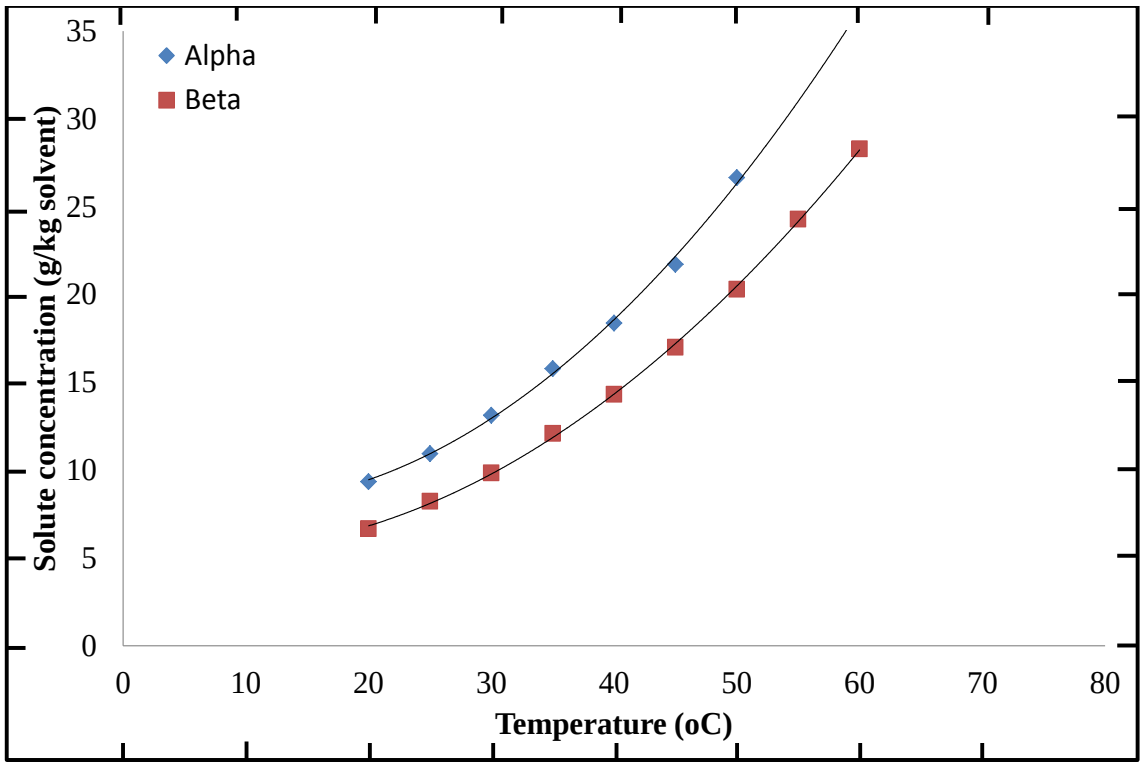

Figure 3-2: Solubility of alpha and beta L-glutamic acid in water[3]

D-Mannitol is also a white powder which has three recognised polymorphs, however, there has been several alternative methods used to name the different polymorphs so in this report the nomenclature used by *Cornel et al*. has been adopted making the three polymorphs: meta-stable α- and β-forms and a thermodynamically stable γ-form.[4] All of these polymorphs crystallise as needle-shaped particles and therefore cannot be distinguished using microscopy. Figure 3-3 shows the solubility of alpha, beta and gamma Mannitol.

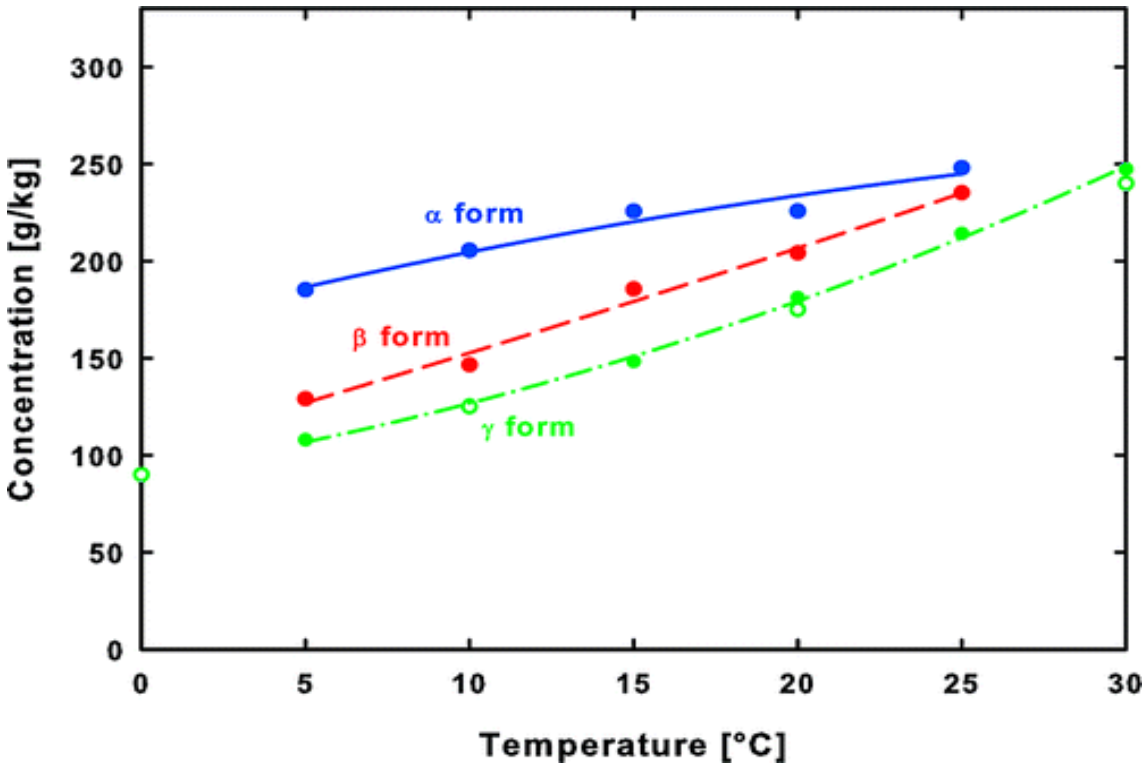

Figure 3-3: Solubility of alpha, beta and gamma D-mannitol in water[4]

3.3 Crystallisation Reactors

3.3.1 Batch Stirred Tank Reactor (STR)

Three different sizes of jacketed reactor were used in the batch STR crystallisation experiments. The smallest reactor consisted of a 350 ml round-bottomed glass vessel with dimensions 8 cm wide by 13 cm tall fitted with a PTFE paddle impeller measuring 5 cm by 2 cm. The 500 ml vessel measured 15 cm wide by 19 cm tall with an internal diameter of 10 cm and was also fitted with a PTFE impeller measuring 7.2 cm by 2.5 cm. The largest stirred tank reactor had a total volume of 1 L with dimensions 14.9 cm wide by 22.8 cm tall with an internal diameter of 10.3 cm and was coupled with a glass paddle impeller measuring 7 by 2.1 cm. The impellers for all reactor sizes were operated using a digital overhead stirrer (IKA RW20 digital, IKA works, Wilmington, USA) with mixing speeds of between 100 and 600 rpm applied during the crystallisation

experiments. The jacket temperature was controlled using a heater-chiller unit and the internal reactor temperature was recorded where possible using a digital thermocouple temperature indicator where readings were taken every minute.

3.3.2 Batch Oscillatory Baffled Reactor (OBR)

The reactors for these experiments consisted of jacketed glass vessels with external dimensions 9.8 cm wide by 37 cm tall holding a total volume of 1 L, and 5.7 cm wide by 31.5 cm tall for the smaller 250 ml vessel. The jacket temperature was controlled using a heater chiller unit and internal temperature measurements were recorded throughout the crystallisation. Mixing within the OBR was created using a baffled string consisting of two equally spaced PTFE orifice baffles for the 1 L and three baffles for the 250 ml reactor. The baffles used to create oscillation in the larger vessel had an outer diameter of 7.1 cm and an inner diameter of 3.4 cm supported by two 5 mm diameter steel rods. The baffles were spaced 8.8 cm apart. The smaller baffles used in the 250 ml vessel had an outer and inner diameter of 3.7 cm and 1.7 cm respectively which were spaced 5.7 cm apart (Figure 3-4). The string was connected to an electrical motor which provided oscillation frequencies of 1-3 Hz and amplitudes of 10-30 mm.

Figure 3-4: Image of the two baffles strings used in the 1 L batch OBR (left) and the 250 ml OBR (right)

Raman measurements were obtained non-invasively in both the batch STR and OBR through the side of the vessels (Figure 3-5) using the Kaiser Raman P^{h}AT probe (section 3.4). The probe was positioned as to avoid the PTFE impellers and baffles in each of the reactors. In the OBR reactors this position was between the bottom two baffles (11.5 cm and 7 cm from the base of the reactor for the 1 L and 250 ml vessels, respectively). Measurements were recorded in the two larger stirred tank vessels approximately half way up the reactor, above the impellor. However, due to the size of the smallest STR, the probe position was restricted to the region either side of the impellor.

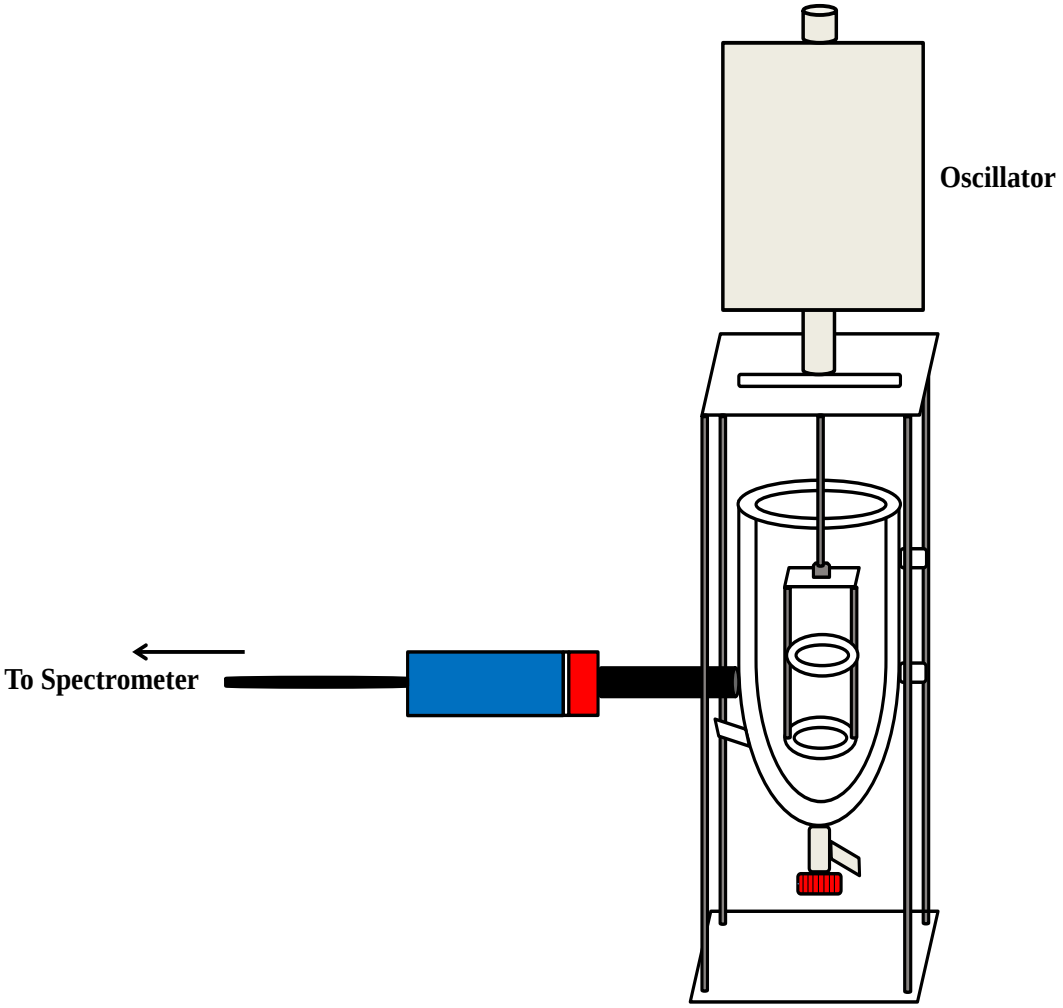

Figure 3-5: Schematic representation of P^{h}AT probe and Batch OBR setup

3.3.3 Continuous Oscillatory Baffled Reactor (COBR)

The reactor consisted of 22 jacketed straight and 11 un-jacketed bend sections with an internal diameter of 1.5 cm with equally spaced orifice baffles 2.2 cm apart which resulted in a total length of 1.8 m and an overall volume of 3.2 L. The reactor was divided into 6 zones and a separate heater-chiller was used to control the temperature in each zone (Figure 3-6) so that a linear cooling profile was obtained. The temperature of each heater-chiller was fixed at a pre-determined temperature calculated in the following

way; firstly, the flow rate was determined from the total volume of the reactor and the residence time required:

$$\boldsymbol{Flow\ rate\ (ml/min)} = \frac{\boldsymbol{Volume\ (cm^3)}}{\boldsymbol{Residence\ Time\ (min)}} \quad \textbf{(3-1)}$$

The velocity of the fluid through the tube was then calculated using equation 3-2:

$$\boldsymbol{Velocity\ m/min} = \frac{\boldsymbol{Flow\ rate\ (m^3/min)}}{\boldsymbol{Area\ (m^2)}} \quad \textbf{(3-2)}$$

Finally, the time required for the fluid to reach a certain distance in the reactor was determined from the length at that position and the velocity, and this value was used to calculate the temperature decrease at that point:

$$\boldsymbol{Time\ (min)} = \frac{\boldsymbol{distance\ (m)}}{\boldsymbol{velocity\ (m/min)}} \quad \textbf{(3-3)}$$

$$\boldsymbol{Temperature\ at\ distance\ x}\ (℃) = \boldsymbol{Initial\ temperature}\ (℃) - (\mathbf{0.5}(\boldsymbol{Time\ for\ distance\ x\ (min)})) \quad \textbf{(3-4)}$$

The temperature calculated at the end of each zone was used as the value for the heater-chiller for that zone. Figure 3-7 shows an overlay of a linear cooling profile obtained in a crystallisation (80-40^{o}C) and the temperature of each heater-chiller in the 6 zones for that crystallisation. The temperature during the crystallisation was measured using a digital thermocouple at the end of each zone to ensure it was the same as the set temperature for the heater-chiller for that zone. The feed solution was prepared in a separate 25 L batch vessel prior to being pumped into the reactor continuously using a peristaltic pump (Model 520S, Watson Marlow, UK). The product was collected continuously for fixed time periods; for a residence time of 80 minutes, the slurry was collected for 10 minute time periods, while for a residence time of 20 minutes, the slurry was collected for 2.5 minute intervals. The collected slurry was then filtered under vacuum and dried in an oven overnight prior to any off-line analysis being carried out.

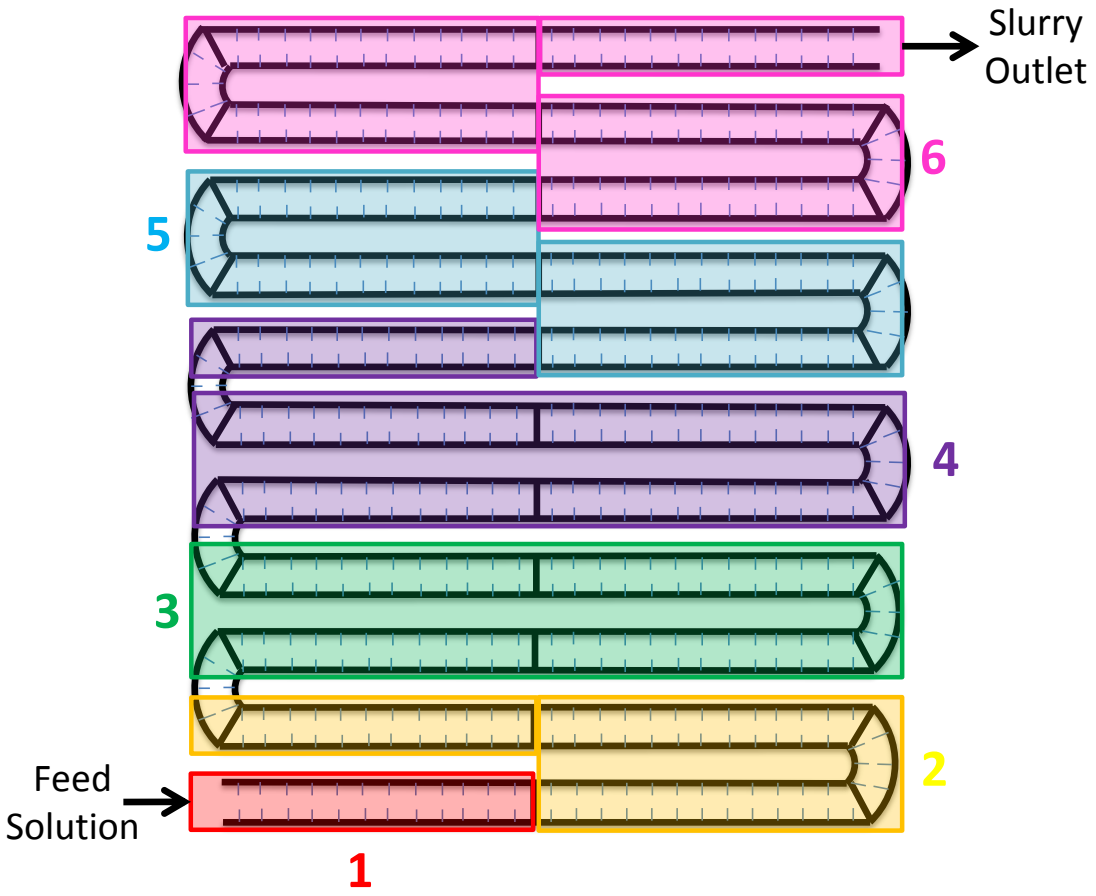

Figure 3-6: Schematic of the continuous OBR showing the six different temperature zones

Raman measurements were obtained in this reactor through the glass wall of the final bend section prior to the slurry outlet (end of zone 6 in Figure 3-6). This section of the vessel was then covered in foil and blackout material in order to reduce the effect on the spectrum from external light sources. The position of the probe was kept as consistent as possible between experiments in order to be able to make comparisons between different operating conditions. The bend sections were selected to collect the data as these were un-jacketed and there were no issues with the type of coolant used in the heater-chiller units which may have affected the measurements. For example, if the coolant used was not water, a spectrum for this fluid could have been obtained which would interfere with the measurements from within the reactor.

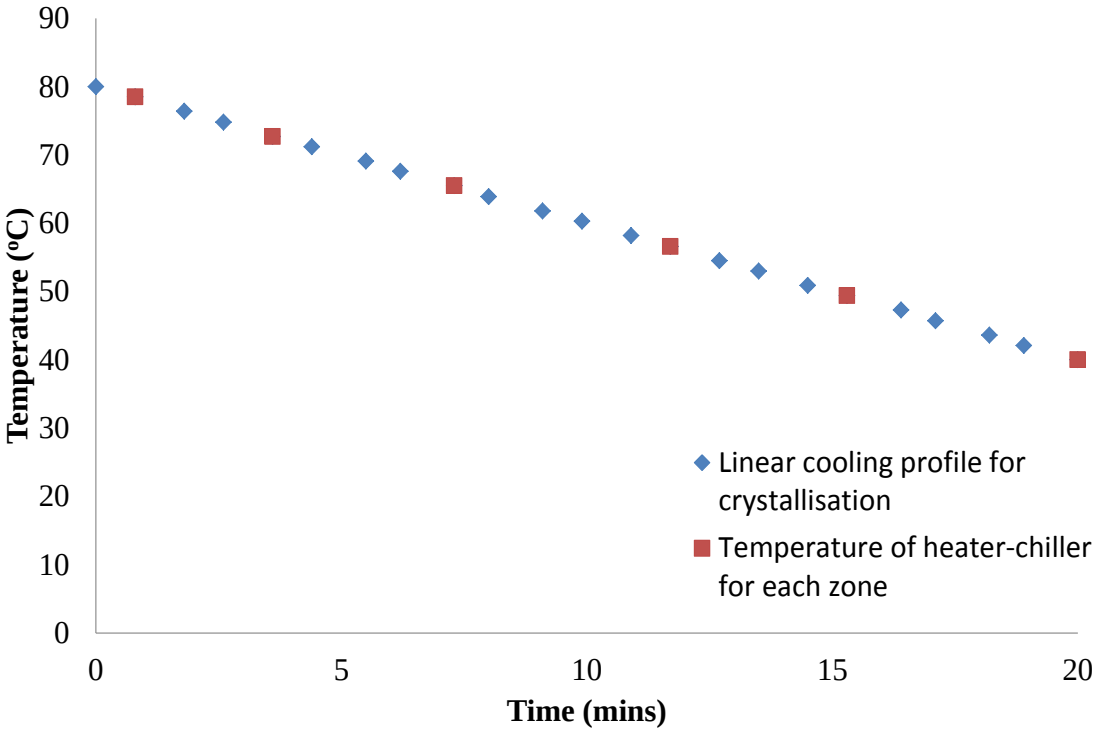

Figure 3-7: Graph showing an overlay of the linear cooling profile (calculated) adopted during a typical cooling crystallisation in a COBR and the fixed temperatures of the heater-chillers

3.3.4 Mixed Suspension, Mixed Product Removal Reactor (MSMPR)

The batch reactor consisted of a 350 ml round bottomed vessel, as described in section 3.1.1. To convert operation to continuous mode, an inlet and outlet tube were added which entered the reactor through separate ports in the vessel lid (Figure 3-8). The inlet tubing was placed above the reactor contents while the outlet tube was fixed at a level where approximately 15.5 ml of the vessel contents were above the tube opening. Two peristaltic pumps were used to control the flow rates in and out of the vessel and both sections of tubing were jacketed to ensure no additional crystallization took place throughout the tubing. The temperature was held the same as that of the feed solution using a second heater-chiller. The feed solution was prepared in a 5 L container and heated on a hotplate which was pumped into the vessel continuously, at a fixed flow rate

once the contents had reached a set temperature and were fully dissolved. A fixed volume of the reactor contents (10% or 15.5 ml) was removed at periodic time intervals depending on the residence time selected.

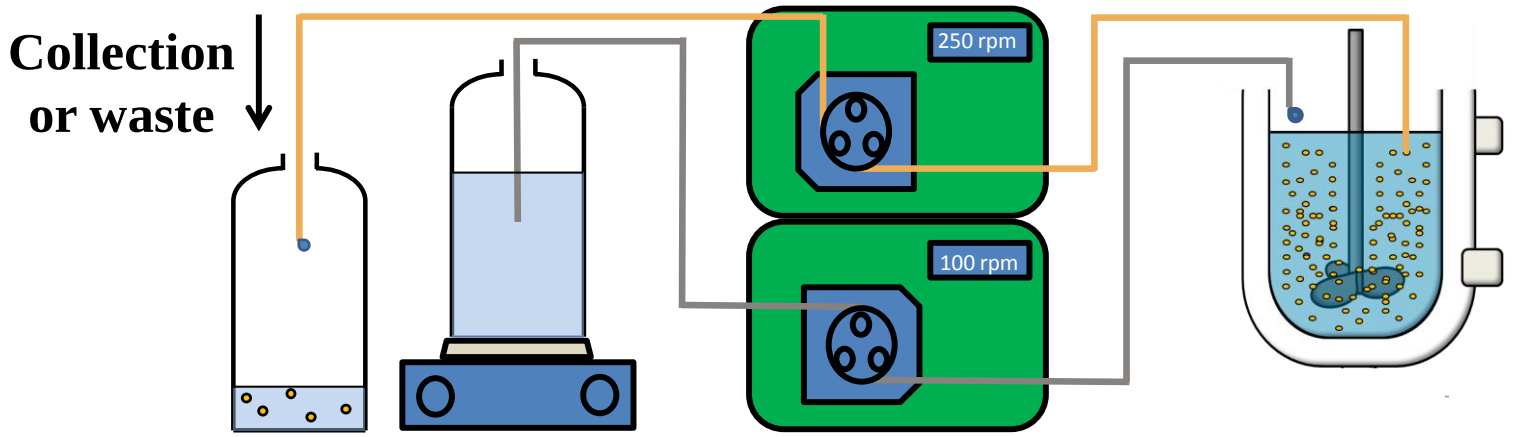

Figure 3-8: Schematic of the Mixed Suspension, Mixed Product Removal Reactor Set-up

3.4 Instrumentation

3.4.1 Kaiser Rxn1 spectrometer

Raman measurements were carried out using a Kaiser Rxn1 spectrometer with a P^{h}AT probe attachment. This choice of probe head enabled non-invasive measurements to be collected during crystallisation processes in both batch and continuous reactors. Figure 3-9 shows the main components which constitute the Rxn1 spectrometer system.[5] The following section will provide a brief description of each of these features of the spectrometer.

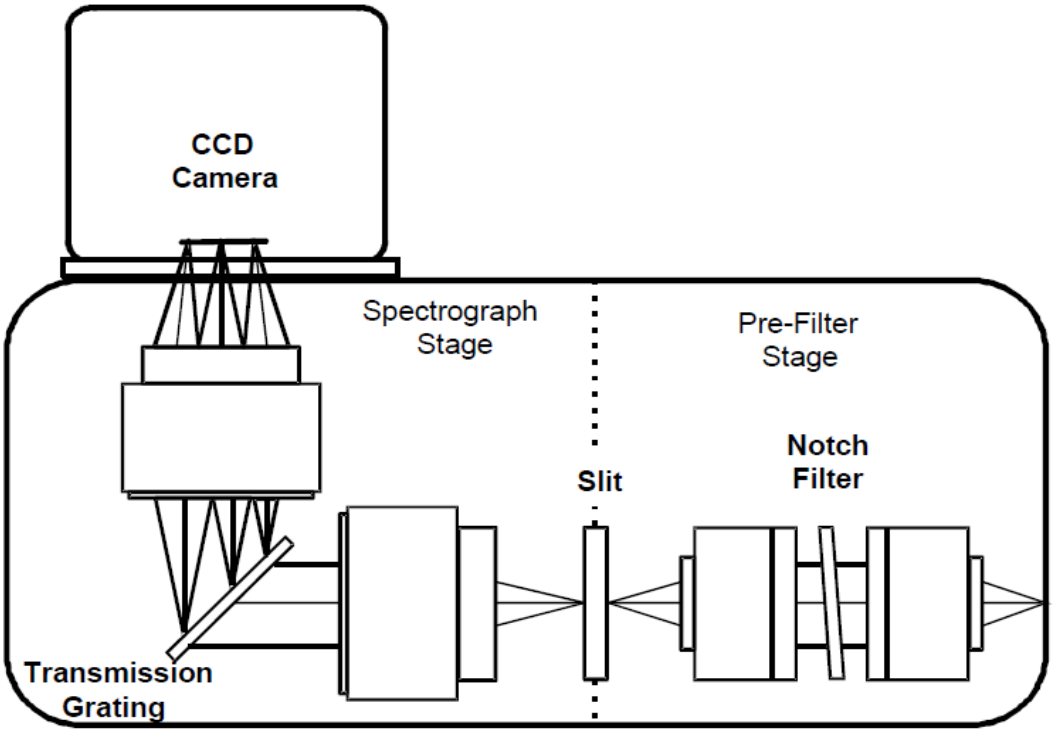

Figure 3-9: Schematic of the interior of a Kaiser Rxn1 spectrometer

After the incident beam is focused onto the sample, the scattered radiation is collected and enters the spectrometer at the pre-filter stage. During this phase, the signal passes through a number of lenses and filters in order to reduce the Rayleigh scattered photons as much as possible. The remaining signal is then focused onto the entrance of the

spectrograph stage whereby using a combination of a transmission grating and a charge coupled device, the entire Raman spectrum can be collected simultaneously.

3.4.1.1 Pre-filter stage

The signal collected from the sample contains a combination of Rayleigh and Raman scattered photons which are passed through an initial lens at the entrance to the spectrometer where this incoming beam is collimated. This then passes through a notch filter which reduces the Rayleigh signal by selectively reflecting a narrow wavelength band in the region of the incident laser wavelength. The remaining wavelengths are transmitted through to the spectrograph stage. It is possible with the use of advanced notch filters to transfer bands within 40 cm^{-1} to the incident laser wavelength; however the filters used alongside the P^hAT system allow bands shifted by 175 cm^{-1} and higher to pass. Notch filters provide many advantages over the conventional edge filter technology employed. These include improved transmission on both sides of the Rayleigh line compared to only one side with the edge filter. In addition, narrow bandwidths, improved transmission at low wavenumbers outside the band and sharp spectral edges are further advantages to notch filter technology.[6] Once the signal has been filtered, it is focused using a second lens onto a spectrograph entrance slit with the aim of minimizing the transmission of stray light into the dispersion stage.[5]

3.4.1.2 Axial transmissive spectrograph

The filtered light entering the spectrograph stage is directed to a multi-element lens prior to being passed through a holographic transmission grating. This component enables the entire Raman spectrum to be collected instantaneously without the need for moving parts. Instead, the scattered light is dispersed onto the detector using optics carrying two separate spectral tracks. Consequently, higher spectral resolution, wide spectral coverage and improved operating stability are obtained over previous spectrometer designs containing a Czerny-Turner grating. These types of scanning gratings mean that different parts of the spectrum are collected at different times making it difficult to obtain a representative measurement of the entire spectrum. A further advantage of the

holographic transmission grating is the measurements are rapid as the entire spectrum is collected simultaneously meaning a higher sample throughput is possible.[7, 8]

3.4.1.3 Charge couple device (CCD)

The CCD component of a spectrometer operates by relating the number of electrons collected in a potential well to the number of photons incident on that pixel and these values are directly proportional. An electron can be excited from the valence to the conduction band when a photon is absorbed by the silicon component in a CCD. This creates a hole which under normal circumstances would recombine with the electron. However, an electric field is applied to avoid this and the electrons are subsequently passed through a highly doped silicon electrode, also known as a gate which causes the electrons to be immobilised in a region called a potential "well" which holds electrons. The CCD consists of a two-dimensional array of wells (or pixels) where one dimension is used to collect the spectral information and the second is most often used for spatial resolution. The P^{h}AT probe system consists of 1024 by 256 pixels of which the 256 pixels are divided into 7 bins which are summed to provide the overall spectrum thereby reducing the noise observed in the resulting readout.[5]

3.4.1.4 P^{h}AT probe

The P^{h}AT probe is a non-invasive attachment with a maximum 25 cm working distance and a variable spot size of 1, 3 or 6 mm (Figure 3-10). When a 785 nm laser is used with the probe, it is possible to record Raman spectra in the region 175-1875 cm^{-1} with the Rxn1 spectrometer. Conventional Raman instruments utilize a spot size in the region of 100 µm, however, by optically broadening the laser beam up to 6 mm in diameter, the problems associated with obtaining a representative measurement of a sample are reduced. The P^{h}AT probe was designed for solid sampling of powders and tablets to increase reproducibility of measurements and ensure representative spectra were obtained without the need for focusing of the laser beam or moving the sample for additional measurements, thus resulting in rapid analysis. It was thought these features

of the P[h]AT probe would be beneficial for crystallisation monitoring, however, this is the first detailed study showing the application of this technique to crystallisation.

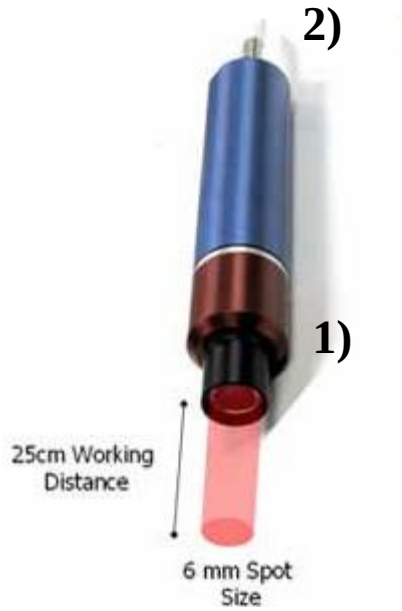

Figure 3-10: Image of the P[h]AT probe head showing the largest spot size used and corresponding working distance. Position 1) shows the interchangeable lens and position 2) the fibre optic attachment[9]

The P[h]AT probe operates as follows: the laser light is passed through the excitation fibre and is collimated using a lens before being passed through a bandpass filter to remove unwanted noise, also known as amplified spontaneous emission (ASE) resulting from the laser (Rayleigh scattering) and the fibre (silica Raman interference). The excitation light is then reflected using a mirror to a combiner before being directed through an exit window and onto the sample using a sample lens. The collected light containing both Rayleigh and Raman scattered light as well as possible fluorescence signals is passed back through the sample lens and through a notch filter. The filtered light is focused onto the collection fibre bundle which normally contains in the region of 50 fibres.[10] Figure 3-11 shows an illustration of the inner components of the P[h]AT probe head.

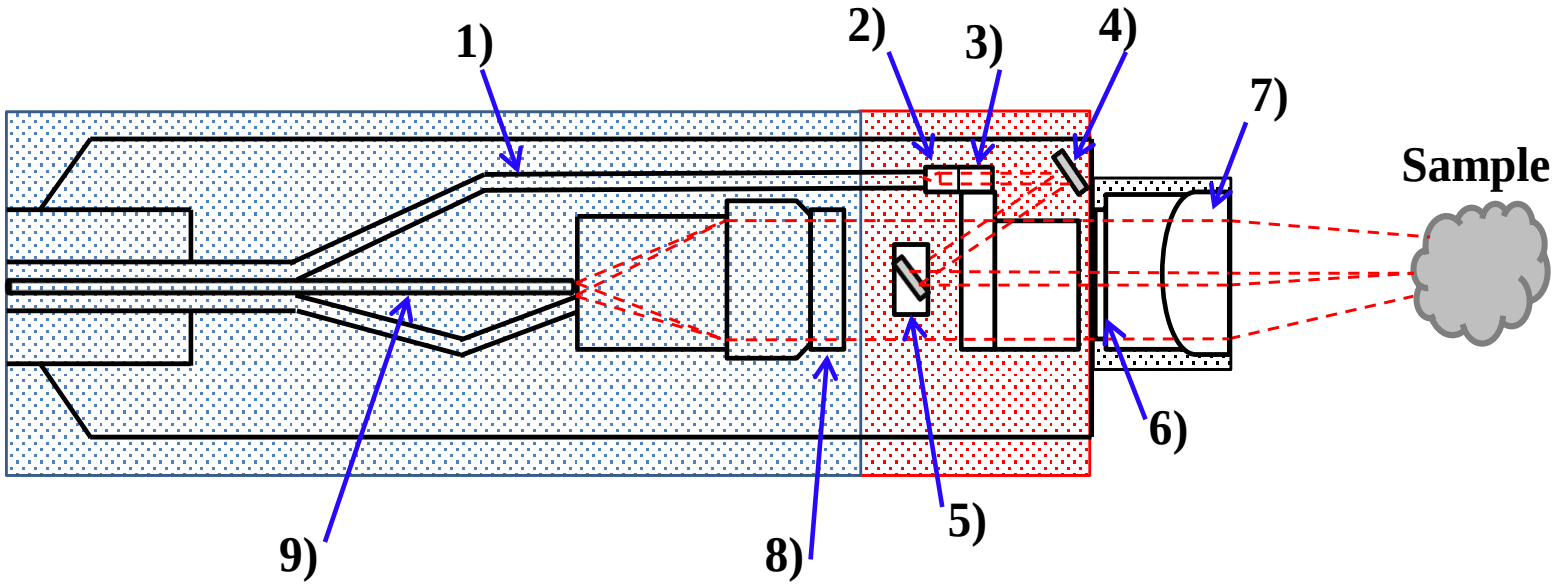

Figure 3-11: Schematic representation of the inside of a PhAT probe head containing the following components: 1) excitation fibre; 2) short focal length lens; 3) bandpass filter; 4) mirror; 5) combiner; 6) exit window; 7) sample lens; 8) notch filter; 9) collection fibre bundle[10]

The data acquisition software utilised with this instrument was iC Raman, which can be used for single measurements and reaction monitoring. Prior to the collection of any measurements, an instrument validation was carried out using cyclohexane. The measurements collected for both the LGA and D-mannitol crystallisations were carried out using a 785 nm laser with a laser power of 400 mW and utilised a 15 second exposure time and 4 accumulations resulting in a measurement being obtained every 90 seconds. The spectral data collected was processed in Matlab using a Savitsky-Golay first derivative filter which utilised a width of 11 data points and a second order polynomial.

3.4.2 Acoustic emission instrumentation

Acoustic emission measurements were carried out using a number of different components from several manufacturers which have been used collectively for acoustic emission monitoring within CPACT for a number of years. Figure 3-12 shows a schematic representation of the components which comprise the acoustic emission instrumentation.

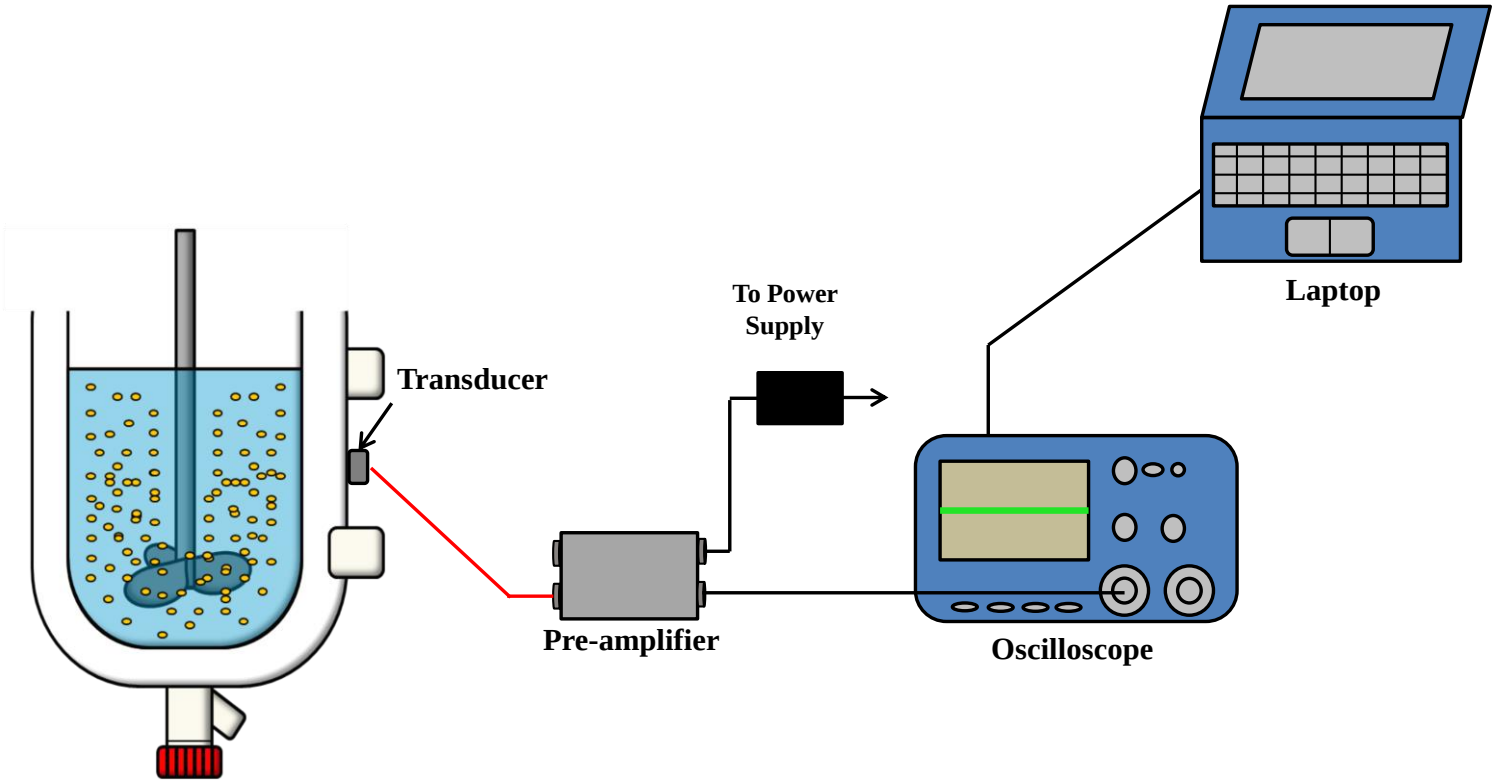

Figure 3-12: Schematic representation of the acoustic emission set-up for crystallisation monitoring

As Figure 3-12 demonstrates a Nano 30 piezoelectric transducer with an operating frequency range of 150-400 kHz (Physical Acoustics Corporation, Princeton, USA) was attached to the outside of the vessel wall using vacuum grease (Dow Corning, Midland, USA) and electrical tape to secure the transducer and ensure air free contact between the ceramic face of the transducer and the glass vessel wall. The signals detected by the transducer were sent to an Agilent 54624A oscilloscope via a 60 db pre-amplifier (Physical Acoustics Ltd) and these were transferred to a laptop PC. The purpose of the pre-amplifier is to filter the noise and therefore amplify the signal from particle collisions which were being monitored.[11] The software used for data collection converted each individual time, voltage trace from the oscilloscope to a separate comma separated variable (CSV) file and was developed in house by Douglas McNab and Robbie Robinson (Centre of Ultrasonic Engineering). A sampling rate of 2 MHz was used for all experiments with a 2 second delay between measurements. The theory behind acoustic emission spectrometry was discussed further in section 2.3.

Signals obtained from acoustic emission monitoring were converted to the power spectrum by carrying out a Fourier transform on each signal using Matlab (Mathworks Inc.) and groups of 32 power spectra were summed to improve the signal-to-noise ratio. The trend obtained by integrating the area under the peaks has been used to compare the results between crystallisation experiments in this work. Figure 3-13 shows an example of a signal obtained from an oscilloscope which has been Fourier transformed into a power spectrum.

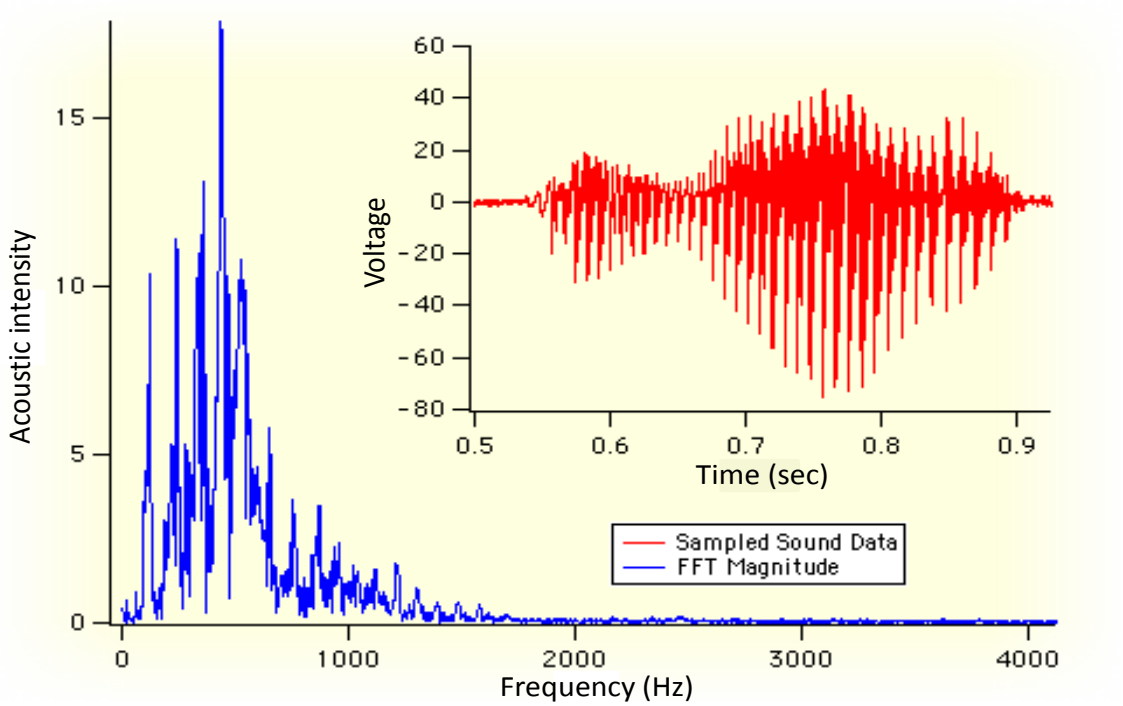

Figure 3-13: Example of the conversion of a signal detected by an oscilloscope and the transformation to the power spectrum using Fourier transform[12]

3.4.3 Malvern Mastersizer

Laser diffraction measurements were carried out using a Malvern Mastersizer 2000 which was coupled with a Hydro2000SM sample accessory cell. Figure 3-14 shows a schematic representation of the Mastersizer laser diffraction system. Samples which had been vacuum filtered and dried overnight in an oven were added to the sample cell containing a saturated solution of LGA and 0.1% Tween 80 to prevent agglomeration of the particles. The samples were added to the cell until a laser obscuration (internal parameter of the instrument to indicate multiple scattering effects) of ~3% was obtained.

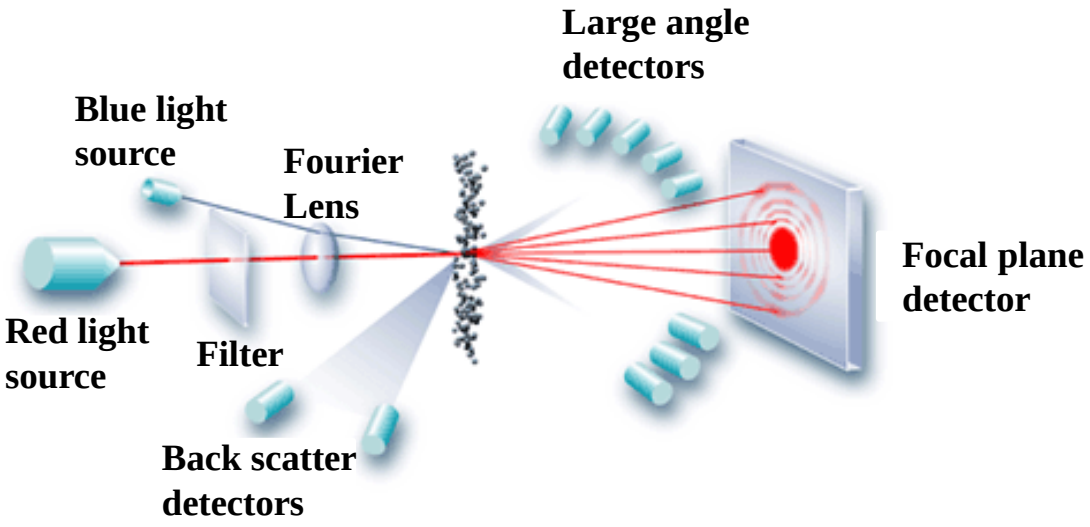

Figure 3-14: Schematic representation of a laser diffraction system[13, 14]

As is shown in Figure 3-14 the laser diffraction system comprises a laser which provides intense light at a fixed wavelength. The Mastersizer 2000 uses two light sources, a 632.8 nm HeNe red light and a 470 nm blue light source. Two light sources are used in laser diffraction instruments in order to facilitate multi-wavelength measurements. The filter enables the vertically and horizontally polarized light to be separated while the Fourier lens placed prior to the sample cell allows particle scattering to be measured at both forward and backscatter angles. A sample presentation system is necessary to ensure the sample is presented to the laser beam as a well dispersed, homogeneous stream of particles. A number of detectors are employed to measure the light pattern produced over a range of angles (discussed further in section 2.4.1). In this case the angle range measured is from 0.02 to 135 degrees. It is possible to measure particle size ranges from 0.02-2000 µm.[13, 15] The laser diffraction measurements provided particle size information of which the volume distribution, the d (0,5), the d (4,3) and the span were used. The volume distribution is given in 100 logarithmically spaced size bins from 0.01 – 10,000 µm, the d (0,5) (µm), is the particle diameter corresponding to 50% of the volume distribution, the d (4,3) (µm) is the volume weighted mean and the span is

calculated using equation 2-5 where d (0,1) and d (0,9) are the particle diameters corresponding to 10 and 90% of the volume distribution, respectively.

$$\boldsymbol{span = \frac{d\,(0,9) - d(0,1)}{d\,(0,5)}} \qquad \textbf{(2-5)}$$

3.4.4 Focused Beam Reflectance Measurement

Focused beam reflectance measurements (FBRM) were carried out using a Lasentec (Mettler Toledo) S400 laboratory scale probe. Figure 3-15 shows a schematic representation of an FBRM probe.

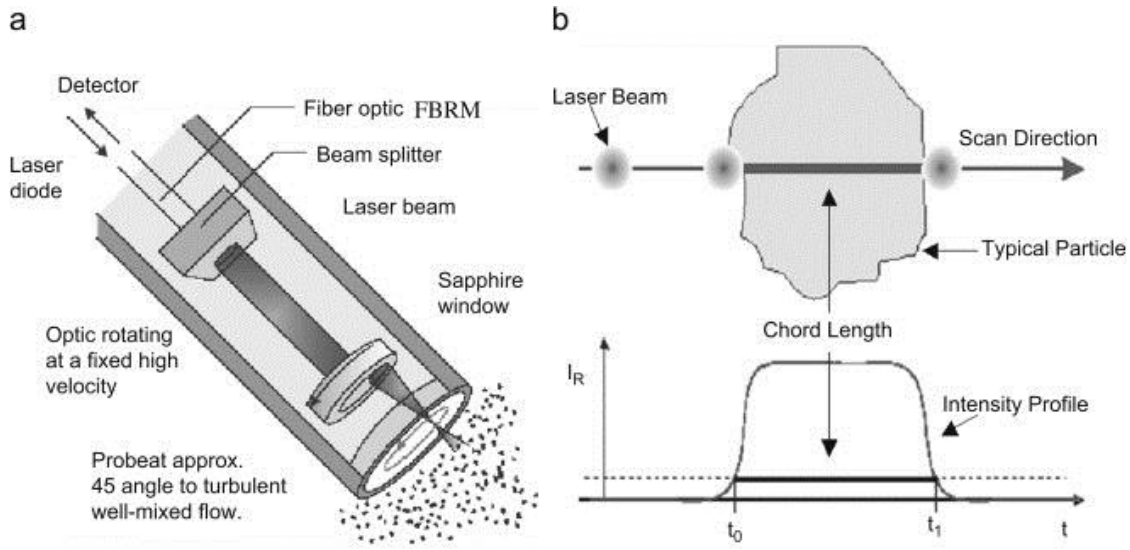

Figure 3-15: Schematic representation of a) a FBRM probe and b) measurement principle behind FBRM[16]

As shown in Figure 3-15 a laser light source of 780 nm is focused into the FBRM probe where a series of lenses and a rotating optic (at approximately 2 ms^{-1}) focus the light to a small spot at the sapphire window. When the probe is immersed into a solution containing particles or droplets, the laser energy is reflected back into the probe by backscatter from the particles. The duration or reflectance time, of the measurement is used to determine the particles chord length.[17] The chord length distribution is the fundamental measurement provided by FBRM and can be used to detect and monitor changes in particle count and size. For the experiments conducted, a probe with an

external diameter of 8 mm and a length of 91 mm was used. FBRM was applied to crystallisations of D-mannitol. *In-situ* measurements were carried out by inserting the probe into the 1 L batch OBR probe port which was secured with a probe sleeve. Off-line measurements were carried out by adding 1 g of each sample into a beaker containing ~50 ml of diethyl ether and stirring applied using a magnetic stirrer. For both the *in-situ* and off-line analysis, a measurement was collected every 15 s. The principles of FBRM are discussed further in section 2.4.2.

3.4.5 X-ray Powder Diffraction

X-ray powder diffraction measurements were undertaken using a Bruker AXS D8Advance transmission diffractometer and a PANalytical X'PERT PRO diffractometer was used for the work carried out in chapter 6 only. Figure 3-16 shows a schematic representation of a typical X-ray diffractometer.

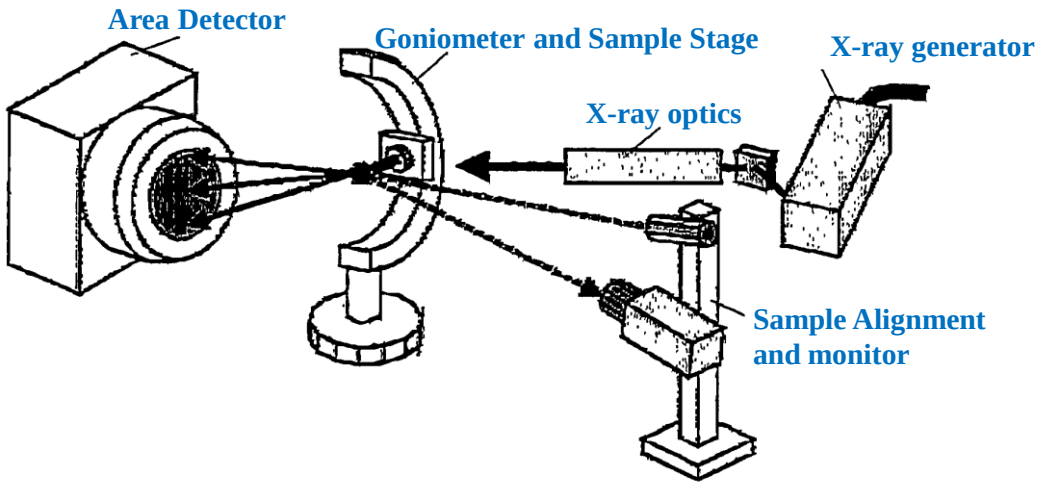

Figure 3-16: Schematic representation of a typical X-ray diffraction system[18]

The main components of an X-ray diffractometer include the X-ray source and optics, goniometer and sample stage, sample alignment and monitor and the detector. The X-ray source ensures the radiation is of the required energy spot size and intensity while the optics condition the primary beam to the necessary wavelength, beam profile and

divergence. The goniometer and sample stage ensures the correct alignment between the primary beam, sample and detector. The X-rays scattered from a sample are recorded and converted to a diffraction pattern by the detector.[18] The theory behind XRD has been discussed in further detail in section 2.5.

The Bruker AXS D8Advance transmission diffractometer was equipped with θ/θ geometry, primary monochromatic radiation (Cu $K_{\alpha 1}$, 0.154 nm), a Braun 1D position sensitive detector (PSD) and an automated multi-position x-y sample stage. Data were generally collected from 4-35° 2θ with a 0.015° 2θ step size and 1 s $step^{-1}$ count time. The samples (having been vacuum filtered and dried in an oven overnight) were prepared by being lightly ground in a pestle and mortar and then a small amount (<0.5 g) was placed on a well plate supported by kapton film (7.5 μm thickness) which could hold up to a maximum of 28 samples. The PANalytical X'PERT PRO diffractometer also had a θ/θ geometry and Cu $K_{\alpha 1}$, 0.154 nm radiation source, however the data was collected from 5-40^{o} 2θ with a 0.0167 2θ step size. Powder samples were placed on a silicon support plate with an aluminium holder.

3.5 References

1. Sigma Aldrich, L-glutamic acid, November 2010, http://www.sigmaaldrich.com/catalog/product/aldrich/w328502?lang=en&region=GB.
2. Sigma Aldrich, D-Mannitol, June 2012, http://www.sigmaaldrich.com/catalog/product/sial/m4125?lang=en&region=GB.
3. J. Schöll, D. Bonalumi, L. Vicum, M. Mazzotti and M. Müller, In Situ Monitoring and Modeling of the Solvent-Mediated Polymorphic Transformation of l-Glutamic Acid, *Crystal Growth & Design*, 2006, **6**, 881-891.
4. J. Cornel, P. Kidambi and M. Mazzotti, Precipitation and Transformation of the Three Polymorphs of d-Mannitol, *Industrial & Engineering Chemistry Research*, 2010, **49**, 5854-5862.
5. Kaiser Optical Systems Inc, PhAT systems operation manual *(*2008487 V2.0*)*, 2004.
6. Kaiser Optical Systems Inc, Holographic Notch Filters (Raman products technical note: number 1050), July 2013. http://www.kosi.com/resources/product_literature_1/rtnote1b/Kaiser_TN1050.pdf,
7. Kaiser Optical Systems Inc, HoloPlex Holographic Transmission Grating (Raman products technical notes: number 1201), July 2013. http://www.kosi.com/resources/product_literature_1/rtnote1b/Kaiser_TN1201.pdf,
8. Kaiser Optical Systems Inc, Axial Transmissive Spectrograph (Raman products technical notes: number 1200), July 2013. http://www.kosi.com/resources/product_literature_1/rtnote1b/Kaiser_TN1200.pdf,
9. Kaiser Optical Systems Inc, PhAT Probe for Quantitative Raman Analysis of Solids, July 2013. http://www.kosi.com/raman-spectroscopy/phat-probe-head.php.
10. H. Owen, D. J. Strachan, J. B. Slater and J. M. Tedesco, *United States Patent (US 7148963 B2)*, 2006.
11. Physical Acoustics Corporation, Voltage Preamplifiers, August 2013. http://www.pacndt.com/index.aspx?go=products&focus=/amplifiers/voltagepreamps.htm.
12. WaveMetrics, Power Spectra, July 2013. http://www.wavemetrics.com/products/igorpro/dataanalysis/signalprocessing/powerspectra.htm.
13. Z. Stojanovic and S. Markovic, Determination of particle size distributions by Laser Diffraction, *Technics-New Materials*, 2012, **21**, 11-20.
14. Malvern, Laser Diffraction Particle Sizing, July 2013. http://www.malvern.com/labeng/technology/laser_diffraction/particle_sizing.htm

15. Malvern, Mastersizer 2000, July 2013. http://www.malvern.com/labeng/products/mastersizer/ms2000/mastersizer2000.htm.
16. D. Greaves, J. Boxall, J. Mulligan, A. Montesi, J. Creek, E. Dendy Sloan and C. A. Koh, Measuring the particle size of a known distribution using the focused beam reflectance measurement technique, *Chemical Engineering Science*, 2008, **63**, 5410-5419.
17. Mettler Toledo, FBRM (Focused Beam Reflectance Measurement) Technology, July 2013. http://us.mt.com/us/en/home/supportive_content/specials/Lasentec-FBRM-Method-of-Measurement.html.
18. B. B. He, Two-dimensional X-ray diffraction, John Wiley & Sons, 2009.

4 Effect of operating conditions on particle properties in batch oscillatory baffled and stirred tank reactors

4.1 Introduction

The batch stirred tank reactor (STR) has been the workhorse for industrial crystallisation for many years and is still widely used especially in the pharmaceutical industry. Despite this there are many problems with product quality and consistency of the end product due to difficulties with optimisation of this technology and reproducibility of crystallisation processes. This is a particular issue in the pharmaceutical industry where changes in the properties of the end product (*e.g.* polymorph, particle size) can at the least affect the downstream processes for the manufacture of that product and at the worst put the consumer at risk (discussed further in section 1.1.). The potential consequences for both the consumer and the companies supplying the drug product have been highlighted in the past with a number of high profile pharmaceutical products. One of these was Ritonavir where a previously unknown polymorph of the compound unexpectedly formed which was more thermodynamically stable and less soluble. This caused the final product to fail the dissolution test costing the company 250 million dollars to reformulate the drug and there was risk of a shortage of a widely used product to treat a life threatening condition.[1] This has led to the use of polymorphic screening to find all polymorphs and select the best solid form for the product.[2] Although the case of Ritonavir is an extreme one, problems with the crystallisation step are commonplace in the pharmaceutical industry and result in much wasted time and cost in finding the cause and rectifying the matter. Therefore, the initial section of work in this study was focused around batch stirred tank reactors to determine if the operating conditions affected the properties of the end product of a model compound and assess the scope for optimisation of this technology. These results were then compared with a relatively recent alternative and comparatively understudied technology, the batch oscillatory baffled reactor to determine if any potential advantages were gained. The use of *in situ* measurement techniques were adopted in order to aid with the

monitoring and control (and therefore optimisation) of the crystallisation process in both reactors.

The model compound selected for this study was L-glutamic acid which is well defined in the literature with respect to crystallisation with stirred tank reactors. This provided the opportunity to develop process understanding of batch OBR reactors and evaluate analytical techniques by using previous results in the literature. Therefore, the potential advantages and disadvantages of implementing OBR technology over conventional stirred tank reactors could be identified for this compound. There are many reports in the literature on the study of the kinetics of the crystallisation of L-glutamic acid, conditions to obtain each of the polymorphs, as well as various *in situ* techniques to provide increased understanding of the processes occurring during the crystallisation. L-glutamic acid comprises two polymorphs: the metastable alpha and the thermodynamically stable beta form. The polymorphism exhibited in LGA is an example of conformational polymorphism and the differences are caused by hydrogen bonding interactions; mainly four hydrogen bond donors and four acceptors.[3, 4] The beta form is easier to crystallise than the alpha form in a batch stirred tank from an aqueous solution, however, although the alpha polymorph can be more problematic to obtain it is most often the desired form due to its crystal habit making it easier to handle for downstream processing.[5] Nevertheless, even for this widely studied compound there are conflicting reports on the methods to obtain both the polymorphs. The beta form is reported to crystallise under slow cooling conditions while the metastable form has been reported to be obtained using a number of different methods.[3, 6, 7]

In the majority of reports using cooling crystallisation for LGA, the alpha form was obtained by using more rapid cooling rates. *Srinivasan et al*. employed rapid, uncontrolled cooling from an initial temperature of 80^{o}C to final temperatures of 1-40^{o}C to determine the conditions to obtain each pure form.[5] It was reported that the pure metastable form was obtained at temperatures below 9^{o}C and the stable beta form between 27 and 34^{o}C with mixtures of the two forms between these two

temperature ranges. This suggested that supersaturation played an important part in the nucleation of the respective forms with a higher supersaturation value resulting in increasing levels of the alpha form.[5] *Kitamura* and *Ma et al*. similarly reported that the alpha polymorph was obtained at a lower final temperature during a cooling crystallisation, however, in these cases, temperature rather than supersaturation appeared to be the determining factor in which polymorph was formed.[8-10] The alpha polymorph has also been reported to be obtained by anti-solvent crystallisation (using iso-propanol as the anti-solvent), pH shift using monosodium glutamate, and with the addition of impurities.[2, 11-14] The solvent-mediated transformation process of L-glutamic acid has also been well studied and the metastable alpha polymorph is supposedly relatively easy to isolate as it remains stable, without transforming for a longer period of time at a lower temperature and also using a faster cooling rate during the crystallisation.[15, 16]

The application of *in situ* measurement techniques to pharmaceutical processes has become an area of increased interest over recent years with many reviews of the most widely used techniques being reported.[17-21] The range of techniques applied specifically to the crystallisation process has been discussed in section 1.4. As L-glutamic acid has been a widely studied compound with respect to crystallisation, it has also been the focus of the investigation of many *in situ* monitoring techniques. The most commonly reported of these techniques are Raman and mid-infrared spectrometries for the measurement of solid concentration and liquid phase concentration, respectively (both techniques discussed further in sections 1.4.1.1 and 1.4.1.3). Mid-infrared spectrometry is a valuable technique for crystallisation monitoring since the solute concentration and supersaturation values can be determined, which are important parameters to monitor during a crystallisation process.[22, 23] However, although several authors have applied this technique to the monitoring of the crystallisation of L-glutamic acid, it was reported that relatively advanced chemometrics were required to provide reliable liquid phase concentration measurements mainly due to the low solubility and hence weak spectra.[2, 24, 25] Therefore, although several preliminary experiments were conducted using this

technique, it was anticipated that little additional information than what is already reported in the literature would be gained.

Raman spectrometry has been applied to the study of the crystallisation of L-glutamic acid in batch stirred tank reactors to obtain quantitative information on solid concentration and also for the monitoring of the polymorphic transformation from alpha to beta LGA. *Ono et al.* used a calibration set of different mixtures of the alpha and beta forms and the corresponding peak height and area values to predict the solid concentration of the alpha polymorph.[6] Additionally, the decreasing concentrations of the alpha form were predicted at different temperatures during the transformation process.[6] *Cornel et al*. employed multivariate data analysis including principal components analysis (PCA) and partial least squares (PLS) to estimate both the liquid and solid phase values of the two polymorphs during seeded and unseeded transformations.[6] It was reported that multivariate analysis was necessary to obtain accurate quantitative information due to the complex nature of Raman spectra which are influenced by both liquid and solid phases and particle size, temperature effects, etc. Additionally, the pre-processing applied to the spectral data significantly impacted the model performance.[26] Many other similar studies have been reported for the quantitative monitoring of the crystallisation of L-glutamic acid.[2, 15, 27] The reported cases of *in situ* Raman monitoring of L-glutamic acid has been with the use of immersion probes which have a relatively small sampling area in the region of 100 µm. Therefore, it was anticipated in the present study that the use of a wide area illumination probe such as the Kaiser Raman $P^{h}AT$ probe (with a 6 mm spot diameter) would result in more representative sampling with the added benefit of non-invasive data collection. This would significantly reduce the issues of probe fouling which are commonplace in crystallisation processes and allow for a novel method of monitoring crystallisations as shown with alternative particulate processes such as powder drying.[28]

The batch oscillatory baffled reactor (OBR) was developed by NiTech Solutions Ltd. as a middle ground between operating in batch stirred tank reactors and transferring to continuous operation in a continuous OBR (chapter 5). Oscillatory mixing has

only relatively recently been applied to crystallisation, however, there are reports of oscillation being used to enhance mixing as early as the 1950s.[29] The OBR reactor has also been applied to other processes including flocculation, polymerisation and fermentation.[30-33] OBR technology (discussed further in section 1.2.2.) claims to provide more uniform mixing and, therefore, results in a product with consistent properties that can be produced repeatedly. The batch OBR reactor is designed to be used to establish optimum operating conditions for the crystallisation of a particular compound on a small scale prior to transferring these conditions and scaling up to the continuous OBR. The majority of the reports dealing with batch OBR reactors have used L-glutamic acid as a model compound. These mainly dealt with the effect of operating conditions on the crystallisation outcome, *e.g.* polymorphic form. It was reported that when the mixing intensity, final temperature and solution concentration were increased, greater levels of the beta polymorph were obtained.[7, 34, 35] However, no *in situ* analysis was implemented with these crystallisation experiments. It was anticipated in the present study that by monitoring the crystallisation of LGA under various operating conditions and undertaking a more systematic approach *e.g.* design of experiments, additional information on the process and how the operating conditions influence a certain particle outcome could be determined. Additionally, the outcomes from the batch OBR crystallisations were not compared in previous studies with similar experiments in a batch STR; the metastable zone width was the only comparison made. Therefore, in this section of work, similar experiments were also carried out in a batch STR to assess the improvements or differences in the end product.

There are many operating conditions which affect the properties of the crystals obtained during a crystallisation process. These include cooling rate, type and intensity of mixing, solution concentration and temperature.[7, 11, 35-39] All these factors influence the metastable zone, and therefore, affect nucleation and growth kinetics resulting in clear differences in the particles obtained.[40] In the following report, *in-situ* Raman spectrometry has been employed to provide information on how different operating conditions affect the formation and growth of particles in real time in two different batch reactors, a stirred tank (STR) and an oscillatory baffled reactor

(OBR). A design of experiments approach was adopted for the study in the OBR and these results were compared and contrasted with those obtained from similar experiments in the stirred tank. The aim of the study was to investigate if particles of a greater quality and consistency were obtained in the OBR due to the more uniform conditions within the vessel. The measurements were able to show differences in the nucleation temperature and growth profiles of the crystals, which helped to explain why a change in experimental conditions had an impact on the physical properties of the crystals. Supplementary information was obtained through off-line X-ray diffraction (XRD) and laser diffraction (LD). This work also demonstrated the potential of using real-time information from Raman measurements to be able to control the properties of the final product in alternative continuous modes of operation by adjusting the conditions in order to control the properties of the end product.

4.2 Experimental

4.2.1 Materials

In this work, L-glutamic acid and distilled water were used for all experiments as described in section 3.2.

4.2.2 Batch STR conditions

The reactor consisted of a 1 L jacketed glass vessel as described in section 3.3.2. Solution concentrations of 15 and 45 g/L of LGA in distilled water were used in all experiments in the STR and heated to 80^{o}C on a hotplate. The solution (1 L) was then added to the STR where the initial temperature was 80^{o}C, and cooling to 40 or 10^{o}C took place at approximately 0.65^{o}C/min for slow cooling (resulting from natural cooling of the heater chiller from 80 to 40 or 10^{o}C). The hot solution (1 L) was added to the reactor with the jacket temperature set at 10^{o}C for rapid cooling. The impeller speed was set to either 100 or 200 rpm. Figure 4-1 shows the cooling profiles of the reactor contents for slow and rapid cooling in the batch STR.

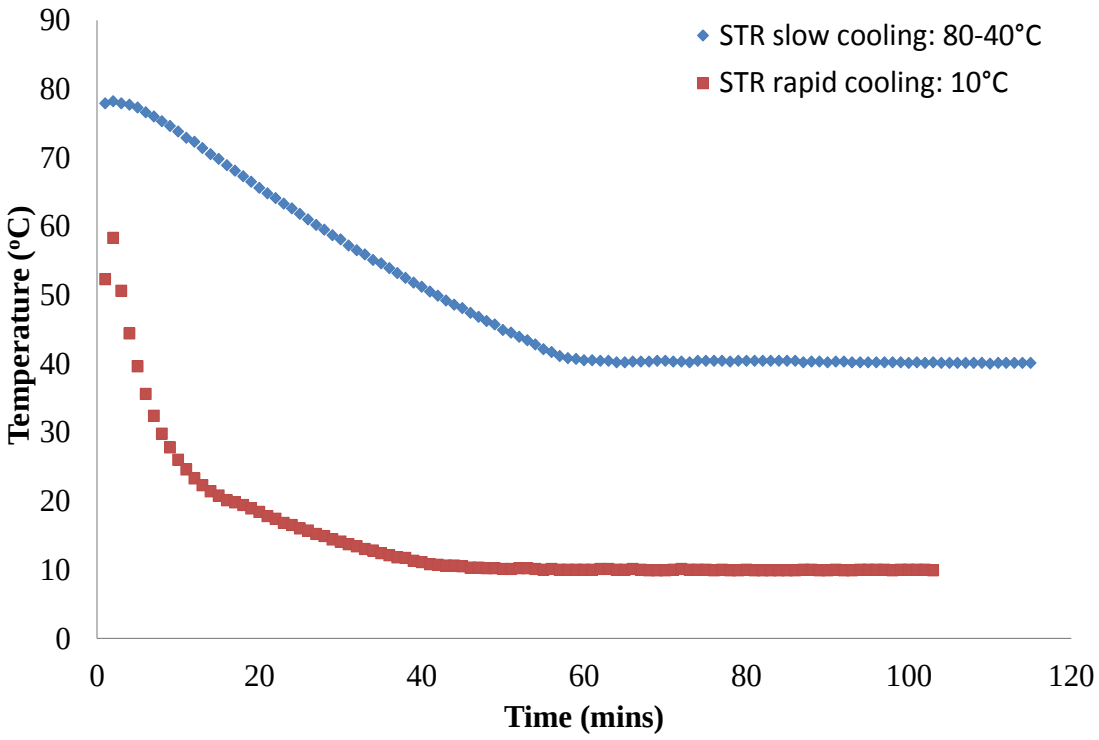

Figure 4-1: Cooling profiles for slow and rapid cooling obtained using a thermocouple placed inside the batch STR

4.2.3 Batch OBR conditions

The reactor for these experiments consisted of a 1 L jacketed OBR vessel as described in section 3.3.2. Two different concentrations (15 and 45 g/L) of LGA solution were used in the OBR. These were first prepared in a beaker and heated to 80^{o}C on a hotplate with stirring. The solution (1 L) was then added to the OBR, which had the water jacket set at an initial temperature of 80^{o}C for slow cooling (approximately 0.65^{o}C/min resulting from natural cooling of the heater chiller from an initial temperature of 80 to 40 or 10^{o}C) or 10^{o}C for rapid cooling. The solutions were oscillated at frequencies of 1, 2 or 3 Hz and amplitudes of 10 or 30 mm. For slow cooling, the solutions were cooled to final temperatures of 40 or 10^{o}C with a cooling rate of approximately 0.5^{o}C/min and were held at the final temperature for an hour. For rapid cooling, the jacket temperature was maintained at 10^{o}C throughout. Figure 4-2 shows the cooling profiles of the reactor contents for slow and rapid cooling in the batch OBR.

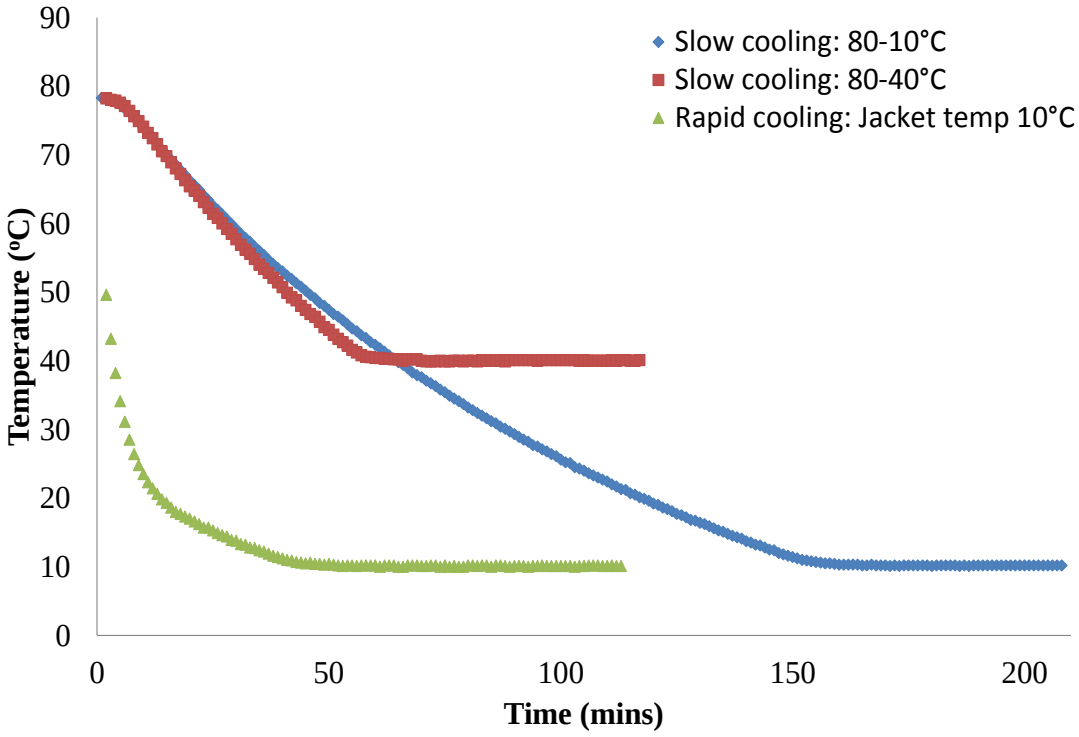

Figure 4-2: Cooling profiles for both slow and rapid cooling obtained using a thermocouple placed inside the batch OBR

The temperature was recorded in both batch reactors using a digital thermocouple temperature indicator where readings were taken every minute of the reactor contents.

4.2.4 Raman Instrumentation - Kaiser RXN1 spectrometer

Raman measurements were carried out using the Kaiser RXN1 spectrometer with the PhAT probe head as described in section 3.4.1. Non-invasive measurements were recorded by directing the laser through the side of the OBR vessel, between the two bottom baffles. The vessel and the probe head were covered in aluminium foil and blackout material to limit any cosmic rays or room lights affecting the spectra. A laser wavelength of 785 nm using a spot size of 6 mm and a laser power of 400 mW were used and an average of four 15 s scans were recorded resulting in a measurement every 90 s. The spectral data collected was processed in Matlab using a Savitsky-Golay first derivative filter which utilized a width of 11 data points and a second order polynomial.

4.2.5 Laser diffraction

Laser diffraction measurements were carried out using a Malvern Mastersizer 2000 as described in section 3.4.3. Approximately 100 ml of a saturated solution of LGA and 0.1% Tween 80 was added to a Hydro2000SM cell. Powder samples of LGA which had been vacuum filtered and dried in an oven overnight were added to the cell until a laser obscuration (internal parameter of the instrument to indicate multiple scattering effects) of ~3% was obtained.

4.2.6 X-ray diffraction

X-ray diffraction measurements were undertaken using a Bruker AXS D8 Advance transmission diffractometer as described in section 3.4.5. Powder samples which had been vacuum filtered and dried in an oven overnight were prepared by lightly grounding the samples in a pestle and mortar before mounting a small amount of the powder (<0.5 g) on a well plate supported by kapton film. Figure 4-3 shows the XRD patterns of the pure forms of alpha and beta L-glutamic acid.

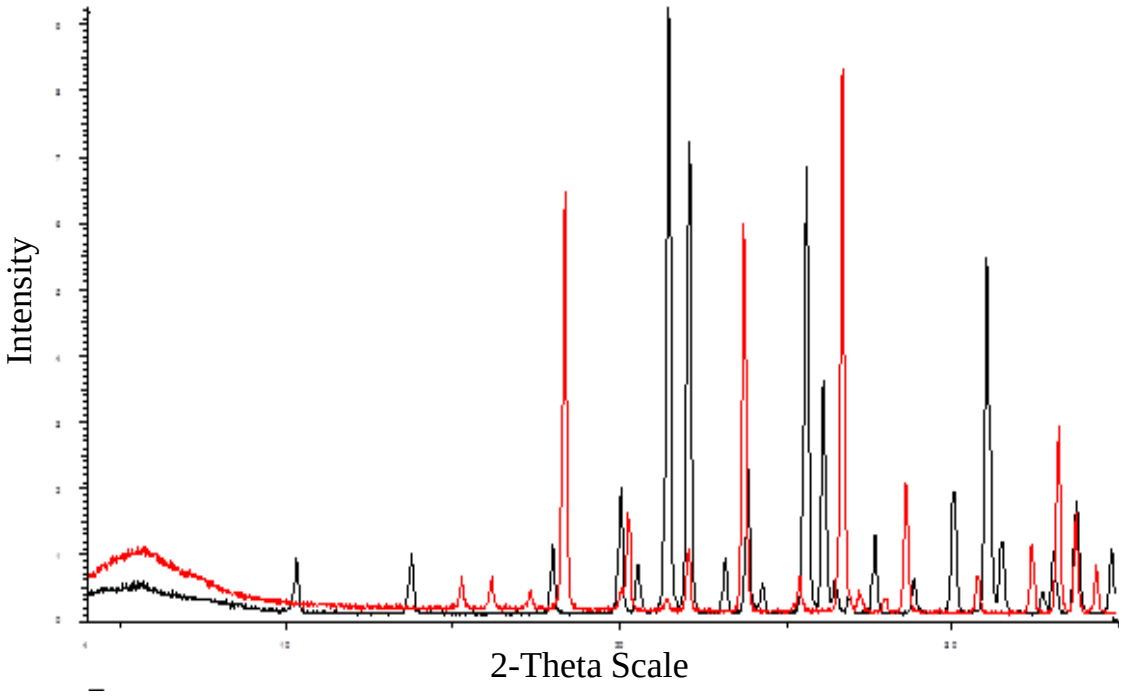

Figure 4-3: X-ray diffraction pattern of alpha (red) and beta (black) L-glutamic acid

4.3 Results and Discussion

4.3.1 Batch OBR DoE

A design of experiments was carried out in the batch OBR to try and gain increased understanding of this reactor using the least amount of experiments possible. By using this approach, it was possible to compare the effects of various operating parameters and determine those which affected the crystallisation the most. A 2-level, 4^{-1} factorial design was conducted initially which gave eight experiments (1-8) comprising various operating conditions. These experiments were monitored using non-invasive Raman spectrometry. Eight additional experiments were then completed to give a full factor design, however, only off-line XRD and LD were carried out for the extra experiments. Four preliminary experiments carried out previously in the batch OBR using different oscillation conditions to those in the DoE were also added to compare the effects of operating conditions on particle properties. The conditions were chosen as it was expected these would have the greatest effect on the outcome of the crystallisation of LGA. The different experiments generated for the DoE (plus four additional experiments) comprising various operating conditions are shown in Table 4-1. The outcome of each crystallisation experiment including the polymorphic form as determined using non-invasive Raman and off-line XRD measurements, particle properties including the d(0,5), d(4,3) and span obtained using off-line laser diffraction and the solid recovery and yield are shown in Table 4-2. The yield was calculated using the solid recovery measurements obtained at the end of the crystallisation and the initial solution concentration.

Table 4-1: Different operating conditions used in the sixteen DoE experiments and additional experiments with the batch OBR

Experiment	Type of Cooling	Concentration (g/L) (A)	Final Temp (^{o}C) (B)	Frequency (Hz) (C)	Amplitude (mm) (D)
1	Slow	15	40	1	30
2	Slow	15	10	3	30
3	Slow	45	40	1	10
4	Slow	45	10	3	10
5	Slow	45	40	3	30
6	Slow	45	10	1	30
7	Slow	15	40	3	10
8	Slow	15	10	1	10
9	Slow	45	10	1	10
10	Slow	15	10	3	10
11	Slow	15	10	1	30
12	Slow	45	10	3	30
13	Slow	15	40	1	10
14	Slow	45	40	3	10
15	Slow	45	40	1	30
16	Slow	15	40	3	30
17	Slow	45	40	2	10
18	Slow	15	10	2	10
19	Rapid	45	10	2	10
20	Rapid	15	10	2	10

Table 4-2: Outcome of the sixteen DoE experiments and additional experiments in the batch OBR showing the polymorphic composition of the final product using Raman spectrometry and XRD, the particle size measurements using laser diffraction and the solid recovery and yield

	Polymorph Obtained						
Experiment	**Raman**	**XRD**	**d (0,5) (µm)**	**d (4,3) (µm)**	**Span**	**Solid Recovery (g)**	**Yield (%)**
1	-	-	-	-	-	-	-
2	α	α	83.5	89.3	1.16	8.04	53.6
3*	α/β	α/β	457.3	558.8	2.22	14.55	32.3
4	α/β	α/β	381.9	395.4	0.85	30.69	68.2
5	α/β	α/β	311.6	382.0	2.33	27.75	61.7
6	-	α/β	522.9	585.6	1.52	30.60	68
7	-	-	-	-	-	-	-
8*	-	α	46.5	106.2	2.81	0.11	0.7
9*	-	α	305.3	468.7	3.34	24.89	55.3
10	-	α	289.0	307.3	1.11	4.06	27.1
11	-	α	181.8	198.2	1.21	6.27	41.8
12	-	α/β	102.7	204	4.87	35.91	79.8
13*	-	-	-	-	-	-	-
14	-	α/β	350.9	384.7	1.31	25.12	55.8
15	-	α/β	364.8	388.3	1.14	24.75	55
16	-	-	-	-	-	-	-
17*	α/β	α/β	395.0	427.6	1.62	15.35	34.1
18*	α/β	α/β	165.8	178.4	1.25	3.91	26.1
19*	α/β	α/β	280.3	304.9	1.41	30.17	67.0
20*	α	α	166.7	180.5	1.30	5.50	36.7

*=poorly suspended experiments; ◯ =major form

Table 4-2 shows that four of the experiments, 1, 7, 13 and 16, produced no crystals at all. This was due to a low solution concentration being used (15 g/L) and a high final temperature (40^{o}C) which meant the nucleation temperature was not reached. The results shown in Table 4-2 are discussed in detail in section 4.3.2, while Table 4-3 shows the calculated main effects and interactions of the measurements in Table 4-2

Table 4-3: Main effects and strongest interactions of the factors used in the DoE experiments in the batch OBR

	Main Effects			
	A	**B**	**C**	**D**
d (0,5)	**239.6**	-53.6	-79.9	-67.9
d (4,3)	**333.3**	-80.1	-67.9	-46.7
span	**1.41**	-1.23	0.07	0.07

	Interaction Effects					
	AB	**AC**	**AD**	**BC**	**BD**	**CD**
d (0,5)	61.6	-116.0	-50.4	-30.0	-35.0	**-133.1**
d (4,3)	**95.1**	-29.5	-15.2	22.8	-10.7	-56.3
span	0.34	0.36	0.46	0.15	-0.09	**1.20**

The main effects shown in Table 4-3 are obtained by combining the data collected at the low level of a given factor (*e.g.* 15 g/L for factor A (solution concentration)) and subtracting this from the total of the data obtained at the high level (45 g/L for factor A) and then dividing this by 2^{n-1}, where n is the number of factors used in the design. To calculate the magnitude of an interaction of factors, firstly the level of the interaction is calculated from the product of the two separate input factors *e.g.* for the interaction between factors A and B, if both factors are high level, the interaction will be high level, however if factor A is high and factor B is low, the interaction will be low level. The effect of the interaction is then carried out using the same method to calculate the main effects. This is shown in equations 4-1 and 4-2.

$$\boldsymbol{Main\ Effect} = \begin{bmatrix} (\sum \boldsymbol{responses\ for\ (+)\ level\ experiments}) - \\ (\sum \boldsymbol{responses\ for\ (-)level\ experiments}) \end{bmatrix} / \boldsymbol{2^{k-1}} \quad \textbf{(4-1)}$$

$$\boldsymbol{Main\ Interaction} = \begin{bmatrix} (\sum \boldsymbol{+\ level\ experiments}) - \\ (\sum \boldsymbol{-\ level\ experiments}) \end{bmatrix} / \boldsymbol{2^{k-1}} \quad \textbf{(4-2)}$$

Table 4-3 shows the calculated main effects and interaction effects for the experiments (1-16) carried out as represented in Table 4-1. Of all the main effects (concentration, frequency, amplitude and final temperature), concentration appeared to have the biggest effect and was a dominant factor on the value of the d (0,5), d (4,3) and the span (defined in section 2.4). As this is a positive value in all cases, the response increases when going from a low to a high concentration. The interaction between frequency and amplitude is larger than the effect of either factor alone for the d (0,5) and the span values. However, for the d (0,5) response, the interaction is negative whereas for the span it is positive. With a low frequency, an increase in the amplitude results in an increase in the response which can be seen in experiments 9 and 6 in Table 4-2 where the average particle size increases from 305.3 at 1 Hz 10 mm to 522.9 at 1 Hz 30 mm. On the other hand, at a high frequency, an increase in amplitude leads to a decrease in the response seen in experiments 4 and 12 where the particle size decreases from 381.9 at 3 Hz 10 mm to 102.7 at 3 Hz 30 mm. For the span value, an increase in frequency or amplitude leads to an increase in the response. The exception to this is the experiments carried out at 1 Hz 10 mm which resulted in a much larger value for the span, which is most likely due to the material not being suspended efficiently and settling on the bottom of the vessel leading to a wider range of particle sizes. The analysis of the effects and interactions suggests the operating conditions can be varied to alter and potentially control the particle size. The interaction between concentration and final temperature had the biggest effect on the d (4,3) value.

Non-invasive Raman spectrometry was employed to monitor the crystallisation process in a number of the experiments in Table 4-1. Previous work where calibration samples containing different mixtures of the alpha and beta polymorphs as well as the pure forms were analysed, provided useful information for non-invasive measurements. An expanded area (800-940 cm^{-1}) of the 1st derivative Raman spectra is shown in Figure 4-4.

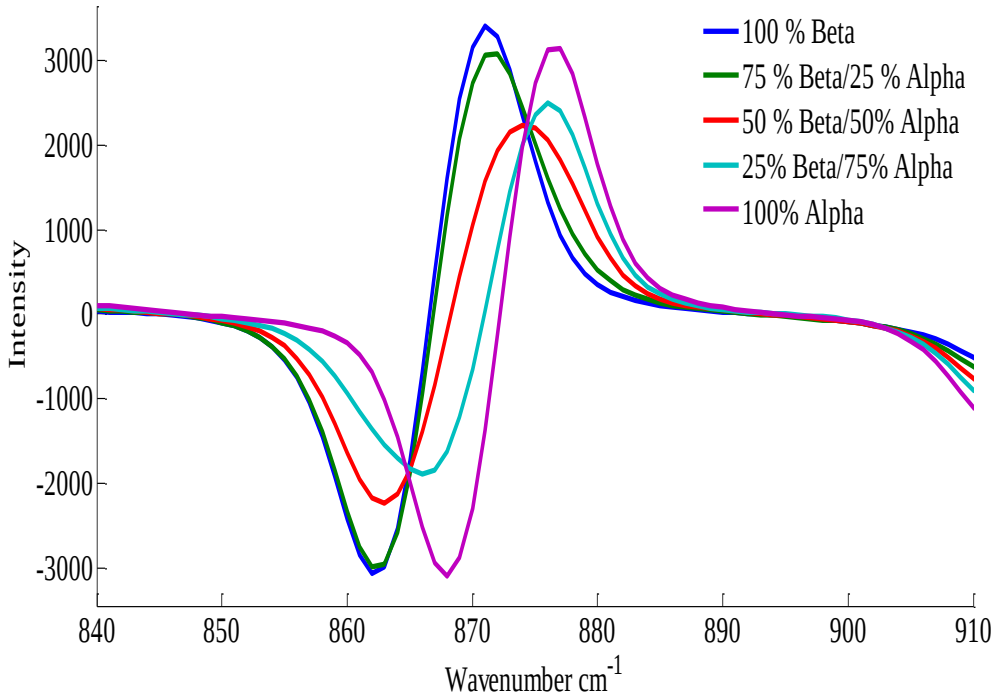

Figure 4-4: 1st derivative Raman spectra of mixtures of alpha and beta L-glutamic acid slurries in the range 840-910 cm^{-1}

Figure 4-4 reveals that the spectra of the pure forms of alpha and beta L-glutamic acid show a single peak at 877 and 872 cm^{-1}, respectively. Whereas a mixture of the two polymorphs exhibits a shift in the peak maximum depending on the relative levels of the polymorphs present. A 50:50 mixture results in a peak maximum of 875 cm^{-1}. There are several separate peaks attributable to each of the two forms which do not overlap, however these are quite low in intensity and are too weak to use to give relative amounts of the two polymorphs from the *in-situ* measurements. Table 4-4 shows the calibration samples analysed and the different mixtures of the two polymorphs. The samples were analysed in triplicate to ensure the differences in the peak position were repeatable and due to the varying amounts of the two polymorphs. The percentage concentration of beta was determined from 100 minus the alpha form value for each sample.

Table 4-4: Calibration samples containing varying amounts of the alpha polymorph

Calibration sample	Percentage alpha form (%)	Wavenumber of peak maximum (cm^{-1})	Solid concentration (g/L)
1	0	871	50
2	8	871	50
3	19	871.5	50
4	25	871.5	50
5	33	873.25	50
6	42	873.5	50
7	50	874.5	50
8	61	875.5	50
9	69	875.75	50
10	75	876	50
11	84	876.25	50
12	93	876.5	50
13	100	876.5	50

Figure 4-5 shows the plot of the peak maximum against the percentage alpha form.

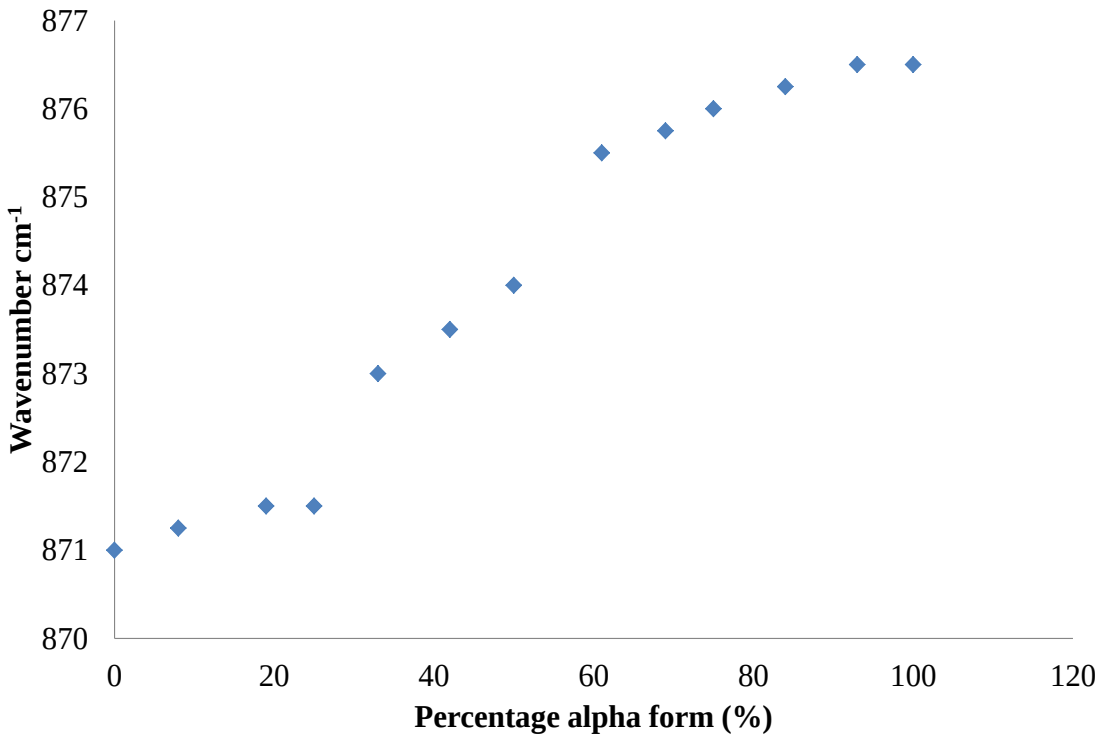

Figure 4-5: Plot of the peak maximum against percentage alpha form for varying mixtures of the two polymorphs of LGA

Figure 4-5 shows that the plot of the wavenumber of the peak maximum against the percentage of the alpha form present resembles a sigmoid shape which suggests there is a relationship between the two values. Therefore, it would be possible to estimate the percentage of each polymorph in an unknown sample by looking at the individual spectra as in Figure 4-4 and consulting the graph in Figure 4-5. However, it was also important to be able to estimate the concentration of solid material during a crystallisation process. Therefore, principal components analysis (PCA) was employed to model both variables with the addition of supplementary additional calibration samples shown in Table 4-5. Again the percentage of the beta polymorph on the calibration samples was determined from 100 minus the alpha form value for each sample.

Table 4-5: Calibration samples containing varying concentrations of pure alpha and beta polymorphs

Calibration sample	Percentage alpha form (%)	Solid concentration (g/L)
14	100	0.5
15	100	1
16	100	3
17	100	5
18	100	8
19	100	10
20	100	30
21	100	50
22	100	100
23	0	0.5
24	0	1
25	0	3
26	0	5
27	0	8
28	0	10
29	0	30
30	0	50
31	0	100

Figure 4-6 shows the PCA plot obtained using the calibration samples in Table 4-4 and Table 4-5.

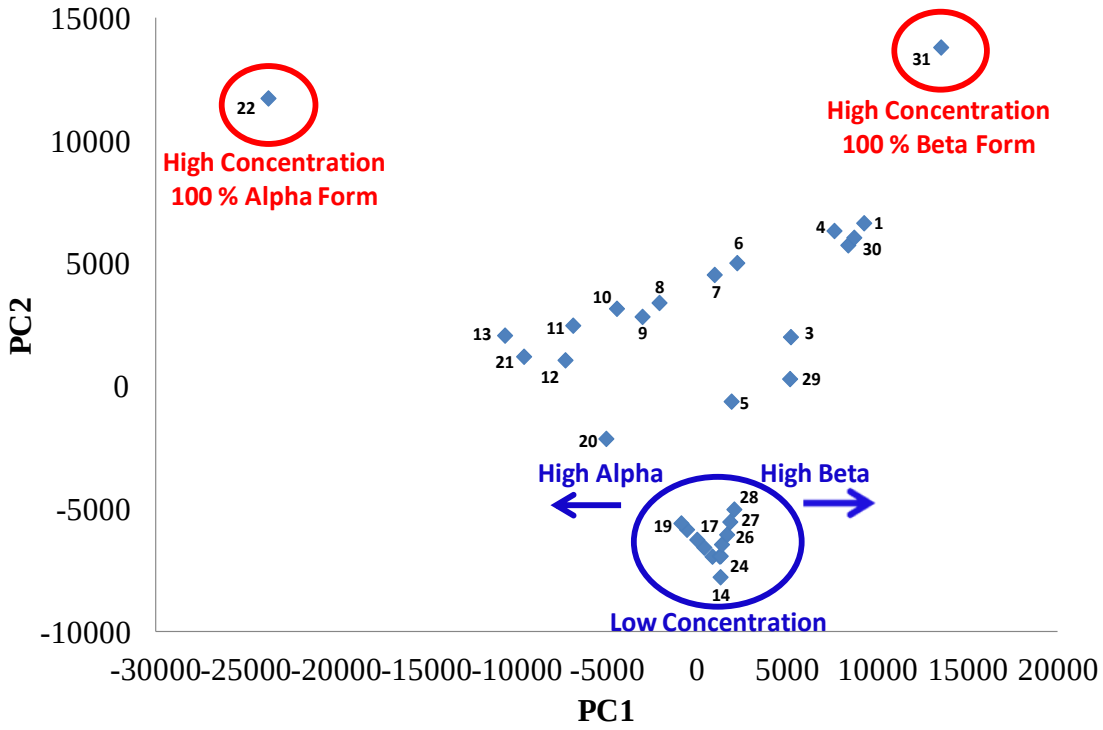

Figure 4-6: PCA plot of principal components 1 and 2 from calibration samples of L-glutamic acid shown in Table 4-4 and Table 4-5

Figure 4-6 shows that the variation in the data could be explained using two principal components: principal component 1 (PC1) which described the relative amounts of the two polymorphs and PC2 which explained the solid concentration of the samples. As shown, the data has been separated into several areas of the plot. Samples 22 and 31 show the opposite extremes with respect to polymorphic composition and are well separated at either sides of the plot with one sample 22 being composed of 100% alpha and sample 31 100% beta form. Both of these samples also have the highest solid concentration and are therefore separated from the other samples on the y-axis. There is also a cluster of samples at the bottom of the plot which all have a low concentration and are organised in a V-shape with the samples at one side being composed of higher levels of the alpha form (17 and 19) whilst on the other side containing higher levels of the beta form (24, 26, 27 and 28). The remaining samples in between these extremes are organised depending on both the solid concentration and the polymorphic composition of the samples. It was then necessary to show that the PCA model was able to predict the solid concentration and polymorphic

composition of several test samples. The test samples used are described in Table 4-6 and the PCA plot of both the calibration samples and test samples is shown in Figure 4-7.

Table 4-6: Test samples containing varying concentrations of pure alpha and beta polymorphs

Test Sample	Percentage alpha form (%)	Solid concentration (g/L)
32	50	1
33	50	5
34	50	10
35	100	50
36	25	50
37	0	50

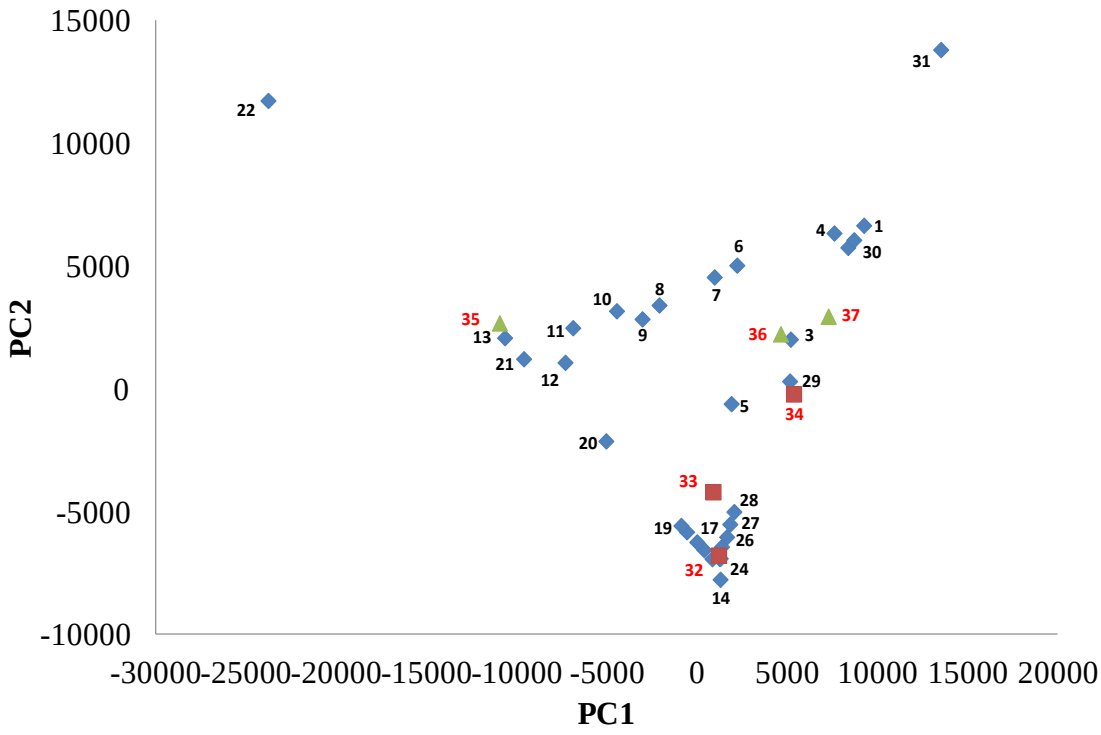

Figure 4-7: PCA plot of principal components 1 and 2 from calibration and test samples of L-glutamic acid in Table 4-4, Table 4-5 and Table 4-6

As Figure 4-7 shows the test samples have been predicted relatively well and have been organised on the plot according to the solid concentration and level of each polymorph in the sample. Partial least squares (PLS) regression was also attempted using the calibration samples to determine if a value for both the solid concentration and polymorphic composition (as a percentage) could be acquired. However, due to the peak shift observed with varying mixtures of polymorphs (Figure 4-4), it was found to be difficult to obtain adequate predictions for solid concentration as the concentration for pure alpha would be at a different peak position to pure beta. Therefore, it would be necessary to have two separate models for the alpha and beta polymorph and the model would not be able to predict the concentration when mixtures of the polymorphs are obtained. As this happened frequently in the batch OBR experiments, it was thought PCA plots were the best method to show the polymorph composition and approximate solid concentration. Therefore, it was thought PLS might be a more appropriate technique for the continuous OBR experiments where only one polymorph was obtained. The PLS method reported in the literature by *Cornel et al.* was found to only use calibration samples of either the alpha or the beta polymorph and therefore the prediction of solid concentration was simpler as the peak shift observed in this study when mixtures of polymorphs were present was not investigated and included in the model.[26]

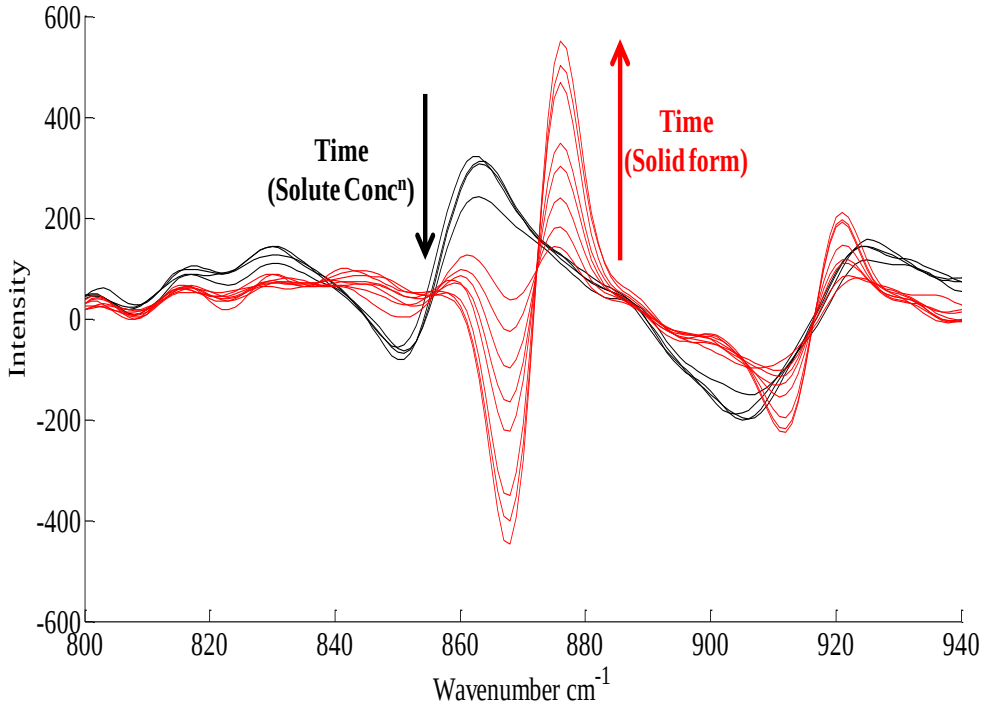

Figure 4-8: Selection of 1st derivative spectra from experiment 5 (45 g/L, 3 Hz 30 mm, 40°C final temp) for crystallisation of L-glutamic acid showing the decrease in signal for solute concentration and increase in alpha concentration at 862 and 876 cm^{-1} respectively

The 1st derivative spectra for one of the experiments (experiment 5) are shown in Figure 4-8. This shows that the first few spectra (black) recorded are relatively broad and describe the liquid phase when LGA is in solution. The sharper, more defined peaks describe the solid phase (red spectra) and become more prominent as the solid phase becomes the major influence on the Raman spectrum. Cooling crystallisation of LGA using the conditions in experiment 5 (45 g/L, 80-40°C, 3 Hz, 30 mm) resulted in approximately 50 % of the alpha form being produced when the Raman spectra were compared to that in Figure 4-4. During the crystallisation experiment in the batch OBR, the signal for the solute concentration at 862 cm^{-1} decreased (black spectra), owing to the diminishing supersaturation of the solution. The reduction in supersaturation arises because nucleation and crystal growth are beginning to take place which can be seen in the strong increase in the Raman intensity for the solid phase (red spectra) with increasing time. As this solid phase peak appears between that of the pure alpha and beta forms it can be concluded that an approximate equal

mixture of polymorphs is obtained. The XRD analysis carried out at the end of the experiment revealed a mixture of polymorphs had been formed during this experiment which agreed with the Raman spectra. As can be seen in Figure 4-8, the peaks for the solute and solid phase overlap slightly in the 1st derivative spectrum. Therefore, this will affect the crystallisation profile obtained for the solid phase and over-estimate the intensity value obtained. However, it is likely that the error associated with the measurement would be greater at the start of the crystallisation, just following nucleation. The contribution and error introduced from the solute phase would decrease as the crystallisation progressed, as the particles become the main influence on the spectrum rather than the liquid phase. It has also been reported that the estimation of solution concentration during the crystallisation of L-glutamic acid is particularly challenging and cannot be achieved using conventional peak height or area quantitative calibration methods due to the significant overlapping with the solid phase.[18]

The crystallisation profiles for the peaks describing the change in solute concentration and solid production are shown in Figure 4-9. The circled points depict the spectra selected in Figure 4-8.

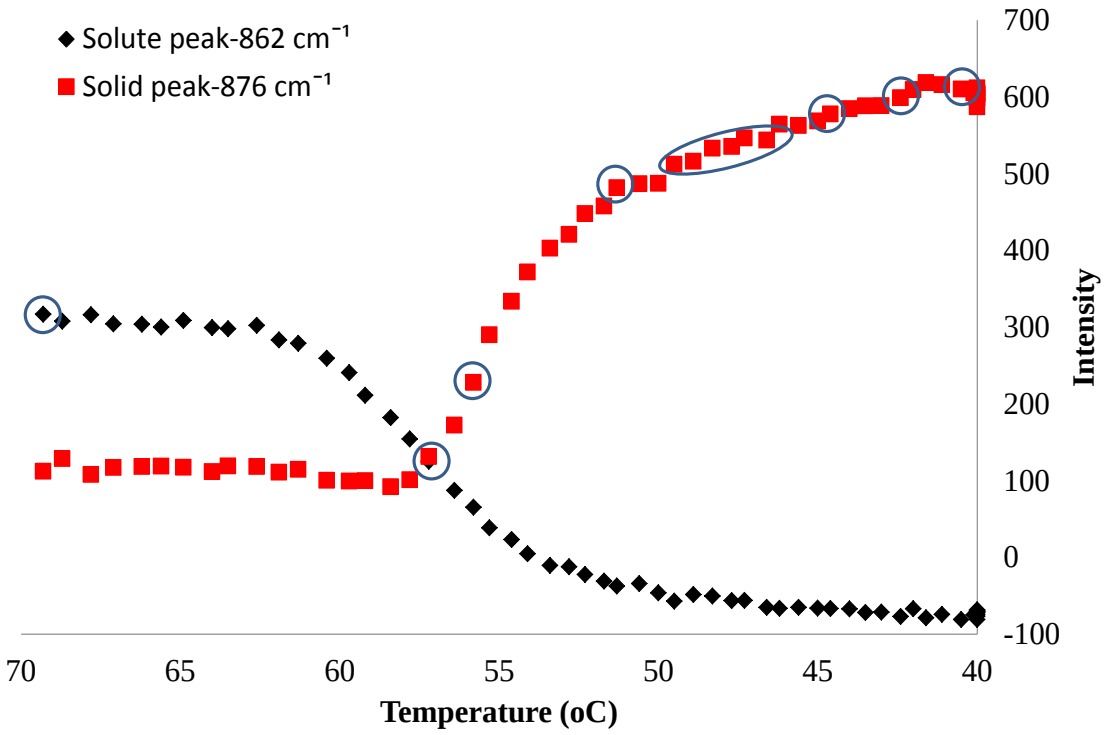

Figure 4-9: Crystallisation profile of L-glutamic acid from experiment 5 (45 g/L, 3 Hz 30 mm, 40°C final temp) based on 1st derivative Raman spectra at 862 and 876 cm^{-1}

As can be seen in Figure 4-9, the intensity of both the solute and solid crystallisation profiles remains steady at first, until approximately 30 minutes (when plotted against time, figure not shown) when the intensity of the solute profile (black) begins to decrease. This indicates the supersaturation of the solution is beginning to decrease as the nucleation temperature is approached. The delay at the start of the measurements is due to a slower cooling profile being employed which means it takes longer to reach the nucleation temperature. At ~36 minutes there is a strong increase in the intensity for the solid phase (red) indicating that nucleation followed by crystal growth are beginning to take place. The intensity of the solid phase is not zero to begin with as this peak overlaps with that of the solute peak. The intensity then begins to level off around 70 minutes and remains steady for the remainder of the measurements indicating that crystal growth is coming to an end and the amount of material being measured in the reactor is relatively constant. The crystallisation profiles observed also provide an indication of the temperature at which nucleation takes place. As Figure 4-9 shows, according to the Raman measurements, nucleation

under these operating conditions takes place at around 57°C. The nucleation temperature is likely to take place a few degrees higher than the temperature indicated in the profile as Raman is not particularly sensitive and a sufficient amount of material (between 3 and 5 g/L) would need to be present before the solid phase is detected.

4.3.2 Effect of operating conditions on polymorphic form and particle size

A selection of the experiments in Table 4-1 were monitored non-invasively using Raman spectrometry to provide information on the polymorphic form of the crystals during the process. Additionally, off-line XRD and laser diffraction were carried out to provide information on the polymorphic form and particle size distribution (PSD) of the end product. This information was used to compare the properties of the particles. Figure 4-10 shows the PSDs obtained for the particles produced in some of the experiments in Table 4-1.

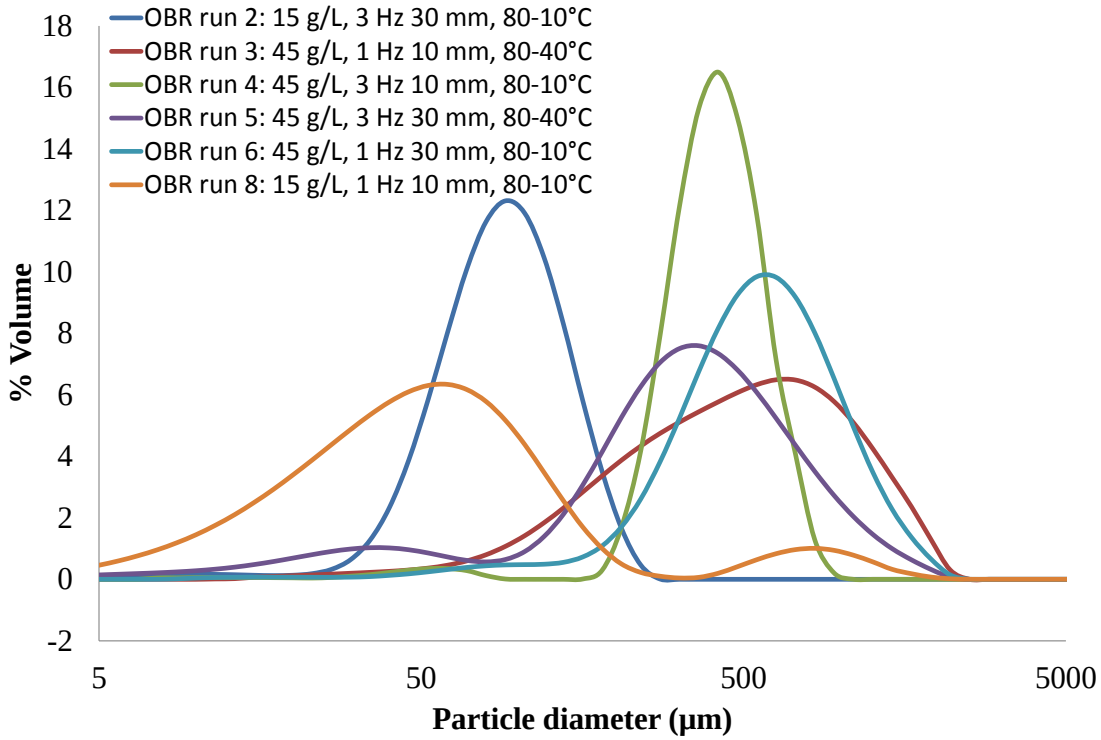

Figure 4-10: Particle size distributions for the end products obtained where the run number corresponds to the experiment number in Table 4-1

Figure 4-10 illustrates that a wide variation of PSDs are acquired when the operating conditions are differed. These differences are discussed further in the next section.

4.3.2.1 Effect of Final Temperature

The experiments in Table 4-1 were carried out using two final temperatures, 10 and 40^{o}C. As a fractional design was carried out initially only 8 of the 16 experiments were monitored using non-invasive Raman spectrometry. Therefore, the final temperature was different for some of the comparisons made between increasing frequency or increasing amplitude with a solution concentration of 45 g/L. Therefore, repeat experiments were carried out using off-line analysis to determine the effect of final temperature on crystal properties whilst keeping the other conditions unchanged. The results of the XRD and LD analysis showed that the final temperature had little effect on the crystal form or the PSD for the majority of the experiments and both the polymorphic composition and particle size distribution were similar for similar experiments with both a final temperature of 40 and 10^{o}C. This contradicts previous work reported by Ni *et al.* where the final temperature affected the crystal polymorph obtained using the same reactor, however that work was carried out using faster cooling rates.[35] Additional work by the same author showed a cooling rate of 0.5^{o}C min^{-1} was found to have a different effect on the MSZW than faster cooling rates.[7]

4.3.2.2 Effect of oscillation frequency on particle properties

The type and degree of mixing within a reactor is known to affect crystal properties. Oscillatory mixing is altered by changing the baffle frequency, the amplitude or both. Figure 4-11 shows the crystallisation profiles obtained from experiments where the frequency was increased while the amplitude was kept constant with a LGA solution concentration of 45 g/L.

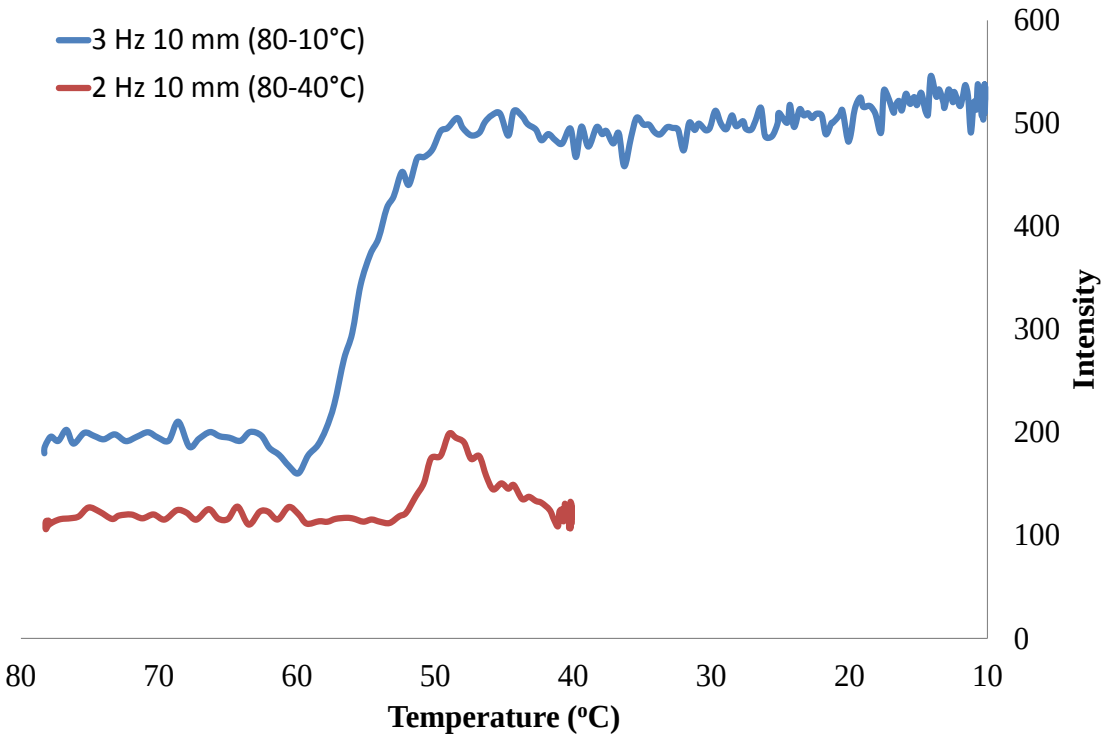

Figure 4-11: Crystallisation profile for L-glutamic acid from two experiments (4 and 17 in Table 4-1) of increasing oscillation frequency, based on 1st derivative Raman intensity at 876 cm^{-1}

Crystallisation monitoring using non-invasive Raman measurements demonstrates that there is quite a considerable difference in the nucleation temperatures as well as the profiles for the generation of the solid phase in Figure 4-11. Both the solid peaks for experiments 4 and 17 appear at 876 cm^{-1} meaning they contain more of the alpha form; however the profiles in Figure 4-11 describe the formation of both the alpha and beta forms. The profile resulting from a higher frequency of oscillation displays a higher nucleation temperature of around 60°C. At this temperature, the intensity increases quite rapidly until it levels off after 10-15 minutes. This contrasts with the results obtained with a frequency of 2 Hz, which exhibit a lower nucleation temperature of 50°C with a small increase in intensity for the solid signal immediately followed by a steady decrease. This trend is most likely observed due to the material not being suspended efficiently at this oscillation intensity. An increase in the signal intensity is observed initially as crystals begin to grow, but as increased levels of crystals are produced, of a larger size, the oscillation intensity is not sufficient enough to suspend the crystals and the material was found to sink to the

bottom of the reactor and this is why a weak Raman signal is obtained in comparison to the higher frequency. In addition, the higher frequency of 3 Hz resulted in double the yield of crystals being obtained (based on mass measured at the end of the experiment) which will also cause the Raman signal to be increased. The profile for the lowest frequency used (1 Hz, experiment 3) is not shown as no solid Raman signal was obtained. This was again thought to be due to the intensity of oscillation being inadequate to suspend the solid material as the majority of the solid material settled at the bottom of the reactor. The differences in nucleation temperature observed suggest that the frequency of oscillation affects the size of the metastable zone, therefore, affecting when nucleation takes place. It would appear that as the frequency is increased, the metastable zone width narrows and nucleation occurs at a higher temperature. This agrees with previous work carried out in the OBR where an increase in mixing intensity resulted in a decrease in the MSZW as well as increased transformation of α-crystals to β-crystals.[35]

The XRD spectra for the products of the 3 experiments (3, 14 and 17) at increasing oscillation frequency all show a similar mixture of polymorphs with the alpha form being the major product which agrees with the Raman spectra. The higher frequency (3 Hz) appears to result in a slightly increased level of β-form whilst the lowest frequency (1 Hz) produced a higher level of α-form. This agrees with previous work carried out in a batch OBR.[35] A mixture of polymorphs was obtained in all three cases according to the off-line XRD analysis, and although the alpha polymorph was the major form, the peak at the wavenumber selected describes the solid phase (i.e. the alpha and the beta polymorph). However the position of the peak confirms that the alpha form is the major product. Figure 4-12 shows the particle size distributions (PSDs) obtained for the three experiments of increasing oscillation frequency.

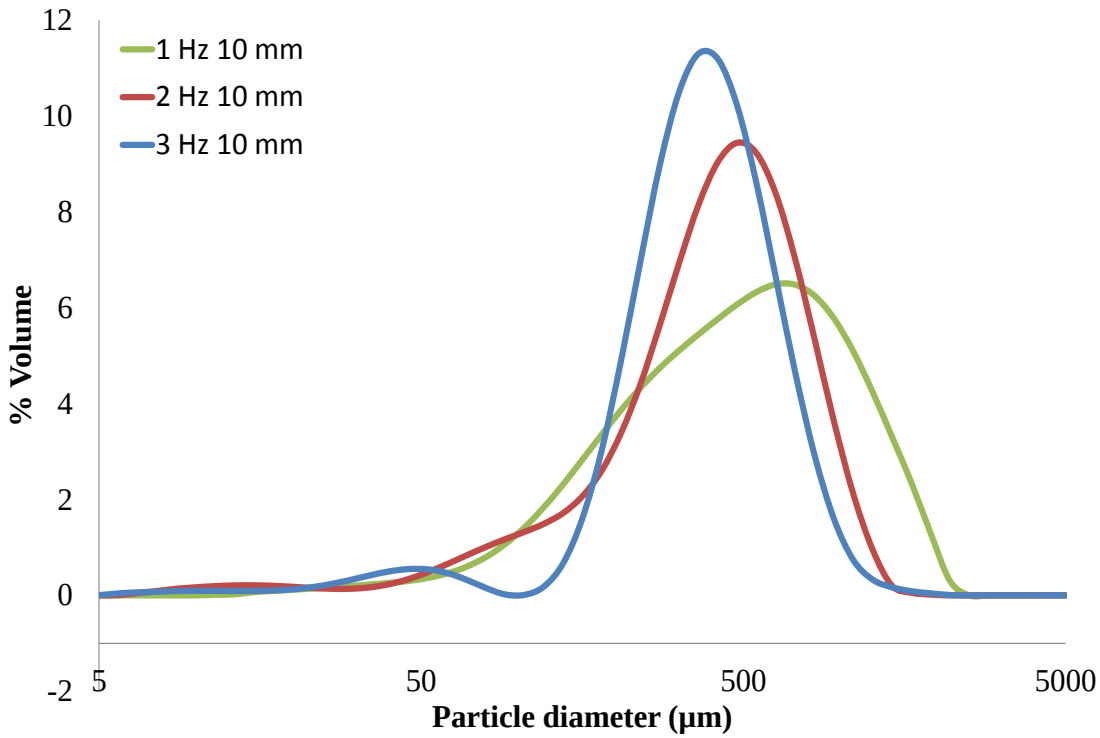

Figure 4-12: Particle size distributions of LGA for experiments 3, 14 and 17 in Table 4-1 when baffle frequency was increased

Figure 4-12 shows the PSD starts off relatively wide at the lowest frequency (green) and becomes narrower as the frequency is increased. As the laser diffraction method assumes the particles shape is spherical, particles which are non-spherical show deviating distributions as the particle shape has a strong impact on the PSD. This is due to the error incurred by using the spherical model to calculate the distribution of particles that diverge from a spherical shape. The orientation of the particles also impacts the measured distribution as this is related to the particle shape; therefore, needle-shaped particles will have a particularly large orientation effect in LD measurements with increasing aspect ratio (length-to-width ratio).[41, 42] Accordingly, the wider, more irregular distribution obtained at 1 Hz would be expected to have a significant amount of needle shaped beta crystals while the narrow distribution at 3 Hz should contain more prismatic alpha crystals. However, the XRD data for the lowest frequency (1 Hz) had slightly more alpha form crystals which is in contrast to the measured particle size distribution which would be expected to contain more of the beta polymorph out of the three distributions. However, the PSD observed could

also be a result of the low intensity of mixing used which meant not all of the material was suspended efficiently and lay at the bottom of the reactor. These conditions could also result in slower nucleation and growth rates over an extended period of time and lead to a wider range of particle sizes being obtained.

4.3.2.3 Effect of oscillation amplitude on particle properties

Figure 4-13 shows the crystallisation profiles obtained from experiments where the amplitude was increased while the frequency was kept constant using a solution concentration of 45 g/L.

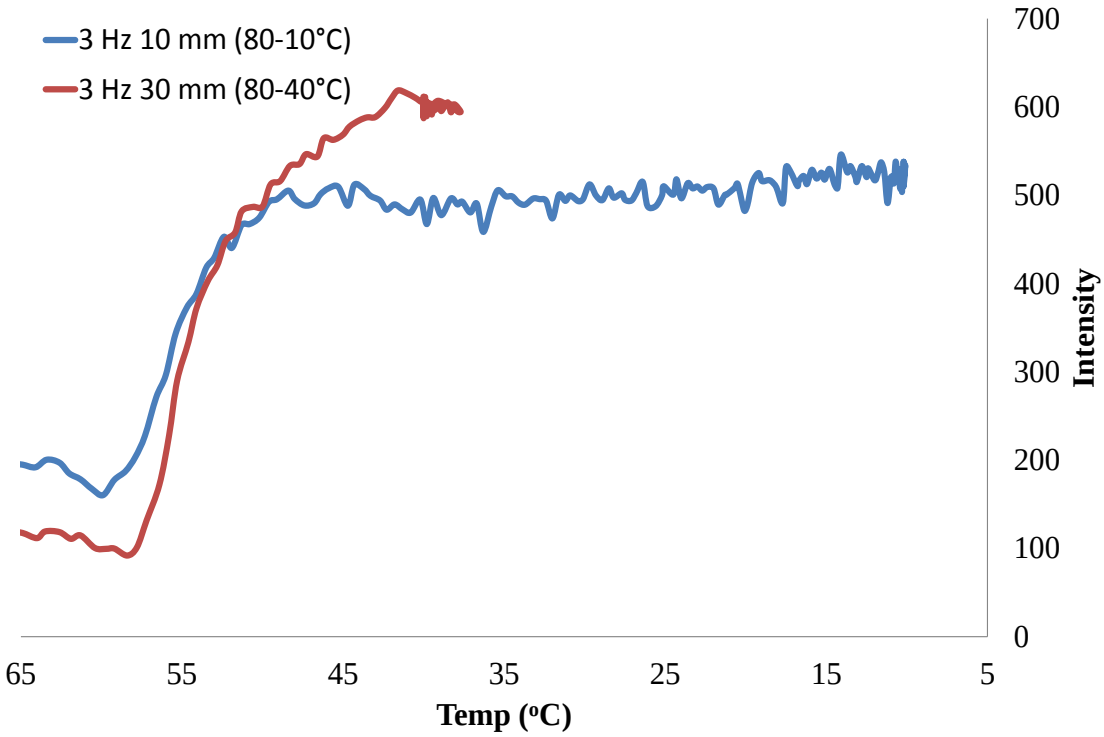

Figure 4-13: Crystallisation profiles for alpha and beta LGA for experiments 4 and 5 in Table 4-1 when baffle amplitude was increased, based on 1st derivative Raman intensity at 876 and 873 cm^{-1}, respectively

The profiles obtained using a frequency of 3 Hz at 10 or 30 mm amplitude result in a strong Raman signal for a mixture of polymorphs. The nucleation temperature is relatively similar for both the higher and lower amplitudes with nucleation occurring at 60°C at 10 mm amplitude and ~58°C at 30 mm. The more noticeable difference in

the profiles is that the intensity of the solid form increases further at a higher amplitude (red), most likely due to the larger amount of particles produced when more intense oscillation is applied. The amplitude has less of an effect than frequency on the nucleation temperature, changing it by only a few degrees. This could suggest a small change in the size of the meta-stable zone is occurring with varying oscillation amplitude which will have an impact on the polymorphic composition of the product and the particle size distribution. However, as the difference observed is relatively small, it could also mean that amplitude has little effect on the nucleation temperature and that it is a result of experimental variation as a small range of different values would be expected with repeat experiments.

As with increasing the frequency, an increase in the oscillation amplitude results in increased formation of beta crystals which was confirmed by XRD and microscopy. Figure 4-14 shows the PSDs obtained from four experiments where the amplitude was increased while the frequency was kept constant at two different values, 1 and 3 Hz using a solution concentration of 45 g/L.

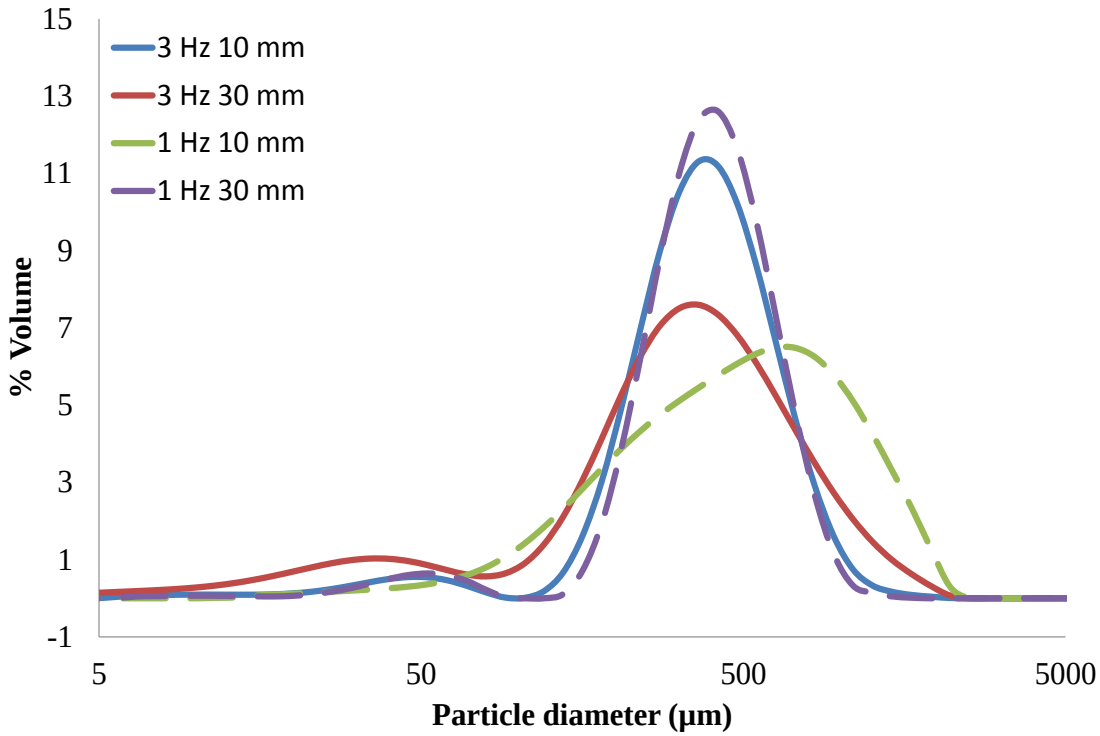

Figure 4-14: Particle size distributions of LGA for experiments 3, 5, 14 and 15 in Table 4-1 when baffle amplitude was increased

At a higher frequency of 3 Hz, the PSD is similar at both amplitudes with only a relatively small difference in the average particle size. This result agrees with the crystallisation profiles in Figure 4-13 where similar profiles were obtained at both amplitudes with little difference in the nucleation temperature. This suggested that particles with similar properties would be obtained which is confirmed in Figure 4-14. The distribution is slightly wider at a higher amplitude, most likely due to the increase in the beta polymorph with an increase in amplitude. The PSD obtained for a frequency of 1 Hz and amplitude of 30 mm resembles those obtained at a higher amplitude. The mean particle size is 50 μm higher than that obtained at 3 Hz 30 mm which is expected as an increase in the frequency was found to result in a decrease in the average particle size as shown in Figure 4-12. The PSD obtained at 1 Hz 10 mm is quite different from the others most likely due to the reasons explained previously (*i.e.* poor suspension of material leading to slow nucleation and growth).

4.3.2.4 Effect of solution concentration on particle properties

Figure 4-15 shows the crystallisation profiles for high and low solution concentrations of LGA obtained at a fixed frequency and amplitude.

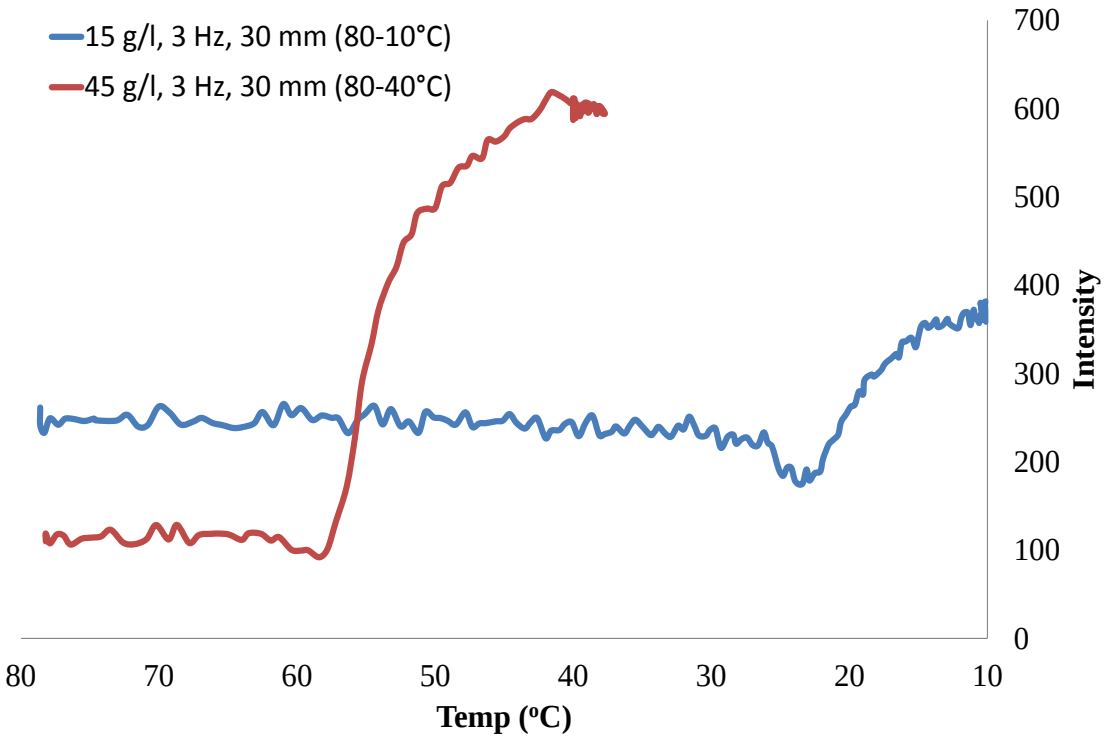

Figure 4-15: Crystallisation profiles for pure alpha and mixed LGA for experiments 2 and 5 in Table 4-1 when solution concentration was increased, based on 1st derivative Raman intensity at 877 and 876 cm^{-1}, respectively

Figure 4-15 demonstrates there is quite a significant difference in the crystallisation profiles for the two different solution concentrations. The higher concentration of 45 g/L has a much higher nucleation temperature of 58°C and produces a more intense signal for the solid phase due to the higher concentration of crystals suspended in the vessel. The 15 g/L solution nucleates considerably later in the crystallisation at a temperature of ~23°C which explains why a number of the experiments in Table 4-1 (1, 7, 13 and 16) resulted in no crystals being produced as the final temperature of 40°C was too high for nucleation and crystal growth to take place. The difference in the two profiles suggests a narrower MSZW for increasing solution concentration due to the much higher nucleation temperature.

The XRD patterns obtained from the end products of both crystallisation experiments show the lower concentration of 15 g/L results in the pure alpha form being obtained while a higher concentration leads to a 50:50 mixture of polymorphs. The solution concentration also affects the mean particle size which increases with an increase in

the concentration. This result is expected as a higher solution concentration means there are more solute molecules in the liquid phase that can be integrated into the crystal lattice resulting in a larger average particle size, i.e. the concentration of molecules surrounding the growing particles is higher.

In previous studies in the OBR by *Ni et al.*, it was found that an increase in concentration led to a decrease in the nucleation rate. This would result in a lower amount of crystals growing to a larger size at a high concentration, whilst at a low solution concentration, there would be increased nucleation and the resultant crystals would be smaller. The outcome for the different solution concentrations also agrees with this previous study where low concentrations favour α-form crystals while higher solution concentrations result in increased levels of β-form crystals. In addition, a larger particle size obtained using a higher solution concentration was also observed.[7] Figure 4-16 shows the PSDs obtained from four experiments where the concentration was increased while the frequency and amplitude were kept constant at two different values, 2 Hz and 10 mm and 3 Hz and 30 mm.

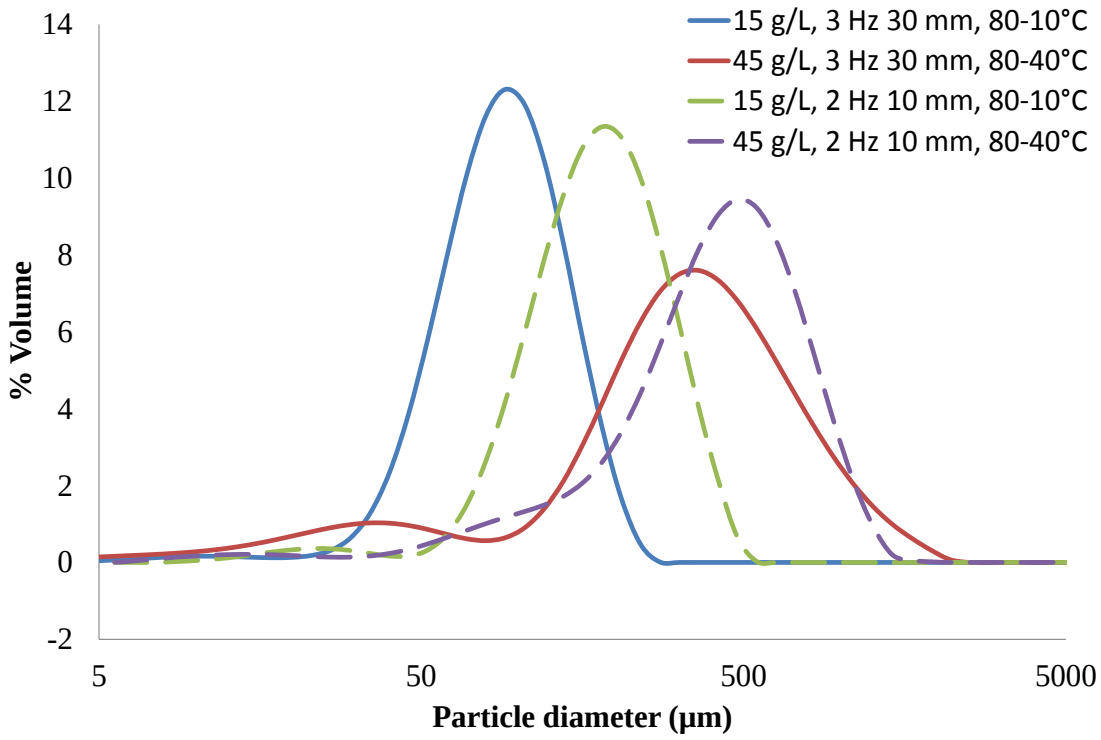

Figure 4-16: Particle size distributions for 4 of the experiments of increasing solution concentration in Table 4-1 using L-glutamic acid.

Figure 4-16 shows that for both the frequency and amplitude combinations used, the average particle size increases for an increase in the solution concentration. This result is expected as a higher solution concentration means there are more solute molecules in the liquid phase that can be integrated into the crystal lattice resulting in a larger average particle size. Additionally, a narrower distribution is obtained for the lower 15 g/L solution concentration. This is due to the solution concentration also having an effect on the polymorph obtained. The lower concentration results in a narrow distribution as the crystals are predominantly prismatic alpha form. Conversely, a higher solution concentration produces a mixture of polymorphs which is why a wider, more irregular distribution is obtained.

4.3.3 Comparison of OBR and STR

A selection of experiments was carried out in a stirred tank reactor (STR) so that the results could be compared to those obtained in the batch OBR. Table 4-7 describes the conditions used for these experiments.

Table 4-7: Additional experiments carried out in the STR

Experiment	Type of Cooling	Concentration (g/L)	Final Temp (^{o}C)	Mixing Intensity (rpm)
21	Slow	45	40	200
22	Slow	45	40	100
23	Slow	15	10	200
24	Slow	15	10	100
25	Rapid	15	10	200
26	Rapid	45	10	200

Table 4-8: Outcome of the experiments carried out in the STR showing the polymorphic composition of the final product using Raman and XRD, the particle size measurements using LD and the solid recovery and yield.

	Polymorph Obtained						
Experiment	**Raman**	**XRD**	**d (0,5) (µm)**	**d (4,3) (µm)**	**Span**	**Solid recovery (g)**	**Yield (%)**
21	β	β	212.3	285.5	2.79	25.02	55.6
22	β	β	285.0	337.6	2.38	18.64	41.4
23	-	-	-	-	-	-	-
24	-	-	-	-	-	-	-
25	-	-	-	-	-	-	-
26	α/β	α/β	274.4	295.5	1.32	34.29	76.2

The crystallisations in Table 4-7 were also monitored using non-invasive Raman spectrometry and off-line XRD and laser diffraction analyses were carried out on the end products. An important difference that was noted between the stirred tank and OBR crystallisations is that no crystals were obtained for any of the conditions used in the stirred tank for a solution concentration of 15 g/L. A combination of the low solution concentration and wider MSZW (slower nucleation) in this type of vessel may mean that conditions within the vessel do not reach adequate levels of supersaturation in order for crystals to form at this concentration. Figure 4-17 shows the crystallisation profiles obtained for two of the experiments at 45 g/L, for impeller speeds of 100 and 200 rpm.

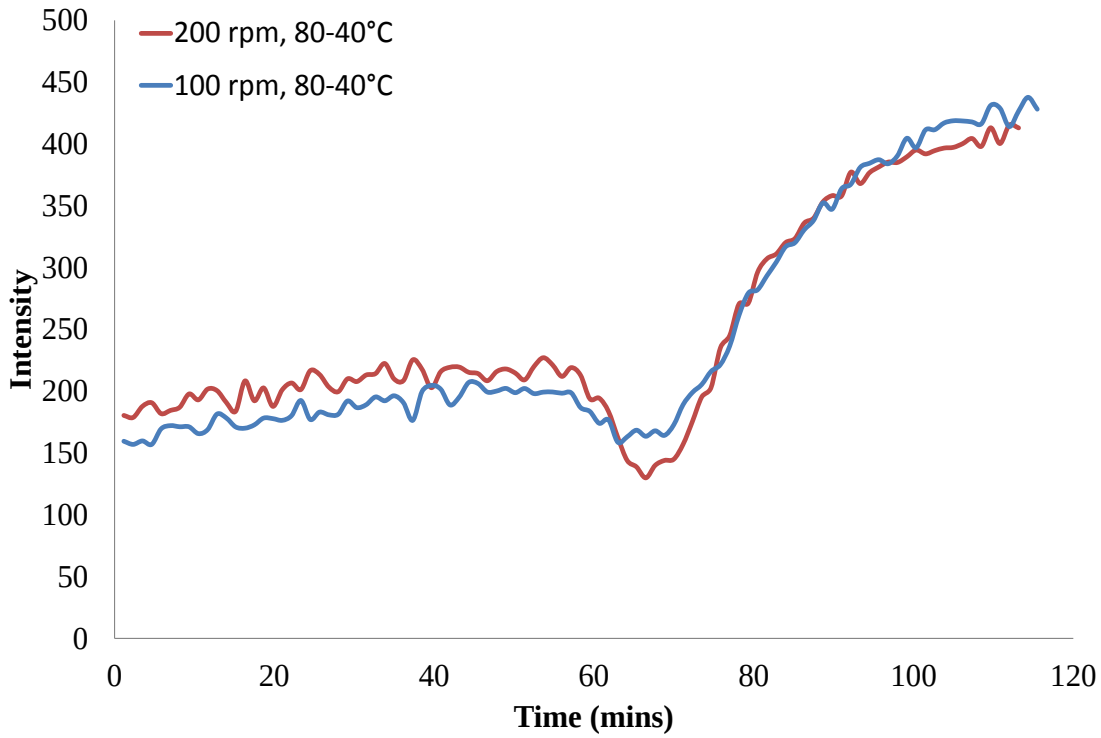

Figure 4-17: Crystallisation profiles for beta LGA for experiments 21 and 22 in Table 4-7 when the speed of mixing was increased in a stirred tank, based on 1st derivative Raman intensity at 872 cm^{-1}

Figure 4-17 shows that an increase in the mixing speed in the STR does not appear to affect the nucleation temperature greatly for the two different impellor speeds attempted in this study. Additionally, the polymorphic form is not impacted as according to both the Raman spectra and XRD patterns, the pure beta polymorph was obtained with either of the mixing conditions described. According to previous work carried out in a STR, agitation intensity affects the MSZW and therefore the nucleation temperature, but this became more apparent at impeller speeds above 200 rpm where a decrease in the MSZW is observed with an increase in the mixing intensity.[43, 44] Figure 4-18 shows the PSDs obtained for the two stirred tank experiments.

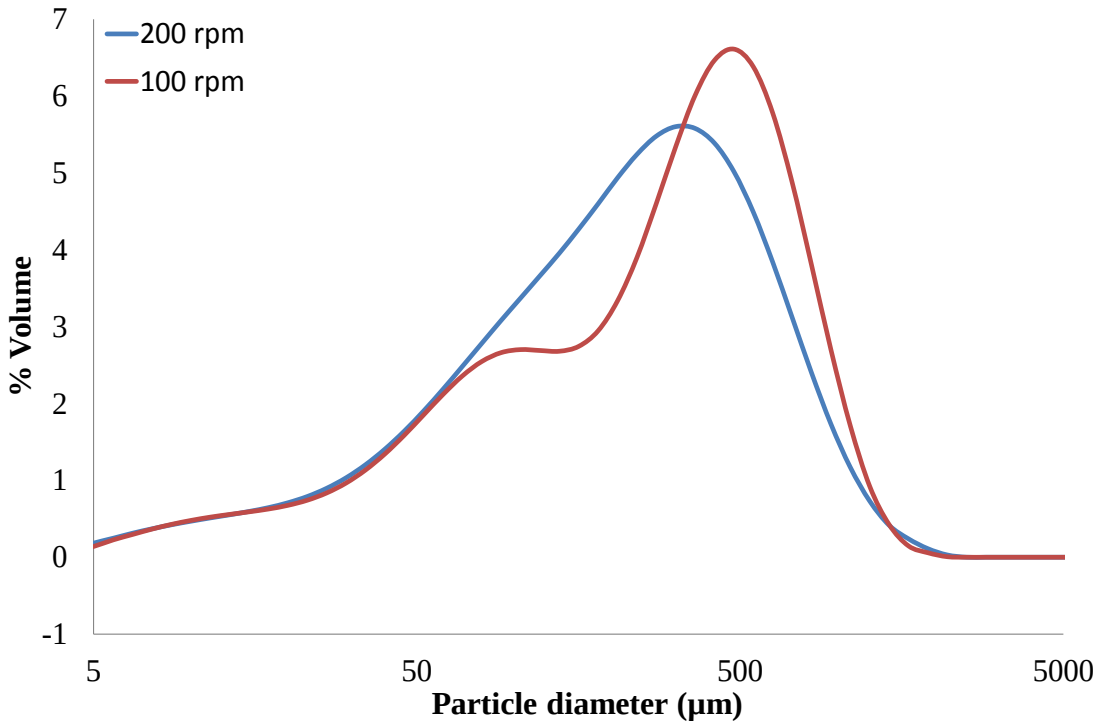

Figure 4-18: Particle size distributions of LGA for experiments 21 and 22 in Table 4-7 when impeller agitation was increased in a stirred tank

The distributions in Figure 4-18 show that the mean particle size decreases as the impeller speed is increased. This could possibly be due to increased particle breakage (attrition) due to the particles colliding with the impeller, walls of the vessel or other particles due to the increased intensity of mixing within the vessel.[35] This observation was also made in relation to operation of the OBR where an increase in the frequency resulted in a decrease in the mean particle size. In addition, the lowest mixing intensity shows a bimodal distribution indicating two different ranges of particle size. This is most likely due to the intensity of mixing being inefficient to suspend all of the material so that some of the material is suspended and the remainder sinks to the bottom of the reactor resulting in the differences in particle growth and the resulting particle size observed. As with the OBR, the low mixing intensity used could also result in slower nucleation and growth rates leading to a wider range of particle sizes. Figure 4-19 shows a comparison of the profiles obtained using intense mixing in the STR and OBR and a solution concentration of 45 g/L.

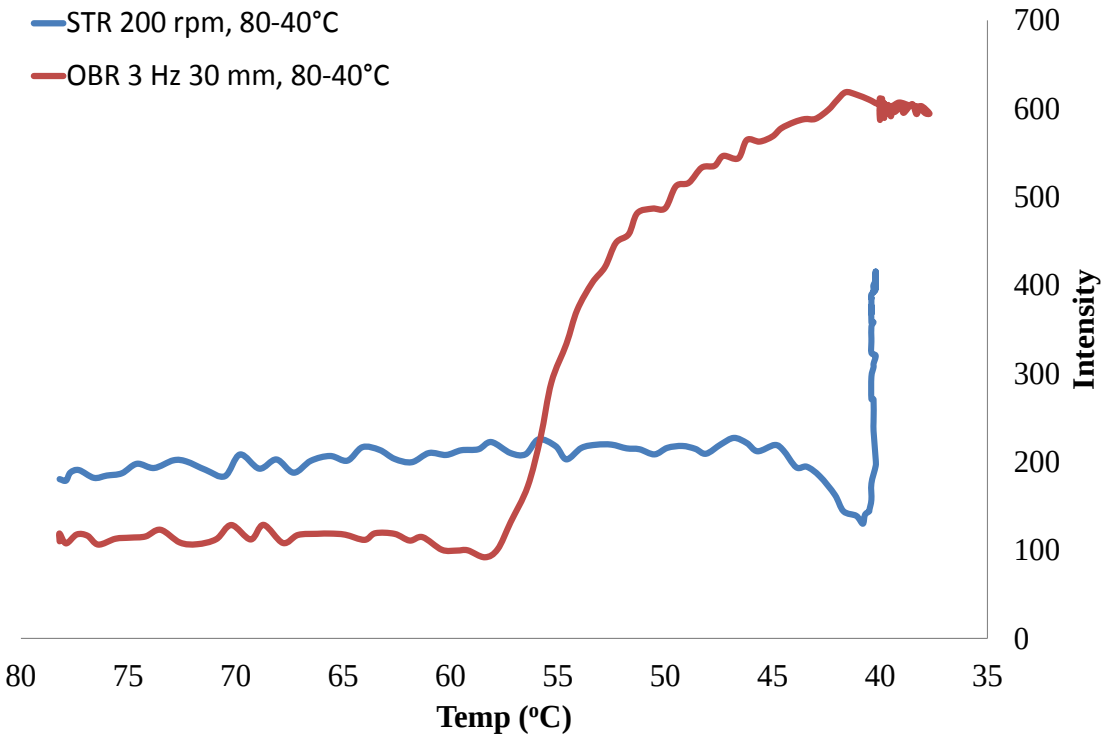

Figure 4-19: Comparison of crystallisation profiles for LGA for experiments 5 and 21 in Tables 4-1 and 4-7 obtained in STR and OBR using intense mixing, based on 1st derivative Raman intensity at 876 and 872 cm^{-1}, respectively

The crystallisation profiles illustrated in Figure 4-19 for the different batch reactors are quite different. At the same solution concentration of 45 g/L, the nucleation temperature is considerably higher in the OBR compared to in the stirred tank by almost 20°C. This could be due to the improved mixing in the OBR giving more uniform temperature and supersaturation levels, resulting in nucleation happening at a higher temperature and therefore a lower supersaturation which also suggests a narrower MSZW in this type of reactor. As nucleation within the stirred tank happened at a much lower temperature, this suggests a much wider MSZW to overcome for nucleation to occur. Studies of L-glutamic acid by *Ni et al.* have shown that when the MSZW for a STR and OBR were compared for similar conditions, crystallisation in the OBR occurred at a higher temperature, which agrees with the results in Figure 4-19. The MSZW in the OBR was found to be smaller than in the STR meaning that nucleation occurs at a higher temperature (lower supersaturation).[34] The Raman and XRD results also show there is a difference in

the polymorphic composition of the end products from the different reactors. The STR produces pure beta LGA while the OBR gives a mixture of both the alpha and beta forms. This suggests the difference in mixing in the two types of reactor may affect the polymorphic composition of the end product. As the alpha form or a mixture of forms was only produced in the OBR using slow cooling, it was thought the baffles may accelerate nucleation and promote the formation of the alpha form.

A comparison of the distributions obtained using intense mixing in the STR and OBR and a solution concentration of 45 g/L are shown in Figure 4-20.

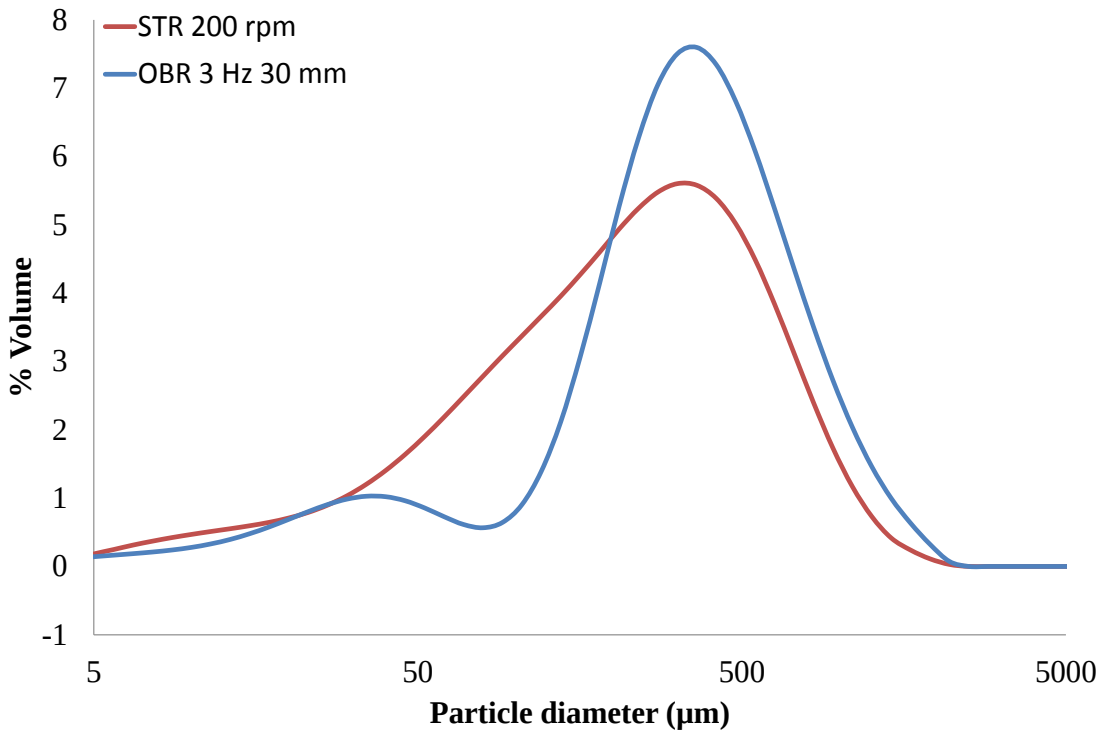

Figure 4-20: Comparison of particle size distributions of L-glutamic acid obtained in STR and OBR using intense mixing

Figure 4-20 shows that the average particle size obtained between the two reactors is approximately the same using the above conditions. However, there is quite a difference in the distributions acquired. The PSD obtained from the product of the OBR has a larger narrower peak and a smaller peak indicating a mixture of polymorphs or a large number of fines. On the other hand, the end product from the

STR shows a much broader distribution. This suggests that there is a difference in the polymorphic composition of the end products from the different reactors. The STR results in the pure beta polymorph being obtained which explains the broad, irregular distribution while the OBR gives a mixture of both the alpha and beta forms which describes why two peaks are observed.

The effect of rapid cooling on particle properties was also compared in the two reactors using a solution concentration of 45 g/L, and the crystallisation profiles and particle size distributions are shown in Figure 4-21 and Figure 4-22, respectively.

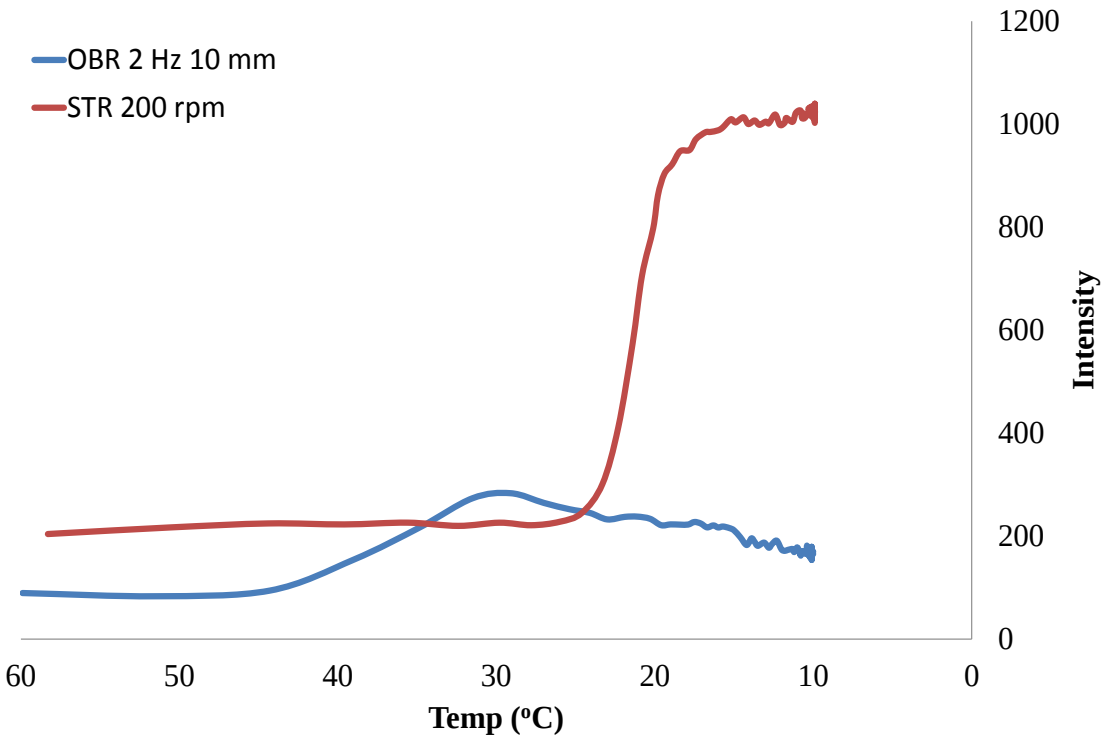

Figure 4-21: Crystallisation profiles of LGA for experiments 19 and 26 in tables 4-1 and 4-7 from STR and OBR using rapid cooling, based on 1st derivative Raman intensity at 876 cm^{-1}

As Figure 4-21 shows, the crystallisation profiles obtained are significantly different for the STR and OBR when rapid cooling is used. Similar observations were made as for slow cooling, i.e. in the OBR; crystals are formed at a much higher temperature than in the stirred tank. It is likely the signal for the solid phase in the OBR was reduced as the crystals gradually sank to the bottom of the reactor; this was also

observed using slow cooling with the same conditions and the crystallisation profile shows a similar trend to that given in Figure 4-11 for slow cooling at the same oscillation intensity.

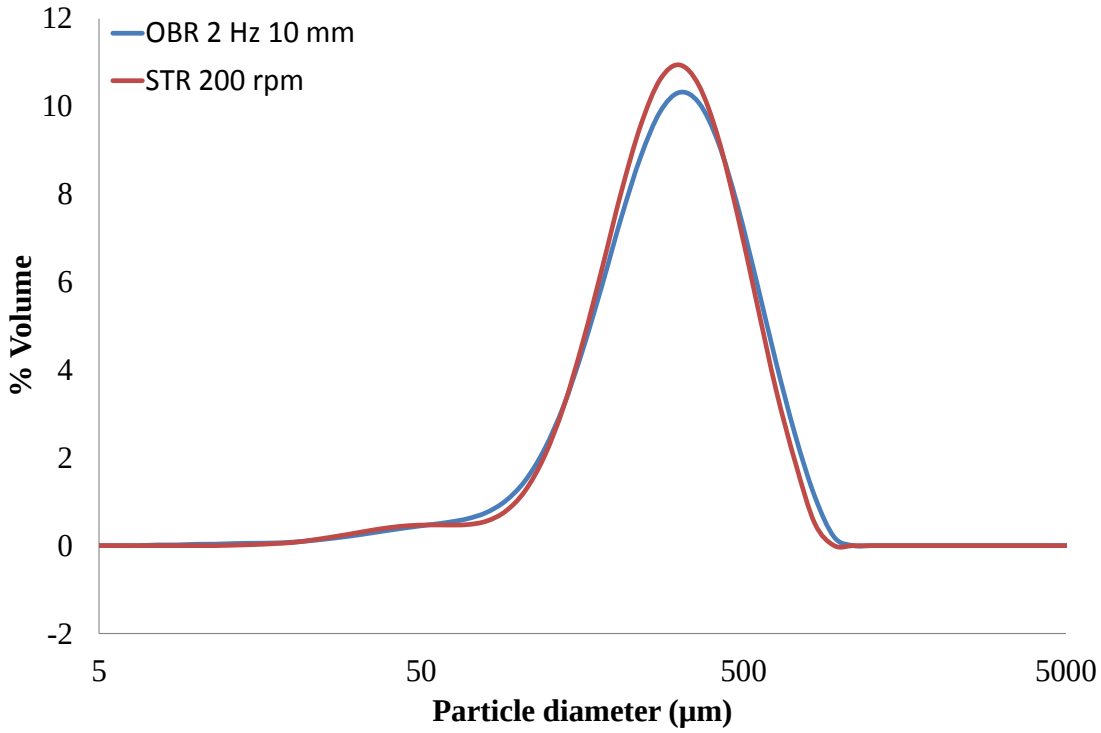

Figure 4-22: Comparison of particle size distributions of LGA for experiments 19 and 26 in tables 4-1 and 4-7 obtained in STR and OBR using rapid cooling

Figure 4-22 shows that very similar distributions are obtained when rapid cooling is employed in both the stirred tank and OBR, suggesting that the products were similar; this was confirmed as the XRD spectra for both products are very similar and show a mixture of polymorphs with alpha crystals being the major form, despite the difference in nucleation temperature. These results suggest that the cooling rate is a major influence on the particle properties as the variation between the PSDs of the products has been removed between the two different reactors. The difference in the nucleation temperature does not seem to affect the final product significantly.

As Figure 4-21 shows the crystallisation profiles obtained are significantly different for the STR and OBR when rapid cooling is used. This is unusual considering the PSDs are so similar. Similar observations are made as for slow cooling in that in the

OBR crystals are formed at a much higher temperature than in the stirred tank. It was thought as the signal for the alpha polymorph in the OBR was so weak that during the crystallisation the material had sunk to the bottom of the reactor which could not be seen during the experiment as the reactor was covered in foil. At the end of the crystallisation a considerable amount of material could be seen to be settled on the base of the vessel and the profile showed a similar trend to that obtained using slow cooling and the same oscillation intensity (Figure 4-11). Therefore the crystallisation profile and PSD obtained for the lower concentration of 15 g/L using rapid cooling was also compared which is shown in Figure 4-23 and Figure 4-24.

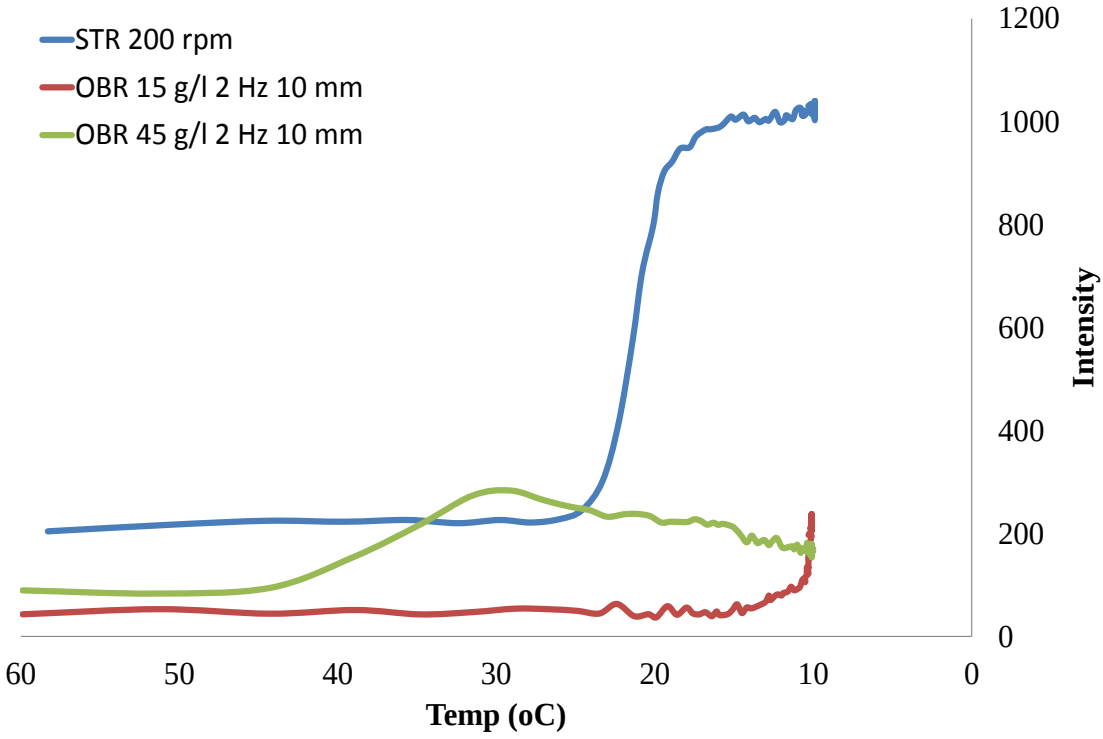

Figure 4-23: Crystallisation profiles for L-glutamic acid from the STR (experiment 26 in Table 4-7) and two different solution concentrations in the OBR (experiments 19 and 20 in Table 4-1) using rapid cooling, based on 1st derivative Raman intensity at 876 and 877 cm^{-1}

Figure 4-23 shows that as well as the clear difference between the experiments in the STR and OBR at the same solution concentration already discussed, the nucleation temperature is much lower for the 15 g/L which was also observed using slow cooling (Figure 4-15).

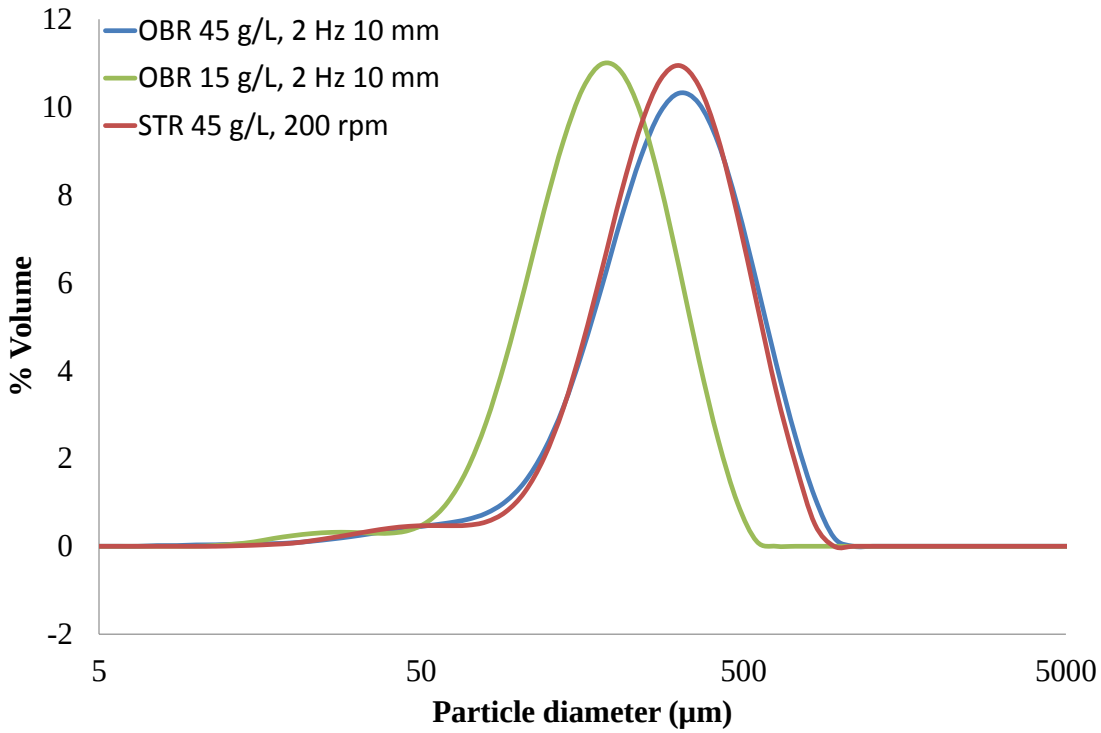

Figure 4-24: Comparison of particle size distributions of L-glutamic acid obtained in the STR and for two solution concentrations in the OBR using rapid cooling

These results suggest that the cooling rate is a major influence on the particle properties as the variation between the PSDs of the products has been removed between the two different reactors. It was thought that rapid cooling of the solutions to 10^{o}C caused faster depletion of the supersaturation due to a large number of small nuclei forming and relatively fast crystal growth meaning the mixing employed had little effect on the properties of the particles and resulted in particles of the same size in both reactors. The difference in the nucleation temperature does not seem to affect the final product however the solution concentration has the same effect as with slow cooling on the average particle size obtained and the polymorphic composition, which is exclusively alpha form for the 15 g/L solution but a 45 g/L solution concentration in both the STR and OBR gives a mixture of forms.

It was also important to investigate if the results obtained in the batch OBR were repeatable and if particles of the desired polymorphic form and particle size could be

produced consistently. Therefore, several of the experiments were repeated three times and Figure 4-25 shows the particle size distributions obtained using a frequency of 1 Hz and 30 mm.

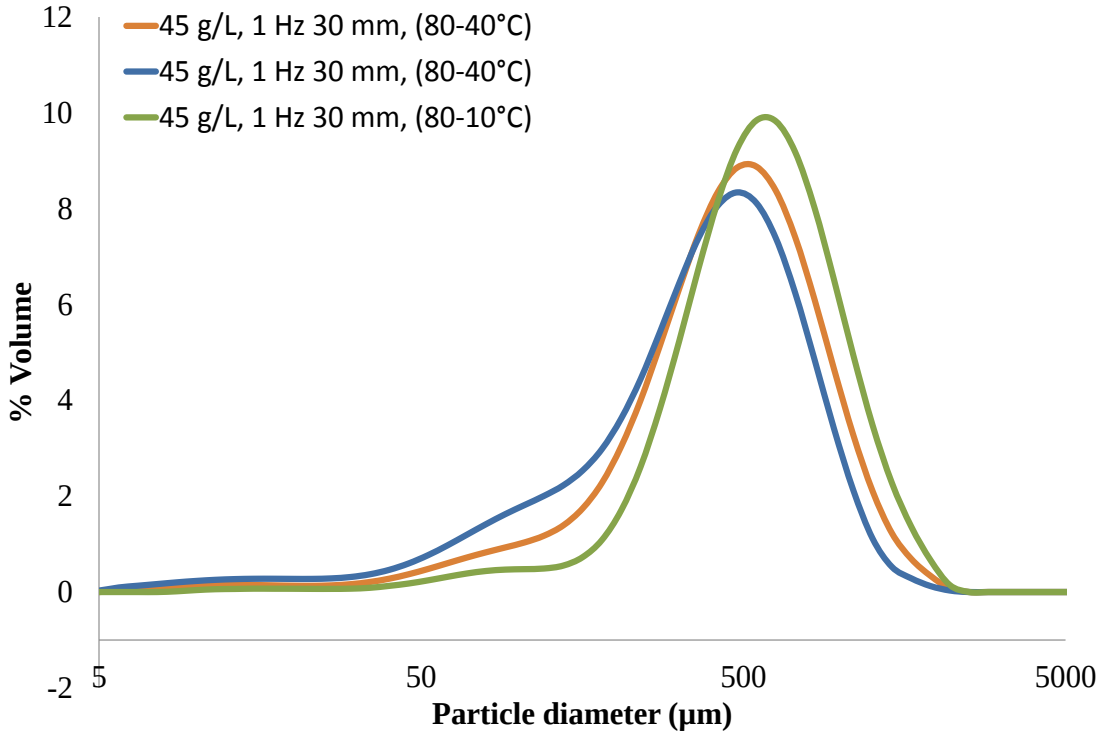

Figure 4-25: Particle size distributions of LGA for two repeat experiments and a third at a lower final temperature using an oscillation intensity of 1 Hz and 30 mm

As Figure 4-25 shows, although not identical, a similar average particle size and distribution is obtained for all three repeat experiments using the same oscillation intensity. The only set of conditions where this was not the case was using an intense oscillation of 3 Hz and 30 mm. As the mixing within this type of vessel is increased beyond a certain magnitude the mixing becomes more chaotic.[45] This will most likely result in decreased reproducibility of particle properties between experiments. This suggested that batch OBR technology does indeed provide more uniform mixing and therefore conditions within the vessel than that obtained in a stirred tank (Figure 4-26). It seems, therefore, that particles of LGA with similar PSDs can be produced repeatedly, which if transferable to other compounds is especially important for the crystallisation of pharmaceutical products.

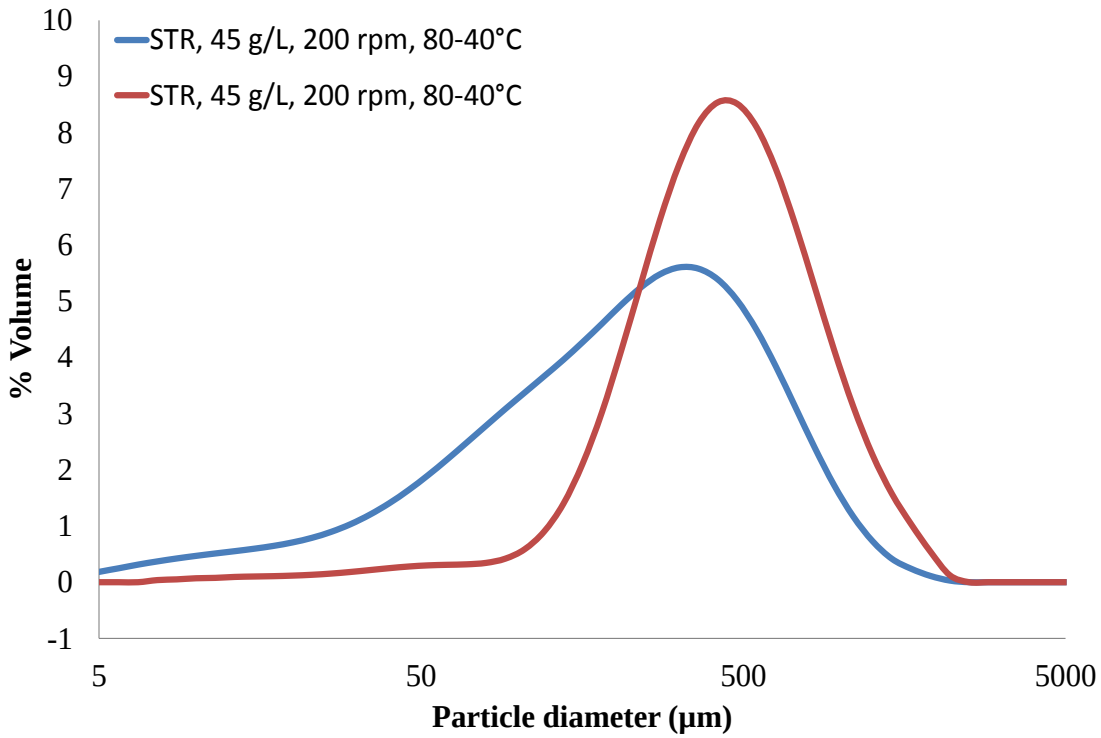

Figure 4-26: Particle size distributions of LGA for two repeat experiments in a stirred tank using a mixing intensity of 200 rpm

4.4 Conclusions

The data presented demonstrates that operating conditions are an important consideration in crystallisation processes. The study carried out in the batch OBR showed that several conditions including the oscillation intensity, solution concentration and final temperature impacted the particle properties including particle size and distribution which has not been reported previously. Additionally, the batch OBR conditions appear to be more important to the outcome of the particle properties than with the batch STR suggesting that conditions could be selected to obtain particles of desired particle size, etc.

The oscillation frequency had an effect on the particle size distribution as well as the polymorphic form. Increasing the frequency at low amplitude gave a narrower distribution and a slightly increased level of the beta form. The opposite effect was observed when increasing the amplitude at a fixed frequency which gave a broader particle size distribution but still resulted in increased levels of beta crystals. The solution concentration had an effect on the particle size and the polymorph. A higher concentration resulted in a greater mean particle size and increased amounts of the beta form.

On comparing the results obtained in the OBR with the STR, several observations were made. When a solution concentration of 15 g/L was used in the STR, crystallization did not occur at any conditions used. At a higher solution concentration, nucleation occurred at a much higher temperature in the OBR than in the STR, which indicated the MSZW in the OBR was smaller and nucleation happened at a lower level of supersaturation. This resulted in a difference in the PSD and polymorphic composition of the products obtained in each reactor. However, when rapid cooling was employed, although similar differences in the nucleation temperatures were observed as when slow cooling was used for the OBR and STR, the effects on the average particle size and distribution were not significant, suggesting that the rate of cooling used is a major influence on the properties of the LGA particles obtained.

The results show that varying the operating conditions in the batch OBR impacts the properties of the particles including the particle size, PSD and polymorphic composition. Repeat experiments also showed that these results could be replicated. This suggests that by controlling the operating conditions, a product with the desired properties can be produced. However, only the pure alpha form and mixtures of the alpha and beta polymorph were obtained in the batch OBR reactor using all the conditions attempted. Non-invasive Raman measurements provided useful information on the difference in nucleation temperature when different conditions and reactors were used which helped to explain the differences in PSD and polymorph of the final product. The pure alpha form was produced in the batch OBR using a number of operating conditions. Slow cooling of a low solution concentration of 15 g/L in combination with a low final temperature of 10^{o}C under all oscillation conditions resulted in the alpha form being obtained. Slow cooling of a 45 g/L solution concentration using a final temperature of 40^{o}C and an oscillation of 1 Hz and 10 mm also produced the alpha form. Alternatively, rapid cooling with a low solution concentration and an oscillation of 2 Hz and 10 mm gave the alpha form. Principal components analysis was beneficial in separating the contributions to the Raman spectra from the solid concentration and the polymorphic form, however, quantitative analysis methods such as PLS were found to be more challenging to apply due to the peak shift associated with a change in the polymorphic composition and it was thought this would be better applied to quantifying the pure forms.

4.5 References

1. J. Bauer, S. Spanton, R. Henry, J. Quick, W. Dziki, W. Porter and J. Morris, Ritonavir: An Extraordinary Example of Conformational Polymorphism, *Pharmaceutical Research,*, 2001, **18**, 859-866.
2. H. Qu, H. Alatalo, H. Hatakka, J. Kohonen, M. Louhi-Kultanen, S. Reinikainen and J. Kallas, Raman and ATR FTIR spectroscopy in reactive crystallization: Simultaneous monitoring of solute concentration and polymorphic state of the crystals, *Journal of Crystal Growth*, 2009, **311**, 3466-3475.
3. J. Bernstein, Polymorphism of L-Glutamic Acid: Decoding the tr--B Phase Relationship via Graph-Set Analysis, *Acta Crystallographica Section B*, 1991, **47**, 1004-1010.
4. N. Hirayama, K. Shirahata, Y. Ohashi and Y. Sasada, Structure of alpha form of L-Glutamic Acid. alpha-beta Transition, *Bulletin of the Chemical Society of Japan*, 1980, **53**, 30-35.
5. K. Srinivasan and P. Dhanasekaran, Nucleation control and crystallization of l-glutamic acid polymorphs by swift cooling process and their characterization, *Journal of Crystal Growth*, 2011, **318**, 1080-1084.
6. T. Ono, J. H. Horst and P. J. Jansens, Quantitative Measurement of the Polymorphic Transformation of l-Glutamic Acid Using In-Situ Raman Spectroscopy, *Crystal Growth & Design*, 2004, **4**, 465-469.
7. X. Ni and A. Liao, Effects of Cooling Rate and Solution Concentration on Solution Crystallization of l-Glutamic Acid in an Oscillatory Baffled Crystallizer, *Crystal Growth & Design*, 2008, **8**, 2875-2881.
8. M. Kitamura, Polymorphism in the crystallization of L-glutamic acid, *Journal of Crystal Growth*, 1989, **96**, 541-546.
9. C. Y. Ma and X. Z. Wang, Simultaneous characterization of multiple properties of solid and liquid phases in crystallization processes using NIR, *Particuology*, 2011, **9**, 589-597.
10. M. Kitamura, Controlling factor of polymorphism in crystallization process, *Journal of Crystal Growth*, 2002, **237–239, Part 3**, 2205-2214.
11. C. Lindenberg and M. Mazzotti, Effect of temperature on the nucleation kinetics of α l-glutamic acid, *Journal of Crystal Growth*, 2009, **311**, 1178-1184.
12. M. Kitamura and T. Ishizu, Kinetic effect of L-phenylalanine on growth process of L-glutamic acid polymorph, *Journal of Crystal Growth*, 1998, **192**, 225-235.
13. M. Kitamura and H. Funahara, Effect of L- And D-Phenylalanine on Crystallization and Transformation of L-Glutamic Acid Polymorphs, *Journal of Chemical Engineering of Japan*, 1994, **27**, 124-126.
14. C. P. M. Roelands, J. H. ter Horst, H. J. M. Kramer and P. J. Jansens, Precipitation mechanism of stable and metastable polymorphs of L-glutamic acid, *AIChE Journal*, 2007, **53**, 354-362.
15. J. Schöll, D. Bonalumi, L. Vicum, M. Mazzotti and M. Müller, In Situ Monitoring and Modeling of the Solvent-Mediated Polymorphic Transformation of l-Glutamic Acid, *Crystal Growth & Design*, 2006, **6**, 881-891.
16. J. C. De Anda, X. Z. Wang, X. Lai, K. J. Roberts, K. H. Jennings, M. J. Wilkinson, D. Watson and D. Roberts, Real-time product morphology monitoring in crystallization using imaging technique, *AIChE Journal*, 2005, **51**, 1406-1414.
17. G. Févotte, In Situ Raman Spectroscopy for In-Line Control of Pharmaceutical Crystallization and Solids Elaboration Processes: A Review, *Chemical Engineering Research and Design*, 2007, **85**, 906-920.

18. G. Févotte, New perspectives for the on-line monitoring of pharmaceutical crystallization processes using in situ infrared spectroscopy, *International Journal of Pharmaceutics*, 2002, **241**, 263-278.
19. T. De Beer, A. Burggraeve, M. Fonteyne, L. Saerens, J. P. Remon and C. Vervaet, Near infrared and Raman spectroscopy for the in-process monitoring of pharmaceutical production processes, *International Journal of Pharmaceutics*, 2011, **417**, 32-47.
20. G. Févotte, J. Calas, F. Puel and C. Hoff, Applications of NIR spectroscopy to monitoring and analyzing the solid state during industrial crystallization processes, *International Journal of Pharmaceutics*, 2004, **273**, 159-169.
21. Y. Roggo, P. Chalus, L. Maurer, C. Lema-Martinez, A. Edmond and N. Jent, A review of near infrared spectroscopy and chemometrics in pharmaceutical technologies, *Journal of Pharmaceutical and Biomedical Analysis*, 2007, **44**, 683-700.
22. F. Lewiner, J. P. Klein, F. Puel and G. Févotte, On-line ATR FTIR measurement of supersaturation during solution crystallization processes. Calibration and applications on three solute/solvent systems, *Chemical Engineering Science*, 2001, **56**, 2069-2084.
23. D. D. Dunuwila and K. A. Berglund, ATR FTIR spectroscopy for in situ measurement of supersaturation, *Journal of Crystal Growth*, 1997, **179**, 185-193.
24. Z. Chen, J. Morris, A. Borissova, S. Khan, T. Mahmud, R. Penchevc and K. J. Roberts, On-line monitoring of batch cooling crystallization of organic compounds using ATR-FTIR spectroscopy coupled with an advanced calibration method, *Chemometrics and Intelligent Laboratory Systems*, 2009, **96**, 49-58.
25. H. Grön, A. Borissova and K. J. Roberts, In-Process ATR-FTIR Spectroscopy for Closed-Loop Supersaturation Control of a Batch Crystallizer Producing Monosodium Glutamate Crystals of Defined Size, *Industrial & Engineering Chemistry Research*, 2003, **42**, 198-206.
26. J. Cornel, C. Lindenberg and M. Mazzotti, Quantitative Application of in Situ ATR-FTIR and Raman Spectroscopy in Crystallization Processes, *Industrial & Engineering Chemistry Research*, 2008, **47**, 4870-4882.
27. H. Alatalo, J. Kohonen, H. Qu, H. Hatakka, S.-P. Reinikainen, M. Louhi-Kultanen and J. Kallas, In-line monitoring of reactive crystallization process based on ATR–FTIR and Raman spectroscopy, *Journal of Chemometrics*, 2008, **22**, 644-652.
28. P. Hamilton, D. Littlejohn, A. Nordon, J. Sefcik, P. Slavin, P. Dallin and J. Andrews, Studies of particle drying using non-invasive Raman spectrometry and particle size analysis, *Analyst*, 2011, **136**, 2168-2174.
29. X. Ni, M. R. Mackley, A. P. Harvey, P. Stonestreet, M. H. I. Baird and N. V. Rama Rao, Mixing Through Oscillations and Pulsations—A Guide to Achieving Process Enhancements in the Chemical and Process Industries, *Chemical Engineering Research and Design*, 2003, **81**, 373-383.
30. X. Ni, Y. Zhang and I. Mustafa, An investigation of droplet size and size distribution in methylmethacrylate suspensions in a batch oscillatory-baffled reactor, *Chemical Engineering Science*, 1998, **53**, 2903-2919.
31. H. K. Gaidhani, B. McNeil and X. Ni, Production of pullulan using an oscillatory baffled bioreactor, *Journal of Chemical Technology & Biotechnology*, 2003, **78**, 260-264.
32. X. Ni, Y. Zhang and I. Mustafa, Correlation of polymer particle size with droplet size in suspension polymerisation of methylmethacrylate in a batch oscillatory-baffled reactor, *Chemical Engineering Science*, 1999, **54**, 841-850.
33. X. Ni, J. A. Cosgrove, R. H. Cumming, C. A. Greated, K. R. Murray and P. Norman, Experimental Study of Flocculation of Bentonite and Alcaligenes Eutrophus in a

Batch Oscillatory Baffled Flocculator, *Chemical Engineering Research and Design*, 2001, **79**, 33-40.
34. X. Ni, A. Valentine, A. Liao, S. B. C. Sermage, G. B. Thomson and K. J. Roberts, On the Crystal Polymorphic Forms of l-Glutamic Acid Following Temperature Programmed Crystallization in a Batch Oscillatory Baffled Crystallizer, *Crystal Growth & Design*, 2004, **4**, 1129-1135.
35. X. Ni and A. Liao, Effects of mixing, seeding, material of baffles and final temperature on solution crystallization of l-glutamic acid in an oscillatory baffled crystallizer, *Chemical Engineering Journal*, 2010, **156**, 226-233.
36. H. A. Mohameed, B. Abu-Jdayil and M. Al Khateeb, Effect of cooling rate on unseeded batch crystallization of KCl, *Chemical Engineering and Processing: Process Intensification*, 2002, **41**, 297-302.
37. M. Moscosa-Santillán, O. Bals, H. Fauduet, C. Porte and A. Delacroix, Study of batch crystallization and determination of an alternative temperature-time profile by on-line turbidity analysis -- application to glycine crystallization, *Chemical Engineering Journal*, 2000, **55**, 3759-3770.
38. C. Y. Ma and X. Z. Wang, Closed-loop control of crystal shape in cooling crystallization of l-glutamic acid, *Journal of Process Control*, 2012, **22**, 72-81.
39. M. Akrap, N. Kuzmanić and J. Prlić-Kardum, Effect of mixing on the crystal size distribution of borax decahydrate in a batch cooling crystallizer, *Journal of Crystal Growth*, 2010, **312**, 3603-3608.
40. K. Sangwal, On the effect of impurities on the metastable zone width of phosphoric acid, *Journal of Crystal Growth*, 2010, **312**, 3316-3325.
41. Z. Ma, H. G. Merkus, J. G. A. E. de Smet, C. Heffels and B. Scarlett, New developments in particle characterization by laser diffraction: size and shape, *Powder Technology*, 2000, **111**, 66-78.
42. X. Renliang and D. G. O. Andreina, Comparison of sizing small particles using different technologies, *Powder Technology*, 2003, **132**, 145-153.
43. D. O'Grady, M. Barrett, E. Casey and B. Glennon, The Effect of Mixing on the Metastable Zone Width and Nucleation Kinetics in the Anti-Solvent Crystallization of Benzoic Acid, *Chemical Engineering Research and Design*, 2007, **85**, 945-952.
44. K. Liang, G. White, D. Wilkinson, L. J. Ford, K. J. Roberts and W. M. L. Wood, An Examination into the Effect of Stirrer Material and Agitation Rate on the Nucleation of l-Glutamic Acid Batch Crystallized from Supersaturated Aqueous Solutions, *Crystal Growth & Design*, 2003, **4**, 1039-1044.
45. P. Stonestreet and P. M. J. Van Der Veeken, The Effects of Oscillatory Flow and Bulk Flow Components on Residence Time Distribution in Baffled Tube Reactors, *Chemical Engineering Research and Design*, 1999, **77**, 671-684.

5 Crystallisation of L-glutamic acid in a continuous oscillatory baffled reactor

5.1 Introduction

Continuous manufacturing has become an area of increased interest and research in recent years in the pharmaceutical industry due to the many potential advantages over current batch methods. These include reduced processing time, equipment size, waste and energy leading to overall cost reduction.[1-3] The potential advantages and the industrial drivers for continuous manufacturing have been discussed previously in chapter 1.3. The investigation of the suitability of continuous manufacturing in the pharmaceutical industry is still in the relatively early stages due to the initial difficulties in development, with only a small number of companies actively evaluating or using this type of technology.[4] Although research is being carried out by various groups on specific unit operations *e.g.* continuous granulation or continuous crystallisation, there is currently limited evidence of the feasibility of a fully continuous manufacturing process. These unit operations are operated as continuous processes in other industries meaning there should already be sufficient knowledge and understanding available, however, they are most often operated at much larger scale than what is required in pharmaceutical production.[5] As mentioned in chapter 1.3, continuous pharma processing is being investigated by the Novartis-MIT Center for Continuous Manufacturing and other similar centres. Until a fully continuous process has been demonstrated to be flexible and reliable, with proven advantages over current batch methods, it is less likely that continuous manufacturing will be widely adopted by the pharmaceutical industry.[6] Additionally, there are likely to be some processes which cannot always be operated in a continuous manner.[7] For example, in the case of crystallisation, there are a number of compounds which are known to be prone to fouling of reactor materials such as stainless steel and glass which would cause the process to not operate at the optimum efficiency and result in blocking of the reactor. It may be that compounds like these may not be viable for continuous operation until after the initial API production. Thus, continuous manufacturing may not be a one size fits all option, however, if a wide number of

commonly produced compounds in the pharmaceutical industry could be manufactured from start to finish in a continuous process, there would be significant benefits.

The study and conversion of current batch to continuous pharmaceutical unit operations includes crystallisation, granulation, drying and tableting.[8-11] This study focused on continuous crystallisation of which there are two main types of reactor design: the plug flow type reactor and the mixed suspension mixed product removal reactor (discussed further in chapter 6).[2, 12] The plug flow system studied in this section was the continuous oscillatory baffled reactor (discussed in chapter 1.2.2.) with the same model compound used previously in the batch study, L-glutamic acid. There are a limited number of reports investigating this type of reactor. *Lawton et al.* transferred a batch process of a model API to operation in a COBR with a dramatic decrease in the successful isolation of the product from over 9 hours in a batch process down to 12 minutes in a COBR.[13] However, the COBR has also shown to be beneficial in organic synthesis of compounds of high purity with the addition of effective cleaning protocols demonstrating that this reactor can be flexible and transferred to the production of a new compound with minimal loss of product.[14] There are also reports of successful continuous crystallisations in alternative plug flow reactor designs.[15, 16]

As there has been limited research in the use of COBRs for crystallisation in comparison to batch STRs, there is also a lack of knowledge of suitable *in situ* analytical techniques for the monitoring and control of the process, which was one of the aims of this section of work. In the limited number of studies reported to date, similar *in situ* techniques used with batch reactors have been implemented for the monitoring of continuous processes. *Ferguson et al.* used measurements obtained by FBRM, PVM and ATR-FTIR to monitor the crystallisation of benzoic acid in a plug flow reactor. This work showed that crystals of a smaller size could be obtained in a plug flow reactor in comparison to batch operation.[15] L-glutamic acid was one of several model compounds studied by *Alvarez and Myerson* in a plug flow reactor. In this case anti-solvent crystallisation was carried

out and the effect of the number of anti-solvent injection points on the crystal size distribution determined using FBRM.[17] In an alternative mixed suspension, mixed product removal (MSMPR) type crystalliser with added baffles, *Narducci et al.* demonstrated how ultrasound could be used to control the properties of the particles produced. Smaller crystal size, improved crystal habit and reduced agglomeration were benefits observed when ultrasound was employed during the crystallisation.[18] *In situ* techniques have also been applied to alternative continuous processes. Near infrared spectroscopy has been employed for the monitoring of solid concentration of an API in continuous powder mixing, while Raman and near infrared spectrometries have been applied to the monitoring of continuous granulation processes to aid in the understanding of the process and to study the effect of varying operating conditions.[19-21] Therefore, it was anticipated that the techniques used for the monitoring of alternative continuous processes, in particular non-invasive Raman spectrometry, could be implemented to monitor continuous crystallisation in a COBR.

In the following section of work, non-invasive Raman spectrometry has been employed to provide increased process knowledge and understanding on the continuous oscillatory baffled reactor using the model compound L-glutamic acid. As a minimal amount of process analysis has been conducted on this type of reactor, it was envisioned that this additional information would help in the explanation of how different operating conditions affect the nucleation and growth processes occurring in the reactor. This would allow a comparison with the study of the crystallisation of L-glutamic acid in the batch OBR in chapter 4 and the alternative continuous reactor in chapter 6. The aim of the study was to determine if the properties of the particles obtained (polymorph, particle size, *etc*.) could be dictated by the set of operating conditions used and whether this was reproducible. Additionally, the operating conditions which allowed the system to reach and maintain steady state were important to identify as well as the fluctuations in the conditions which may disrupt steady state. Along with supplementary information provided by off-line laser diffraction and x-ray diffraction, it was possible to determine

how operating conditions affected nucleation time, growth profiles and the time to reach steady state.

5.2 Experimental

5.2.1 Materials

In this work, L-glutamic acid and distilled water were used for all experiments as described in section 3.2.

5.2.2 Continuous OBR Conditions

The reactor comprised 32 jacketed straight and 8 un-jacketed bend sections for the preliminary experiments (section 5.3.1) and 22 straight and 11 bend sections for the remaining experiments as described in section 3.3.3 (Figure 1-7 and Figure 3-6). The solutions (20, 25, 30 or 45 g/L) were prepared and contained in a 25 L batch reactor at a temperature of 80^{o}C prior to being fed into the COBR. The reactor would initially be filled with water due to cleaning following the previous crystallization. Therefore, once the temperature zones had reached the correct temperature, the hot solution was pumped as quickly as possible through the reactor to replace the water and remove any air bubbles. Once the reactor was filled with LGA solution, the oscillation was started to begin the crystallization process. For the longer reactor set-up the solutions were cooled to a final temperature of 40^{o}C using a flow rate of 29 ml/min resulting in a cooling rate of 0.5^{o}C/min and an 80 minute residence time. For the shorter reactor length the solutions were cooled to final temperatures of 40 or 10^{o}C using a flow rate of either 40 or 161 ml/min resulting in a cooling rate of 0.5 or 2^{o}C/min and a residence time of 80 or 20 minutes, respectively.

Figure 5-1 shows the cooling profiles for 0.5 and 2^{o}C/min in the COBR. Due to the reactor length, the 2^{o}C/min profile could only be achieved if the solution was rapidly cooled from 80-50^{o}C in the first straight then a linear cooling profile was employed from

50-10°C by 2°C/min for the remaining length of the reactor. The solutions were oscillated in the COBR at frequencies of 1 or 3 Hz and amplitudes of 10 or 30 mm. The slurry was collected at the outlet at 8 equal time intervals per residence time (either every 10 minutes for a 0.5 °C/min cooling rate or every 2.5 minutes for a 2°C/min cooling rate) for off-line laser diffraction and x-ray diffraction. Prior to off-line analysis, the slurry was filtered under vacuum and then dried in an oven overnight.

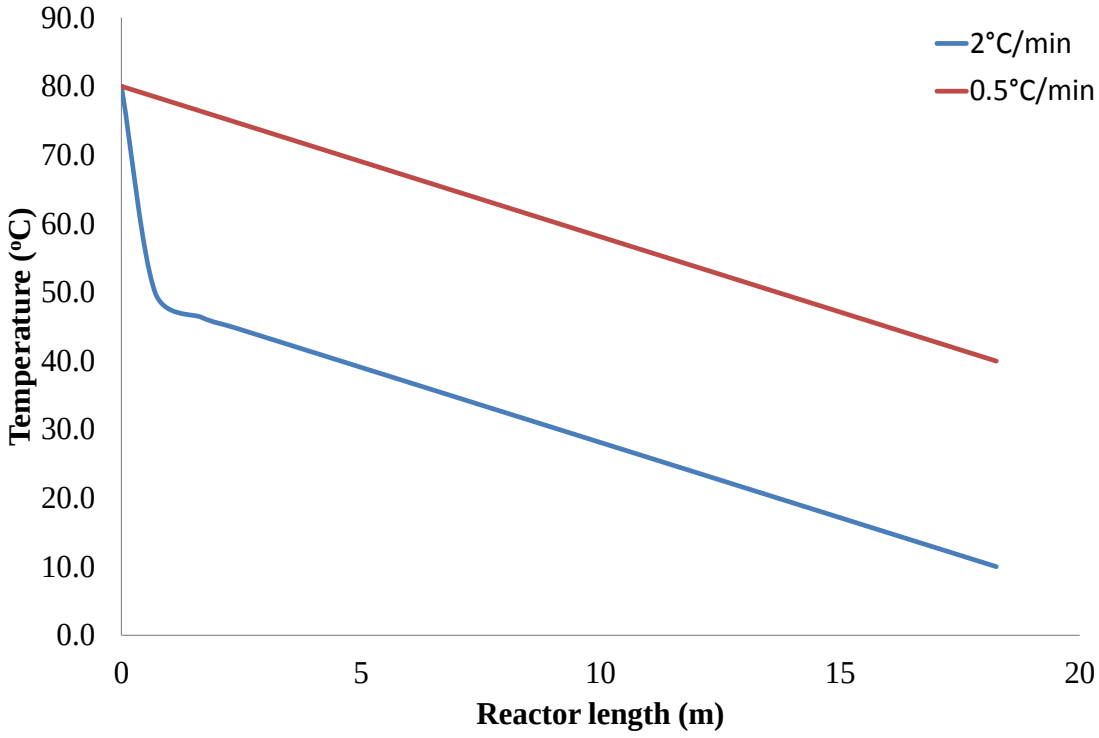

Figure 5-1: Cooling profiles calculated in the COBR using 0.5 and 2°C/min

5.2.3 Raman Instrumentation-Kaiser RXN1 spectrometer

Raman measurements were carried out using a Kaiser RXN1 spectrometer with the P^{h}AT probe head as described in section 3.4.1. Non-invasive measurements were recorded by directing the laser light at the final bend section of the COBR reactor. The bend section and probe head were covered in aluminum foil to limit and cosmic rays or room lights affecting the spectra. A spot size of 6 mm using a 785 nm near-IR laser with

a laser power of 400 mW were used and an average of four 15 s scans was recorded, resulting in a measurement being acquired every 90 s. The spectral data collected was processed in Matlab using a Savitsky-Golay first derivative filter which utilised a width of 11 data points and a second order polynomial.

5.2.4 Laser diffraction

Laser diffraction measurements were carried out using a Malvern Mastersizer 2000 as described in section 3.4.3. Approximately 100 ml of a saturated solution of LGA and 0.1% Tween 80 was added to a Hydro2000SM cell. Powder samples of LGA which had been vacuum filtered and dried in an oven overnight, were added to the cell until a laser obscuration (internal parameter of the instrument to indicate multiple scattering effects) of ~3% was obtained.

5.2.5 X-ray diffraction

X-ray diffraction measurements were undertaken using a Bruker AXS D8 Advance transmission diffractometer as described in section 3.4.5. Powder samples of LGA which had been previously vacuum filtered and dried in an oven overnight were lightly ground in a mortar and pestle before a small amount (< 0.5 g) was added to a well plate supported using kapton film. Figure 4-3 in section 4.2.6 shows the XRD patterns of the pure forms of alpha and beta L-glutamic acid.

5.3 Results and Discussion

5.3.1 Preliminary COBR experiments

Some preliminary experiments were carried out in the continuous reactor following on from the results obtained in the batch OBR (section 4.3.1). A saturated solution was prepared at 30^{o}C since crystals would be expected to be monitored at a single point in the reactor at this or a similar temperature in a cooling crystallisation, and 25 g of beta LGA was added. The mixture was then fed into the continuous OBR at 30^{o}C, at a flow rate of 58 ml/min and baffle oscillations of 2 Hz and 20 mm were applied. Non-invasive Raman spectrometry was employed to see if similar measurements could be made as in the batch set-up. These measurements were made in several of the bend sections of the reactor as these were not jacketed and a number of the heater chillers used oil in the temperature jacket. Figure 5-2 shows the 1st derivative spectra obtained at three different points along the length of the reactor.

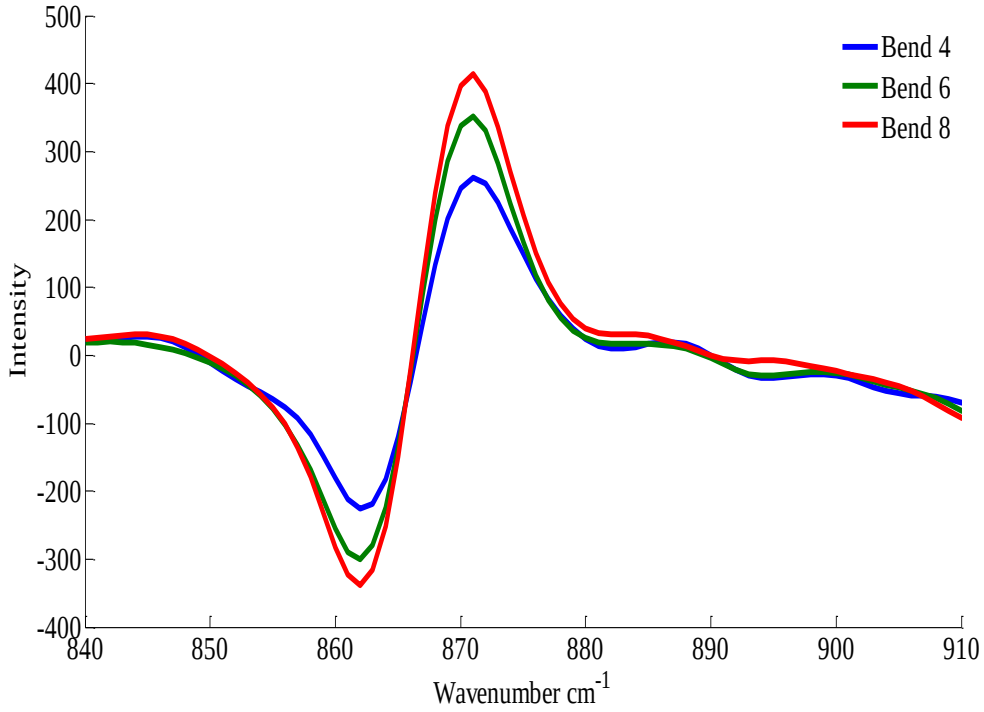

Figure 5-2: Expanded area of 1st derivative Raman spectra of beta L-glutamic acid showing the increase in signal at different points along length of the reactor at a constant temperature of 30^{o}C

It is likely that the solution may have been slightly supersaturated rather than saturated and this led to a small amount of crystal growth which explains the increase in the Raman signal observed as the probe was moved to locations further down the length of the reactor. Nevertheless, this experiment showed that Raman measurements could be made at any of the bend sections and potentially in the early stages of the crystallisation, which could be used to confirm whether the right polymorph has been formed.

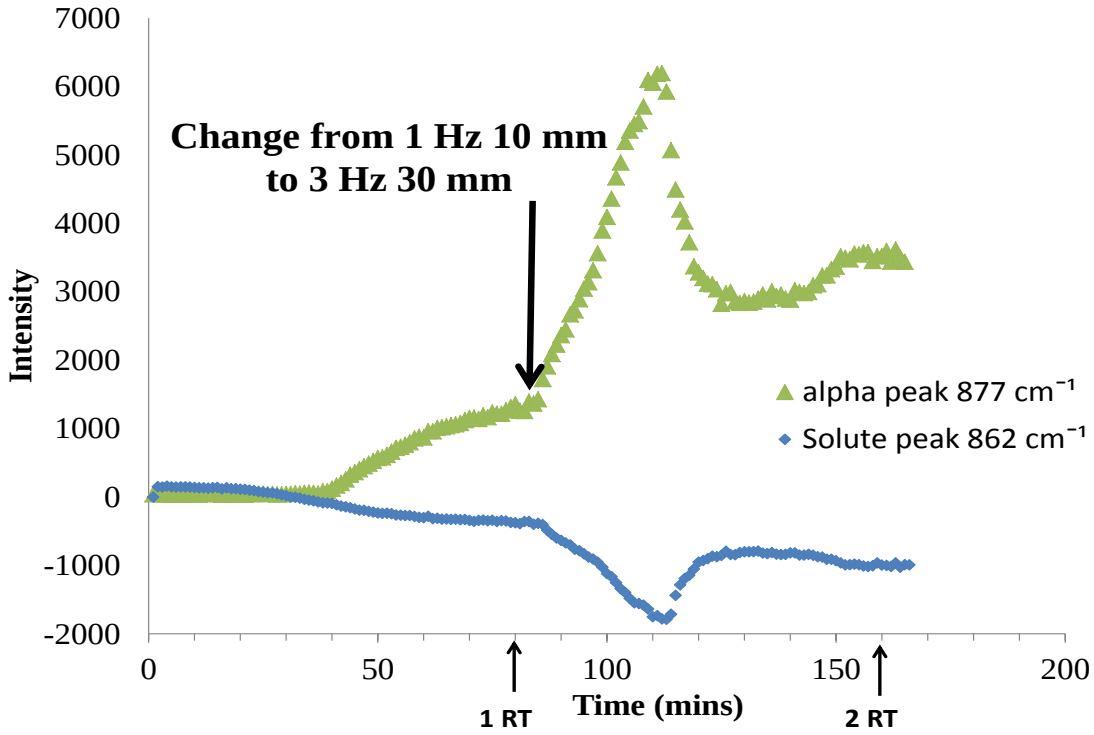

Figure 5-3: Crystallisation profile for L-glutamic acid solution and alpha L-glutamic acid monitoring the change in oscillation conditions using a residence time of 80 minutes, based on 1st derivative Raman intensity at 862 and 877 cm^{-1}, respectively

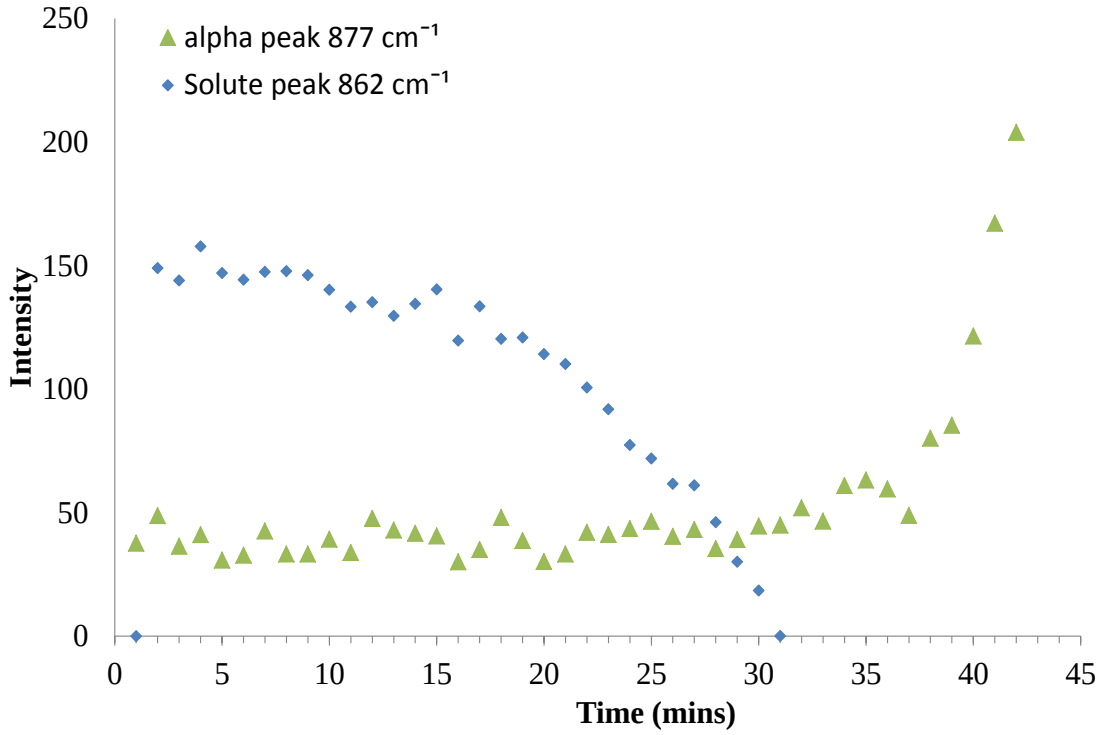

Figure 5-4: Crystallisation profile for L-glutamic acid solution and alpha L-glutamic acid showing the first 45 minutes using a residence time of 80 minutes, based on 1st derivative Raman intensity at 862 and 877 cm^{-1}, respectively

Figure 5-3 shows the Raman intensity profiles for alpha LGA particles and the LGA solute obtained when the oscillation intensity was increased during the crystallisation of a 45 g/L solution. As can be seen the profile for the solute phase mirrors that of the solid phase after nucleation has occurred due to the overlapping in the Raman peaks (discussed further in section 4.3.1.) The starting temperature of the inlet solution was 80^{o}C and a cooling rate of 0.5^{o}C/min was employed with the final temperature set to 40^{o}C (29 ml/min flow rate). The crystallisation was monitored using starting conditions of 1 Hz and 10 mm. After 1 residence time of 80 minutes, the oscillation was increased to 3 Hz 30 mm. The residence time describes the time spent by the solution in the reactor from the point it enters the vessel to the slurry outlet. For the initial 40 minutes (shown in Figure 5-4), the Raman spectra recorded at the outlet were dominated by the solute concentration, thereafter, crystals were detected as indicated by the steady

increase in the Raman signal for the solid phase with increasing time. A change in the profile occurred when the frequency and amplitude of oscillation were increased; a sharp increase in the signal intensity occurred due to the greater amount of crystals being produced or suspended. The signal then reached a maximum before it decreased and began to level off. This suggests the system was starting to reach steady state. For steady state to occur, the conditions at different points along the reactor must remain constant with increasing time. It was thought that the signal increased initially between 40 minutes to 80 minutes due to nucleation and crystal growth at the starting conditions of 1 Hz 10 mm. The next 40 minutes showed the transition period as the intensity of oscillation was increased. The signal increased rapidly possibly due to a combination of effects. A higher intensity of oscillation results in a higher nucleation temperature, which would happen earlier on in the reactor, and so might be expected to result in a larger amount of crystals. In addition, sedimentation was observed at the lower oscillation conditions and it is likely that the sudden increase in oscillation caused this material to be dislodged and passed through the reactor which would contribute to the increase in signal observed. The decrease in the signal would then be due to the new set of conditions being the only effect on the crystals which is why the Raman signal begins to level off. However, additional experiments would need to be performed to investigate this further.

These results showed that crystallisation experiments in the COBR could be monitored using non-invasive Raman spectrometry as in the batch OBR. However, it is difficult to be able to compare the data obtained in both the batch and continuous OBR since in the COBR; measurements were taken at a fixed point at a constant temperature whereas in the batch experiments the crystallisation is monitored throughout the temperature decrease. Altering the oscillation conditions could be seen to have an effect on the crystals produced by the changes observed in the Raman measurements. This demonstrates the potential of using the technique for real-time optimisation of the crystallisation process in a COBR.

5.3.2 Effect of particle size on Raman measurements

The effect of the size of the particles produced during a crystallisation process on the Raman signal was investigated further to determine if the signal was influenced by both the concentration of the solid form present and the particle properties. It was therefore important to know how significantly the particle size affected the Raman signal. Alpha form LGA particles, which are prismatic in their habit, were sieved into several particle size fractions and suspended in a saturated solution (50 g/L) at 20^{o}C which reflected the temperature of the final sections of the continuous OBR in many of the crystallisation experiments. Figure 5-5 shows an expanded area of the first derivative spectra of the various particle size fractions.

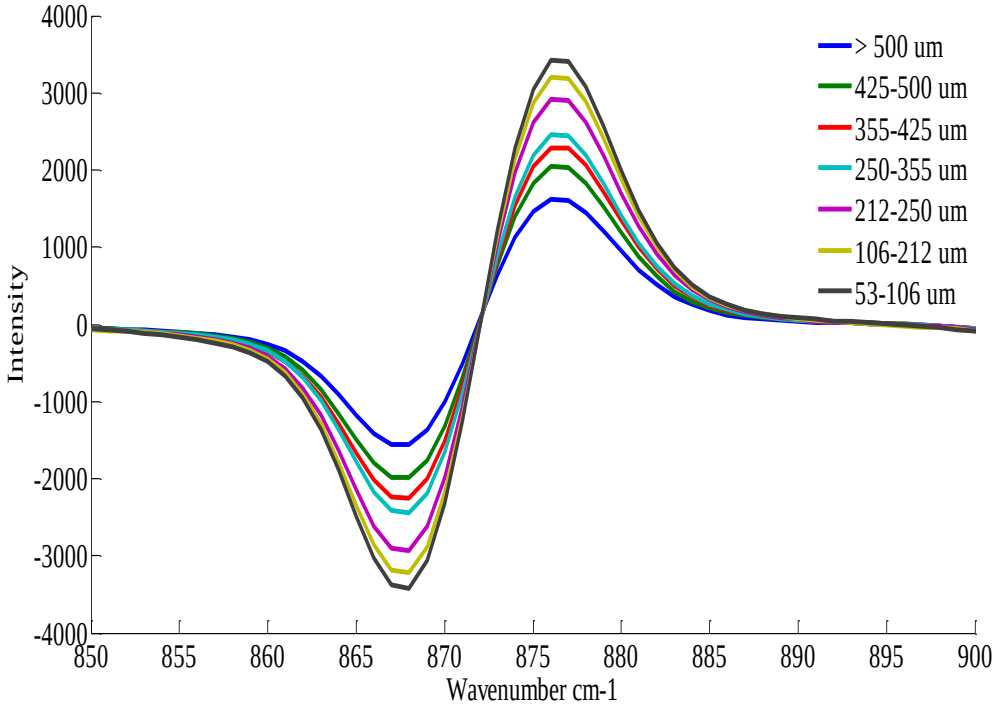

Figure 5-5: Expanded area of 1st derivative spectra of 50 g/L alpha L-glutamic acid slurries of increasing particle size

Figure 5-5 shows the most intense alpha form peak at 877 cm^{-1} in the 1st derivative spectra of increasing particle size of L-glutamic acid. It can be seen that the particle size has quite a significant effect on the Raman intensity. As the particle size decreases, the

signal intensity increases and there is quite a substantial difference in the intensity between the two extremes of particle size (> 500 µm and 53-106 µm). Figure 5-6 shows a plot of the intensity versus the particle size (µm).

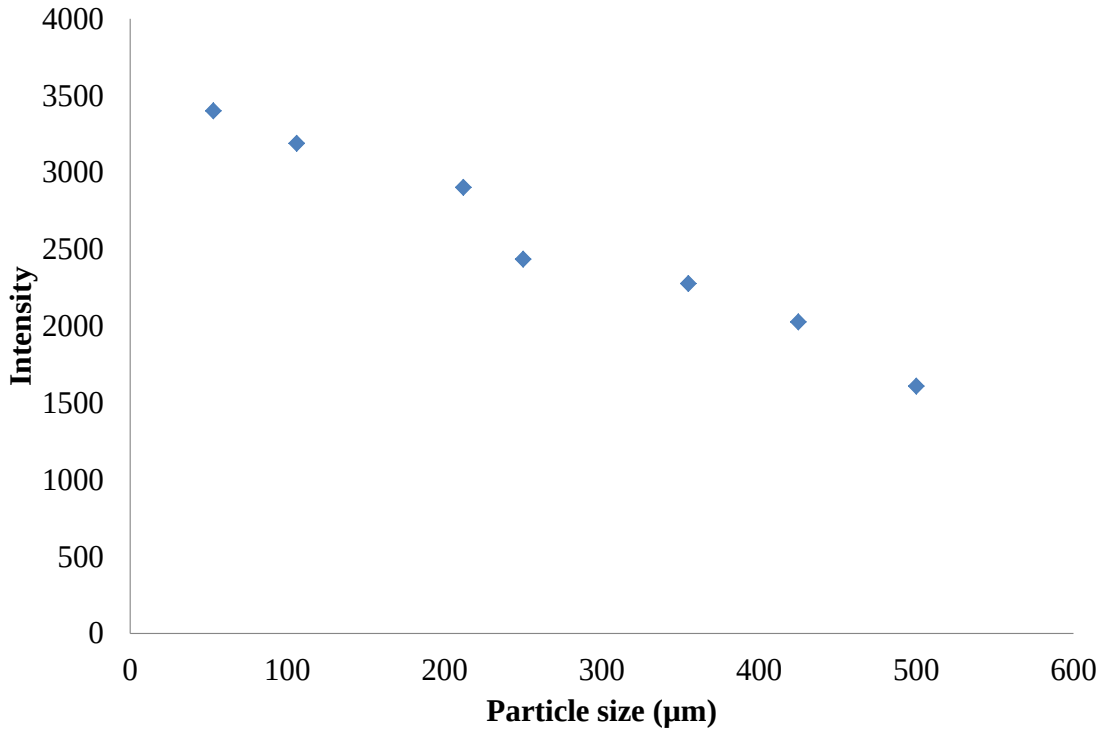

Figure 5-6: Plot of Raman intensity (at 877 cm^{-1}) with increasing particle size from the 1st derivative spectra of alpha L-glutamic acid

Figure 5-6 shows the trend of the Raman intensity with increasing particle size. It can be seen that as the particle size increases the Raman signal intensity decreases and this response is relatively linear. It was expected that the Raman signal intensity would be higher at decreased particle sizes since it has been shown that at smaller particle sizes there is increased scattering.[22, 23] However, it can be seen that there is a significant difference in the signal intensity between the smallest and the largest particle size range used. Therefore it would appear that the particle size as well as the solids concentration has a significant impact on the Raman signal in the case of L-glutamic acid. Consequently, it is not possible to rely on the Raman crystallisation profiles alone to determine if the continuous OBR is operating at steady state as there are significant

contributions to the signal from both the concentration of solid material being produced and the particle size of this material. As shown previously in this section, the Raman signal has suggested the crystallisation is operating at steady state when the particle size is not constant. This would suggest that an in-line particle size technique would be beneficial to provide complementary information to the non-invasive Raman measurements. This would mean it would be possible to know when the system is truly operating at steady state when the solids concentration and the particle size values are both consistent.

5.3.3 Effect of operating conditions on particle properties in the continuous OBR

The effect of operating conditions on the particle size distribution and particle size was investigated in the COBR. As in the previous experiment, a solution concentration of 45 g/L and a cooling rate of 0.5^{o}C/min were used from a starting temperature of 80^{o}C to a final temperature of 40^{o}C. This gave a residence time of 80 minutes and samples were collected from the end of the COBR 8 times each residence time (every 10 minutes) for particle size analysis. In this case, the oscillation conditions were changed from 1 Hz 10 mm to 3 Hz 10 mm.

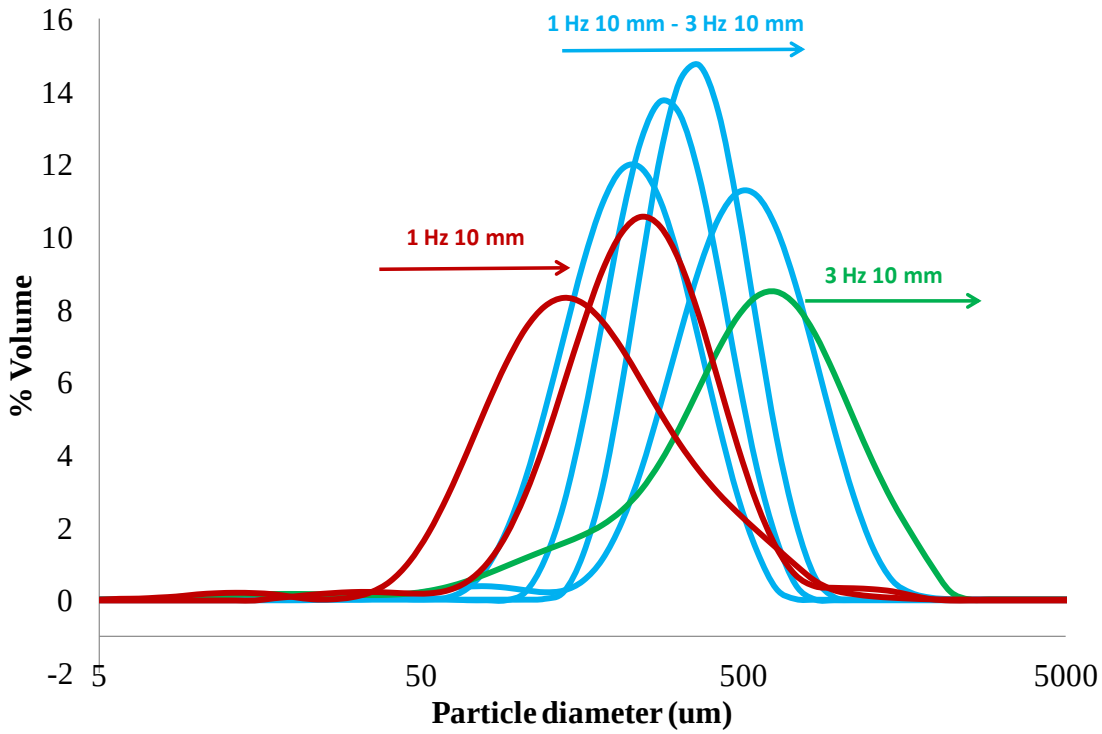

Figure 5-7: Particle size distributions of LGA when baffle frequency was increased from 1 Hz 10 mm (red) showing the transition period (blue) to a higher frequency of 3 Hz 10 mm (green) in the COBR

Figure 5-7 shows the change in particle size distribution (PSD) observed when the frequency of oscillation was increased. The slurry was collected for one residence time following nucleation at the initial set of conditions before the oscillation was increased and slurry collection was continued every 10 minutes. At the start of the crystallisation, the average particle size increased with time at the less intense oscillation conditions, which is shown by the red distributions. When the frequency was increased, there was a period of transition when the average particle size increased further as shown by the blue PSD plots in Figure 5-7. The green distribution shows the average particle size continuing to increase as the third residence time is entered and the higher oscillation conditions should have full influence on the system. Figure 5-8 shows a plot of the average particle size against time. The circled points depict the distributions selected for Figure 5-7.

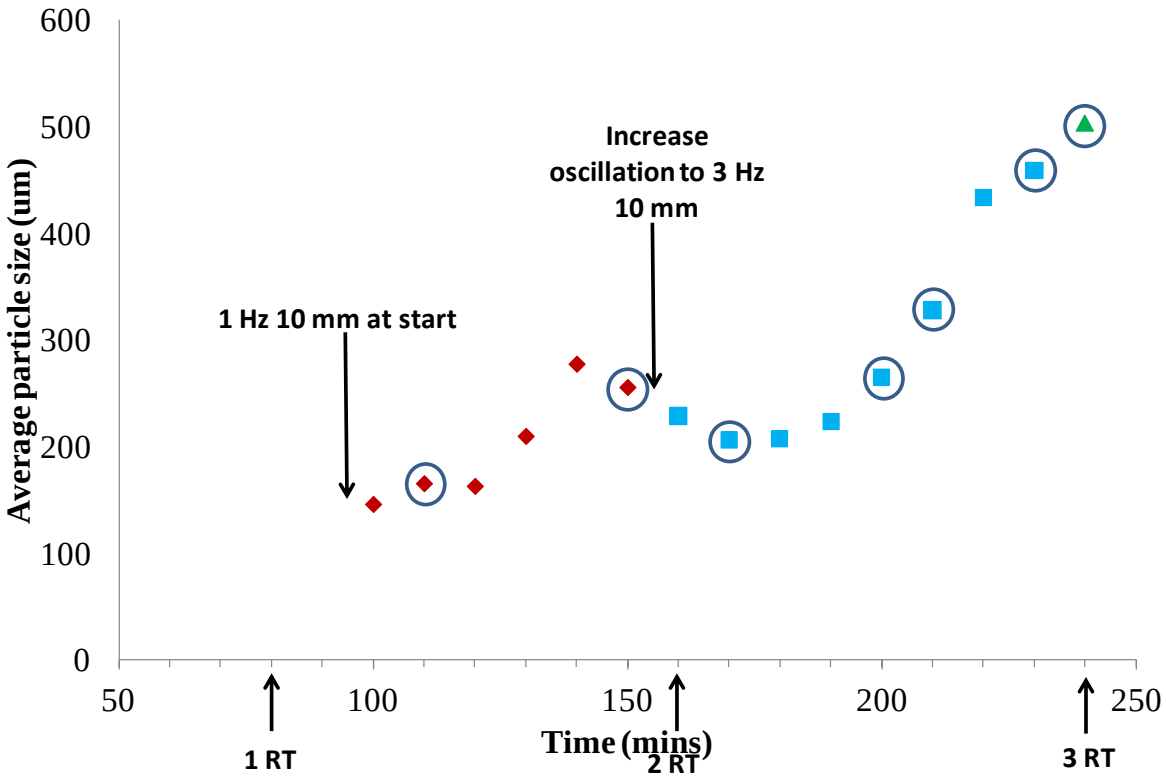

Figure 5-8: Plot of average particle size with increasing time as the frequency was raised during the crystallisation of L-glutamic acid in the COBR (cooling rate of 0.5°C/min) showing the initial set of conditions of 1 Hz 10 mm (red), the transition period (blue) and the final conditions of 3Hz 10 mm (green). The circled points show the distributions used in figure 5-7

As Figure 5-8 shows, the average particle size increases steadily with time as crystal growth progresses. The frequency of oscillation is then increased and the average particle size begins to level off between ~180 and 220 minutes before the change in conditions begins to take effect and the particle size increases once more quite rapidly. It had been planned to collect particles for four full residence times, however, the reactor blocked less than half way through the third residence time. Therefore, the experiment was repeated with a higher cooling rate as this causes an increase in the flow rate and was expected to reduce the problems with blocking in the reactor. A flow rate was selected which gave a cooling rate of 2°C/min. The residence time is also reduced from 80 to 20 minutes at this cooling rate and as before 8 samples were collected every

residence time, but this time each sample was collected every 2.5 minutes. Figure 5-9 shows the overlay of the experiments carried out at the two different cooling rates.

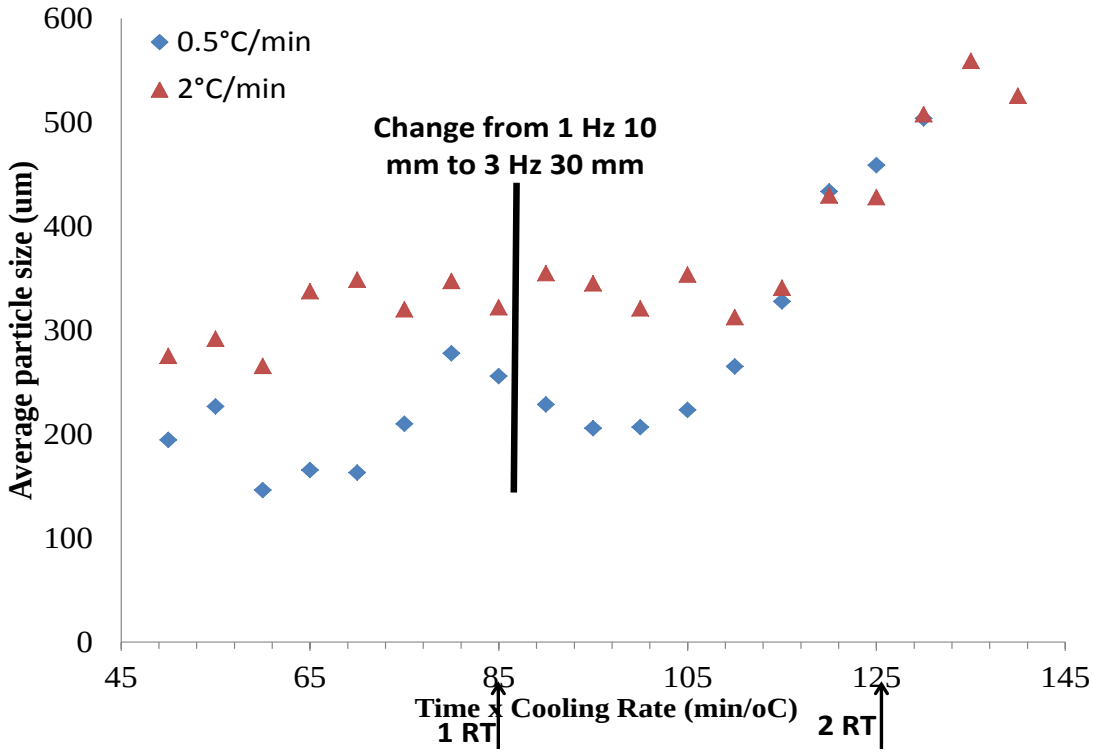

Figure 5-9: Plot of average particle size with increasing sample number as the frequency was raised during the crystallisation of 45 g/L L-glutamic acid using a cooling rate of 0.5°C (blue) and 2°C/min (red) in the COBR

As the cooling rate is increased from 0.5 to 2°C/min, an improvement is observed in the consistency of the particles obtained. At the lower oscillation conditions, the average particle size becomes consistent much quicker and so particles of a similar size were produced for longer, at the higher cooling rate. The change in the oscillation intensity then causes the same increase in the particle size as observed at the lower cooling rate. The experiment lasted slightly longer using a 2°C/min cooling rate and was stopped towards the end of the third residence time due to blocking so the higher cooling rate did not fully solve the blocking problem. XRD showed that the alpha form was produced using both cooling rates.

a)

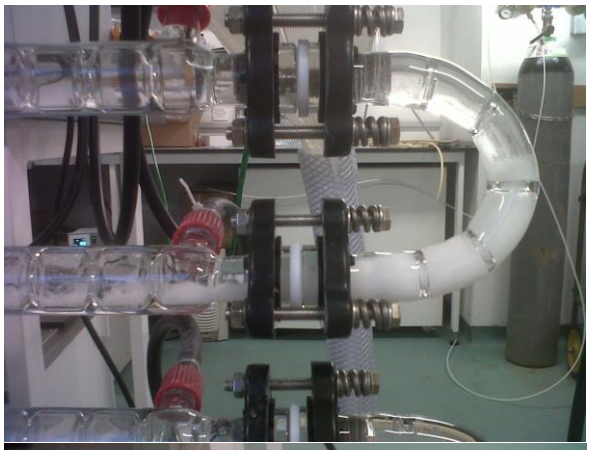

b)

Figure 5-10: Images of the COBR showing (a) the gathering of material in the bend sections and (b) the sedimentation in the straight sections

Figure 5-10 shows the causes of the blocking which occurs in the COBR using a relatively high concentration of 45 g/L LGA. As the crystallisation proceeds and more crystals are produced, the material begins to gather at the bend sections and the oscillation is not sufficient to push enough material along the reactor. Therefore, blocking eventually occurs which can be problematic if this is not monitored, as the build-up in pressure eventually causes the bellow attached to the oscillator to split. A further problem that was encountered was sedimentation, which was obvious on several of the final straight sections. Although the position of the Raman probe was limited to the bend sections in this case, the level of sedimentation observed would interfere with any Raman measurements that might be taken in the last few straight sections of the reactor, which could be a potential disadvantage. Therefore, it was decided that a

solution concentration of 45 g/L was too high for the continuous system and a lower concentration of LGA was used for the subsequent experiments.

5.3.4 Continuous OBR DoE

Following on from the preliminary experiments which showed that changes in operating conditions had an impact on the PSD of the particles during the crystallisation of LGA, a design of experiments was carried out similar to that undertaken with the batch OBR to investigate the effects further. A 2-level, 3-factor design was conducted which gave a total of eight experiments comprising various combinations of operating conditions. These experiments were monitored using non-invasive Raman monitoring and off-line samples were collected frequently for analysis by LD and XRD. The conditions used in these experiments are shown in Table 5-1.

Table 5-1: Different operating conditions used in the eight DoE experiments in the continuous OBR

Experiment	Concentration (g/L)	Frequency (Hz)	Amplitude (mm)
1	30	3	30
2	30	3	10
3	30	1	30
4	30	1	10
5	20	3	30
6	20	3	10
7	20	1	30
8	20	1	10
9	25	2	20

Table 5-2: Outcome of the eight DoE experiments in the continuous OBR showing the polymorph of the product as determined by Raman and X-ray diffraction

	Polymorph Obtained	
Experiment	**Raman**	**XRD**
1	α	α
2	α	α
3	α	α
4	α	α
5	α	α
6	-	-
7	-	-
8	-	-
9	α	α

Table 5-2 shows that three of the experiments, 6, 7 and 8, produced no crystals at all. All these experiments were carried out using the lower solution concentration of 20 g/L which appeared to be too low a concentration for nucleation to occur unless the most intense oscillation conditions were applied (3 Hz, 30 mm-experiment 5). This was unexpected as a lower concentration of 15 g/L had been successfully used to produce crystals in the batch OBR. As with the batch OBR experiments, peaks from the first derivative spectra between the range 872 (pure beta) and 877 (pure alpha) cm^{-1} were monitored to provide information on the process including the nucleation temperature and the growth profile of the solid phase. When a mixture of forms was present, the Raman peak was found to be located in between these two pure phase peaks (as described previously in section 4.3.1), for example when a 50:50 mixture of alpha and beta LGA was formed the peak shifted to 875 cm^{-1}.

5.3.4.1 Effect of oscillation frequency on particle properties

The information obtained from non-invasive Raman measurements as well as the off-line laser diffraction and x-ray diffraction measurements were used to compare the

properties of the particles obtained when different operating conditions were used. Figure 5-11 shows the crystallisation profiles obtained from experiments where the oscillation frequency was increased while the amplitude was kept constant with a LGA solution concentration of 30 g/L.

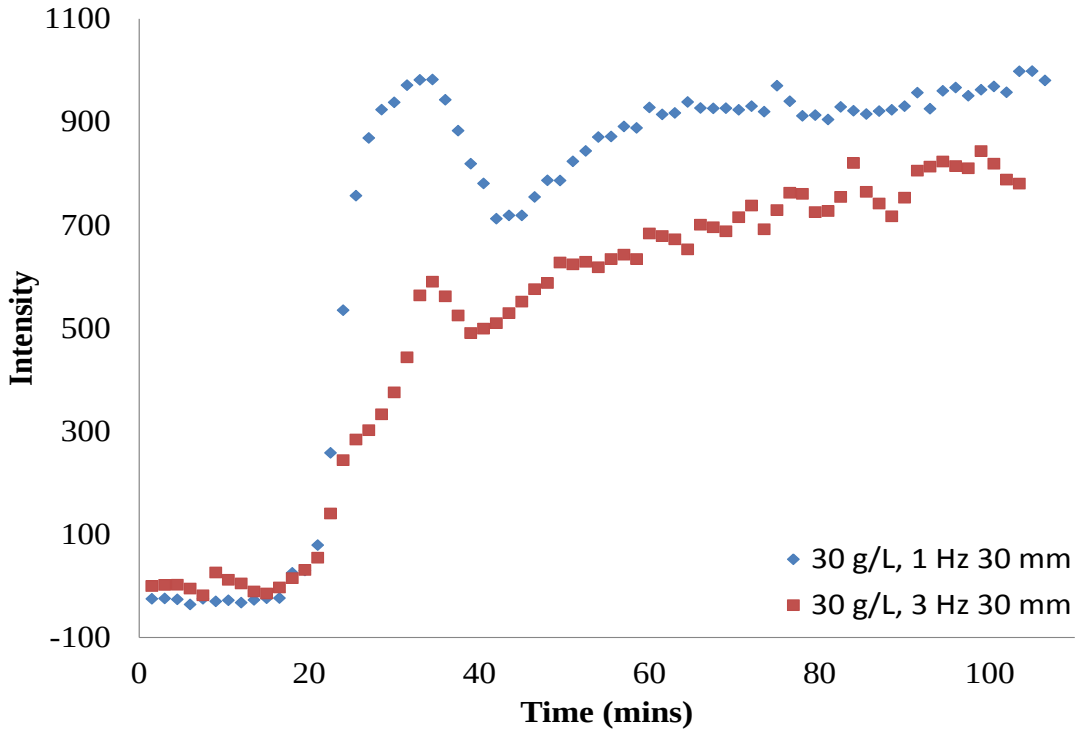

Figure 5-11: Crystallisation profile for L-glutamic acid from two experiments (1 and 3 in Table 5-1) of increasing oscillation frequency, based on 1st derivative Raman intensity at 877 cm^{-1}

Figure 5-11 shows that the crystallisation profiles obtained when varying the oscillation frequency at a fixed high amplitude of 30 mm are relatively similar. The nucleation temperatures are comparable at both frequencies meaning the initial nuclei which could be detected by Raman reached the final bend at a similar time. The growth profile is relatively similar at both oscillation frequencies: there is a sharp increase following nucleation describing crystal growth, which reaches a maximum after approximately half a residence time (10 minutes). The intensity then decreases followed by a slight increase before the signal begins to level off at around 60 minutes (2 residence times following nucleation). The unusual trend in the Raman signal observed following

nucleation could be due to the supersaturation being consumed rapidly in the initial stages of the crystallisation. As this happens, there is a sharp increase in the signal for the solid form as a large number of nuclei are formed and growth takes place quickly. Once this is complete and the supersaturation has been used up the signal starts to decrease as the rate of nucleation and crystal growth slowdown. It was found that the solute signal had no impact on the Raman solid peak at 877 cm^{-1} selected for the crystallisation profile in Figure 5-11 (as overlapping of the peaks was found to be an issue in the early stages of nucleation) and therefore this was thought to be unlikely to be responsible for the trend observed at around 30 minutes. There is a second increase shortly after due to supersaturated solution being continuously pumped through the reactor leading to a second smaller increase in nucleation and growth of the crystals. This is followed by the signal levelling off suggesting a consistent level of crystals is being produced. The main difference with changing the frequency is a decrease in the intensity of the profile with an increase in the frequency of oscillation. This could potentially be due to a lower amount of solid being produced at a higher frequency or a difference in the size of the particles. Figure 5-12 shows plots of the weight of solid collected over the same time interval (2.5 min) during the two experiments when the frequency was increased. The number of residence times following nucleation are also highlighted.

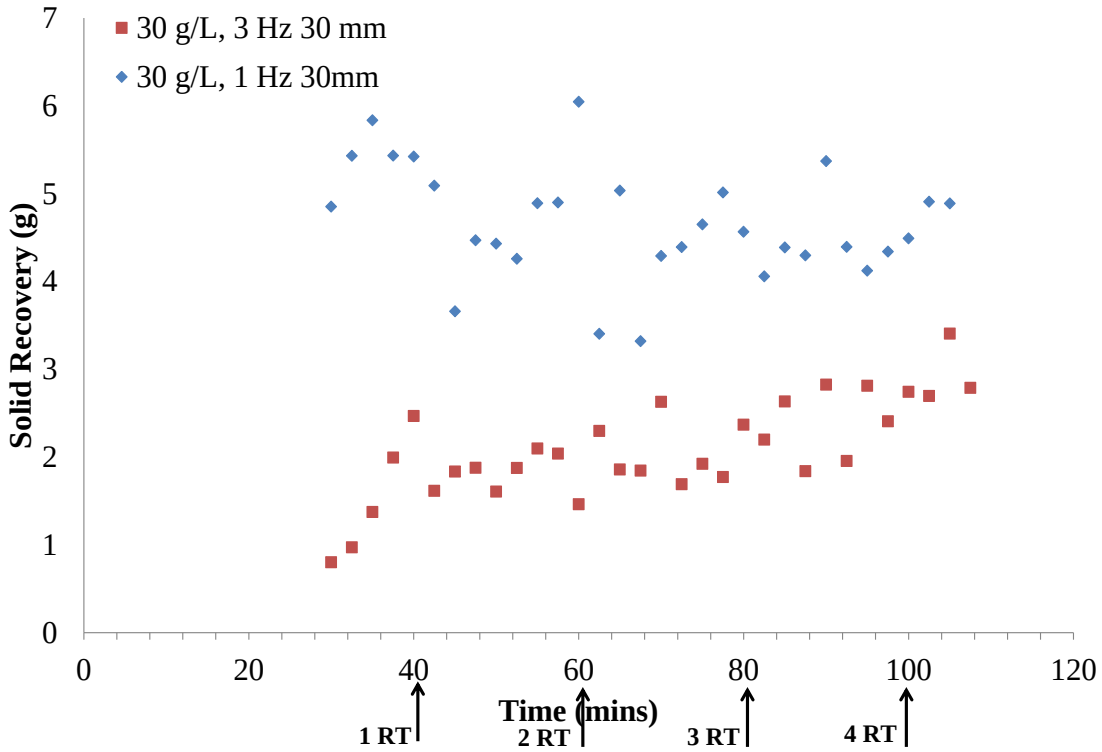

Figure 5-12: Plot of solid recovery every 2.5 minutes for experiments 1 and 3 in Table 5-1, when baffle frequency was increased

Figure 5-12 shows the amount of solid produced during the crystallisation at the lower frequency of 1 Hz is approximately double that produced at the higher frequency, but is more variable. This accounts for the higher intensity Raman signal obtained at these conditions and could be due to more efficient nucleation and crystal growth at the more intense oscillation conditions (3 Hz, 30 mm). Figure 5-13 shows the overlay of the Raman measurements and solid recovery measurements at the higher oscillation frequency of 3 Hz.

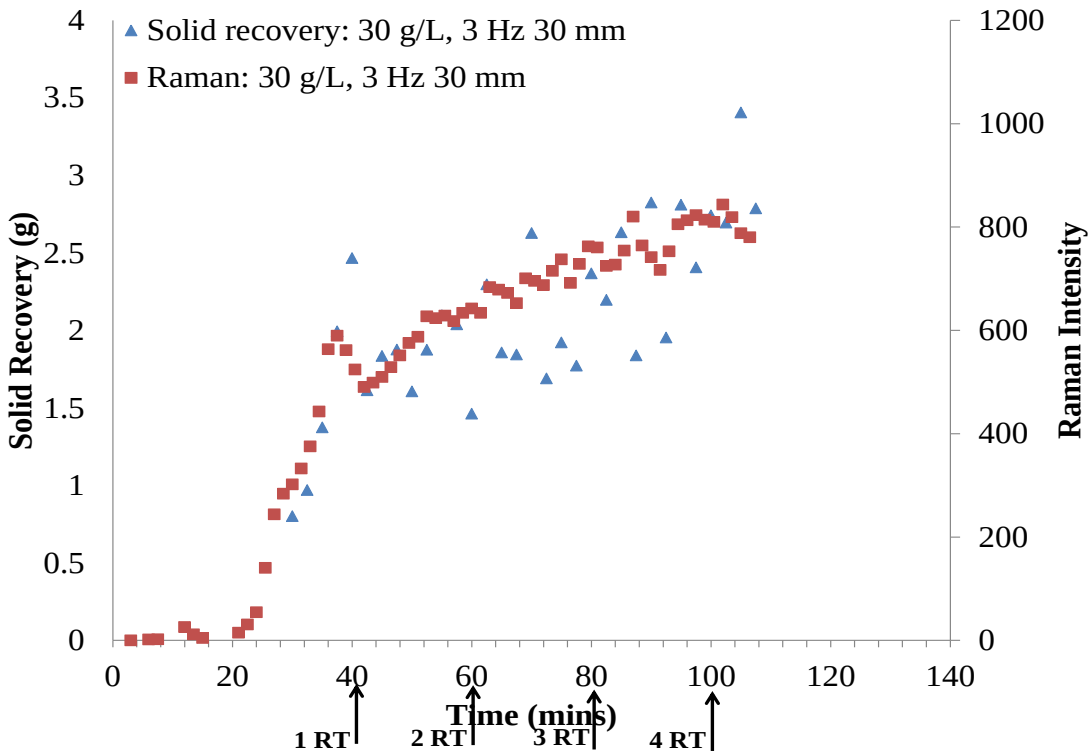

Figure 5-13: Plot of Raman measurements and solid recovery for experiment 1 in Table 5-1 when baffle frequency was increased

As Figure 5-13 shows, when both the Raman and solid recovery measurements are overlaid the trends are relatively similar although, the measurements for the amount of solid collected during the process fluctuates more. This suggests that the majority of the Raman signal describes the changing concentration of the solid material.

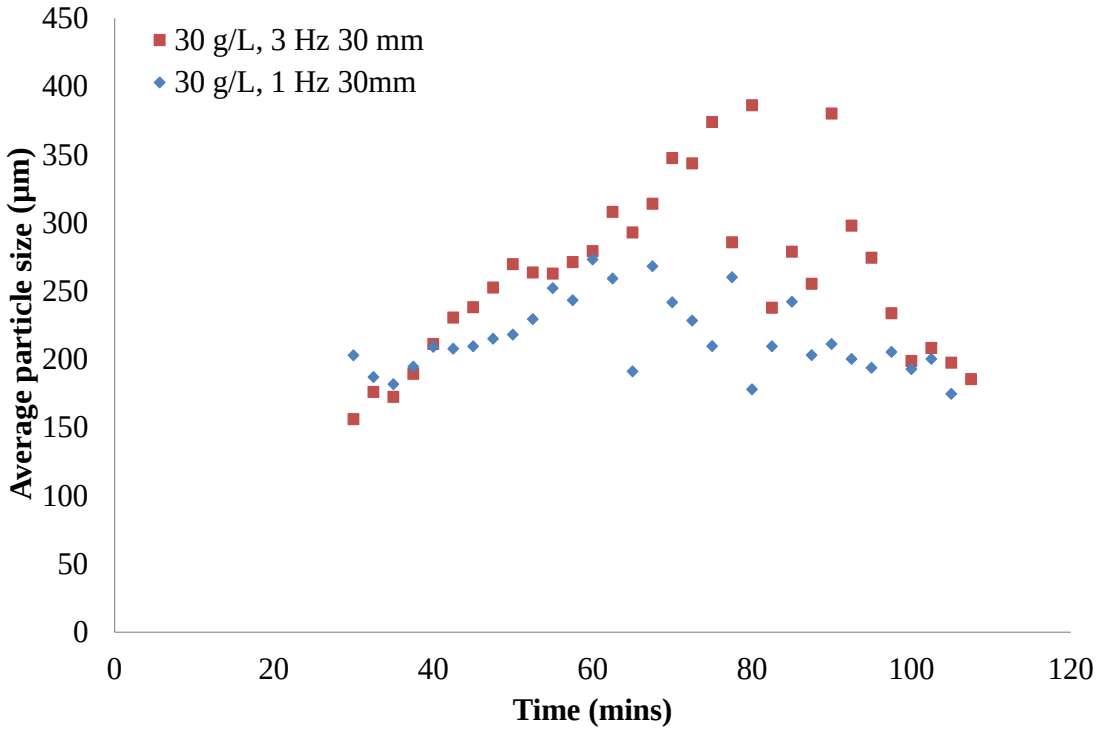

Figure 5-14: Plots showing average particle size (d(0,5)) measurements obtained by laser diffraction for experiments 1 and 3 in Table 5-1 as baffle frequency was increased

Figure 5-14 shows the average particle size (d(0,5)) of the off-line samples collected during the two experiments (3 Hz 30 mm and 1 Hz 30 mm). The average particle size increases steadily at a higher frequency of 3 Hz and an amplitude of 30 mm, however, instead of levelling out the particle size then decreases to close to the initial size from the first few samples collected following nucleation. This could possibly be due to the intense oscillation conditions causing the particles to break up at higher solid concentrations due to collisions with the walls and baffles of the reactor and also between the particles themselves. The trend of the particles from the volume-weighted mean values (d(4,3)) shows that this mirrors the trend of the Raman measurements more closely and becomes more consistent towards the end of the crystallisation (Figure 5-15). The particle size throughout the crystallisation using a lower frequency of 1 Hz remains within a narrower range of 150 to 250 µm. It appears to become more consistent at around 200 µm from ~85 minutes onwards (3 residence times following nucleation).

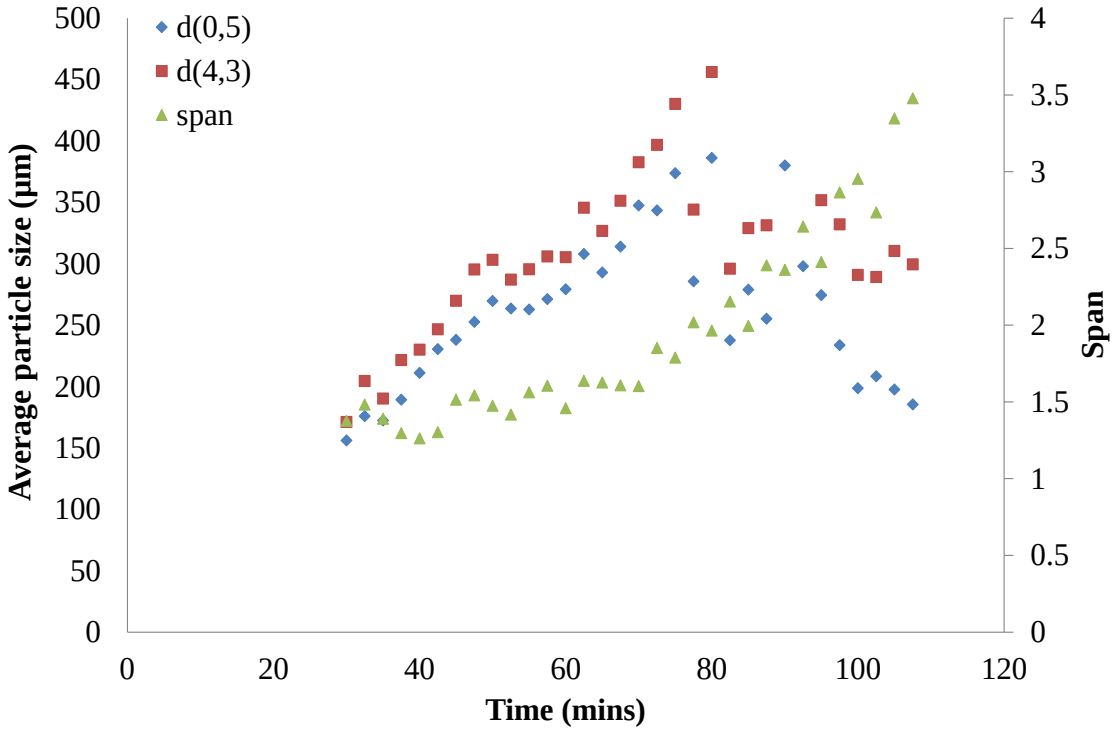

Figure 5-15: Plots showing average particle size (d(0,5)), volume-weighted mean (d(4,3)) and span of the distribution measurements obtained by laser diffraction for experiment 1 in Table 5-1 when a frequency of 3 Hz and a amplitude of 30 mm was used

The differences observed between the d(0,5) and d(4,3) trends could be explained by attrition of the particles during the crystallisation causing an overall decrease in the mean particle size while the span of the particle size distribution continued to increase during this period due to there being a wider variation of particle sizes resulting from particle breakage. As the span was increasing while the mean particle size was decreasing, this resulted in a fairly consistent d(4,3) value during this time. Figure 5-16 shows the crystallisation profiles obtained from Raman measurements when the frequency was increased from 1 to 3 Hz at a fixed low amplitude of 10 mm.

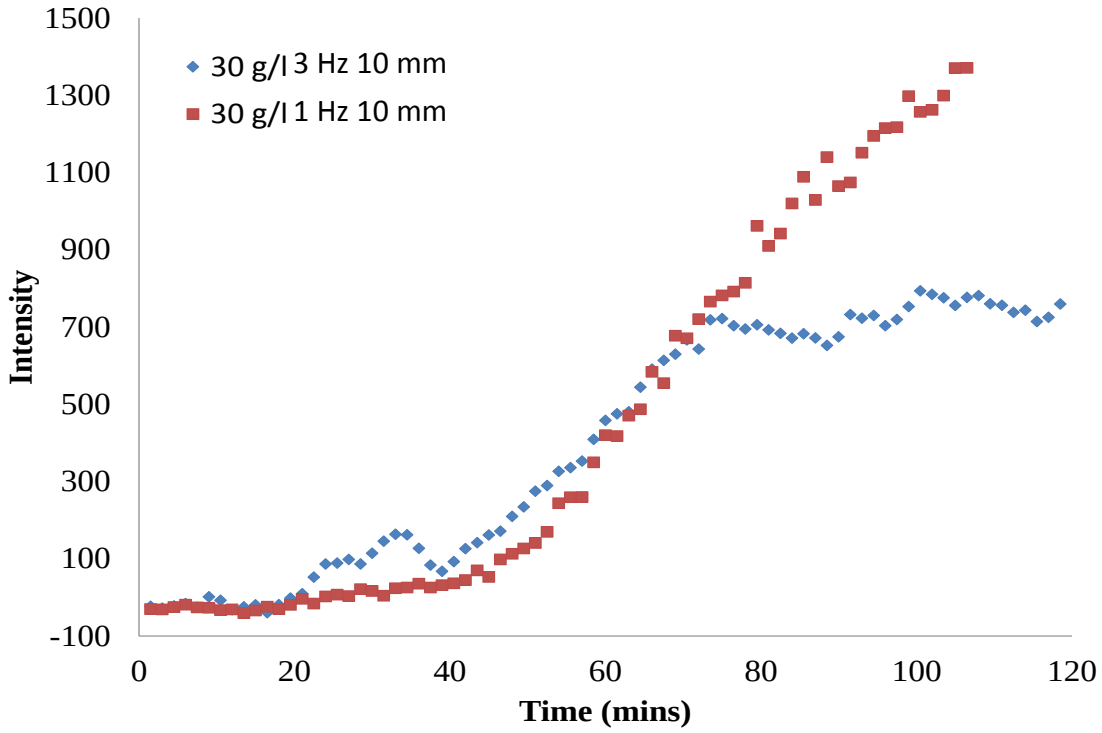

Figure 5-16: Crystallisation profile for L-glutamic acid from two experiments (2 and 4 in Table 5-1) of increasing oscillation frequency, based on 1st derivative Raman intensity at 877 cm^{-1}

Figure 5-16 shows that when the frequency was increased at a fixed low amplitude and a fixed solution concentration of 30 g/L, the nucleation temperature is similar for both frequencies used. As with the experiments at a fixed amplitude of 30 mm, the Raman intensity is much higher at a lower frequency of 1 Hz. Again this was found to be mostly due to the differences in solid formed during the crystallisation as a higher concentration of solid material was produced in the later stages of the crystallisation (~1.5 grams more) at a lower frequency (figure not shown). This could be due to the difference in nucleation and growth rates at a lower frequency with a smaller number of nuclei being formed during nucleation followed by slow growth rates resulting in growth of the nuclei into bigger particles. The particle size measurements were also found to be larger for particles obtained using the least intense oscillation conditions of 1 Hz 10 mm.

5.3.4.2 Effect of oscillation amplitude

The effect of oscillation amplitude on particle properties was also investigated and this is shown in Figure 5-17.

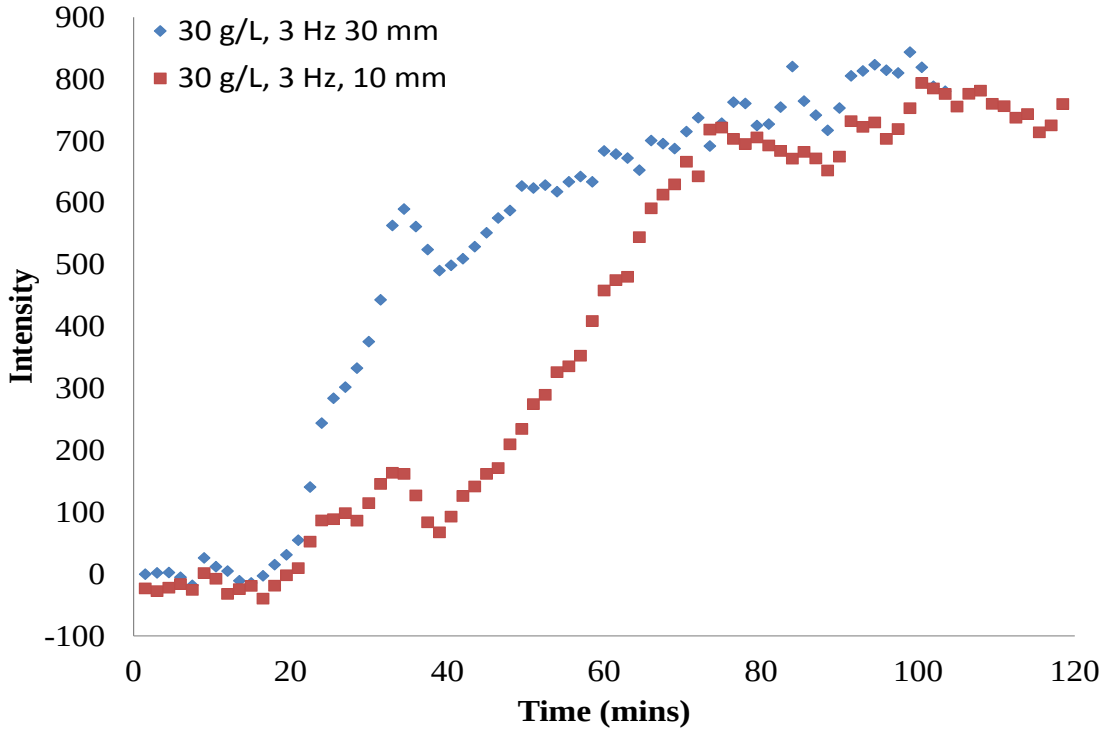

Figure 5-17: Crystallisation profile for L-glutamic acid from two experiments (1 and 2 in Table 5-1) of increasing oscillation amplitude, based on 1st derivative Raman intensity at 877 cm^{-1}

Figure 5-17 shows that as with varying the oscillation frequency, the amplitude does not impact the nucleation temperature greatly with nucleation taking place at approximately 20 minutes under both sets of conditions. In addition, there is also a small peak in Raman intensity shortly after nucleation as with the experiments in Figure 5-11, however, they are less pronounced in this case. The signal intensities toward the end of the crystallisation also stabilise at a similar value, suggesting an equivalent concentration of solid was being produced. The main effect of oscillation amplitude appears to be during crystal growth with a lower amplitude resulting in a much slower growth profile. The majority of crystal growth was complete within 50 minutes (30

minutes following nucleation) at a high amplitude of 30 mm. However, decreasing the amplitude increased this period of crystal growth to 60 minutes. Figure 5-18 shows the different weights of solid material collected during the two crystallisation experiments.

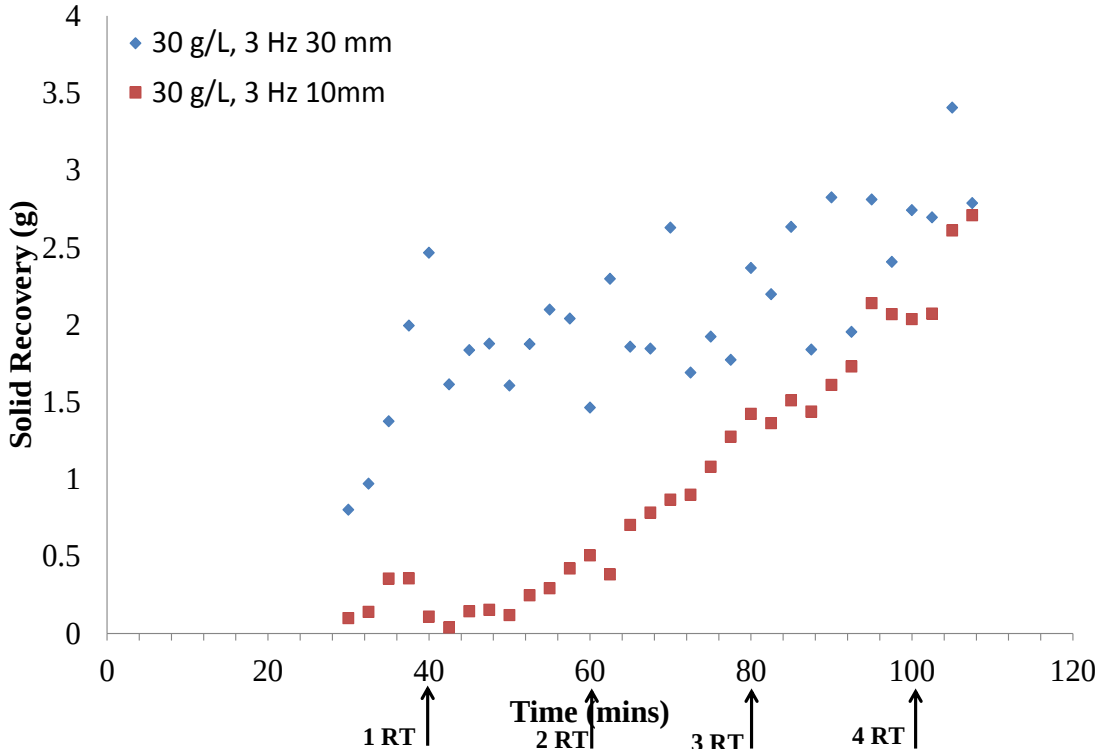

Figure 5-18: Plot of solid recovery every 2.5 minutes for experiments 1 and 2 in Table 5-1, when baffle amplitude was increased

Figure 5-18 shows the trends for solid recovery are in good agreement with the crystallisation profiles obtained in Figure 5-17 describing the crystal growth stage. It can be seen that there is a much more rapid increase in the amount of crystals being produced initially at a higher oscillation amplitude of 30 mm. This shows that the crystal growth rates are faster and the majority of crystal growth is complete within a relatively short time period. In contrast, the mass of particles produced following nucleation is reduced using a lower amplitude. There appears to be a slower steadier growth of the crystals until a similar mass of particles was attained in the final 20-30 minutes. The main difference between the Raman measurements and the mass of particles produced

during the crystallisation is that in the crystallisation profiles deduced from the Raman measurements, the system appears to be at steady state from approximately 70 minutes when both oscillation amplitudes are applied. The amount of solid recovered during the crystallisation using an oscillation of 3 Hz 30 mm appears to become more consistent earlier than when using a lower amplitude, however, this is still within a fairly large range of between 2-3 g per 2.5 min period. Figure 5-19 shows the plot of the average particle size of the off-line samples collected during both crystallisation experiments.

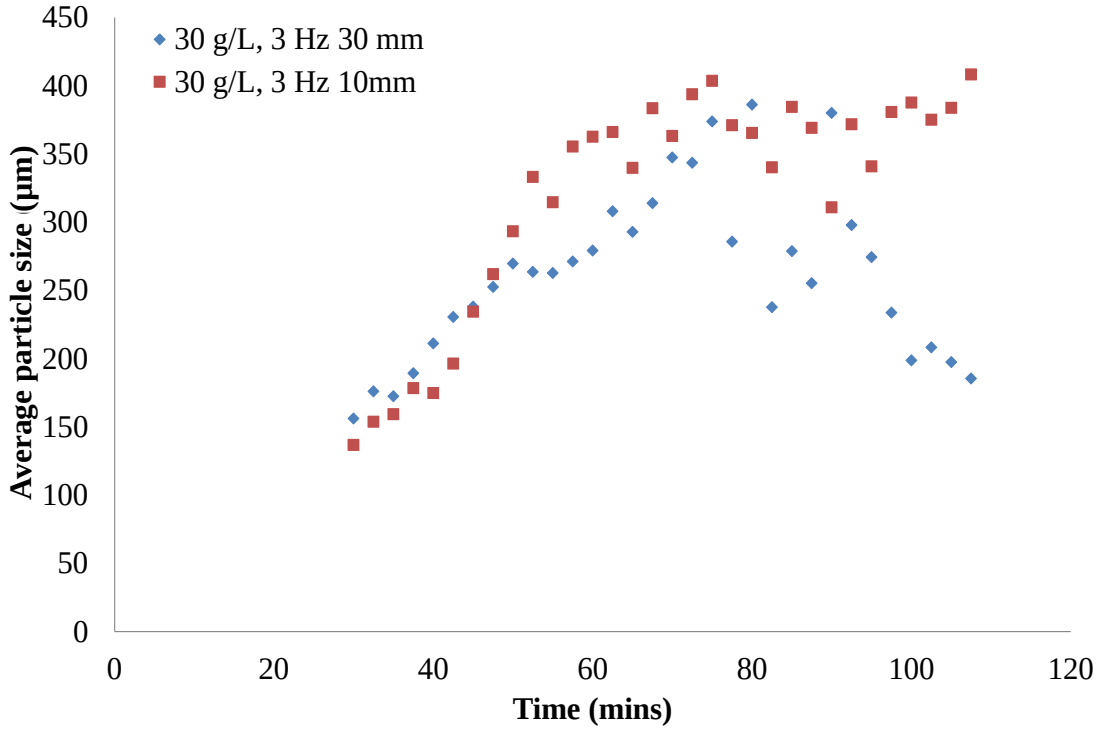

Figure 5-19: Plots showing average particle size (d(0,5)) measurements obtained by laser diffraction for experiments 1 and 2 in Table 5-1 as baffle amplitude was increased

Figure 5-19 shows that during the crystallisation at 3 Hz and 10 mm although the mass of particles does not become consistent (Figure 5-18), the average particle size levels off after approximately 1.5-2 residence times following nucleation and remains within a 50 µm range until the crystallisation is concluded 60 minutes later. However, when the crystallisation is carried out at 3 Hz and 30 mm, the particle size appears to level out briefly before it decreases quite steadily over the remainder of the crystallisation until it

reaches a size similar to that obtained in the initial stages following nucleation (~150 µm). It would appear that the Raman measurements are influenced by the trend of the solid concentration in this case rather than the particle size obtained whereas when oscillation conditions of 3 Hz and 10 mm are used, the Raman measurements follow the same trend as the off-line particle size measurements. Therefore, it would appear that when the Raman signal indicates that the system may be operating at steady state, it may be that it is either the solid concentration or the particle properties that are consistent, or potentially both, but this cannot be determined from the Raman measurements alone. Figure 5-20 shows a selection of the particle size distributions from the off-line samples collected throughout the crystallisation.

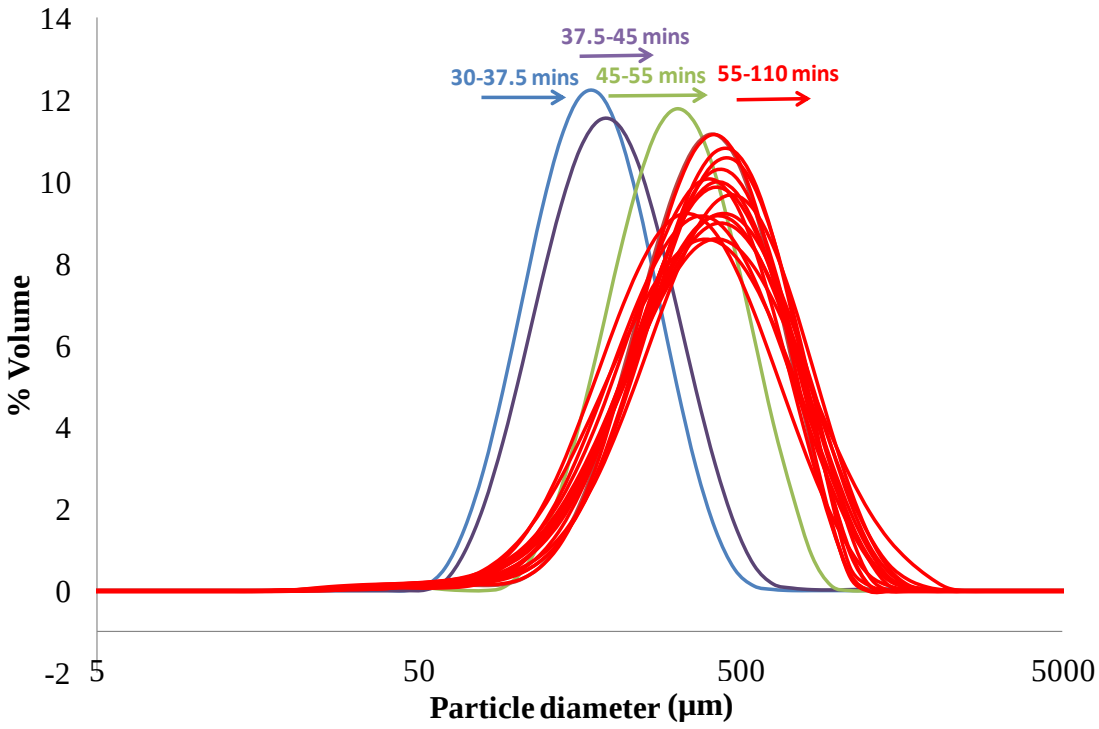

Figure 5-20: Particle size distributions obtained using laser diffraction of off-line samples of L-glutamic acid obtained at 3 Hz and 10 mm in a COBR

As mentioned previously, it is important to know that the system has reached steady state during the crystallisation and how long it takes for the particle properties to become

consistent. Figure 5-20 shows how the PSD changes from the start of the measurements as the particle size increases during growth. From 55 minutes onwards (1.5 residence times following nucleation), the distributions overlay relatively well until the experiment is concluded. Throughout the crystallisation the span of the PSD of the off-line samples collected every 2.5 minutes (8 times per residence time) remains fairly constant and is relatively narrow staying below a value of 1.7. A narrow PSD is a desired property in the production of solid material through crystallisation processes and so obtaining a consistent average particle size as well as a consistently narrow particle size distribution is beneficial. It was also important to know that the outcomes of the experiments were reproducible. Figure 5-21 shows a plot of the average particle size against time for 2 replicate experiments carried out using a frequency of 3 Hz and amplitude of 10 mm.

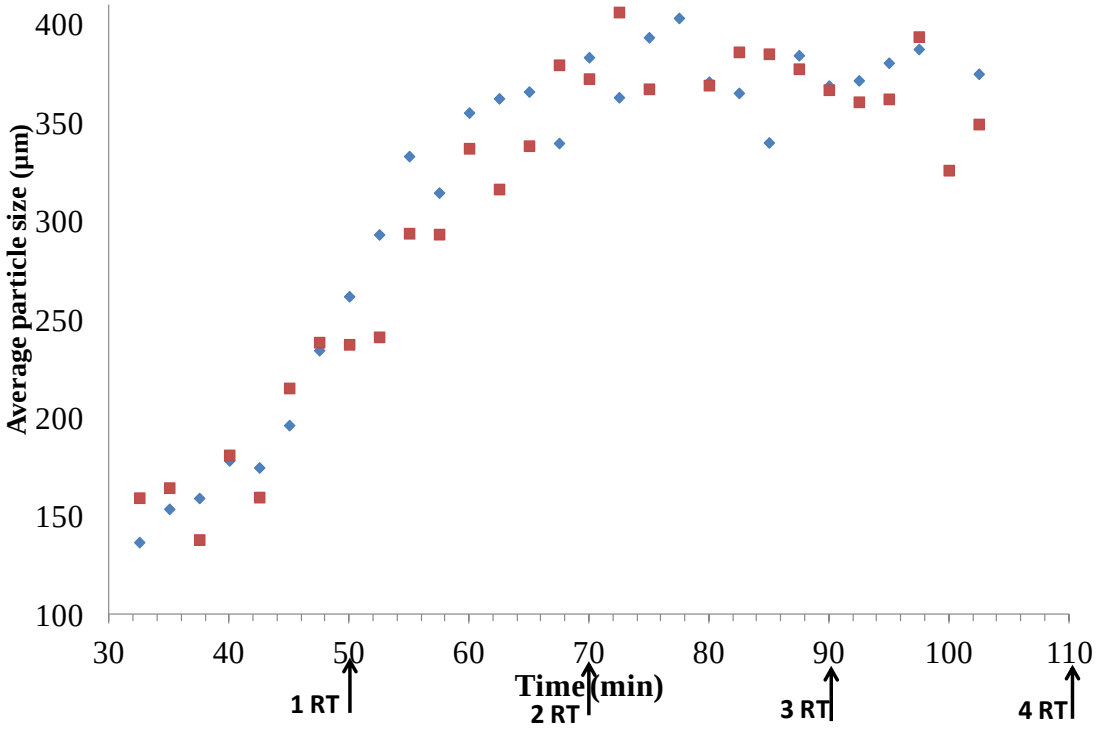

Figure 5-21: Plot of average particle size obtained using laser diffraction against time for 2 replicate experiments for the crystallisation of L-glutamic acid using a concentration of 30 g/L and oscillation conditions of 3 Hz and 10 mm

Samples were collected for four residence times following nucleation and the particle size started to become consistent after 1.5-2 residence times (3 residence times from the start of the experiment). This suggests the system is running close to steady state from 2 residence times following nucleation (according to the particle size and Raman measurements) and the average particle size remains within a 50 µm range. The experiment was repeated and the trend in the particle size of the slurry collected was relatively similar showing that the results are reproducible using this set of conditions (3 Hz 10 mm). XRD showed that the pure alpha form was produced in both repeat experiments.

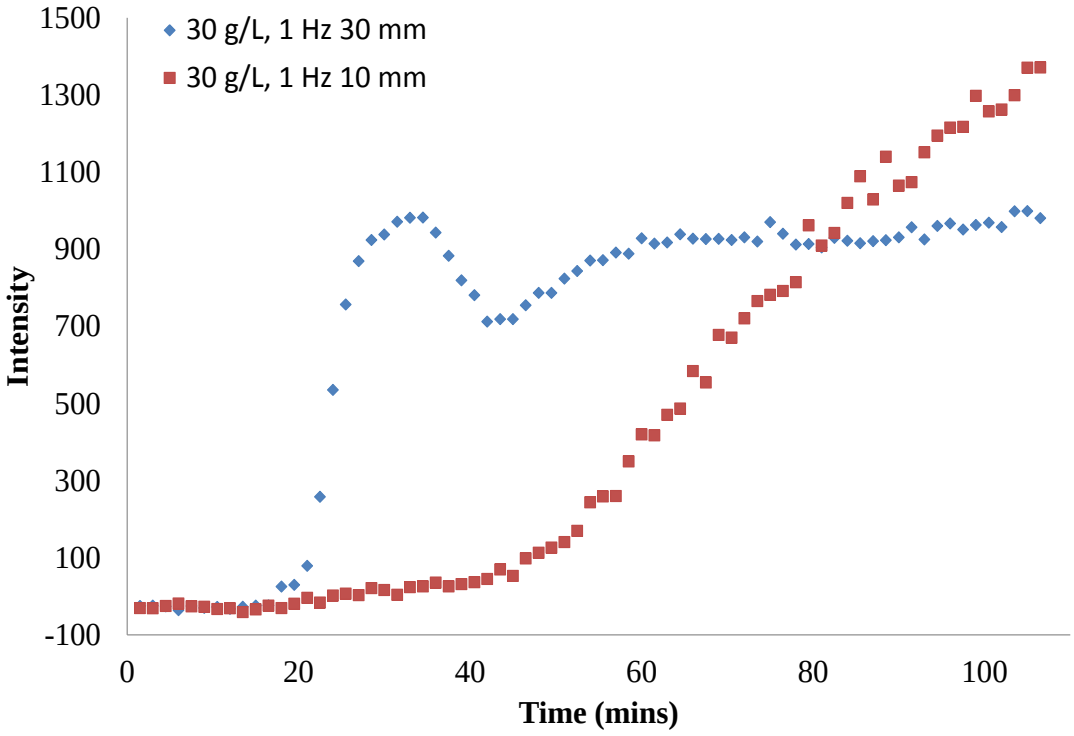

Figure 5-22: Crystallisation profile for L-glutamic acid from two experiments (3 and 4 in Table 5-1) of increasing oscillation amplitude, based on 1st derivative Raman intensity at 877 cm^{-1}

Figure 5-22 shows the effect of oscillation amplitude at a fixed low frequency. When the oscillation amplitude was increased at a low frequency of 1 Hz, a similar trend was observed as that in Figure 5-17 where a significantly slower increase in the Raman intensity was evident. However, in this case the profiles do not end up at a similar signal

intensity towards the end of the crystallisation. Whereas the intensity begins to level out from 60 minutes onwards using conditions of 1 Hz and 30 mm, the combination of a low frequency and a low amplitude appear to significantly affect the growth rates and crystal growth is still not complete by the end of the crystallisation (after 4 residence times). Figure 5-23 shows the solid recovery details for the two crystallisation experiments.

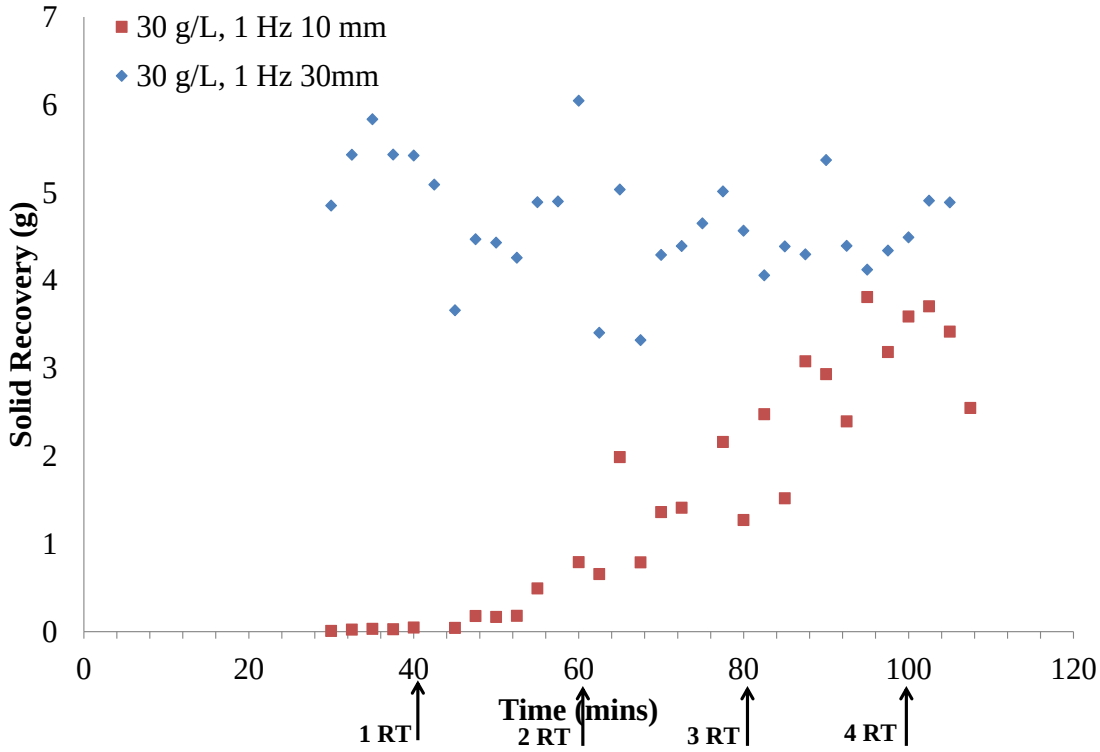

Figure 5-23: Plot of solid recovery every 2.5 minutes for experiments 3 and 4 in Table 5-1, when baffle amplitude was increased

Figure 5-23 shows there is a significant difference in crystal production when the amplitude is increased at a low frequency. Crystal growth occurs rapidly at the higher amplitude and reaches a maximum value relatively quickly. This value then decreases slightly and remains fairly consistent for the remainder of the crystallisation. However, when oscillation conditions of 1 Hz and 10 mm are applied, the amount of crystals being produced in the initial stages is considerably lower than at a higher amplitude. This was followed by a slow, steady increase in the mass of crystals produced suggesting relatively slow growth rates at these conditions which did not appear to be complete by

the end of the measurements. Alternatively, there could have been a smaller amount of nuclei formed initially and so a smaller number of crystals available to grow. The Raman measurements in Figure 5-22 show that the Raman signal increases to a final value higher than that observed at 1 Hz 30 mm oscillation. However, the values for the solid concentration are in a similar range towards the end of the crystallisation so this would not explain the increase in the Raman signal. It was observed that when a low frequency and amplitude were used in combination, this resulted in sedimentation in the second half of the crystallisation which gradually accumulated and would affect the Raman measurements made causing the intensity to be higher than expected.

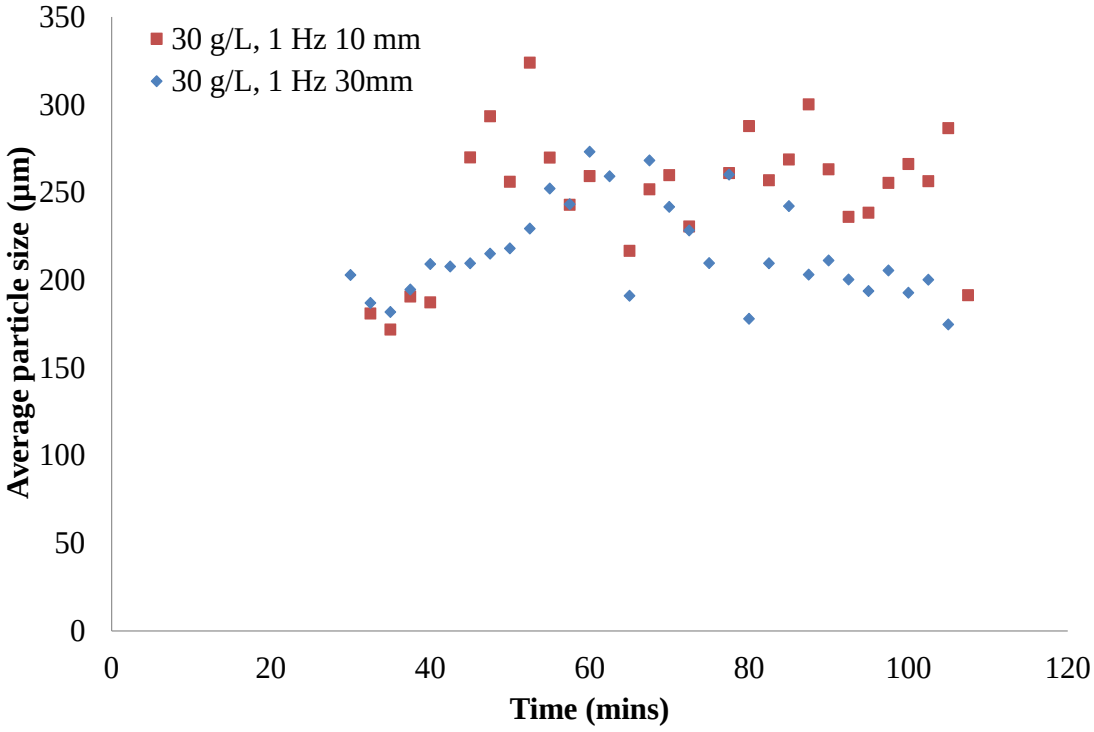

Figure 5-24: Plots showing average particle size (d(0,5)) measurements obtained using laser diffraction for experiments 3 and 4 in Table 5-1 as baffle amplitude was increased

Figure 5-24 shows the off-line particle size measurements from the experiments of increasing amplitude. The particle size remains within a relatively small range of between 250 and 300 µm shortly after the start of collection of the solid material when a low amplitude of 1 Hz is used. This was unexpected as the solid recovery measurements

suggested a slow growth rate so it would be expected that the particle size would increase slowly during the crystallisation. It is possible that the low frequency and low amplitude caused a decreased amount of particles to be produced, but the particles appeared to be of a relatively consistent size shortly following nucleation as they had the opportunity to consume the supersaturation quickly as there was a smaller amount of nuclei present that could grow to a larger size. When a higher amplitude was applied, the particle size reaches a maximum value at around 60 minutes which then decreases slightly. However, the particle size remains close to 200 µm for the remainder of the experiment.

5.3.4.3 Effect of solution concentration

Figure 5-25 shows the effect on the Raman measurements when two different solution concentrations were used in the crystallisation experiments at a fixed frequency and amplitude.

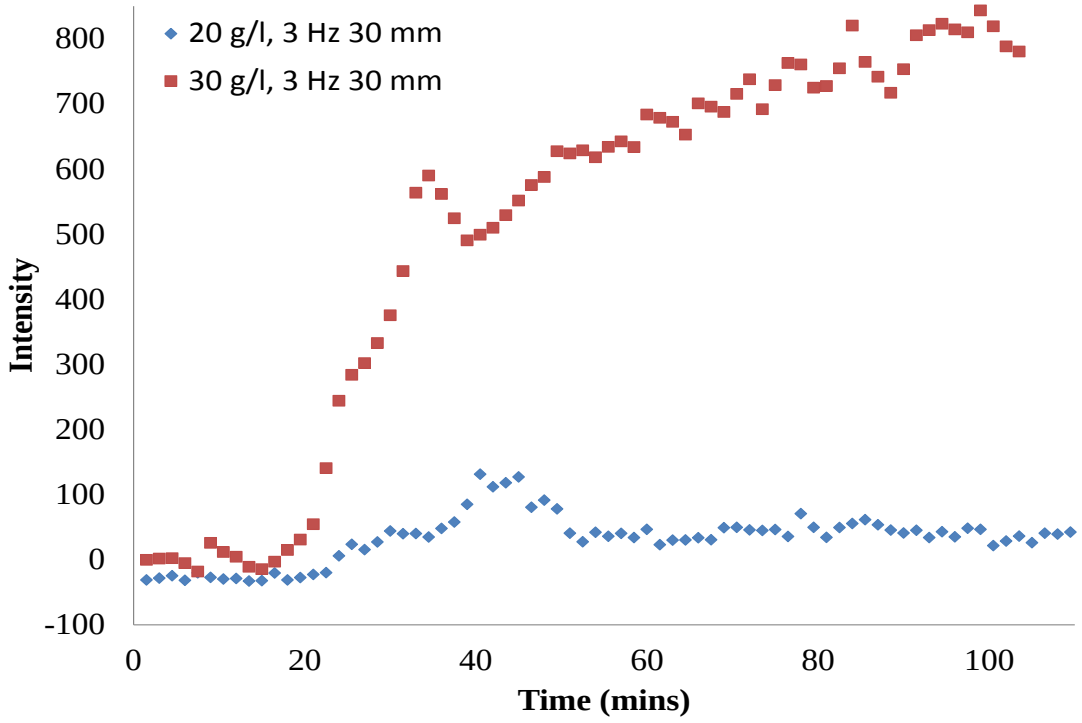

Figure 5-25: Crystallisation profile for L-glutamic acid from two experiments (1 and 5 in Table 5-1) of increasing solution concentration, based on 1st derivative Raman intensity at 877 cm^{-1}

When a higher solution concentration of 30 g/L was used in Figure 5-25, nucleation appears to occur slightly earlier than at a lower concentration of 20 g/L. There is also a quick increase in the Raman signal following nucleation suggesting rapid crystal growth at these conditions. A greater amount of crystals would be expected to be produced using a higher solution concentration. When a solution concentration of 20 g/L was used there was a slow increase in the Raman signal over a period of 20 minutes following nucleation at around 25 minutes. This reached a maximum and was followed by a slight decrease before the signal leveled off for the remainder of the experiment. There was not a large amount of solid material detected by Raman using these operating conditions. Figure 5-26 shows the mass of crystals collected during the two crystallisation experiments.

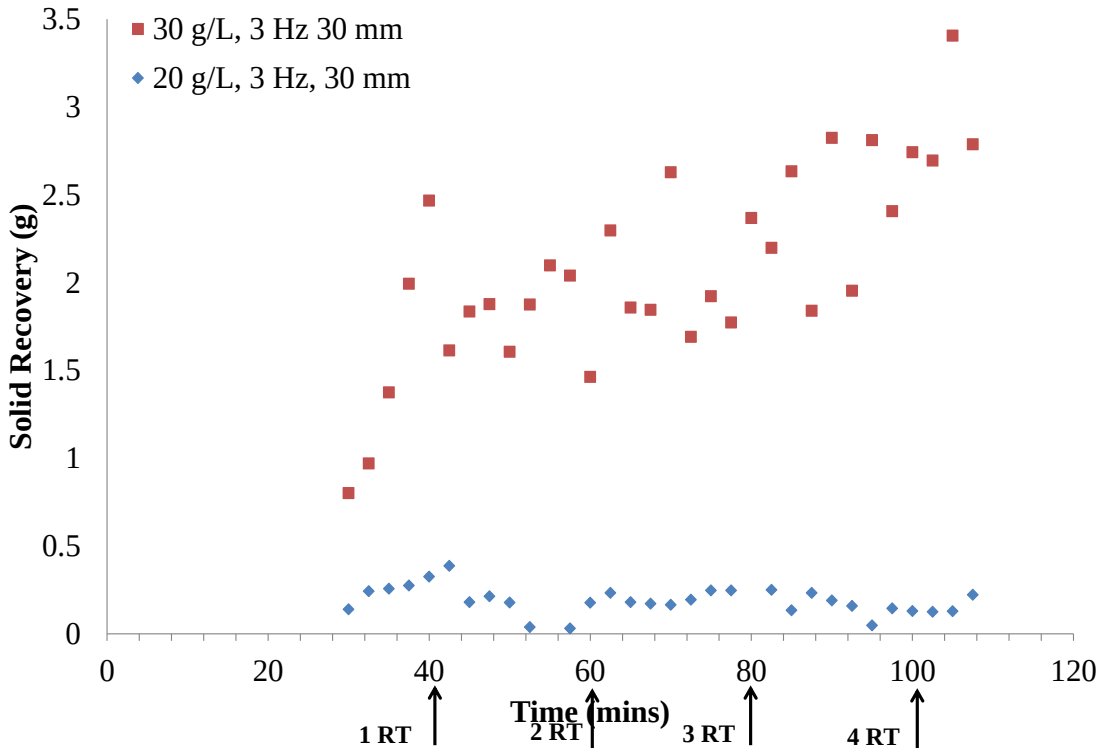

Figure 5-26: Plot of solid recovery every 2.5 minutes for experiments 1 and 5 in Table 5-1, when solution concentration was increased

Figure 5-26 shows that the mass of particles produced during the crystallisation using a solution concentration of 20 g/L is significantly lower than that produced using the same

conditions at 30 g/L. This explains why the crystallisation profile obtained from the Raman signal is relatively low and the trend of the solid concentration is similar in that there is an initial slow increase in particles during crystal growth in the initial 10-15 minutes followed by a decrease when the amount of solid material being produced becomes fairly consistent from approximately 60 minutes onwards. In the final 2-3 residence times, when the solid concentration measurements level out, approximately 1.5-2 g of material was produced using a solution concentration of 20 g/L. This is compared with over 15 g of material per residence time at a higher concentration of 30 g/L. Table 5-1 also shows that from the four experiments conducted using a solution concentration of 20 g/L, only the most intense oscillation conditions of 3 Hz and 30 mm resulted in any crystals being produced. Figure 5-27 shows the average particle size of the solid material as the crystallisations at the two concentrations progressed.

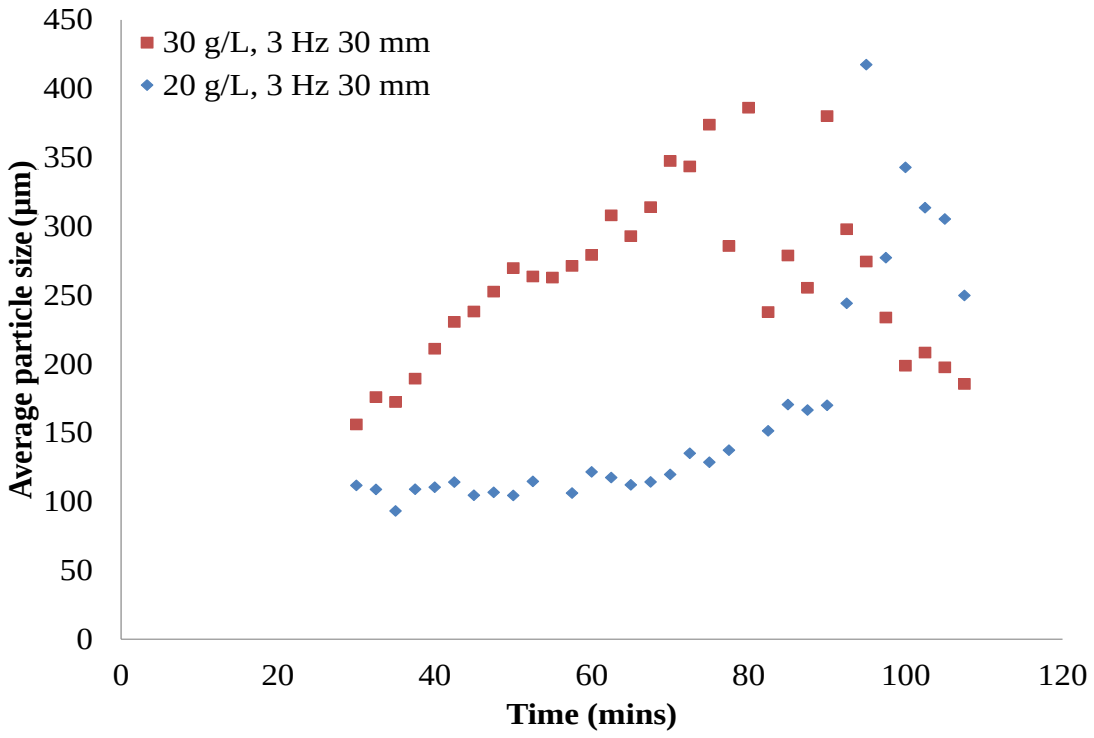

Figure 5-27: Plots showing average particle size (d(0,5)) measurements for experiments 1 and 5 in Table 5-1 as solution concentration was increased

It would be expected that the average particle size of the off-line samples collected during the crystallisation would be smaller when a lower solution concentration was used. During the crystallisation at 30 g/L, there is a steady increase in the average particle size following nucleation until this reaches a maximum value at around 80 minutes. Instead of the particle size then leveling off as seen with the other experiments using this concentration, the particle size then decreases until it reaches a value similar to that obtained from the initial samples collected (~150 μm). As mentioned previously, it was thought this was due to the intense oscillation conditions causing the particles to break up due to particle-particle collisions and contact with the reactor wall and baffles. In contrast, the particle size increases relatively slowly over a longer period of time for 20 g/L LGA. However, towards the end of the crystallisation the particle size increases quite significantly to a value larger than that obtained at 30 g/L at the same stage in the crystallisation. As there was significantly less solid material produced and no significant decrease in the particle size towards the end of the crystallisation using 20 g/L, it is possible that there was not significant contact between the particles and the reactor surfaces or each other despite the intense oscillation conditions applied, allowing the particles to grow to a larger size.

5.3.5 Comparison of batch and continuous OBR

It has been reported in the literature that it is potentially easier to scale up from a batch OBR to operate in continuous mode (COBR) than with traditional batch stirred tank reactors.[13] This would mean that crystallisation experiments could be carried out in small lab-scale batch OBR reactors and when the conditions have been optimized these operating parameters could then be transferred to the continuous OBR and the solid material could be produced at a larger scale for extended periods of time. However, although the mixing within both the batch and continuous reactors can be described as oscillatory, the way in which this mixing is achieved is quite different. In the batch OBR set-up the baffles are moved at different frequencies and amplitudes to oscillate the reactor contents. In contrast, the continuous OBR is composed of fixed baffles and it is

the fluid which is oscillated at various intensities. It would be expected that there would be some differences in the particle properties between the two different reactors when the same operating conditions are employed. It has been shown in section 4.3.3 that particles can be produced repeatedly in a batch OBR with improved properties such as particle size distribution than can be achieved in a conventional batch STR. It has also been shown in this section that by varying the operating conditions in the continuous OBR, the particle size of the solid material can be altered and in most cases the particle size remains fairly consistent once steady state has been attained.

It is difficult to truly compare the results obtained from the non-invasive Raman measurements in the batch and continuous OBRs. The Raman measurements are collected over a range of temperatures during a cooling crystallisation in the batch OBR and information on the entire crystallisation process, i.e. nucleation and crystal growth can be obtained. In comparison, the Raman probe is focused on a single section of the continuous OBR which is at a fixed temperature throughout the crystallisation. Due to the fact that in these experiments the Raman probe was positioned at the bend prior to the slurry outlet, nucleation would not be detected as this took place at an earlier section of the reactor. The first crystals were detected once nucleation had already taken place and crystal growth had begun once the particles had moved down the reactor to the point where the Raman measurements were being made. However, the effect of the operating conditions on the particle properties can be used to make a comparison between the two reactors.

A significant difference between the two reactors is the range of solution concentrations that can be accommodated. In the batch OBR, the highest concentration attempted for crystallisation of LGA was 45 g/L and the lowest was 15 g/L. The reactor could be operated relatively efficiently at both these extremes of concentration as long as the final temperature of the crystallisation was below the nucleation temperature for the 15 g/L starting solution. In addition, it was found that with increasing concentration, a rise in

the oscillation intensity was required to ensure that the material was suspended adequately. When a low frequency and amplitude was applied the solid material descended to the bottom of the reactor and therefore uncontrolled crystal growth resulted leading to a wide particle size distribution (with spans in the region of 3). When these concentrations were attempted for crystallisation in the continuous OBR, a high solution concentration resulted in significant sedimentation of the crystals on the reactor wall which built up until blocking of the reactor occurred within 2 residence times following nucleation. Even though the cooling rate was increased (increased flow rate) in an effort to reduce the problems encountered at this concentration, blocking still occurred in a relatively short period of time. Therefore the concentration was lowered to 30 g/L and it was found that the reactor could be operated for at least 4-5 residence times at this concentration with little evidence of sedimentation and so it may be that the reactor could be operated for many more residence times before blocking potentially became an issue. When a low concentration of 15 g/L was attempted as in the batch OBR, nucleation was not observed even after 4 residence times. It was thought that in a batch OBR the movement of the baffles can cause some contact with the reactor walls and therefore this scraping can help to initiate nucleation at a higher temperature than what would occur normally. This was observed in section 4.3.3 where at the same solution concentration, nucleation took place at a higher temperature in the batch OBR than in a STR. In addition, a low concentration of 15 g/L resulted in no crystals being formed when the crystallisation was carried out in a stirred tank, however when a batch OBR was used crystals were produced. It is possible that at a low solution concentration, nucleation did not occur in the continuous OBR since the baffles are fixed and no contact between the baffles and the reactor wall took place to induce nucleation similar to what was observed in a batch STR. When the concentration was increased to 20 g/L in the COBR, nucleation was only observed when the most intense oscillation conditions were applied. Therefore, the workable concentration range that was possible in the case of L-glutamic acid was above 20-25 g/L and ideally below 35 g/L. This is an extremely narrow range of solution concentrations and does not allow much optimisation of the mass of solid produced. However, with continuous reactors once the operating

conditions have been optimised to produce particles of the desired polymorph, size and distribution, the yield can be increased by operating the reactor for longer periods of time so this issue can be overcome.

The obvious other difference between the batch and continuous OBR was the polymorphic composition of the crystals produced. In the batch STR the beta form was produced using slow cooling for all operating conditions attempted. The only occasion a mixture of forms was obtained was when rapid cooling was employed, however, the pure alpha form was not formed under any of the conditions attempted in section 4.3.3. Conversely, in the batch OBR, the pure beta form was not produced in any of the experiments conducted (Table 4-2). In most cases, especially using a high solution concentration, a mixture of forms was produced. However, the pure alpha form could also be obtained under certain combinations of operating conditions such as a low solution concentration and a low final temperature. It was thought that as the contact of the baffles with the reactor wall caused nucleation to take place at a higher temperature than in the batch STR that this promoted the nucleation of the metastable alpha form initially, as at a higher temperature the solution would be in the metastable form of the alpha rather than the beta form. The continued cooling of the solution would then lead to nucleation of the beta form or continued nucleation and growth of the alpha form depending on the initial solution concentration. This would explain the mixtures of polymorphic forms produced at 45 g/L and the pure alpha form obtained at lower solution concentrations, *e.g.* 20 g/L. However, in the continuous OBR, the pure alpha form was produced in all the experiments, using different operating conditions including solution concentration. It was observed that in the majority of the crystallisation experiments conducted in the continuous OBR, nucleation took place in the same approximate area of the reactor despite the conditions used. As nucleation always appeared to take place in the areas of the reactor where the temperature was in the region of 20-25^{o}C (from visually inspecting the area of the reactor where nucleation first took place), it was thought that this was always in the metastable zone for the alpha

polymorph at all the conditions used. As the majority of nucleation continued to take place in this relatively small section and crystal growth took place in the remaining sections of the reactor where the temperature was decreasing with increasing length, it was thought this was why a mixture of forms was not observed.

Despite the obvious differences between the two reactors, the effect of varying operating conditions such as oscillation frequency and amplitude on the particle properties could be compared. In the case of oscillation frequency, the effect on the particle size, particle size distribution and yield of solid recovered could be contrasted. In the batch OBR experiments of increasing frequency (1, 2 and 3 Hz) at a fixed amplitude of 10 mm, a decrease in the mean particle size of the final product was observed with a corresponding increase in the oscillation frequency. In addition, the particle size distribution became narrower with increasing frequency. An increase in the amount of particles obtained at the end of the crystallisation was also observed when the frequency was increased whilst all other parameters including the duration of the crystallisation remained the same. Therefore, it was relatively easy to determine that an increase in the oscillation frequency in the batch OBR resulted in particles with a smaller mean size, narrower distribution produced at increased yields, which are all beneficial attributes in industrial crystallisation. In contrast, the opposite was observed in the continuous OBR. When the oscillation frequency was increased from 1 to 3 Hz at a fixed amplitude of 10 mm, the mean particle size increased quite significantly. However, an increase in the amount of solid material produced during the crystallisation was observed at a lower frequency. The particle size distributions determined from the off-line samples collected throughout the crystallisation were relatively similar at both frequencies. Therefore, this suggests that the different methods in which oscillatory mixing is achieved in the batch and continuous reactors does have an impact on the particle properties and that the conditions cannot be directly transferred from one reactor to the other with the same outcome. It would, therefore, most likely be more beneficial to start with a smaller lab-scale continuous OBR in order to optimize conditions for potential new compounds to

be produced in this manner before scaling up to a larger COBR. However, this does not mean that the batch OBR should be completely discounted. As shown in this section and section 4.3.3 this reactor can provide benefits for compounds conventionally produced in a batch STR. It has been shown to produce particles with improved properties such as the PSD and by altering the operating conditions, particles of different particle sizes and PSDs can be produced repeatedly which has been shown to be difficult to achieve in a batch stirred tank reactor. In the case of L-glutamic acid, the metastable form, which is the industrially desired form, could also be produced without difficulty in the batch OBR. This is particularly important for compounds which are not compatible with the continuous OBR, for example, those which require a high solids loading for crystallisation experiments and would cause issues with blocking of the reactor. Although these systems cannot be transferred from conventional batch STR operation to this type of continuous reactor, it may be possible to optimize the conditions in a batch OBR and obtain a product with improved particle properties than that possible when produced in a batch STR.

5.4 Conclusions

The data presented in this chapter demonstrates the potential advantages and also some of the drawbacks of converting a batch process to continuous operation and in particular a continuous oscillatory baffled reactor. The study carried out in the continuous OBR using the model compound L-glutamic acid showed that as with the batch OBR the operating conditions such as oscillation frequency and amplitude affect the properties of the particles obtained. In this case, it was more difficult to determine the effect of solution concentration on the crystallisation process since only a narrow range of concentrations could be used. This means optimization of the yield is fairly limited although a range of particle sizes could be produced using various combinations of oscillation frequency and amplitude.

Increasing the oscillation frequency resulted in a decrease in the solid recovery throughout the crystallisation with an increased mean particle size than that obtained at a lower frequency. In comparison, an increase in the oscillation amplitude resulted in an increase in the solid material produced and a slightly lower particle size. In all of the experiments conducted, the alpha form was the sole polymorph produced. This could possibly be due to nucleation always taking place in a section of the reactor where the temperature is in the metastable zone for the alpha form (approximately 25^{o}C). Due to the fact nucleation appeared to be confined to this temperature section and the areas immediately surrounding this section during the crystallisation it was thought that this is why only formation of the alpha form was observed. It would appear that in the case of L-glutamic acid, seeding would be necessary in order to obtain the thermodynamically stable beta form, however due to the fact the alpha form is the industrially preferred form it could be a potential advantage that this is the only polymorph obtained. At this stage, it is difficult to know whether the continuous reactor will always result in a metastable form being continuously produced or whether this is compound specific, so this will need to be investigated with alternative compounds. However, if it is the case that the COBR can always be used to obtain the metastable form of a compound, this would be another potential advantage of this type of reactor since the metastable form is often the industrially desired polymorph and can be challenging to obtain in its pure form.

The continuous OBR is also shown to reach steady state under certain oscillation conditions which is an advantage as the particle properties will be consistent during this time. In some cases although the Raman measurements suggested the system was at steady state, not all of the particle properties were consistent. This showed the importance of having a complementary particle size technique in addition to the non-invasive Raman measurements to ensure all particle properties including solids concentration and particle size are consistent so it can be determined when the system is truly operating at steady state. By comparing the non-invasive Raman measurements and

the off-line particle size measurements it was possible to determine quicker which oscillation conditions resulted in the crystallisation reaching steady state for all particle properties. In the case of L-glutamic acid, the oscillation conditions of medium intensity including 1 Hz 30 mm and 3 Hz 10 mm resulted in steady state being attained within 1.5-2 residence times following nucleation and both the solids concentration and particle size were relatively consistent during this time. More intense oscillation conditions resulted in attrition of the particles once a certain level of crystal growth had taken place. Lower intensity oscillation conditions gave rise to extremely slow growth rates whereby crystal growth was not complete when the crystallisation was stopped 4 residence times following nucleation.

It was also discovered that it was not possible to transfer the operating conditions established in a batch OBR to a continuous OBR since the end result was not comparable. In most cases, the opposite effect was observed in batch than continuous when the effect of operating conditions was investigated. This was most likely due to the difference in the mixing used to create oscillation where the baffles are oscillated in the batch OBR whereas the baffles are fixed and the fluid oscillated in the continuous OBR.

5.5 References

1. K. Plumb, Continuous Processing in the Pharmaceutical Industry: Changing the Mind Set, *Chemical Engineering Research and Design*, 2005, **83**, 730-738.
2. J. Chen, B. Sarma, J. M. B. Evans and A. S. Myerson, Pharmaceutical Crystallization, *Crystal Growth & Design*, 2011, **11**, 887-895.
3. S. D. Schaber, D. I. Gerogiorgis, R. Ramachandran, J. M. B. Evans, P. I. Barton and B. L. Trout, Economic Analysis of Integrated Continuous and Batch Pharmaceutical Manufacturing: A Case Study, *Industrial & Engineering Chemistry Research*, 2011, **50**, 10083-10092.
4. T. Laird, Continuous Processes in Small-Scale Manufacture, *Organic Process Research & Development*, 2007, **11**, 927-927.
5. Manufacturing Chemist Pharma, Turn batch to continuous processing, October 2013. http://www.manufacturingchemist.com/technical/article_page/Turn_batch_to_continuous_processing/54954.
6. A. Pellek and P. V. Arnum, Continuous Processing: Moving with or against the Manufacturing Flow, *Pharmaceutical Technology*, 2008, **9**, 52.
7. B. Swichtenberg, Moving Beyond the Batch, October 2013. http://www.pharmamanufacturing.com/articles/2008/010.html?page=1.
8. C. Vervaet and J. P. Remon, Continuous granulation in the pharmaceutical industry, *Chemical Engineering Science*, 2005, **60**, 3949.
9. J. Vercruysse, D. Córdoba Díaz, E. Peeters, M. Fonteyne, U. Delaet, I. Van Assche, T. De Beer, J. P. Remon and C. Vervaet, Continuous twin screw granulation: Influence of process variables on granule and tablet quality, *European Journal of Pharmaceutics and Biopharmaceutics*, 2012, **82**, 205-211.
10. J. Burgschweiger and E. Tsotsas, Experimental investigation and modelling of continuous fluidized bed drying under steady-state and dynamic conditions, *Chemical Engineering Science*, 2002, **57**, 5021-5038.
11. R. Singh, M. Ierapetritou and R. Ramachandran, System-wide hybrid MPC–PID control of a continuous pharmaceutical tablet manufacturing process via direct compaction, *European Journal of Pharmaceutics and Biopharmaceutics*, 2013, **85**, 1164-1182.
12. N. G. Anderson, Practical Use of Continuous Processing in Developing and Scaling Up Laboratory Processes, *Organic Process Research & Development*, 2001, **5**, 613-621.
13. S. Lawton, G. Steele, P. Shering, L. Zhao, I. Laird and X. Ni, Continuous Crystallization of Pharmaceuticals Using a Continuous Oscillatory Baffled Crystallizer, *Organic Process Research and Development*, 2009, **13**, 1357-1363.
14. C. Ricardo and N. Xiongwei, Evaluation and Establishment of a Cleaning Protocol for the Production of Vanisal Sodium and Aspirin Using a Continuous Oscillatory Baffled Reactor, *Organic Process Research & Development*, 2009, **13**, 1080-1087.

15. S. Ferguson, G. Morris, H. Hao, M. Barrett and B. Glennon, In-situ monitoring and characterization of plug flow crystallizers, *Chemical Engineering Science*, 2012, **77**, 105-111.
16. H. Gros, T. Kilpiö and J. Nurmi, Continuous cooling crystallization from solution, *Powder Technology*, 2001, **121**, 106-115.
17. A. J. Alvarez and A. S. Myerson, Continuous Plug Flow Crystallization of Pharmaceutical Compounds, *Crystal Growth & Design*, 2010, **10**, 2219-2228.
18. O. Narducci, A. G. Jones and E. Kougoulos, Continuous crystallization of adipic acid with ultrasound, *Chemical Engineering Science*, 2011, **66**, 1069-1076.
19. A. U. Vanarase and F. J. Muzzio, Effect of operating conditions and design parameters in a continuous powder mixer, *Powder Technology*, 2011, **208**, 26-36.
20. L. Saerens, C. Vervaet, J.-P. Remon and T. De Beer, Visualization and Process Understanding of Material Behavior in the Extrusion Barrel during a Hot-Melt Extrusion Process Using Raman Spectroscopy, *Analytical Chemistry*, 2013, **85**, 5420-5429.
21. M. Fonteyne, S. Soares, J. Vercruysse, E. Peeters, A. Burggraeve, C. Vervaet, J. P. Remon, N. Sandler and T. De Beer, Prediction of quality attributes of continuously produced granules using complementary pat tools, *European Journal of Pharmaceutics and Biopharmaceutics*, 2012, **82**, 429-436.
22. Y. Hu, H. Wikström, S. R. Byrn and L. S. Taylor, Analysis of the Effect of Particle Size on Polymorphic Quantitation by Raman Spectroscopy, *Applied Spectroscopy*, 2006, **60**, 977-984.
23. H. Wang, C. K. Mann and T. J. Vickers, Effect of Powder Properties on the Intensity of Raman Scattering by Crystalline Solids, *Applied Spectroscopy*, 2002, **56**, 1538-1544.

6 Mixed suspension mixed product removal (MSMPR) as an alternative continuous reactor in the preferential crystallisation of L-glutamic acid polymorphs

6.1 Introduction

Mixed suspension mixed product removal (MSMPR) reactors are an alternative continuous vessel to tubular plug flow reactors (e.g. COBR). They are commonly used for the study of crystallisation kinetics including nucleation and growth rates when the crystallisation is operating at steady state.[1, 2] MSMPR and plug flow reactors are the two main types of continuous reactor available for crystallisation and often the choice of which reactor to use depends on the type of material which is being studied. For example, compounds which require long residence times for the crystallisation to take place are normally carried out in MSMPR reactors. This is due to tubular crystallisers requiring increasingly long lengths of reactor as the residence time is increased. Therefore, compounds which require shorter residence times are more suited to plug flow reactors.[3]

An MSMPR crystalliser is operated by feeding a hot solution into the vessel where it is mixed as uniformly as possible and cooling is applied to create supersaturation. Once a certain level of supersaturation is reached, nucleation and crystal growth can take place. The slurry is continuously withdrawn from the vessel and it is assumed that this has the same composition as that contained in the reactor.[4] The product from the vessel will exhibit a distribution of particle sizes due to the fact the crystals will have varying residence times within the reactor. This residence time distribution in an ideal MSMPR reactor is a decaying exponential function and shows that a large number of the particles will be removed after one residence time, however there will be a number of particles which will remain in the vessel for numerous residence times although this value will decrease with the increasing number of residence times.[5] MSMPR reactors can be operated at a fixed point on the solubility diagram for a selected compound and this can be achieved by keeping the vessel at a fixed temperature or keeping the solution concentration constant while the temperature of the reactor is altered. This can often be a successful way of obtaining the required polymorph as a point on the phase diagram is chosen where this form is most likely

to nucleate at a given temperature and concentration. However, there are several operating conditions which affect the properties of the particles obtained including the solution concentration and the residence time. The supersaturation is affected by the inlet solution concentration as this determines the supersaturation within the vessel and affects nucleation and growth rates.[6] The residence time is another important parameter: a longer residence time results in crystals with a larger average particle size, while a shorter residence time may result in a high level of fines due to the fact there is less time for the crystals to grow before they are withdrawn from the vessel in the outlet slurry. This means the supersaturation builds up in the vessel which favours nucleation rather than crystal growth. The residence time also affects the mass of crystals produced; a longer residence time usually results in a larger yield due to the increased levels of nucleation and growth possible. Therefore, a balance between the residence time and the solution concentration needs to be met which can give the desired production rate, average particle size and distribution.[6-8] However, the operating conditions alone can only control the particle size distribution (PSD) to a certain extent and it is known that crystalliser design also determines the range of particle sizes possible. For example, the operating conditions can be controlled in this type of reactor to produce a fixed mass of material, however, it is more difficult to control whether these particles are small, large or a range of sizes.[9]

MSMPR reactors are subject to oscillations following the start-up of the crystallisation. This means that the properties of the particles are affected and can change whilst these oscillations are taking place.[10] It takes, on average, ten residence times for this type of system to reach steady state and this is when the crystallisation kinetics can be determined.[11] A sample of the slurry is obtained to determine the crystal size distribution and this information can be used to establish nucleation and crystal growth rates at a certain residence time.[12, 13] Determining the crystallisation kinetics for a given compound in a MSMPR can be troublesome due to the complex relationship between supersaturation and the nucleation and growth rates. This is due to these variables changing during the crystallisation causing a feedback loop between the supersaturation, the total surface area and the size distribution (Figure 6-1).[9] There are several assumptions made when determining crystallisation kinetics

in a MSMPR. These include there being no crystals present in the feed solution, no attrition or agglomeration within the vessel and that the reactor contents are well mixed.[4, 14] It is, therefore, common for MSMPR crystallisations to be operated at small scale to ensure adequate mixing in the vessel and also to reduce the amount of material used prior to steady state being reached.[11] However, problems can be encountered with blockages occurring in the inlet and outlet tubes due to low flow rates used at a smaller scale.[14] In reality, many MSMPR reactors do not operate under these ideal conditions and agglomeration, growth rate dispersion and size dependent growth can cause discrepancies in the determined crystallisation kinetics for certain compounds.[1, 15] Growth rate dispersion and size dependent growth result in there being a larger number of fines as well as larger crystals than usually expected.[16] Even when the system is believed to be operating at steady state, there can be temporary periods which cause disturbances in the system and thus affect the nucleation and growth rates even when the operating conditions are kept constant. For example, a change in the production rate will influence the nucleation rate and cause a knock-on effect to the total surface area and growth rates.[9]

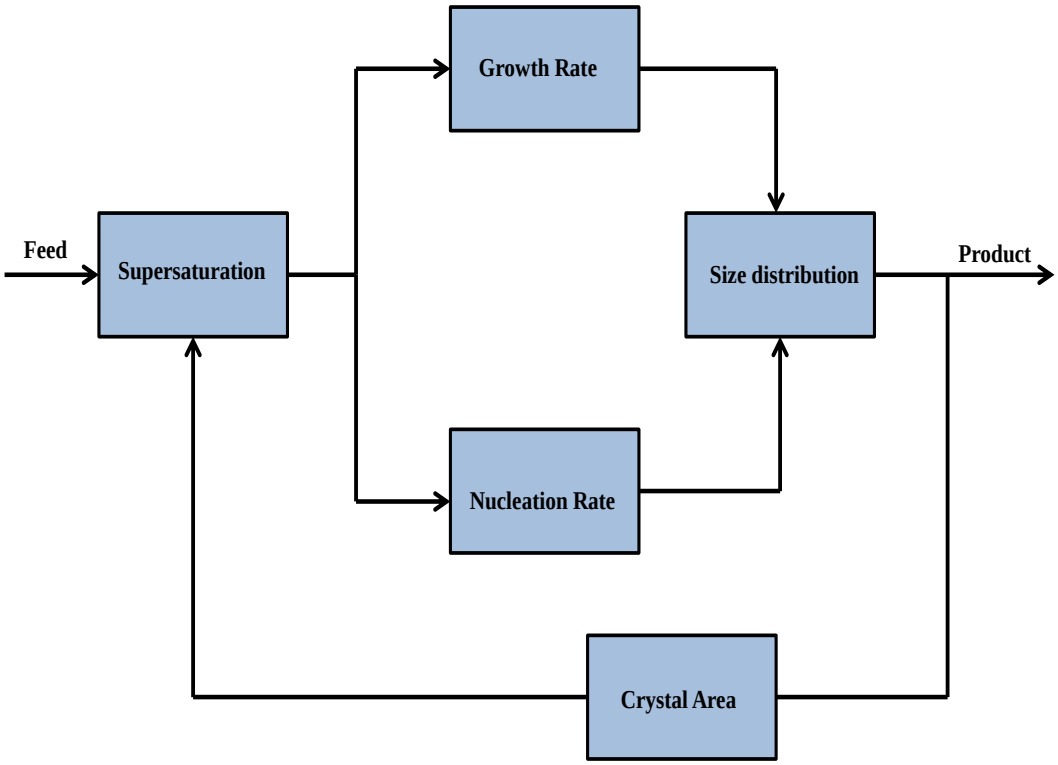

Figure 6-1: Illustration showing the relationship between crystallisation parameters[16]

The physical properties of particles are extremely important especially in the pharmaceutical industry where characteristics of the product such as particle size and polymorphic form can affect the bioavailability of the drug in the body. Particles of a relatively small size (< 100 μm) are usually preferred for most drug products due to the higher surface area and so improved dissolution in the body. One method of producing particles of a smaller average particle size is to control nucleation so that primary nucleation takes place rather than secondary nucleation. This can be achieved by operating the crystallisation using a higher level of supersaturation which means that nucleation is favoured over crystal growth resulting in a large number of crystals with a small mean particle size.[7] However, most industrial continuous crystallisers are currently operated to produce larger crystals due to the low supersaturation and long residence times employed and, therefore, milling is often necessary to obtain particles of the necessary size.[6] This can add significant costs to the manufacturing of a drug product due to the increased manpower and energy required for this additional unit operation. In addition, secondary nucleation is the most common mechanism in stirred tank reactors due to contact nucleation (particle-particle, particle-impeller, particle-wall collisions) and so these become an additional source of nuclei.[2]

An alternative way in which the properties of particles such as particle size and PSD can be manipulated is through seeding. Seeding involves introducing crystals of known characteristics, *i.e*. particle size and polymorph, at a pre-determined point during the crystallisation to control subsequent nucleation and growth. If the seeds are added at an appropriate time in the crystallisation, batch experiments which have previously had problems with product consistency can be repeated with reproducible results using this method. However, if the seeds are introduced at the wrong point in the process, the opposite effect can be experienced, whereby nucleation is encouraged and not necessarily of the desired polymorph. Therefore, it is important that seeding takes place at the desired point in the metastable zone, such that the seed particles do not induce nucleation, but instead act as substitutes for those nuclei that would have been formed through spontaneous nucleation. This means that the majority of growth takes place on the seed crystals so that the size can be determined

by controlling the supersaturation and the polymorphic form can also be regulated.[17] Therefore, it is a more complex process than just adding seeds of a certain form during the crystallisation, nevertheless, the seeding approach, like crystallisation have conventionally been carried out with a trial and error approach. The physical properties other than the polymorphic form of the seed crystals are also of importance. It has been shown that the concentration of seeds added (seed loading), the mean particle size, seeding type (dry or slurry) and the method of seeding (continuous or intermittent) can have an impact on the final product properties.[18, 19]

Seeding has been widely used in batch crystallisation as a method to obtain a product with preferred properties. Seeding the solution prior to nucleation taking place keeps the supersaturation low which helps to avoid secondary nucleation.[19] Therefore more control over the PSD is possible and it has been shown that it is possible to influence the final crystal size with the size of the initial seeds; a larger seed size results in a larger end particle size.[19, 20] In addition, seeding can be used to preferentially obtain either a unimodal or bimodal particle size distribution by altering the seed loading. A low seed loading results in a higher supersaturation than with an increased concentration of seeds and therefore secondary nucleation is more likely which results in a bimodal distribution.[19] Seeding has also been employed in continuous MSMPR reactors as a means to make start-up operation more efficient. By introducing seed crystals of pre-determined properties, it is possible to reduce the time necessary to reach steady state significantly compared with an unseeded crystallisation.[21] The use of seeding to selectively produce one enantiomeric form over another has also been successfully carried out in a continuous MSMPR reactor. [20] However, there has been little research on the use of seeding to preferentially obtain polymorphic forms in continuous crystallisers and in particular in an MSMPR reactor. The work undertaken in the following section addressed this understudied area of the mechanisms of polymorphic formation in continuous single-stage MSMPR reactors through both unseeded and seeded crystallisation experiments.

A number of analytical techniques have been successfully used to monitor crystallisations in different types of vessel including MSMPR reactors. These include

FBRM which has been used to determine when a crystallisation in this type of reactor is operating at steady state and subsequently this information can be used to obtain crystallisation kinetics.[10, 11] In addition, information on the particle size distribution of the slurry within the vessel can also be obtained.[3, 22] This technique has also been effectively used to monitor and control the number of seed particles in a batch stirred tank vessel. When the number or size of seeds strays from the desired levels, a heating or cooling cycle is employed to bring the seeds back to a more uniform size and therefore maintain the properties which result in the desired final product.[23, 24] As mentioned previously (chapter 4), Raman spectrometry has commonly been used in batch crystallisation to monitor polymorphic transformations in many systems in combination with ATR-FTIR spectrometry for liquid phase measurements[25] and FBRM to provide additional information on particle formation.[26] However, in these cases, an immersion probe was used which can be prone to fouling and also the probe only has a small sampling spot size in the region of ~100 μm. Additionally, there has been very little reported on the use of Raman spectrometry in the monitoring of crystallisations in continuous MSMPR reactors, mainly due to these reactors mainly being used to obtain crystallisation kinetics rather than for the study of polymorphic systems. Therefore, by using a non-invasive, wide-area illumination probe such as the Kaiser systems P^hAT probe for crystallisation monitoring, issues of representative sampling are reduced as a spot size of up to 6 mm can be utilized. In addition, as the P^hAT probe is non-invasive it does not interfere with the process so problems with probe fouling, which can encourage polymorph transformation, are removed. The polymorphic transformation of L-glutamic acid has been well studied in batch STRs and the crystallisation kinetics have been well described for this process.[27, 28] However, little work has been carried out for this system in continuous crystallisers including MSMPR reactors with the use of non-invasive Raman monitoring, which was another reason for the current study.

In the following work, non-invasive Raman spectrometry has been employed to monitor crystallisation of L-glutamic acid within a continuous MSMPR crystalliser to compare with the results obtained using the continuous oscillatory baffled reactor

studied previously (Chapter 5). The primary aim of the study was to investigate, with the use of the phase diagram of LGA, if the conditions could be altered to selectively form the metastable alpha and stable beta polymorphs. Monitoring of the crystallisation using Raman spectrometry was able to provide information on how the polymorphs formed, *i.e.* directly or via a transformation process and also whether the system was reaching steady state or not. The measurements taken during the seeded experiments were useful in showing what effect, if any, the seeds had on the crystallisation process.

6.2 Experimental

6.2.1 Materials

In this work, L-glutamic acid and distilled water were used in all experiments as described in section 3.2.

6.2.2 Batch STR conditions

The reactor consisted of a 350 ml round-bottomed jacketed glass vessel as described in section 3.3.1. A solution concentration of 40 g/L was used, which was first prepared in a flask and heated to 80^{o}C on a hotplate with stirring. A total volume of 155 ml of the hot solution was then added to the STR where the jacket temperature was fixed at either 45 or 25^{o}C. The impeller speed applied was 300 rpm.

6.2.3 Continuous MSMPR conditions

The reactor was the same as that described in section 3.3.4. As with the batch STR experiments, a solution concentration of 40 g/l was used which had been heated to 80^{o}C on a hotplate. The jacket temperature was fixed at either 45 or 25^{o}C. A volume of 155 ml of the hot solution was added initially to the reactor before the inlet pump, which fed in the hot solution continuously, and outlet pump, which removed the product slurry periodically, were started. The inlet pump flow rate was 2.5, 5.1 or 9.8 ml/min depending on the residence time, which was either 60, 30 or 15 minutes, respectively. The outlet pump was set on a timer so that 10% of the reactor volume (15.5 ml of the slurry) was removed at set time intervals (either 6, 3 or 1.5 minutes). The slurry was collected at certain time points for 30 minute intervals and filtered under vacuum and dried in an oven. These samples were then used for off-line analysis. The impeller speed used was 300 rpm for the 45^{o}C experiments and for the 25^{o}C experiments the agitation was increased from 300 to 600 rpm to maintain suspension of the greater amount of particles formed.

For the seeded experiments, a 5-10% dry seed loading of beta form seeds of a known size (in the region of 20 µm) were added to the vessel prior to nucleation and before the pumps were started. The maximum possible yield (100%) of solid material was

calculated from the equation of the solubility curve of beta LGA (Figure 6-2) and the equation ΔC=C-C* (equation 1-3, chapter 1.1) and the seed loading is then determined from this value (either 5 or 10%). The equilibrium solute concentration is determined from the quadratic equation at a certain temperature (in this case 45^{o}C) and therefore 5% of the mass can be obtained and this value is used as the seed load. For example to calculate the equilibrium solute concentration, the temperature is substituted as the value for x (equation and temperature value taken from Figure 6-2):

$$\boldsymbol{y = 0.00799x^2 - 0.10432x + 5.71442} \quad \textbf{(6-1)}$$

$$\boldsymbol{y = 0.00799(45^2) - \left(0.10432(45)\right) + 5.71442}$$

$$\boldsymbol{y = 17.20\ g}$$

Then the equilibrium solute concentration is substituted into equation 6-2 using the solute concentration which as shown in Figure 6-2 is 40 g/kg:

$$\boldsymbol{\Delta C = C - C^{*}} \quad \textbf{(6-2)}$$

$$\boldsymbol{\Delta C = 40\text{-}17.20}$$

$$\boldsymbol{\Delta C = 22.8\ g}$$

Finally, the seed mass is calculated as follows using a water mass of 155 g:

$$\boldsymbol{Seed\ mass\ (g) = \Delta C(seed\ loading \div 100) \times mass\ water\ (kg)} \quad \textbf{(6-3)}$$

<u>Seed mass</u>: $\boldsymbol{5\% = 0.177\ g, 10\% = 0.353\ g}$

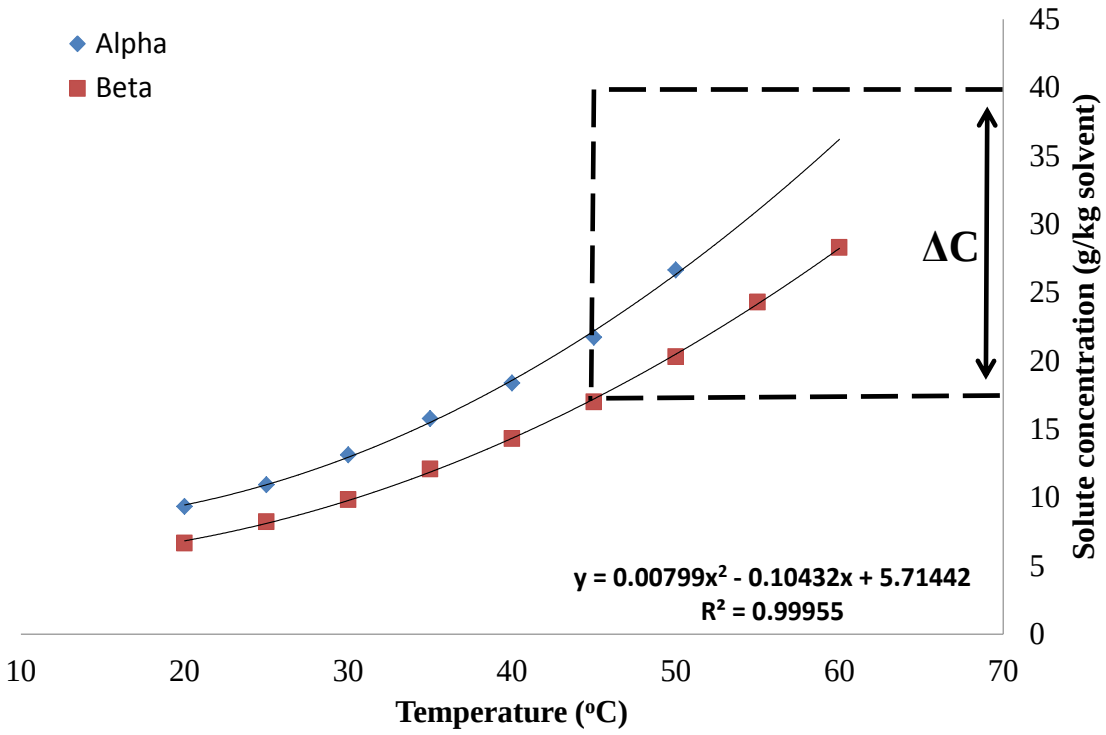

Figure 6-2: Solubility curves of alpha and beta L-glutamic acid showing the method for calculating the seed load

For the experiments seeded with 100% (assuming maximum theoretical yield) beta particles, the crystallisation was operated in batch mode until the seeds of the desired polymorph had been formed. The inlet and outlet pumps were then started to convert the operation to continuous MSMPR operation.

6.2.4 Raman Instrumentation- Kaiser RxN2 spectrometer

Raman measurements were carried out using a Kaiser RxN2 spectrometer with the PhAT probe head which has the same inner components as the RxN1 system described in section 3.4.1. The RxN2 system has an additional immersion probe which was not used for this work. A 785 nm near-IR laser with a 6 mm spot diameter and 400 mW laser power was utilised for all measurements. An exposure time of 15 s was employed with 4 accumulations resulting in a measurement being obtained every 90 s.

6.2.5 Laser diffraction

Particle size measurements were carried out using a Malvern Mastersizer 2000 as described in section 3.4.3. A saturated solution of LGA and 0.1% polysorbate 20 was added to a Hydro2000SM cell. Powder samples of LGA which had been vacuum filtered and dried in an oven were added to the cell until a laser obscuration (internal parameter of the instrument to indicate multiple scattering effects) of ~3% was obtained.

6.2.6 X-ray diffraction

For this section of work, an alternative PANalytical X'PERT PRO diffractometer was used as described in section 3.4.5. Samples were lightly ground with an agate mortar and pestle and ~50 mg was placed on a silicon support plate with an aluminium holder. The diffraction patterns for alpha and beta LGA are shown in figure 4-3.

6.3 Results and Discussion

6.3.1 Batch STR

Several batch STR experiments were carried out to establish the conditions at which to operate the MSMPR. Initially the MSMPR was going to be operated at two sets of conditions (corresponding to two fixed points on the phase diagram) where the concentration would be changed to obtain either the alpha (point 1) or beta form (point 2) at a fixed temperature (Figure 6-3).

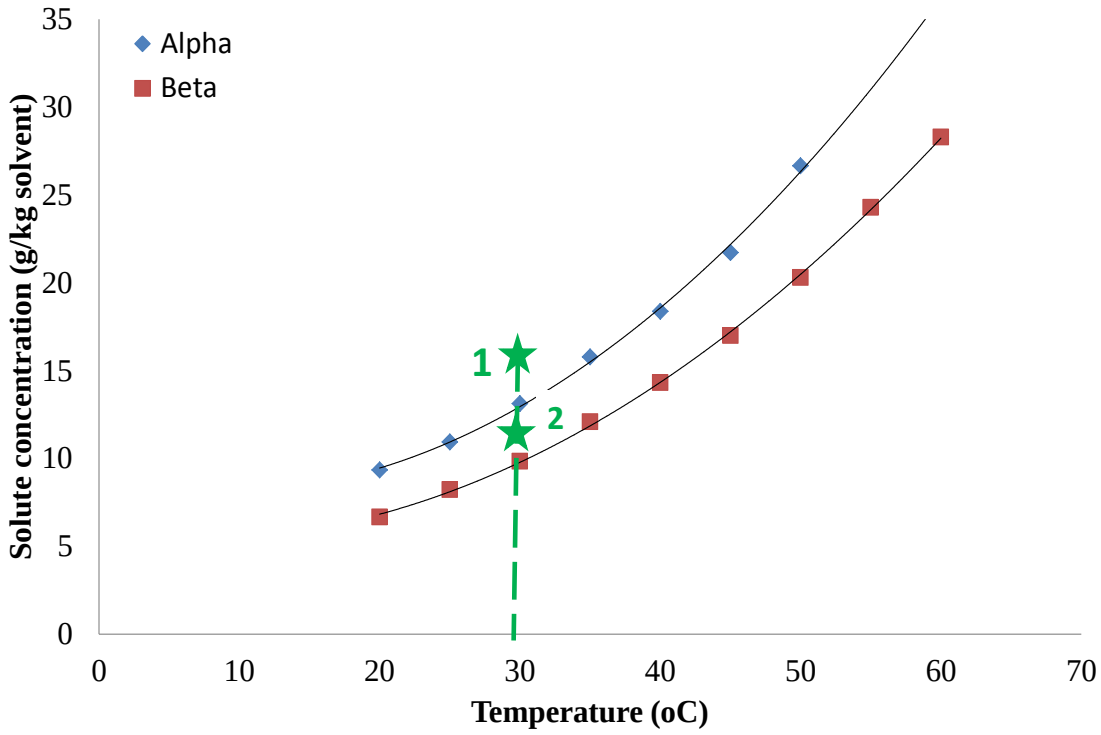

Figure 6-3: Solubility curves of alpha and beta L-glutamic acid in water showing the potential operating points of the MSMPR using a solution concentration of 10 and 15 g/kg at 30°C

However, after carrying out a batch experiment using a concentration of 20 g/L with the aim of obtaining the alpha form it was found that using this concentration gave a relatively low yield. Due to the fact that a lower solution concentration would need to be used to potentially obtain the beta form, it was thought that this would result in yields too low to have sufficient material especially for use in off-line analysis. Therefore, a different approach was adopted where the solution concentration was kept constant while the temperature was altered to obtain the pure alpha and beta forms. The two temperatures used were 25 and 45°C, respectively (Figure 6-4).

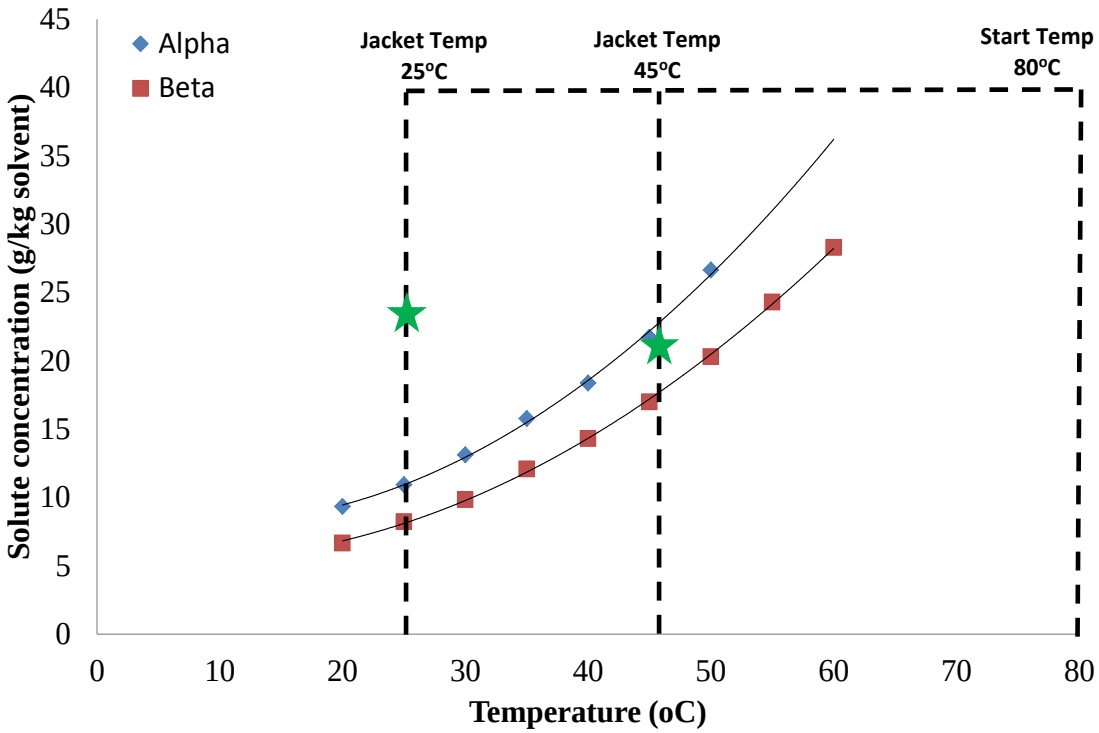

Figure 6-4: Solubility curves of alpha and beta L-glutamic acid in water showing the liquid phase concentrations at 25°C and 45°C obtained during the batch STR experiments

As Figure 6-4 shows, it would be expected from the two points on the solubility diagram that the alpha form would be obtained using a jacket temperature of 25°C and the beta form using 45°C when cooled from an initial temperature of 80°C and a solution concentration of 45 g/L. Figure 6-5 and Figure 6-6 show data measured during the batch STR experiments carried out at 25°C and 45°C, respectively, obtained using non-invasive Raman spectrometry.

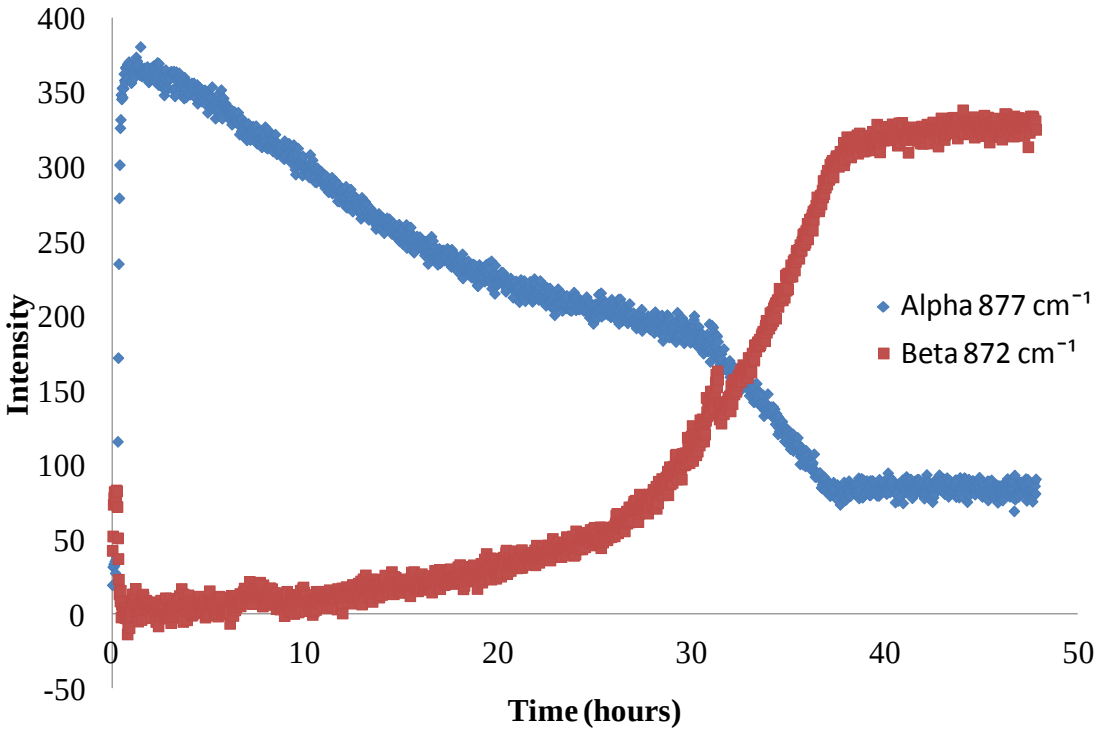

Figure 6-5: Crystallisation profile showing the transformation from alpha to beta L-glutamic acid in a batch STR at 25°C based on 1st derivative Raman intensity at 877 and 872 cm^{-1}, respectively

As Figure 6-5 shows, a jacket temperature of 25°C resulted in the pure alpha polymorph being formed initially. As this is the unstable polymorph it was expected that this would eventually transform into the thermodynamically stable beta form. As can be seen, dissolution of the metastable alpha form began after an hour; however the beta polymorph did not begin to form until 12-14 hours. This is most likely due to the different solubility's of the alpha and beta polymorph and a certain level of dissolution of the more soluble alpha form was necessary before formation of the beta form could begin. The initial transformation was relatively slow and significant growth of the beta form did not begin until around 25 hours. The transformation was then fairly rapid and by 38 hours complete conversion to the beta polymorph had taken place. The signals at the start of the measurements (0-0.5 hours) show a rapid increase in the alpha form while there appears to be an initial amount of beta crystals present which decrease rapidly also. However, as the peaks for the solute and the beta polymorph overlap, it is likely that this decrease observed at the start of the

measurements in the beta signal is in fact the decrease in the solute concentration prior to nucleation.

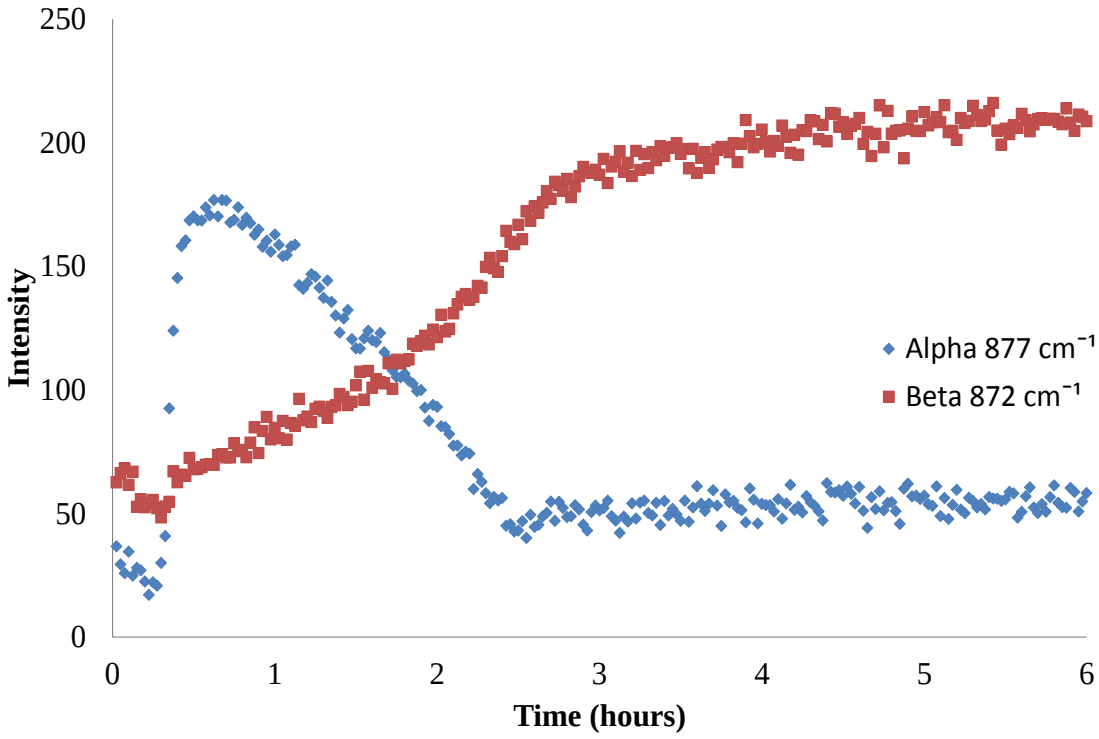

Figure 6-6: Crystallisation profile showing the transformation from alpha to beta L-glutamic acid in a batch STR at 45°C, based on 1st derivative Raman intensity at 877 and 872 cm^{-1}, respectively

Figure 6-6 shows that a jacket temperature of 45°C resulted in a mixture of the forms being obtained initially with the alpha polymorph being the major form. As shown previously in Figure 6-5, an initial decrease in the signal for the beta form is observed at the start of the measurements, again thought to be due to the overlapping of the solute and beta form peaks. However, as the signal for the beta form doesn't decrease to an intensity of close to zero (as in Figure 6-5), a mixture of forms appeared to have nucleated with the alpha polymorph having a faster initial nucleation rate. Although it was expected that the beta form would be obtained from the solubility diagram in Figure 6-4, it is possible that the alpha polymorph nucleated while the solution was being cooled to the jacket temperature where the solution would have been in the metastable zone for the alpha polymorph for a period of time.

Despite the fact the pure beta form was not obtained using 45°C to begin with, the transformation to the stable polymorph was completed much quicker than at 25°C due to the presence of beta crystals in the vessel that nucleated along with the alpha form, which encouraged and accelerated the transformation. The levels of beta form steadily increased after 1 hour, at the same time the signal for the alpha form decreased more rapidly and by 3 hours the transformation was complete. Therefore, although the pure beta form was not obtained in the first instance, as the transformation was relatively rapid, this temperature was used in the MSMPR experiments, as well as the lower temperature of 25°C for the metastable form.

6.3.2 MSMPR unseeded experiments

Initial MSMPR experiments were carried out at 25°C to determine whether the alpha polymorph could be produced as in the batch experiment (Figure 6-5) and if the transformation would occur more rapidly or slowly. The results of the first attempt using a 30 minute residence time are shown in Figure 6-7.

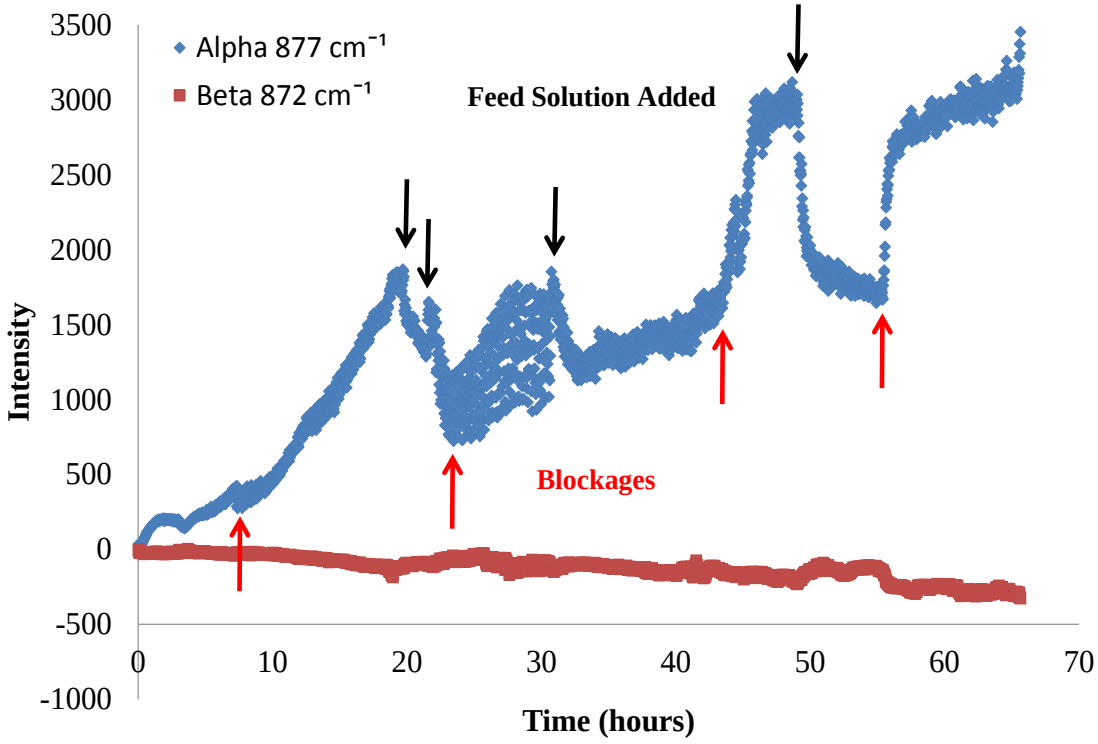

Figure 6-7: Crystallisation profile of alpha and beta L-glutamic acid obtained in a MSMPR at 25°C using a 30 minute RT, based on 1st derivative Raman intensity at 877 and 872 cm^{-1}

As Figure 6-7 shows, the MSMPR was operated continuously for just under 70 hours and the alpha polymorph appears to have been formed preferentially without transforming to the stable form. However the profile obtained highlighted some difficulties with operating a continuous reactor for extended periods of time. First of all, it was apparent that the crystallisation did not reach and remain at steady state. There were several points at which steady state appeared to be obtained for a short period of time (e.g. between 45 and 50 hours), however, it became obvious when looking at the trend that the signal intensity dropped quite dramatically at certain points during the crystallisation. It was found that this matched up to the times when the feed solution was refilled. It was thought that because the crystallisation was being operated for a long period of time and the feed solution was at a high temperature, evaporation was an issue, which was affecting the concentration of the feed solution meaning steady state was more difficult to achieve and maintain. Another problem was blocking of the outlet tube, which caused the signal intensity to increase rapidly when additional nucleation and crystal growth took place, consuming all of the supersaturation. Therefore, in an attempt to overcome these problems, a condenser was added to the feed solution to reduce evaporation and the outlet tube was cleaned regularly to reduce the chances of blockages. Figure 6-8 shows the results of the repeat experiment carried out at 25^{o}C.

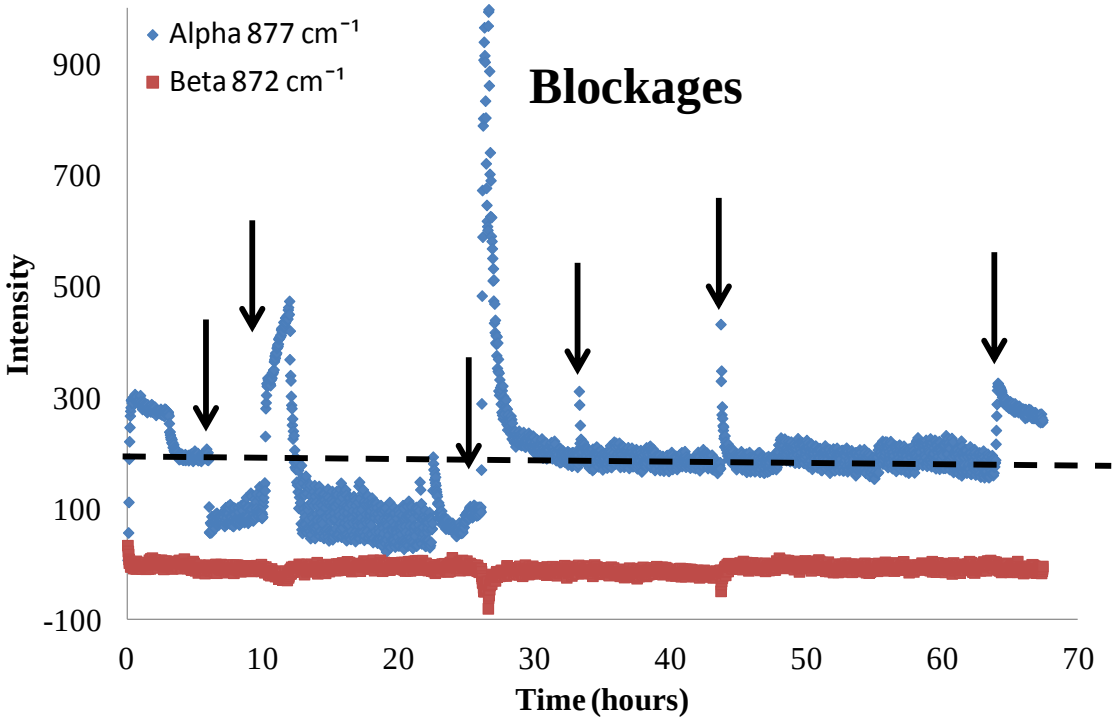

Figure 6-8: Crystallisation profile of alpha and beta L-glutamic acid obtained in a MSMPR at 25°C using a 30 minute residence time, based on 1st derivative Raman intensity at 877 and 872 cm^{-1}, respectively

Figure 6-8 shows that the problems encountered in Figure 6-7, owing to the changing concentration of the feed solution have been removed with the use of a condenser. Although the outlet tube was cleaned regularly, blockages were still an issue especially when the experiment was left for longer periods unsupervised (i.e. overnight). To try and eliminate this issue, the outlet tube was heated using a heater-chiller to attempt to prevent precipitation in the tube. The signal intensity is much lower throughout the crystallisation in Figure 6-8 than the previous figure showing that cleaning the outlet tube regularly helped to reduce the number and duration of blockages in the outlet tubing. The signal intensity reached in excess of 1500 in the first half of the measurements in Figure 6-7 due to the initial blockage (at approximately 10 hours) which was not rectified for over 10 hours meaning feed solution was continuing to be pumped in but no slurry was being removed causing the drastic increase in intensity observed due to the continued formation of crystals. The crystallisation appeared to reach steady state after around 5 hours (10 residence

times) however, several blockages in the system meant that this was not maintained. The profile shows that once the blockages had been cleared, the signal decreased rapidly and reached a similar steady state once more (after 30 hours), shown by the black line in Figure 6-8. Therefore, it was possible to produce the alpha polymorph continuously for up to 70 hours using a temperature of 25^{o}C. This was unusual as it was thought that a transformation may occur whilst operating continuously for such a prolonged period of time (~140 residence times) as it would be expected that particles would become attached to the impeller or perhaps in cracks in the vessel and these would transform to the stable form. Once a number of trapped particles had transformed this would encourage the transformation of other particles in the reactor and seed the supersaturated solution which is constantly being added and would, therefore, lead to the beta form being produced. Previous experiments by the author have shown that the alpha form transforms to the beta form in 8-10 hours when stirred in water at room temperature.

As steady state was not maintained for the entire crystallisation, the physical properties, such as the particle size of the crystals, may not be consistent. Figure 6-9 shows the average particle size (d(0,5)) of samples collected and analysed off-line at various points during the crystallisation, and the solid recovery over a number of 30 minute periods.

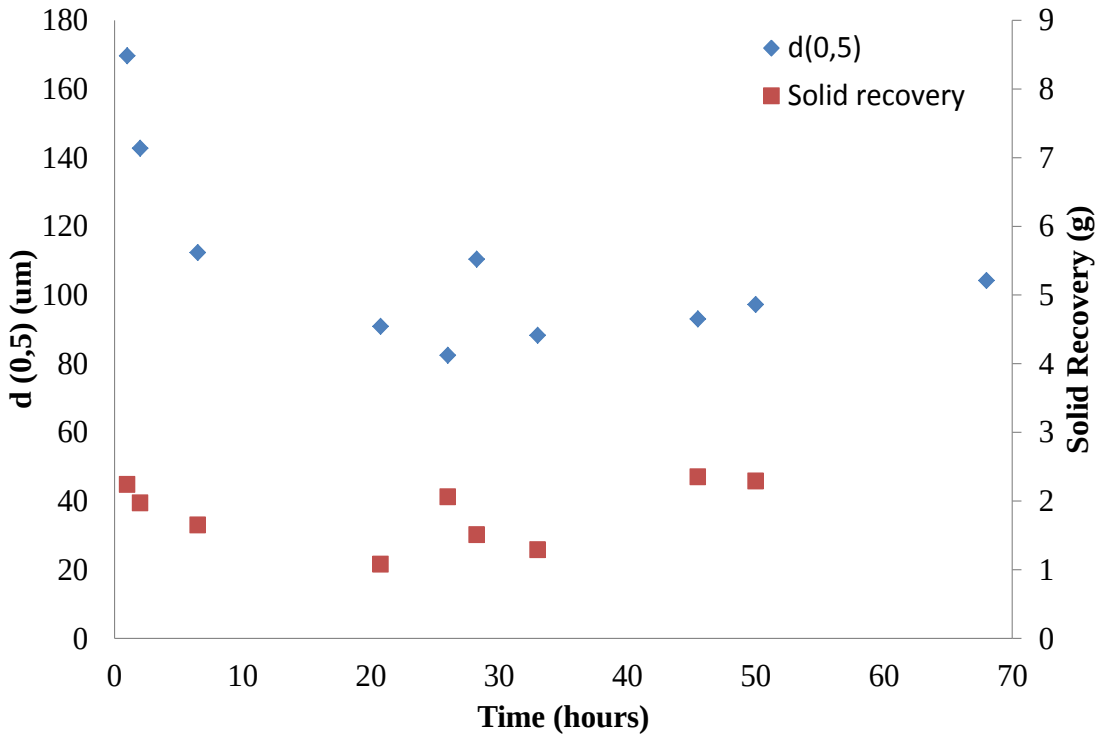

Figure 6-9: Plot of average particle size and solid recovery over 30 minute periods at different stages during the crystallisation of L-glutamic acid in an MSMPR at 25°C and with a 30 minute RT

Figure 6-9 shows that although there was frequent blocking within the system, the mean particle size (d(0,5)) and the solid recovery over 30 minute intervals remained fairly constant once the system first reached steady state after around 5 hours. The larger particles appeared to be removed preferentially in the first few hours of the crystallisation leaving particles with a relatively small average particle size of ~100 µm. This could also mean that the growth rates were initially higher resulting in larger particles but decreased once steady state had been reached. Figure 6-10 shows a similar MSMPR experiment, but this time at a higher temperature of 45°C.

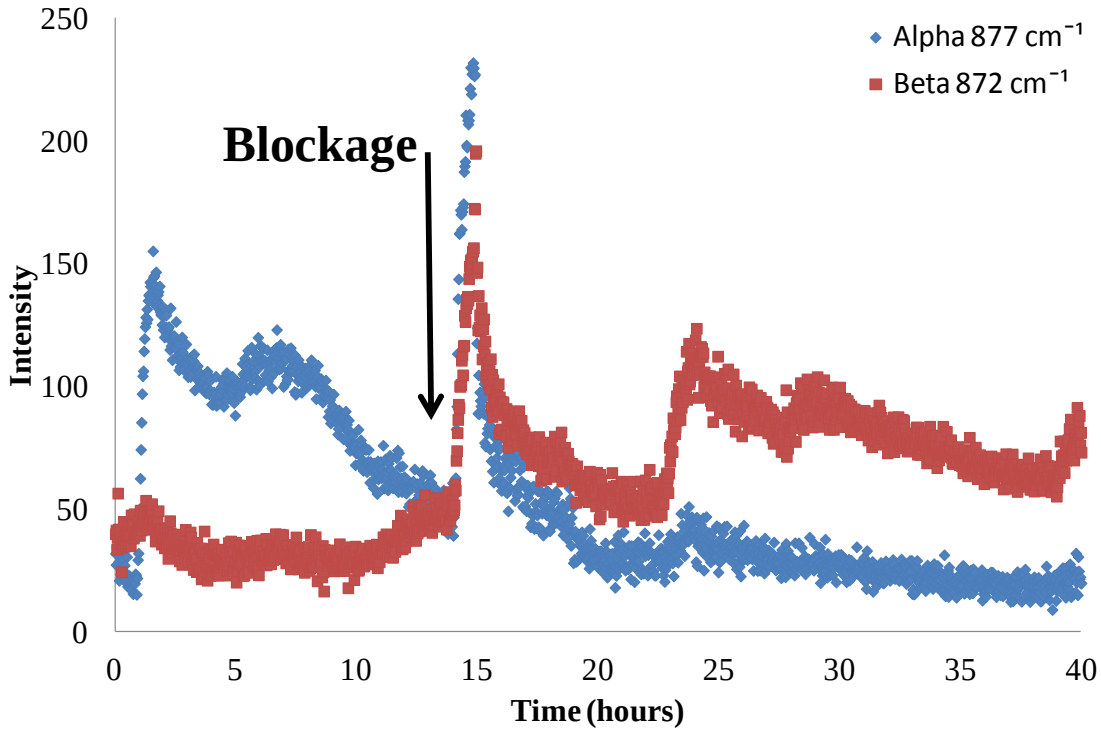

Figure 6-10: Crystallisation profile of alpha and beta L-glutamic acid obtained in an MSMPR at 45°C using a 30 minute residence time, based on 1st derivative Raman intensity at 877 and 872 cm^{-1}, respectively

Figure 6-10 shows that at a higher jacket temperature of 45°C, a mixture of forms was produced (~80:20; α:β) initially as in the batch experiment (Figure 6-6). The percentage composition of polymorphs was estimated from the shift observed from the peak for the pure component (discussed further in chapter 4.3.1), *i.e.* it was observed that the pure alpha form resulted in a peak at 877cm^{-1}, while the pure beta form gave a peak at 872cm^{-1}. When a 50:50 mixture of the two forms was analysed, a single peak appeared at 875cm^{-1}, and this peak position shifted depending on the relative percentages allowing for an estimation of the polymorphic composition to be made. The signal for the alpha form reached a maximum at around 2 hours when it started to decrease in intensity for the remainder of the experiment. The transformation began to take place after 10 hours where increased levels of the beta polymorph started to form. Although the outlet tube became blocked at 15 hours, once this was cleared the trend continued and by 20 hours the transformation had progressed to ~20:80; α:β and by 25 hours the conversion to the stable form was

complete. It was shown that carrying out the crystallisation in an MSMPR using a 30 minute residence time meant that the transformation was significantly slower than that carried out as a batch experiment. The trend in Figure 6-10 shows oscillations in intensity which are common in MSMPR reactors prior to steady state being reached. Figure 6-11 shows the average particle size of samples analysed off-line at various points during the crystallisation and the solid recovery over a number of 30 minute periods.

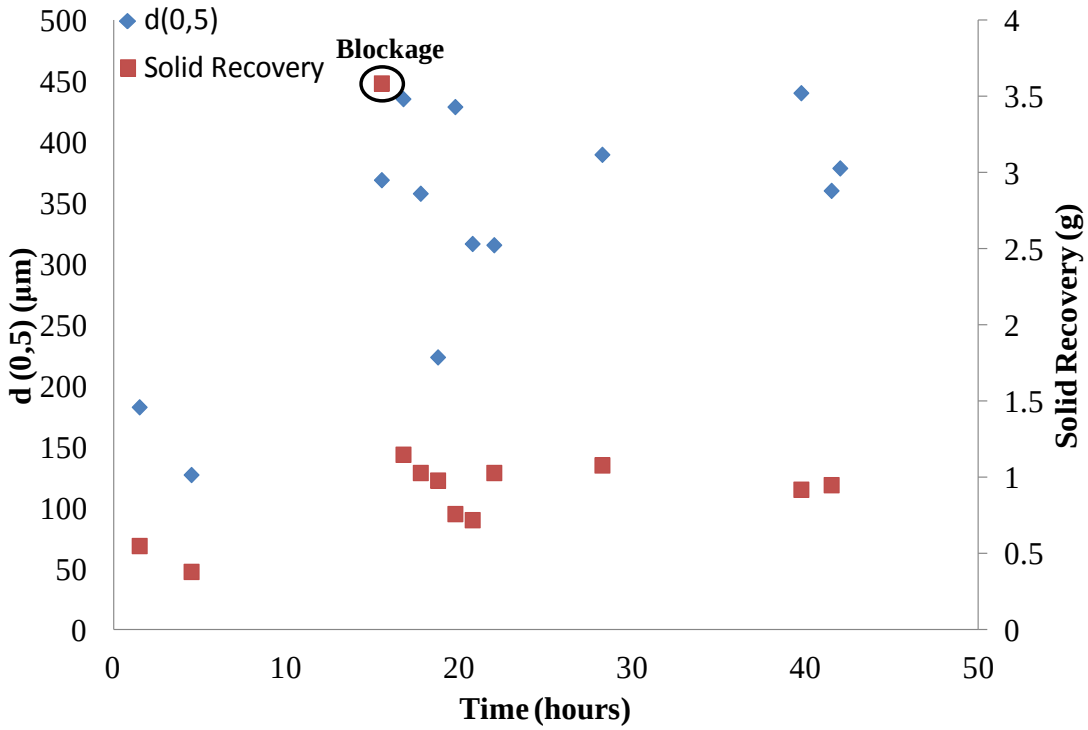

Figure 6-11: Plot of average particle size and solid recovery over 30 minutes at different stages during the crystallisation of L-glutamic acid in an MSMPR at 45°C using a 30 minute RT

Figure 6-11 shows that the average particle size started off relatively small (~150 µm) when the majority of the particles are of the alpha form. The particle size started to increase significantly between 15 and 20 hours, which is at the point the transformation from alpha to beta is advancing and so the shape of the particles changed from prismatic to needle-shaped. The change in morphology during the crystallisation means the samples collected for off-line particle size analysis may not produce accurate results due to the laser diffraction method assuming the particles are spherical. Therefore, the results obtained prior to the transformation will be more

accurate when the particles are prismatic (closer to spherical shape) than with the results obtained from 15 hours onwards when the majority of particles are needles (discussed further in chapter 7.1) The particle size remained fairly constant (~400-450 μm) for the remainder of the crystallisation. The amount of solid recovered during the crystallisation was fairly consistent after 15 hours apart from the time period following the outlet being blocked where solid material had built up in the reactor. Although the beta form was obtained in the MSMPR at 45°C, it took over 20 hours to acquire this polymorph so additional experiments were carried out where the residence time was altered in order to see if this affected the outcome of the experiment and whether the transformation would occur quicker. A lower flow rate giving a longer residence time of 60 minutes was used and Figure 6-12 shows the outcome.

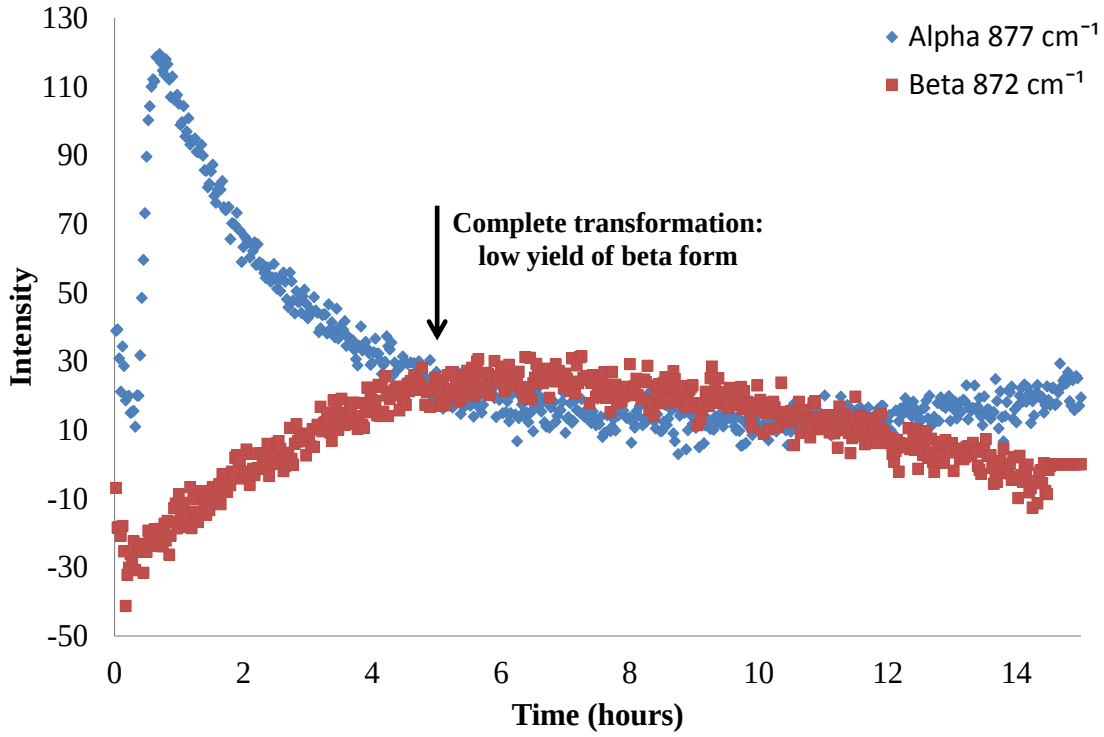

Figure 6-12: Crystallisation profile of alpha and beta L-glutamic acid obtained in an MSMPR at 45°C using a 60 minute residence time, based on 1st derivative Raman intensity at 877 and 872 cm^{-1}, respectively

Figure 6-12 shows that the signal for the alpha form resulted in a similar trend initially as to that in Figure 6-10 using a 30 minute residence time. The intensity

reached a similar maximum value and then began to decrease after 1 hour, however, in this case the intensity decreased much more rapidly. This suggested that a similar initial concentration of alpha particles was formed as with the 30 minute residence time crystallisation but dissolution appears to occur at a quicker rate than in Figure 6-10. As the Raman intensity obtained is predominantly due to the solid concentration, the intensities can be compared between experiments and provide an indication of whether a similar amount of solid material has been produced or not. The profile for the beta form shows that there were no beta crystals detected by Raman spectrometry in the initial stages, however, the intensity started to increase as the signal for the alpha form decreased. By 4 hours, the transformation to the beta form was complete; however, the signal for the beta form was relatively weak and gradually decreased over a number of hours until no solid material was detected. At the end of the transformation, the mass recovered was only 2% of that produced when using a 30 minute residence time which is also suggested when comparing the Raman intensities observed at the end of the measurements. Confirmation of the polymorphic form was obtained by XRD and microscopy of the isolated material collected at the outlet. Figure 6-13 shows the microscopy images obtained from samples at the end of the crystallisation showing the particles observed are needle in shape and contain larger particles as well as smaller particles and fragments of particles which are common with needles as they are susceptible to breakage. The attrition of particles is most likely due to the agitation within the vessel but could also be due to the pumping of the slurry, which was at a relatively high flow rate, through the outlet tubing.

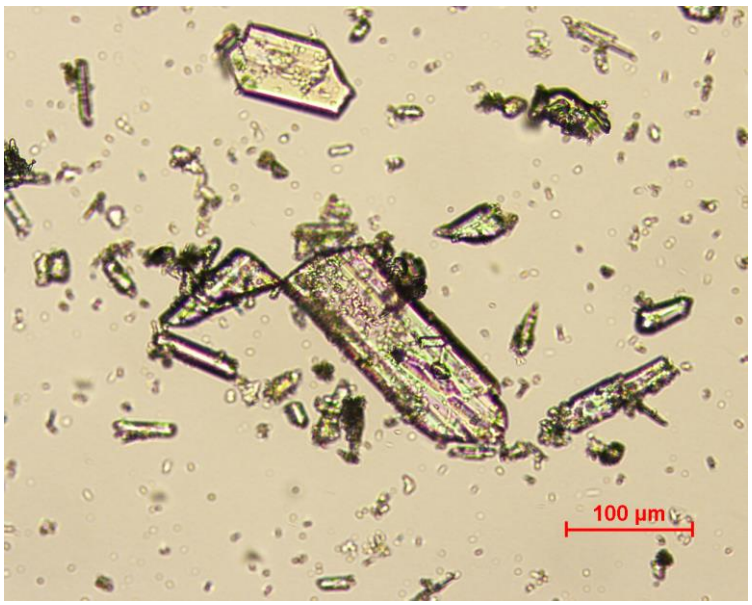

Figure 6-13: Microscopy images of L-glutamic acid samples collected at the end of a continuous crystallisation in a MSMPR reactor at 45°C using a 60 minute residence time

Prior to the experiment being stopped at 15 hours, the alpha form signal began to increase again slightly. This could be due to nucleation of this polymorph happening once more as the supersaturation was gradually restored in the vessel due to the low levels of beta form present and the continuous removal of slurry from the reactor. Although the transformation to the stable form occurred much quicker using a 60 minute residence time (4 hours compared to 25 with a 30 minute residence time), the mass of crystals produced was significantly reduced which makes it difficult to monitor the crystallisation using Raman spectrometry. Figure 6-14 shows the average particle size of off-line samples taken at various points during the crystallisation and the solid recovery collected over a number of 30 minute periods.

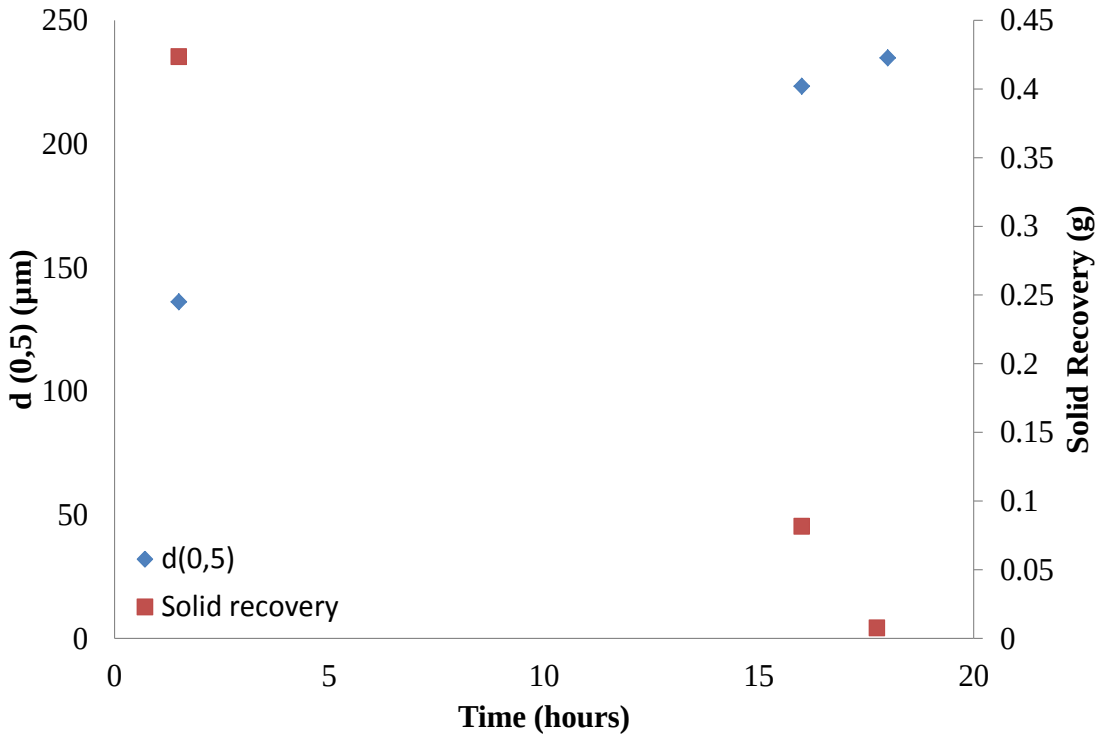

Figure 6-14: Plot of average particle size and solid recovery over 30 minutes at various stages during the crystallisation of L-glutamic acid in an MSMPR at 45°C using a 60 minute RT

Figure 6-14 shows that in the initial stages of the crystallisation, the average particle size was relatively small (~130 µm) and the solid recovered between 60 and 90 minutes was just under 0.5 g, which is similar to that obtained using a 30 minute residence time (Figure 6-11). It appears that in both the 30 and 60 minute residence time experiments, the particles formed at the outset were mainly the alpha form and of a small particle size. However, the samples isolated towards the end of the crystallisation in Figure 6-14 following the transformation, showed an increase in the mean particle size with a corresponding decrease in the amount of crystals collected. The increase in the particle size observed with the formation of the beta polymorph is consistent with the outcome of the 30 minute residence time experiment. However, the considerably lower yields obtained suggests that there was a smaller amount of crystals in the vessel, but that these few particles grew to quite a significant size. It was expected that with a longer residence time, a larger mean particle size would be obtained due to the crystals spending more time in the vessel. This is confirmed in Figure 6-13 which shows the majority of the beta particles are of a larger size.

Due to the fact a longer residence time resulted in a significantly lower production of particles, a shorter residence time of 15 minutes was also attempted to see if this could give adequate conditions to provide a rapid transformation with a sufficient amount of crystals. This profile is shown in Figure 6-15.

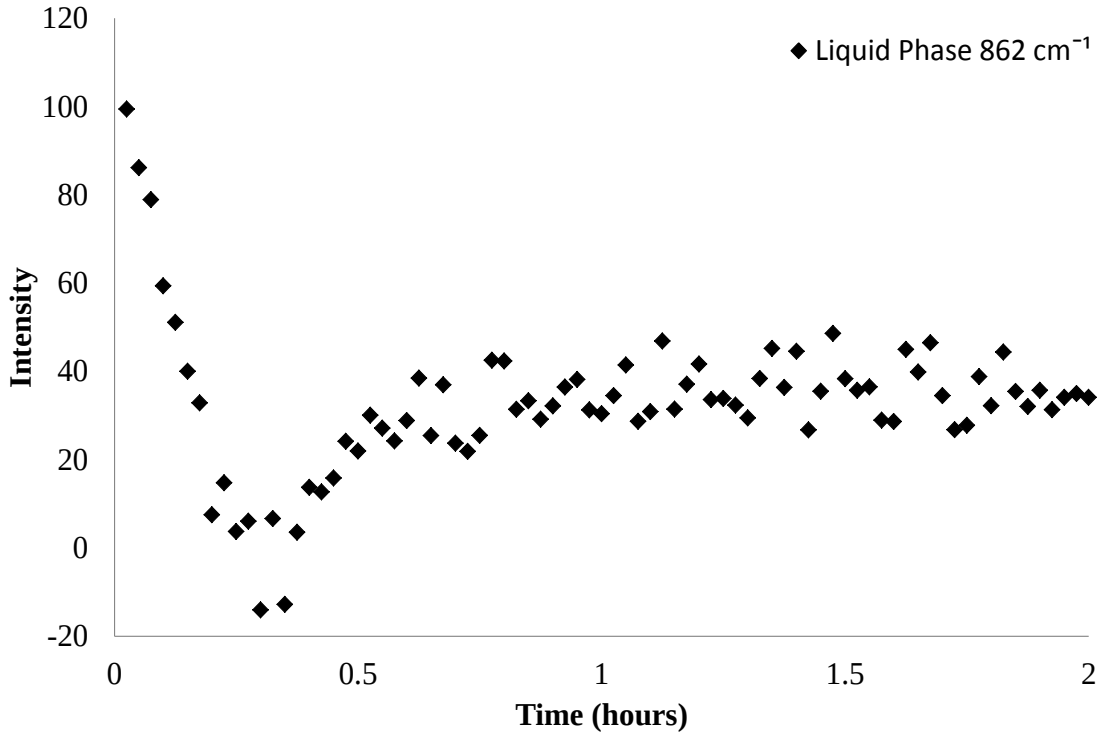

Figure 6-15: Crystallisation profile of L-glutamic acid solution obtained in a MSMPR at 45°C using a 15 minute residence time, based on 1st derivative Raman intensity at 862 cm-1

Using a 15 minute residence time resulted in no Raman signal being detected for the solid phase. Figure 6-15 shows the profile for the liquid phase. The signal gradually decreased from the start of measurements until it reached a minimum intensity at around 20 minutes. This describes the supersaturation of the solution decreasing prior to nucleation taking place. The signal then increased and levelled off for the remainder of the experiment. It is likely that a small level of nucleation took place as the temperature or the solution decreased at around 15-20 minutes (although not sufficient enough to be detected by Raman) as the supersaturation of the solution decreased, however, the residence time appears to be too short for further nucleation and growth to take place and it is likely that the initial nuclei were removed over

time from the vessel which caused the supersaturation of the solution to increase once more.

Therefore, although the beta form was successfully obtained in the MSMPR reactor using a jacket temperature of 45^{o}C, it was mostly through transformation from the metastable alpha form. The residence time influenced the timescale for the transformation and also the mass of solid produced greatly. A residence time of 30 minutes resulted in a sufficient amount of material being produced, however the beta form was only obtained in its pure form after 25 hours, which was the time taken for complete transformation of the alpha form produced in the initial stages. A longer residence time of 60 minutes resulted in a quicker transformation of around 4 hours, however, the beta form was produced in such low quantities that this could not be detected using Raman monitoring. A residence time of 15 minutes was too short to allow sufficient nucleation or crystal growth to take place and as a result only the liquid phase could be monitored using Raman. The next step was to employ seeding in an effort to promote and maintain the formation of the desired polymorph.

6.3.3 MSMPR seeded experiments

As a 30 minute residence time resulted in the most solid product in the unseeded crystallisations, this was used for the seeding experiments. Due to the fact the alpha form had been produced successfully at 25^{o}C, the experiment was seeded with beta form crystals at the start (prior to nucleation) to see if this would influence the polymorph that was produced or encourage transformation. Figure 6-16 shows the outcome of this experiment.

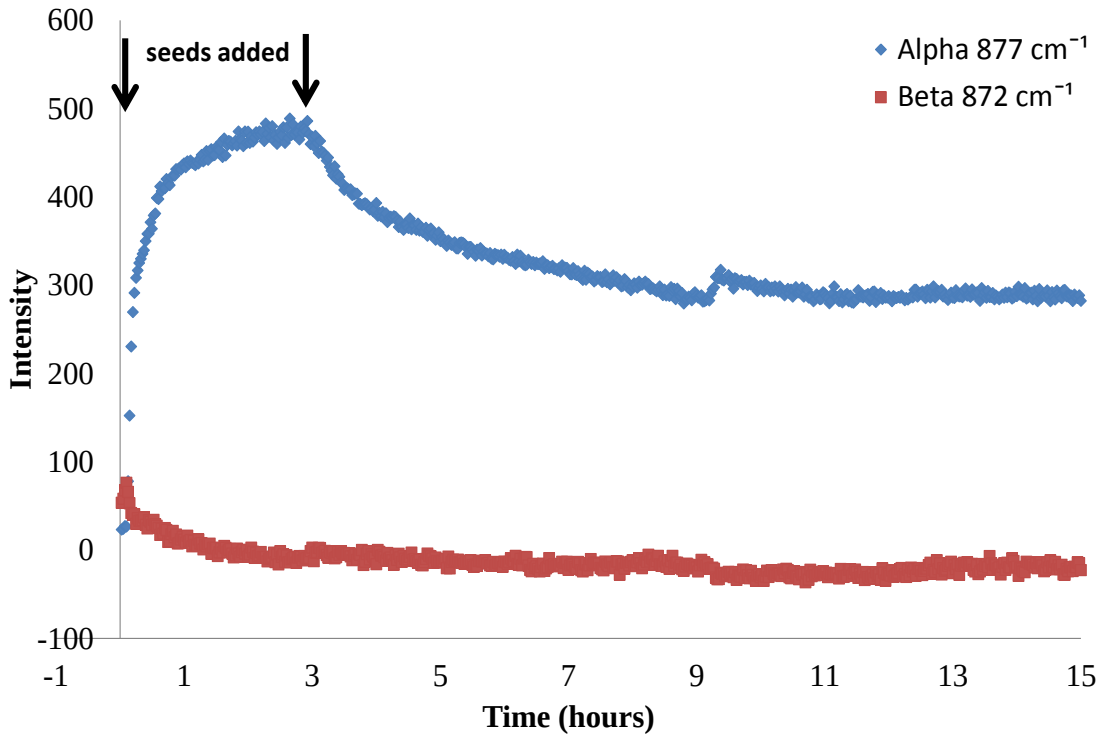

Figure 6-16: Crystallisation profile of alpha and beta L-glutamic acid when a 25°C MSMPR experiment was seeded with 5% mass (0.177 g) of beta crystals using a 30 minute residence time, based on 1st derivative Raman intensity at 877 and 872 cm^{-1}, respectively

Figure 6-16 shows that when the beta seeds were introduced at the start of the experiment, prior to any crystal formation, a small signal for the beta form was observed by Raman, most likely from the seeds themselves. The signal for the alpha form increased rapidly from the start of the measurements much like in the unseeded experiment in Figure 6-8. The beta signal then decreased until no more crystals of this form were detected using Raman suggesting that these crystals did not seed the solution and promote the nucleation of further beta crystals, but were removed gradually from the vessel. Once it was apparent that the initial seeds had not affected the crystallisation, the vessel was seeded once more with a further 5% of beta crystals at approximately 3 hours. This resulted in a slight decrease in the intensity for the alpha form over a number of hours suggesting that dissolution of this form was taking place and it may have been beginning to transform to the beta form. However, the signal then levelled off to a similar signal intensity as that observed in the unseeded experiment using the same conditions (Figure 6-8) and there was no

increase in the beta form detected in the vessel. Therefore, it appeared that the beta seeds were again removed from the reactor before they could encourage a transformation to occur. Operating the MSMPR at 25°C was found to favour the continued formation of the metastable polymorph even when seeded with quite a significant amount of the beta form. Figure 6-17 shows the outcome of seeding at 45°C using 5% beta seeds.

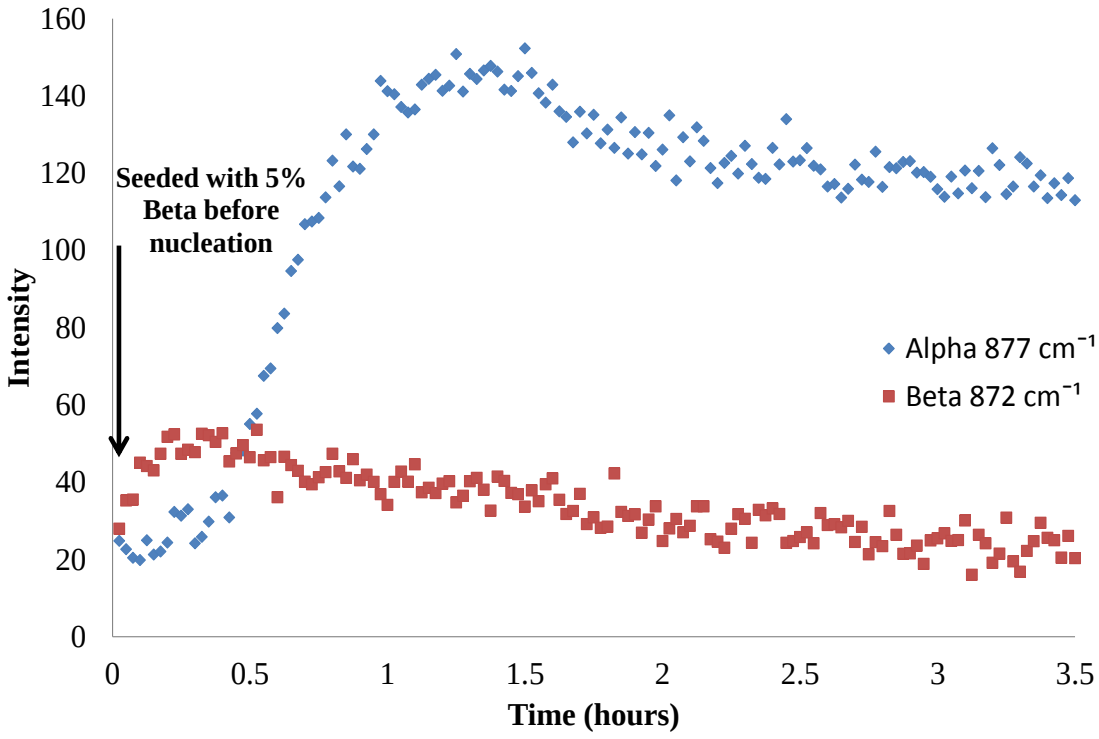

Figure 6-17: Crystallisation profile of alpha and beta L-glutamic acid when a MSMPR at 45°C was seeded with 5% beta (0.177 g) using a 30 minute residence time, based on 1st derivative Raman intensity at 877 and 872 cm^{-1}, respectively

Figure 6-17 shows that seeding with 5% beta crystals prior to nucleation resulted in a slight increase in the signal for the beta polymorph followed by nucleation and growth of the alpha form at around 30 minutes. This was compared with the unseeded experiment carried out at 45°C (Figure 6-10), as shown in Figure 6-18.

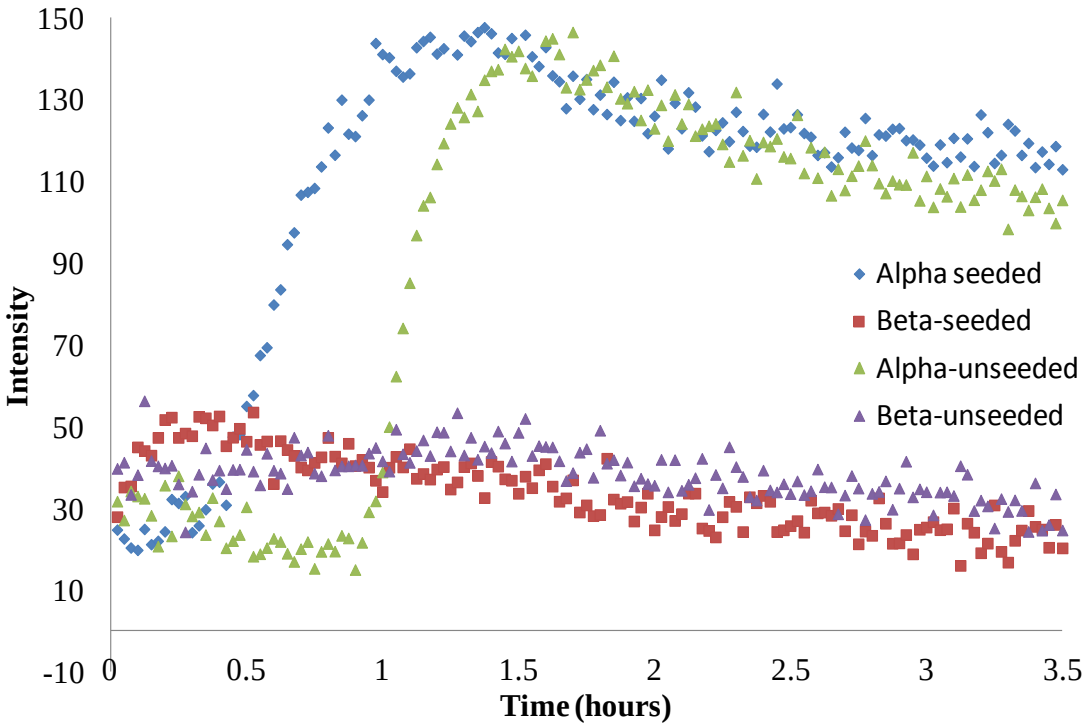

Figure 6-18: Comparison of the seeded and unseeded experiments of alpha and beta L-glutamic acid in a MSMPR at 45°C using a 30 minute residence time, based on 1st derivative Raman intensity at 877 and 872 cm^{-1}, respectively

Figure 6-18 shows that there is little effect to the outcome of the crystallisation when the experiment is seeded with 5% beta crystals. The signal for the beta form was slightly higher initially but then this decreased as the seeds were removed from the vessel. It is possible that as the seeds were added as a dry powder to the slurry, they stuck together and, therefore, were removed almost immediately from the vessel. If they had remained in the vessel longer the agitation would have separated them.[17] The main difference is that seeding the solution caused nucleation of the alpha form to occur 30 minutes earlier than in the unseeded experiment; however the crystallisation then proceeded as before and followed the same trend. Therefore, the seed loading added to the vessel initially was increased to 10% beta form and the results are shown in Figure 6-19.

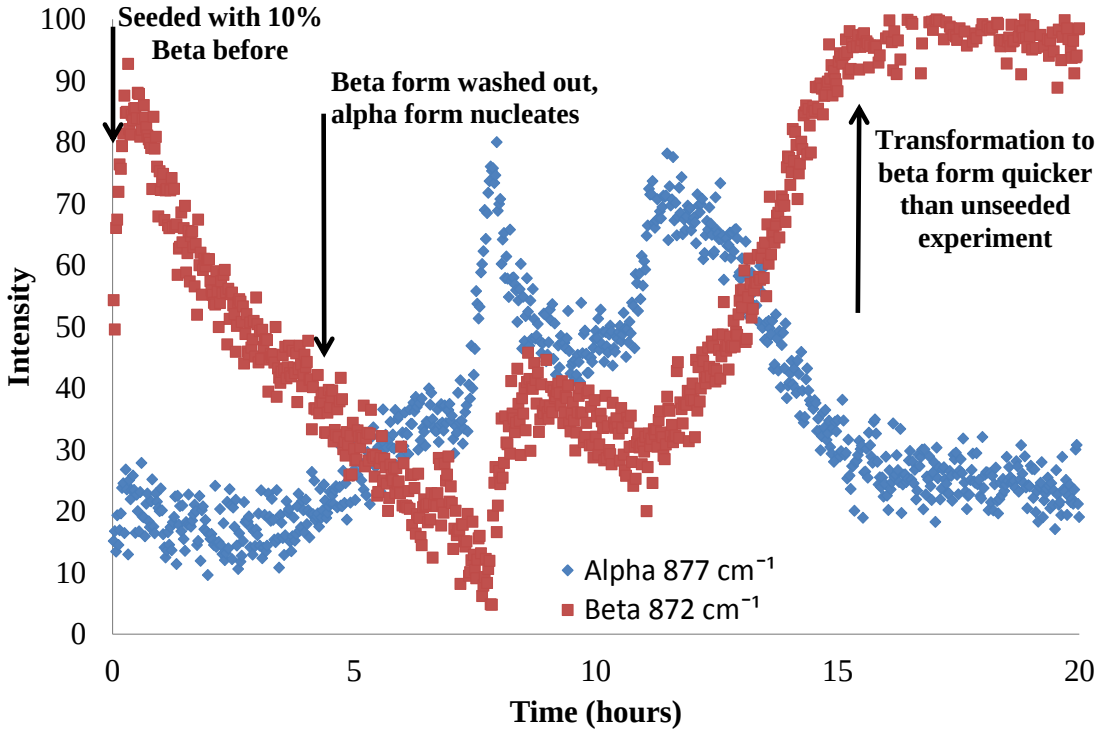

Figure 6-19: Crystallisation profile of alpha and beta L-glutamic acid when a MSMPR at 45°C was seeded with 10% beta (0.353 g) using a 30 minute residence time, based on 1st derivative Raman intensity at 877 and 872 cm^{-1}, respectively

Figure 6-19 shows that seeding the L-glutamic acid solution with 10% beta crystals altered the outcome of the crystallisation quite significantly compared to using only 5% beta seeds (Figure 6-17). The beta seeds introduced initially prevent the nucleation of the alpha form for almost 5 hours. However, as with the previous seeded experiments, the beta seeds, instead of promoting further nucleation and growth of that polymorph were gradually 'washed out' as they appeared to be removed from the reactor faster than they were able to grow or promote further formation of crystals. The majority of the beta crystals had been removed by 4 hours (as shown in Figure 6-19), however, the decrease in signal continued until ~7.5 hours. Following the removal of the majority of the beta seeds, the alpha form nucleated (at 5 hour point) and this signal increased steadily for 3 hours until a rapid increase in intensity (at 7 hour time point) over approximately 1 hour period along with a corresponding increase in the signal for the beta form, however this was a slower process. This was followed by a decrease in the signal for the alpha form

where, for around 4 hours, the intensity for the alpha and beta forms overlapped suggesting that there was ~50:50, α:β forms. After 12 hours of operation, there was a second increase in the intensity of both the alpha and beta forms, however, this time transformation to the beta polymorph progressed which caused dissolution of the alpha form and subsequent growth of the beta form, as indicated between 12 and 15 hours in Figure 6-19. So, although the beta seeds added initially did not result in the sole continued formation of this form, the complete transformation to the stable polymorph occurred in a considerably shorter timescale than the unseeded experiment shown in Figure 6-10 (around 10 hours shorter). It is likely that a small number of the initial seeds remained in the vessel and helped to accelerate the transformation once the supersaturation had been consumed once more by the apparent excessive nucleation of the alpha form at approximately 7.5 hours. Figure 6-20 shows the particle size distributions obtained from the off-line samples collected during the seeded MSMPR experiment (Figure 6-19).

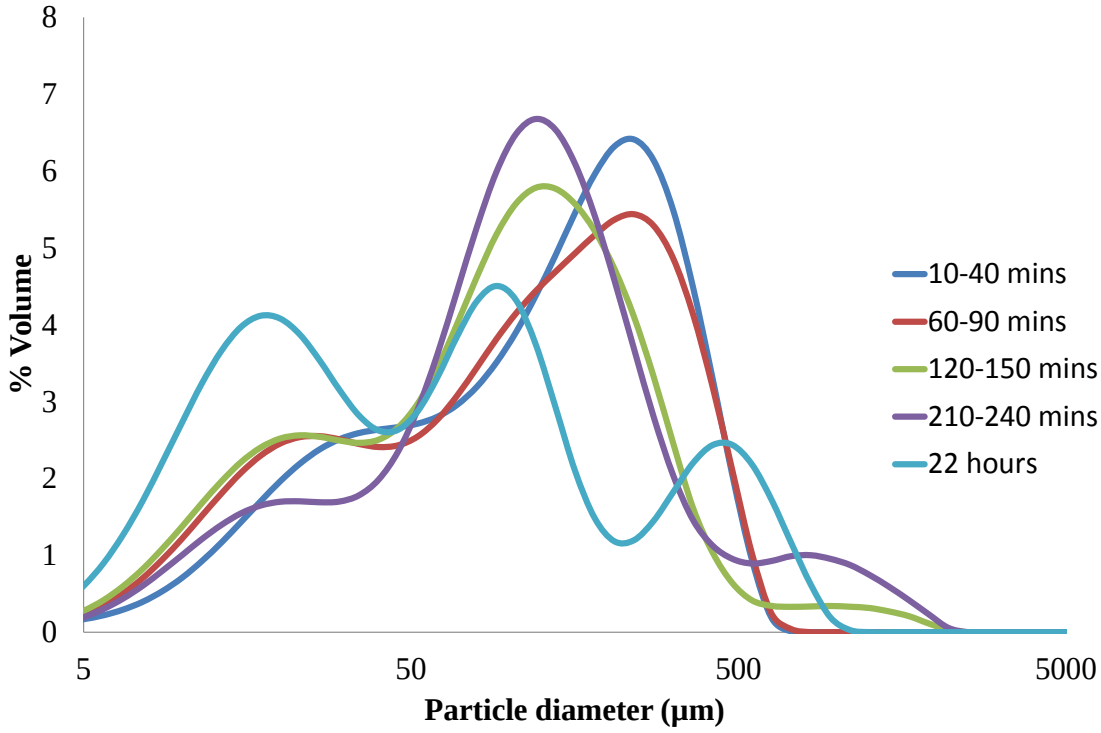

Figure 6-20: Particle size distributions of LGA for off-line samples from a seeded MSMPR experiment at 45°C using a 30 minute residence time

Figure 6-20 shows that the samples collected intermittently during the first 90 minutes consisted mostly of particles of a larger size and the distribution did not change significantly during this period. By comparing these results and the Raman measurements in Figure 6-19 it can be suggested that the beta seeds added initially grew to a larger size over a relatively short period of time and depleted the supersaturation within the vessel. Therefore, at approximately 30 minutes, the intensity for the beta form began to decrease as the slurry was being continually removed whilst the supersaturation was not sufficient enough for nucleation to occur or the nucleation rate was extremely slow. The particle size distributions between 2 and 4 hours show that the larger particles are being preferentially removed from the vessel as the majority of these particles are smaller than in the initial 90 minutes of the crystallisation. The final distribution describes the particles which were collected when the entire slurry was removed from the vessel when the crystallisation was concluded. As can be seen this shows a trimodal distribution over a significantly large range of particle sizes. This is due to the fact that different particles will have different residence times in the reactor. The larger particles are likely to have remained in the reactor longer and continued to grow over time whereas the smaller particles have nucleated more recently and have had less time in the reactor to grow. In addition, a bimodal distribution can also be due to the particle size measurement of needle-shaped crystals where some of the needles are measured by the longest length while some are measured by the shortest width). So, two different sizes of crystals with a similar length or width could lead to a trimodal distribution.

As seeding the experiment with 10% beta particles did not produce the beta polymorph without a transformation from the metastable form, an alternative approach was adopted where the crystallisation was essentially seeded with 100% beta form crystals. This was carried out by operating a batch stirred tank crystallisation at 45^{o}C until a complete transformation to the beta polymorph had occurred (as monitored by Raman spectrometry) and then the MSMPR was started. The crystallisation profile obtained is shown in Figure 6-21.

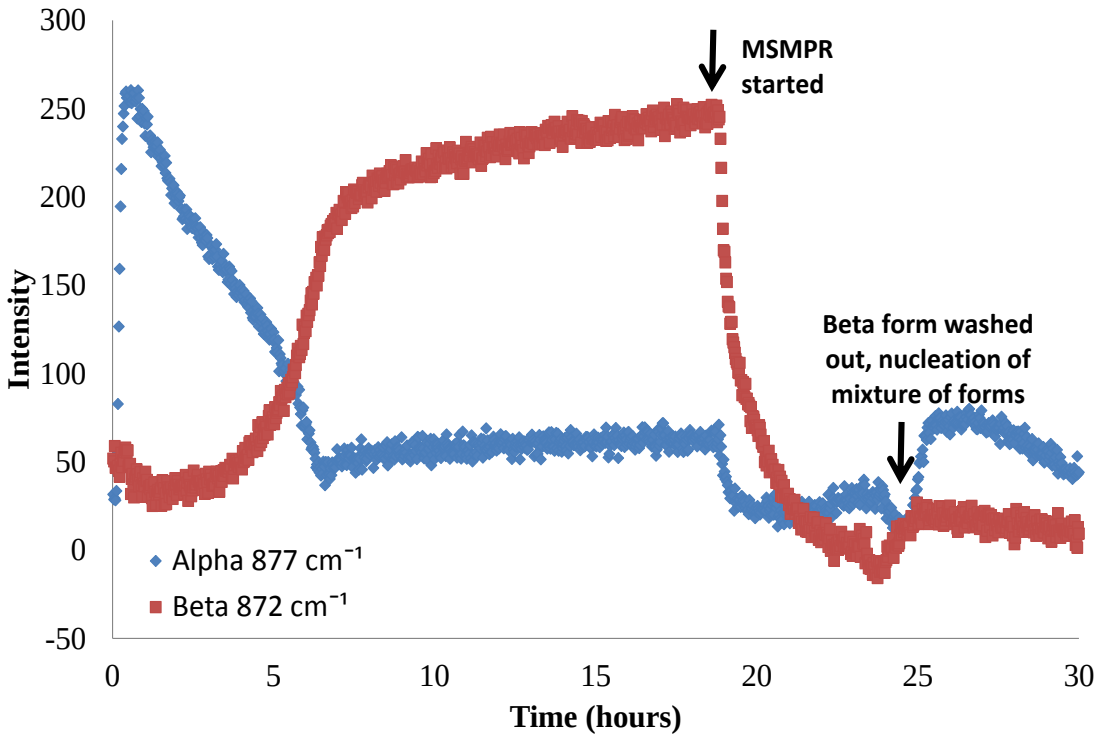

Figure 6-21: Crystallisation profiles of alpha and beta L-glutamic acid obtained when an MSMPR at 45°C was seeded with 100% beta form using a 30 minute residence time, based on 1st derivative Raman intensity at 877 and 872 cm^{-1}, respectively

Figure 6-21 shows that the crystallisation was operated in batch mode for 20 hours when in this time transformation to the beta polymorph had taken place. At approximately 20 hours, the inlet pump adding the LGA solution to the reactor and the outlet pump removing the product slurry from the vessel were started converting the crystallisation to continuous MSMPR operation. As can be seen from Figure 6-21, as soon as the pumps were started, the intensity of the beta form started to decrease dramatically over an extremely short period of time. By approximately 21 hours, there appeared to be very little material remaining in the reactor which could be detected from the Raman measurements. However, when the MSMPR was left to operate, the supersaturation within the vessel seemed to be restored by 25 hours (4 hours later) and nucleation occurred once more, which resulted in a profile similar to that observed in the unseeded experiment under the same conditions. This is compared in Figure 6-22.

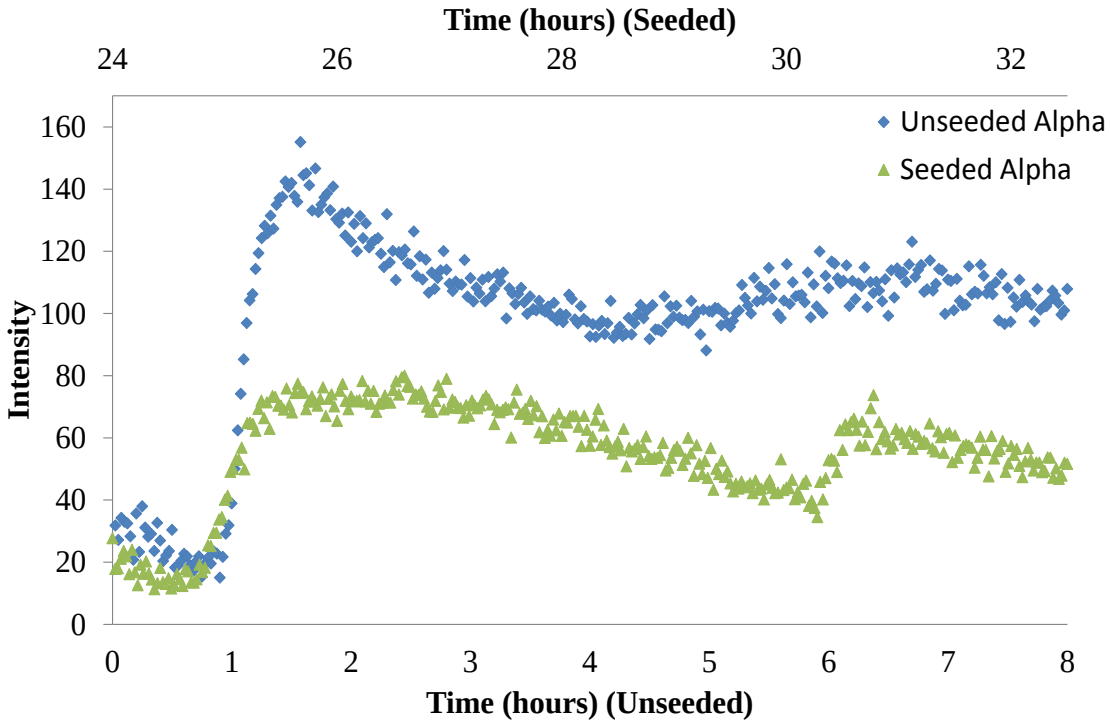

Figure 6-22: Comparison of the seeded and unseeded experiments of alpha L-glutamic acid in a MSMPR at 45°C using a 30 minute residence time, based on 1st derivative Raman intensity at 877 cm^{-1}

Figure 6-22 shows that the profile obtained in the seeded experiment from 24 hours onwards shows a similar trend to that of the initial time period of the unseeded experiment. The main difference is that the profile for the seeded experiment is lower in intensity most likely because the level of supersaturation is not as high as in the initial stages of a crystallisation prior to nucleation. In the seeded experiment, the supersaturation was diminished initially and no further nucleation could occur until a required level of supersaturation was restored. Figure 6-23 shows the average particle size of off-line samples taken at various points during the crystallisation (once the pumps had been started) and the solid recovery over a number of 30 minute periods.

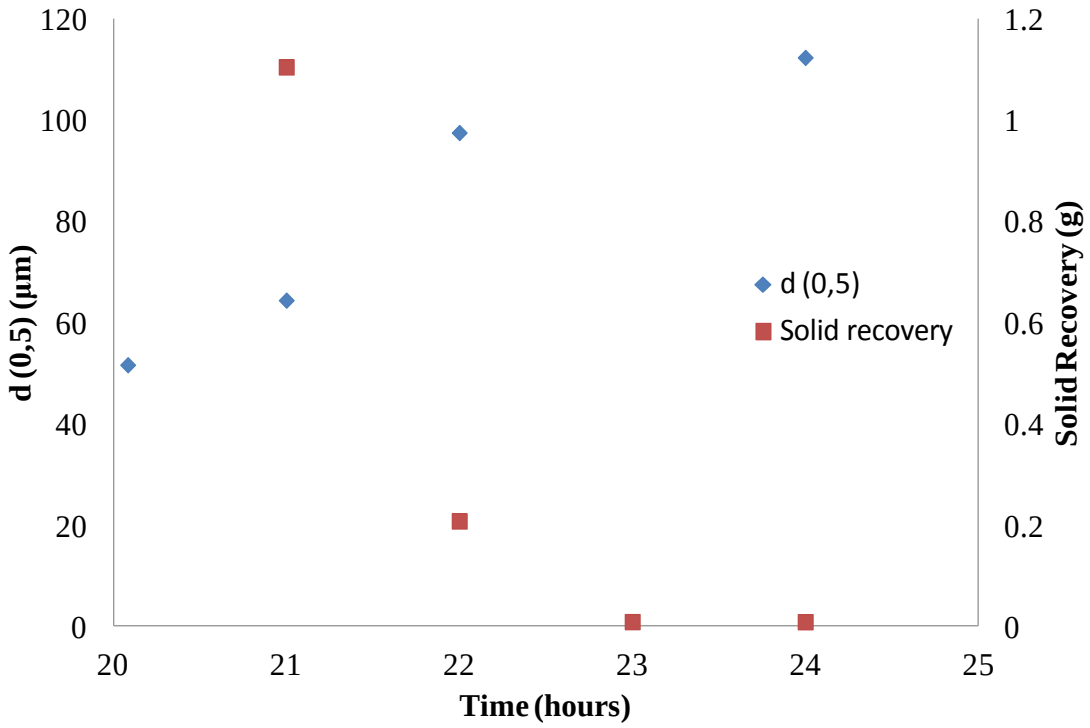

Figure 6-23: Plot of average particle size and solid recovery over 30 minutes at various stages during the crystallisation of L-glutamic acid in an MSMPR seeded with 100% beta at 45°C using a 30 minute RT

Figure 6-23 shows that the concentration of particles in the reactor was significantly higher at the start of the MSMPR operation (after 20 hours in Figure 6-21) and decreased considerably over an hour. This is consistent with the rapid drop in the signal intensity for the beta form in the Raman profile. However, while the number of solid particles in the vessel was reducing, the average particle size increased steadily over several hours. This suggests that after moving to continuous MSMPR operation, particles were removed at a much faster rate than new particles nucleated. However, the crystals that do remain in the vessel appeared to grow steadily in size. Figure 6-24 shows the average particle size and the span of the particle size distributions of the off-line samples.

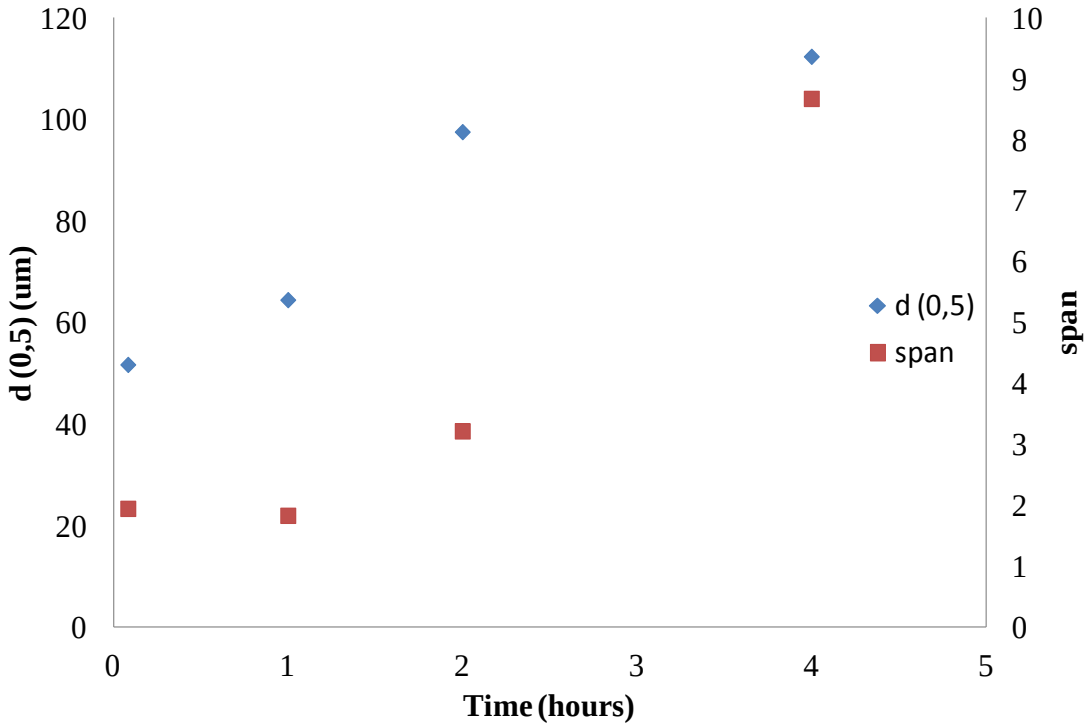

Figure 6-24: Plot of average particle size and solid recovery over 30 minutes during the crystallisation of L-glutamic acid in an MSMPR seeded with 100% beta at 45°C using a 30 minute RT

Figure 6-24 shows that along with the increase in the average particle size, the span of the particle size distribution also increased quite significantly over the first few hours of the MSMPR operation. This is due to a range of particle sizes being present in the vessel including the initial seeds from the batch STR which differ in size due to the different times they spend in the reactor, new nuclei formed when the MSMPR is started, and the subsequent growth of these as well as new nuclei forming during the continued operation of the crystallisation. A PSD span of ~10 as obtained for the sample from 4 hours of MSMPR operation is an extremely wide range of particle sizes and is not a desirable property for crystallisation processes, especially in the pharmaceutical industry where a narrow range of particle sizes is desirable.

6.3.4 Comparison of Continuous Oscillatory Baffled and Mixed Suspension, Mixed Product Removal technology

When comparing the continuous OBR and MSMPR crystallisers, it is important to note that it is unlikely that there will be a "one size fits all" option for continuous reactor technology. As mentioned previously in the section, this is very much compound specific and for example, a certain compound which offers a successful outcome in a continuous OBR may not be able to be replicated with the next compound. This is due to the wide variation in nucleation and growth rates from compound to compound and the operating limits of the reactors themselves i.e. there will be a critical length above which a tubular reactor fails to achieve adequate mixing and approach plug flow conditions and so this will determine the maximum residence time possible in that reactor type.

In the case of L-glutamic acid, it is possible to make certain comparisons between these two main types of continuous reactor since successful crystallisations were conducted in both. Since the main component of a MSMPR reactor is a batch stirred tank vessel, it was possible to accommodate a wider range of solution concentrations (up to 40 g/L) similar to that possible in the batch STR and OBR study (chapter 4). However, due to inlet and outlet tubing being incorporated to convert this batch vessel to a continuous reactor, blocking did become an issue at higher concentrations with increasing time. Conversely, a much narrower range of solution concentrations (20-30 g/L) was possible for crystallisations in the COBR due to blocking at higher concentrations and an absence of any nucleation at lower concentrations. This limits the use of altering the solution concentration as an influence on particle properties, which has been shown to be one of the main effects on both the particle size and the particle size distribution (chapter 4.3). Additionally, the alternate continuous reactors have also been found to provide different outcomes regarding the polymorphic form produced during the crystallisation. All experiments carried out in the continuous OBR resulted in the meta-stable alpha form being obtained (discussed in section 5.3), however, in the MSMPR reactor both pure forms and mixtures were obtained in the unseeded experiments. Therefore, in unseeded crystallisations it was possible to only obtain one polymorph of L-glutamic acid in the COBR (metastable form), whereas

both forms were obtainable in the MSMPR reactor. As seeding experiments were not studied in the COBR, a comparison with the results of the seeded MSMPR experiments could not be made.

As discussed previously, the reactor design as well as the operating conditions also determines the limits of crystal size distribution possible. It is known that particles produced in tubular reactors have a narrower distribution than possible in alternative reactor types and this was obvious with the results obtained using L-glutamic acid. Significantly wider distributions (span of between 4 and 10 compared to less than 2 in the COBR) were observed with the products attained in the MSMPR reactor and in some cases a bimodal distribution was achieved most likely due to the increased secondary nucleation in stirred tank reactors due to collisions. The start-up time was also significantly different between the two reactors. The time to reach steady state operation in the MSMPR was greater than ten residence times (or 5 hours using the average RT) which obviously would waste a great deal of material (if recycling of the material was not employed) if it was necessary to wait for particle properties to become consistent prior to collection of the product. On the other hand, steady state appeared to be attained by two residence times under certain conditions using the COBR, which is a significant advantage over the MSMPR reactor.

6.4 Conclusions

As described at the start of this chapter, the aims of this section of work were to study the mechanisms of polymorph formation of L-glutamic acid in both unseeded and seeded experiments in a continuous mixed suspension, mixed product removal reactor and make comparisons with the study of crystallisation in the continuous oscillatory baffled reactor. The results obtained show that different reactors can provide very different outcomes and that there can be advantages and limitations to both. The decision of which reactor to choose is very much dependent on the compound (i.e. crystallisation kinetics, solubility) and also the desired end result

such as the target polymorph (stable or metastable) and whether properties such as particle size distribution are important.

The unseeded MSMPR experiments carried out at 25^{o}C using a 30 minute residence time resulted in the metastable alpha form being produced continuously for as long as 70 hours (140 residence times). However, due to the crystallisation being operated for such a considerably long time, blocking of the outlet tube was an issue, which despite being heated to prevent precipitation and being flushed through regularly could not be fully overcome. Despite this, once the system had initially reached steady state, the blocking only affected the crystallisation for a short period of time and once this had been cleared the signal returned back to a similar intensity suggesting it had reached steady state once more. The solid production and the average particle size also remained fairly constant once steady state conditions had been reached (after approximately 14 residence times).

When the operating temperature was increased to 45^{o}C using the same residence time, a mixture of forms was obtained with the alpha polymorph being the major form. This was unexpected as the liquid phase measurements obtained during a batch STR experiment using this temperature predicted the beta polymorph would be formed. However, the pure beta form was eventually obtained at this temperature via a solvent mediated transformation process, although this took 25 hours to complete. When the residence time was increased to 60 minutes, the transformation took place much quicker, however, there was significantly less material produced and as the yield gradually decreased, a simultaneous increase in the average particle size was observed. It was expected that the particles would be larger in size as they remained in the vessel longer; however, the fact that there was a smaller mass of particles suggests that crystal growth was the dominant process over nucleation. When a shorter residence time of 15 minutes was attempted, no solid phase could be detected using Raman monitoring. It is likely that some nuclei were formed; however, the residence time appeared to be too short for any substantial nucleation and crystal growth to take place. Therefore, although the beta polymorph could also be formed in a MSMPR this was via a transformation process and the optimum residence time

of 30 minutes did not produce the most desired outcome giving an adequate amount of material, but a slow transformation time of ~25 hours.

When the crystallisation was seeded with 5% beta particles at 45^{o}C using a 30 minute residence time, the outcome was relatively unchanged to that of the unseeded experiment. There was a slight increase in the signal for the beta form initially, but the seeds appeared to be washed out rapidly. However, the seeds did promote the nucleation of the alpha form 30 minutes earlier than in the unseeded crystallisation. It is likely that the seeds stuck together in the vessel and so were removed before they could affect the outcome of the process. When the initial seed loading was increased to 10%, the alpha form was prevented from nucleating for over 4 hours. There was a strong signal for the beta form initially, but this decreased in intensity gradually over a number of hours as these were again washed out from the reactor. It appeared that the beta particles were being removed from the reactor quicker than they could be replaced through nucleation and crystal growth, suggesting the nucleation rate for the beta form was relatively slow. When the MSMPR experiment was seeded with 100% beta formed directly from the batch experiment, the beta seeds were washed out rapidly over a very short period of time. It then took a number of hours for supersaturation to be replenished in the vessel before nucleation of a mixture of forms took place once more.

Therefore, although it was possible to continuously produce the alpha polymorph using a temperature of 25^{o}C in the MSMPR reactor, production of the beta form was more challenging. The stable polymorph could not be formed directly in the unseeded experiments and was only obtained in its pure form following a transformation process. When the crystallisation was seeded with substantial amounts of the beta form, these had little effect on the outcome and were washed out of the reactor for nucleation of a mixture of forms to take place as in the unseeded experiments, once the supersaturation had been restored.

6.5 References

1. A. G. Jones, J. Budz and J. W. Mullin, Crystallization kinetics of potassium sulfate in an MSMPR agitated vessel, *AIChE Journal*, 1986, **32**, 2002-2009.
2. M.-R. Chen and M. A. Larson, Crystallization kinetics of calcium nitrate tetrahydrate from MSMPR crystallizer, *Chemical Engineering Science*, 1985, **40**, 1287-1294.
3. H. Zhang, J. Quon, A. J. Alvarez, J. Evans, A. S. Myerson and B. Trout, Development of Continuous Anti-Solvent/Cooling Crystallization Process using Cascaded Mixed Suspension, *Mixed Product Removal Crystallizers*, *Organic Process Research & Development*, 2012, **16**, 915-924.
4. A. S. Myerson, ed., Handbook of industrial crystallization, 2nd edn., Butterworth-Heinemann, Woburn, 2001.
5. A. G. Jones, Crystallisation Process Systems, Elsevier Butterworth-Heinemann, Oxford, 2002.
6. D. W. Griffin, D. A. Mellichamp and M. F. Doherty, Reducing the mean size of API crystals by continuous manufacturing with product classification and recycle, *Chemical Engineering Science*, 2010, **65**, 5770-5780.
7. R. Grosch, M. Mönnigmann and W. Marquardt, Integrated design and control for robust performance: Application to an MSMPR crystallizer, *Journal of Process Control*, 2008, **18**, 173-188.
8. N. Moldoványi, B. G. Lakatos and F. Szeifert, Model predictive control of MSMPR crystallizers, *Journal of Crystal Growth*, 2005, **275**, 1349-1354.
9. A. D. Randolph and M. A. Larson, Transient and steady state size distributions in continuous mixed suspension crystallizers, *AIChE Journal*, 1962, **8**, 639-645.
10. E. Kougoulos, A. G. Jones, K. H. Jennings and M. W. Wood-Kaczmar, Use of focused beam reflectance measurement (FBRM) and process video imaging (PVI) in a modified mixed suspension mixed product removal (MSMPR) cooling crystallizer, *Journal of Crystal Growth*, 2005, **273**, 529-534.
11. E. Kougoulos, A. G. Jones and M. W. Wood-Kaczmar, Estimation of crystallization kinetics for an organic fine chemical using a modified continuous cooling mixed suspension mixed product removal (MSMPR) crystallizer, *Journal of Crystal Growth*, 2005, **273**, 520-528.
12. J. Mydlarz and A. G. Jones, An assessment of MSMPR crystallization kinetics data for systems modelled by size-dependent crystal growth rate functions, *The Chemical Engineering Journal and the Biochemical Engineering Journal*, 1994, **55**, 69-80.
13. J. Mydlarz and D. Briedis, Growth rate dispersion vs size-dependent growth rate for MSMPR crystallizer data, *Computers & Chemical Engineering*, 1992, **16**, 917-922.
14. J. W. Mullin, Crystallization, 4th edn., Elsevier Butterworth-Heinemann, Oxford, 2001.
15. L. D. Shiau and K. A. Berglund, Model for a cascade crystallizer in the presence of growth rate dispersion, *Industrial & Engineering Chemistry Research*, 1987, **26**, 2515-2521.

16. A. D. Randolph and M. A. Larson, Theory of Particulate Processes, 2 edn., Academic Press Inc., London, 1988.
17. B. O'Sullivan, B. Smith and G. Baramidze, Recent Advances for Seeding a Crystallization Process, *Mettler Toledo White Paper*, 2012.
18. S. M. Nowee, A. Abbas and J. A. Romagnoli, Optimization in seeded cooling crystallization: A parameter estimation and dynamic optimization study, *Chemical Engineering and Processing: Process Intensification*, 2007, **46**, 1096-1106.
19. N. Kubota, N. Doki, M. Yokota and A. Sato, Seeding policy in batch cooling crystallization, *Powder Technology*, 2001, **121**, 31-38.
20. S. Qamar, M. Peter Elsner, I. Hussain and A. Seidel-Morgenstern, Seeding strategies and residence time characteristics of continuous preferential crystallization, *Chemical Engineering Science*, 2012, **71**, 5-17.
21. H. Takiyama and M. Matsuoka, Design of seed crystal specifications for start-up operation of a continuous MSMPR crystallizer, *Powder Technology*, 2001, **121**, 99-105.
22. A. J. Alvarez, A. Singh and A. S. Myerson, Crystallization of Cyclosporine in a Multistage Continuous MSMPR Crystallizer, *Crystal Growth & Design*, 2011, **11**, 4392-4400.
23. A. N. Saleemi, G. Steele, N. I. Pedge, A. Freeman and Z. K. Nagy, Enhancing crystalline properties of a cardiovascular active pharmaceutical ingredient using a process analytical technology based crystallization feedback control strategy, *International Journal of Pharmaceutics*, 2012, **430**, 56-64.
24. M. R. A. Bakar, Z. K. Nagy and C. D. Rielly, Seeded Batch Cooling Crystallization with Temperature Cycling for the Control of Size Uniformity and Polymorphic Purity of Sulfathiazole Crystals, *Organic Process Research & Development*, 2009, **13**, 1343-1356.
25. H. Hao, M. Barrett, Y. Hu, W. Su, S. Ferguson, B. Wood and B. Glennon, The Use of in Situ Tools To Monitor the Enantiotropic Transformation of p-Aminobenzoic Acid Polymorphs, *Organic Process Research & Development*, 2011, **16**, 35-41.
26. Y. Hu, J. K. Liang, A. S. Myerson and L. S. Taylor, Crystallization Monitoring by Raman Spectroscopy: Simultaneous Measurement of Desupersaturation Profile and Polymorphic Form in Flufenamic Acid Systems, *Industrial & Engineering Chemistry Research*, 2004, **44**, 1233-1240.
27. J. Schöll, D. Bonalumi, L. Vicum, M. Mazzotti and M. Müller, In Situ Monitoring and Modeling of the Solvent-Mediated Polymorphic Transformation of l-Glutamic Acid, *Crystal Growth & Design*, 2006, **6**, 881-891.
28. T. Ono, J. H. Horst and P. J. Jansens, Quantitative Measurement of the Polymorphic Transformation of l-Glutamic Acid Using In-Situ Raman Spectroscopy, *Crystal Growth and Design*, 2004, **4**, 465-469.

7 Non-invasive monitoring of the batch crystallisation of D-mannitol using Raman and Acoustic emission spectrometries

7.1 Introduction

D-mannitol was selected as the compound for the last section of this project as it was relevant to industrial crystallisation; however, it is also less well studied than L-glutamic acid and has not been investigated for its compatibility with oscillatory baffled reactor technology. This compound is used to treat several medical conditions including renal failure and cystic fibrosis, and is commonly used in the pharmaceutical industry as an excipient for freeze-dried and tablet formulations.[1, 2] There has been more investigation into alternative particulate processes using D-mannitol including freeze-drying and spray drying.[2-4] As with crystallisation, the polymorph and particle size obtained at the end of these processes are of the upmost importance due to the improved compaction properties of certain forms (when used as a tablet excipient) and optimal range of particle sizes for absorption in the body (when inhaled for the treatment of certain conditions *e.g.* cystic fibrosis). D-mannitol comprises three polymorphs; two meta-stable forms (alpha and beta) and the thermodynamically stable gamma form, all of which have a needle-shaped crystal habit. The crystallisation of D-mannitol has been studied using Raman spectrometry to a lesser extent than L-glutamic acid; however, this has also been carried out using an immersion probe in all reported cases. Therefore, the use of a wide area illumination probe (such as the PhAT probe used in this study), has not been applied to the study of the crystallisation of D-mannitol and offers many potential advantages including the ability to make more representative, non-invasive measurements. *Cornel et al* reported that the crystallisation of D-mannitol in a small scale batch STR was influenced strongly by the solution concentration. Below a certain supersaturation threshold, the gamma polymorph formed, however, above this value, the least stable alpha polymorph nucleated initially, followed by a transformation to the thermodynamically stable form via the beta polymorph.[5] Additionally, it was inferred from simulated process models that the solution concentration would also impact the induction time for nucleation, although, this was not explored experimentally.[5] The

induction time is defined as the time period between supersaturation being attained and the start of formation of a new phase (*i.e.* solid phase). This value can be used to determine the nucleation rate and is affected by the solution temperature and supersaturation.[6] Due to the fact the polymorphs of D-mannitol do not have the same nomenclature in the literature, the three forms were identified as in the report by *Cornel et al*.[5] *Hao et al* also used *in-situ* Raman spectrometry to monitor the transformation of the metastable alpha form to the stable gamma form (named beta in this case) in a batch STR as well as obtaining information on the supersaturation by monitoring the solution concentration. However, in this case, the alpha form was observed to transform straight to the gamma form without any detection of the second metastable (beta) form as an intermediate as reported by *Cornel et al*.[5, 7] Previous work by the same authors incorporated FBRM and particle vision measurement (PVM) alongside Raman measurements to investigate the effect of experimental conditions (temperature, solvent, etc.) on the transformation time when alpha form crystals were added to a saturated solution. It was found that FBRM could also be used to track the transformation process and monitoring particles in the range 1-20 μm could be attributed to the alpha form while an increase in coarser particles above this range indicated the formation of the stable gamma form.[8]

There have been several studies carried out into particle sizing methods available and each are known to have advantages and limitations. Laser diffraction (LD) and FBRM are both light scattering methods and were the two techniques used throughout this project. LD measurements (chapter 4, 5 and 6) assume that particles are spherical which in the case of L-glutamic acid means that particle size distributions (PSDs) obtained for the alpha form (prismatic crystals) will be more accurate than those obtained from beta form crystals (needle-shaped).[9] This means that this method can only really be used qualitatively and that caution needs to be taken when comparing the distributions obtained from pure alpha and pure beta form particles.[10] On the other hand, FBRM measurements (or the chord length distribution (CLD)), of needle-shaped particles are

known to be dominated by the width rather than the length of these particles.[11] However, the orientation of the particle at the measurement window will impact the data collected and in a small number of measurements, the length of the particle rather than the width may be measured which will impact the chord length distribution obtained.[12, 13] Since all of the known polymorphs of D-mannitol (the compound for this section of work) are needle-shaped it was expected that there would be less error in the measurements between polymorphs and these could be compared with more ease. As the data collected from the laser diffraction and FBRM methods in all four chapters would not be compared directly, the difference in instrumentation used and the inherent differences in the principles behind each was thought not to be such an issue.

There are a number of different analytical techniques which have been explored for *in-situ* crystallisation monitoring including Raman, mid and near-infrared spectrometries (as discussed previously in chapter 1.4.1.), however, there are other analytical methods which have been not been applied greatly to this unit operation. One of these techniques is acoustic emission spectrometry (AES) which has shown promise in many particulate processes including powder blending, fluidized bed granulation and reaction monitoring.[14-17] In contrast, active acoustics, where an ultrasound wave is generated and the change detected in the wave is related to the process under study, has been investigated more widely than passive acoustic emission for crystallisation monitoring (see chapter 1.4.2.).[18] It has been reported, however, that AES can be used to obtain information on both the liquid and solid state since the signal obtained will change with a corresponding phase change (*e.g.* the formation of particles in a crystallisation process).[19, 20] *Sawada et al.* used a resonant transducer which means the transducer has a given frequency where it will be especially sensitive to acoustic emission however, it will also have a range of frequencies around this that it will be responsive to and the resulting spectrum obtained will be dependent on the transducer response characteristics. There have been many processes monitored using this type of transducer including heterogeneous reactions; high shear granulation and the progression of slurries through

pipelines.[21-23] It was reported that the effects of solid concentration and particle size were difficult to separate using this type of transducer due to the loss of frequency information following signal analysis which was especially problematic when both these factors caused an increase in the signal amplitude. Additionally, information is likely to be lost due to the short frequency operating range of the transducer.[21] Therefore, in this study, broadband acoustic measurements were made which results in signals being collected over a wide frequency range providing significantly more information than with alternative resonant transducers. Although a wider frequency range is covered using this type of transducer, there will still be a characteristic response that will vary between each transducer causing areas of improved and reduced sensitivity in the resulting spectrum. Particles being monitored during a process by AES will be subject to particle collisions with the components of the vessel, such as the wall and impeller, and also between the particles themselves.[24] These collisions will have an impact on the acoustic frequencies generated which also depend on the properties of the particles such as particle size, shape and density that affect the kinetic energy with which the particles collide. The operating conditions, especially the mixing intensity will also influence the energy of particle collisions and how often they occur.[25] Therefore, any changes in the process that affect these particle collision characteristics will alter the intensity and possibly the frequency distribution of the acoustic waves detected.

Several studies on model systems have shown the effect of increasing collisions (related to solid concentration) and the size of the object colliding (relating to particle size). It was found that when the number of objects colliding increased, this resulted in an increase in the amplitude with little effect on the frequency, while an increase in the size of the objects resulted in a decrease in the frequency and a corresponding increase in the amplitude.[26, 27] AES has been shown to provide information on particle properties during powder blending and also give an indication of when blend homogeneity has been attained. An increasing mass of particles was shown to result in an increase in the overall acoustic signal which was also observed with an increasing particle size

however, a more prominent increase at lower frequencies could be attributed to particles of a larger size.[15] These features of the acoustic emission spectra were also observed during the monitoring of a heterogeneous reaction which made the monitoring of crystallisation using AES an encouraging prospect.[14]

Acoustic emission spectrometry has several potential advantages for the monitoring of particulate processes and in particular, crystallisation. Similar to Raman spectrometry (chapter 4, 5 and 6), measurements can be made non-invasively, which means the problems associated with probe fouling during crystallisation monitoring are removed. However, unlike Raman spectrometry and many of the current crystallisation monitoring techniques, the instrumentation is comparably low cost with an average acoustic set-up costing around $1/10^{th}$ of a Raman spectrometer. Nevertheless, there are several issues which have most likely prevented acoustic emission spectrometry as being adopted as a widely used particle process monitoring technique. The most important of these is the lack of chemical information since AES detects changes in physical properties, whereas certain techniques such as NIR can provide information of both chemical and physical properties (*e.g.* particle size).[28] Additionally, issues with low sensitivity due to the high signal-to-noise can make AES appear a less attractive option to alternative spectroscopic techniques. A loss of signal intensity is commonplace due to the measurements being non-invasive and the acoustic wave having to propagate through the crystallisation medium (*e.g.* water) and the reactor wall. Signal interference from background noise during the crystallisation such as the heater-chiller, and operating conditions including the impeller speed, are also important considerations and this needs to be separated from the information attributable to the effect of the particles on the acoustic spectrum.[29] This is often more complex than alternative spectroscopic techniques where a certain peak(s) position is identified and information on how this peak (*e.g.* intensity, peak area) varies with time can be related to a given property such as concentration.

One of the few examples of acoustic emission monitoring of batch crystallisation showed that the nucleation event could be detected, and at an earlier point than alternative sensors available. Additionally, the purity of the crystals produced influenced the acoustic emission obtained; when impurities were known to be present, the signal was more prominent in different frequency regions than when the chemical purity was high.[25] However, monitoring of the progression of the crystallisation process (*i.e.* crystal growth, steady state) was found to be more difficult information to obtain from AES in this case. *Bouchard et al* were able to obtain some particle size and solid concentration information from batch crystallisation data obtained by acoustic emission, however, relatively complex data analysis was required to achieve this along with an extensive calibration data set.[30] Therefore, to obtain additional information on the progression of the particle size during the crystallisation process, focused beam reflectance measurement (FBRM) was used in this study to relate the acoustic signals obtained and determine any particle size effects.

In the following work, non-invasive Raman spectrometry has been employed to monitor the crystallisation of D-mannitol within a batch STR and batch and continuous OBR. Additionally, acoustic emission spectrometry was employed as a second non-invasive measurement technique to determine if complementary information could be obtained to that already established using Raman spectrometry as a crystallisation monitoring technique (chapter 4, 5 and 6). The primary aims of the study were to obtain additional knowledge to that already in the literature on the batch crystallisation of D-mannitol including the factors which affect the formation and transformation of the three known polymorphs. Secondly, the compatibility of this compound with oscillatory baffled reactor technology was investigated and comparisons drawn with the study undertaken using L-glutamic acid (chapter 4 and 5). Monitoring of the crystallisation using Raman spectrometry was able to provide information on whether the stable or metastable polymorph (or a mixture) nucleated initially and how the transformation progressed. The effect of operating conditions including solution concentration, mixing intensity and

reactor scale on the crystallisation could also be determined using the Raman data collected. Acoustic emission monitoring also provided information on nucleation and growth trends similar to that obtained by Raman spectrometry. Additionally, by comparing with the FBRM measurements it was possible to determine that the acoustic emission trends obtained appeared to be influenced more by the particle size changes during the process than the Raman measurements. This showed the potential for these two techniques being used in combination to provide information on both chemical and physical changes during a crystallisation process.

7.2 Experimental

7.2.1 Materials

In this work, D-mannitol and distilled water were used in all experiments as described in section 3.2.

7.2.2 Batch STR conditions

The reactors used consisted of 350 ml, 500 ml and 1 L round-bottomed jacketed glass vessels as described in section 3.3.1. Solution concentrations of D-mannitol in distilled water between 200 and 350 g/kg were used, which were first prepared in a flask and heated to 60^{o}C on a hotplate with stirring. The hot solution (155 ml for 350 ml vessel, and full volume for 500 and 1000 ml vessels) was then added to the STR where the jacket temperature was fixed at 10^{o}C. The impeller speed applied was either 300 or 400 rpm. Figure 7-1 shows the cooling profiles from a typical crystallisation in both the 1 L and 500 ml STRs using a mixing intensity of 300 rpm.

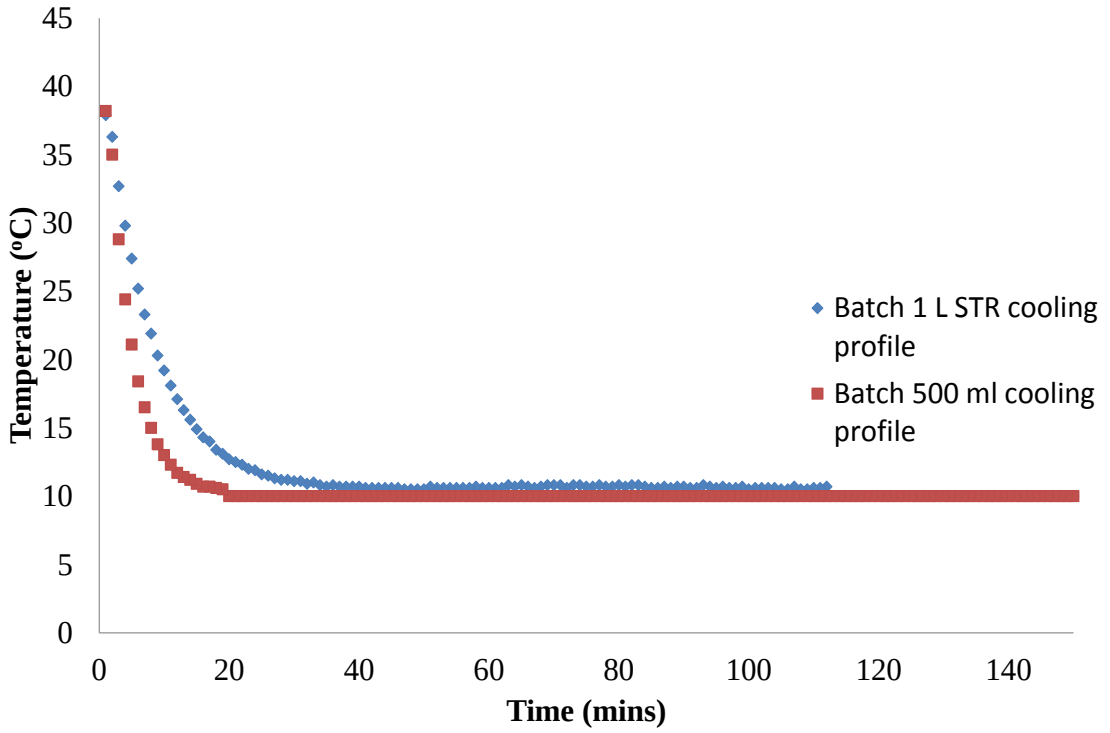

Figure 7-1: Cooling profiles of the reactor contents obtained for both the 500 ml and 1 L batch STR crystallisations using a thermocouple

7.2.3 Batch OBR conditions

The reactors used for this work consisted of 250 ml and 1 L batch jacketed OBR vessels as described in section 3.3.2. Solution concentrations of D-mannitol in distilled water between 300 and 350 g/kg of D-mannitol were used in the OBR. These were first prepared in a beaker and heated to 60^{o}C on a hotplate with stirring. The solution was then added to the OBR, which had the water jacket set at a temperature of 10^{o}C for rapid cooling. The solutions were oscillated at frequencies of 1 or 3 Hz and amplitudes of 10 or 30 mm. Figure 7-2 shows the cooling profile for rapid cooling in both the 250 ml and 1 L batch OBR.

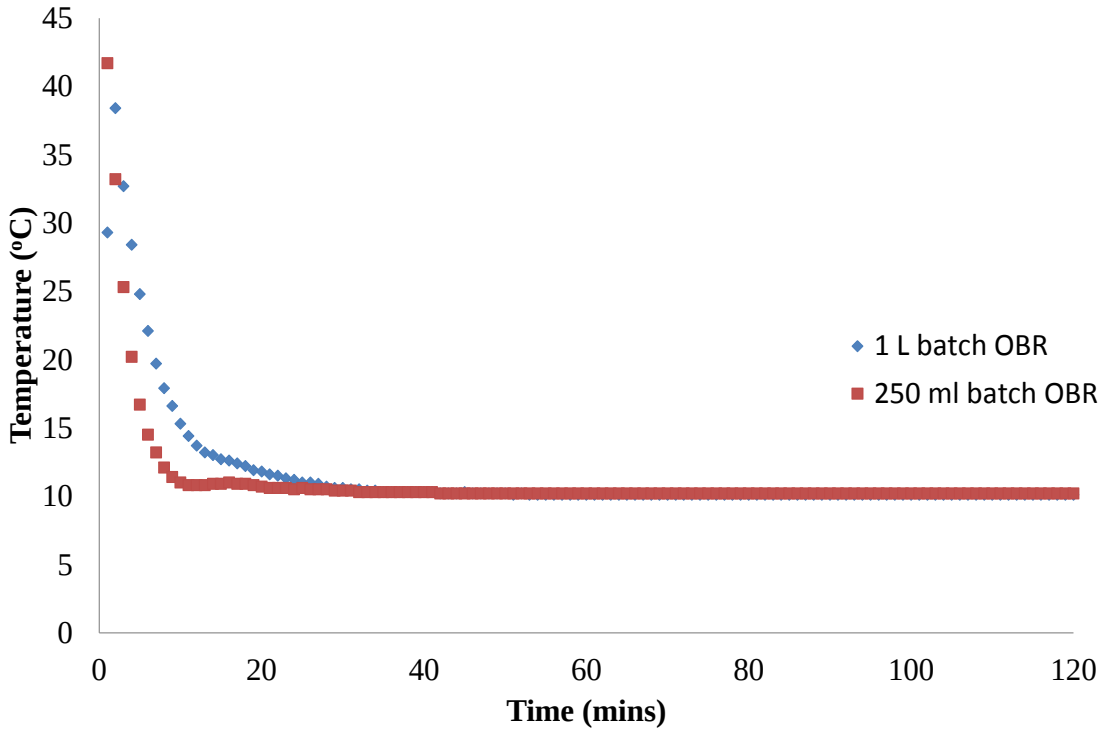

Figure 7-2: Cooling profiles of the reactor contents obtained for both the 250 ml and 1 L batch OBR crystallisations using a thermocouple

7.2.4 Raman Instrumentation- Kaiser RxN1 spectrometer

Raman measurements were carried out using a Kaiser RxN1 spectrometer with the $P^{h}AT$ probe head as described in section 3.4.1. The set-up for Raman measurements is shown in Figure 3-5. A 785 nm near-IR laser with a 6 mm spot diameter and laser power of 400 mW was employed using an exposure time of 15 s and 4 accumulations resulting in a measurement being obtained every 90 s.

7.2.5 Acoustic emission monitoring

Acoustic emission measurements were carried out using the instrumentation described in section 3.4.2. A sampling rate of 2 MHz was used for all experiments with a 2 second

delay between measurements. The acoustic emission measurements were obtained using the set-up in 3-12.

7.2.6 Focused beam reflectance measurement

Focused beam reflectance measurements (FBRM) were carried out using a Lasentec (Mettler Toledo) S400 laboratory scale probe as described in section 3.4.4. *In-situ* measurements were carried out by inserting the probe into the 1 L batch OBR probe port which was secured with a probe sleeve. Off-line measurements were carried out by adding 1 g of each sample (which had been vacuum filtered and dried in an oven) into a beaker containing ~50 ml of diethyl ether and stirring applied using a magnetic stirrer. For both the *in-situ* and off-line analysis, a measurement was collected every 15 s.

7.2.7 X-ray diffraction

X-ray powder diffraction measurements were undertaken using a Bruker AXS D8Advance transmission diffractometer as described in section 3.4.5. Powder samples of D-mannitol which had been vacuum filtered and dried in an oven were lightly ground using a mortar and pestle and a small amount (<0.5 g) was placed on a metal well plate supported by kapton film.

7.3 Results and Discussion

7.3.1 Batch STR

Several preliminary experiments were carried out to establish whether a change in the solution concentration (or supersaturation) affected which polymorph formed initially, as this relationship had been reported by *Cornel et al*.[5] These experiments were conducted on a relatively small scale so as to replicate the experimental conditions of *Cornel et al.* as closely as possible. The solution concentration with the corresponding

supersaturation values with respect to each of the three polymorphs are shown in Table 7-1.

Table 7-1: Initial solution concentrations and corresponding supersaturation values with respect to each polymorph for crystallisation experiments of D-mannitol carried out at 10oC[5]

	Initial Supersaturation		
Solution Concentration (g/kg)	**Alpha form**	**Beta form**	**Gamma form**
200 g/kg	0.97	1.36	1.62
250 g/kg	1.22	1.71	2.02
300 g/kg	1.46	2.05	2.43
350 g/kg	2.83	2.39	2.83

As with the previous study in the batch STR and OBR using L-glutamic acid (chapter 4), the 1st derivative Raman spectra obtained during the crystallisations were investigated and peaks selected that were attributable to the solute concentration and the alpha and the gamma polymorphs. Figure 7-3 shows an expanded area (1000-1090 cm^{-1}) of a selection of the 1st derivative Raman spectra for one of the crystallisations (300 g/kg, 250 ml scale, 300 rpm) showing the solute, and alpha and gamma polymorph peaks selected to produce the crystallisation profiles in all subsequent figures in this chapter.

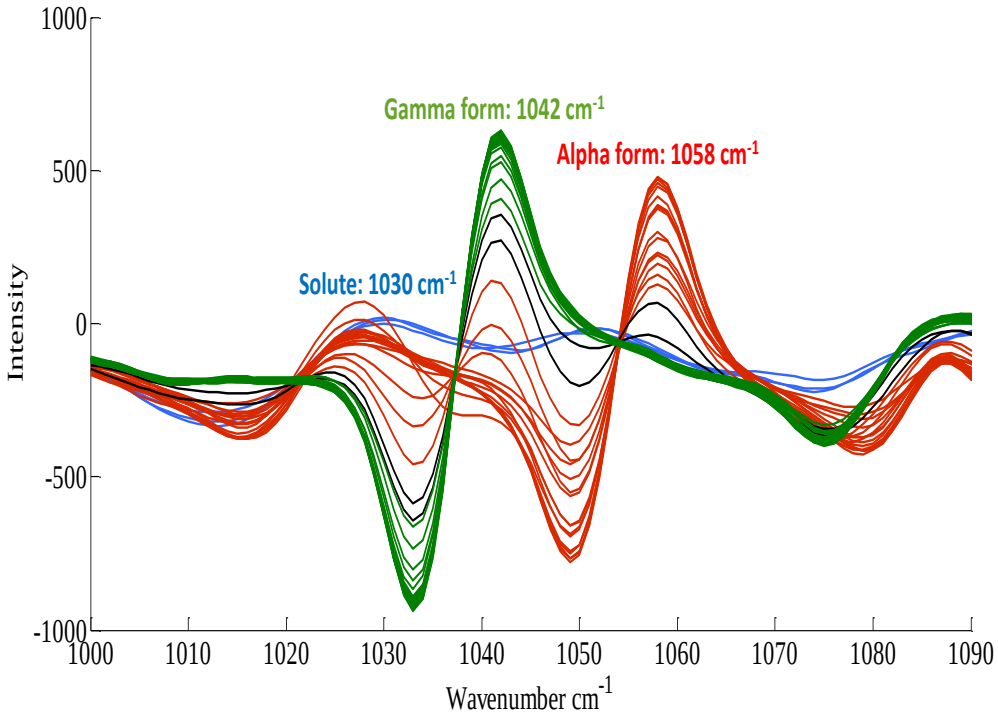

Figure 7-3: Expanded area of a selection of the 1st derivative Raman spectra of D-mannitol for a batch STR experiment at 10°C in a 250 ml vessel with a solution concentration of 300 g/kg and 300 rpm agitation showing the solute (blue), alpha (red) and gamma (green) peaks used to obtain the crystallisation profiles

The crystallisation profiles were formed by plotting the change in the Raman 1st derivative intensity at 1058 cm^{-1} (alpha) and 1042 cm^{-1} (gamma). Figure 7-3 shows that the solute peak (blue) is located at a similar wavenumber to the negative peak of the gamma form (green) and a positive peak for the alpha form (red). This meant the solute profile (*e.g.* in Figure 7-4) becomes a negative mirror image of the gamma form once this begins to increase in intensity. Therefore, the solute profile can really only be interpreted until nucleation of the solid form commences and so was not included in subsequent plots.

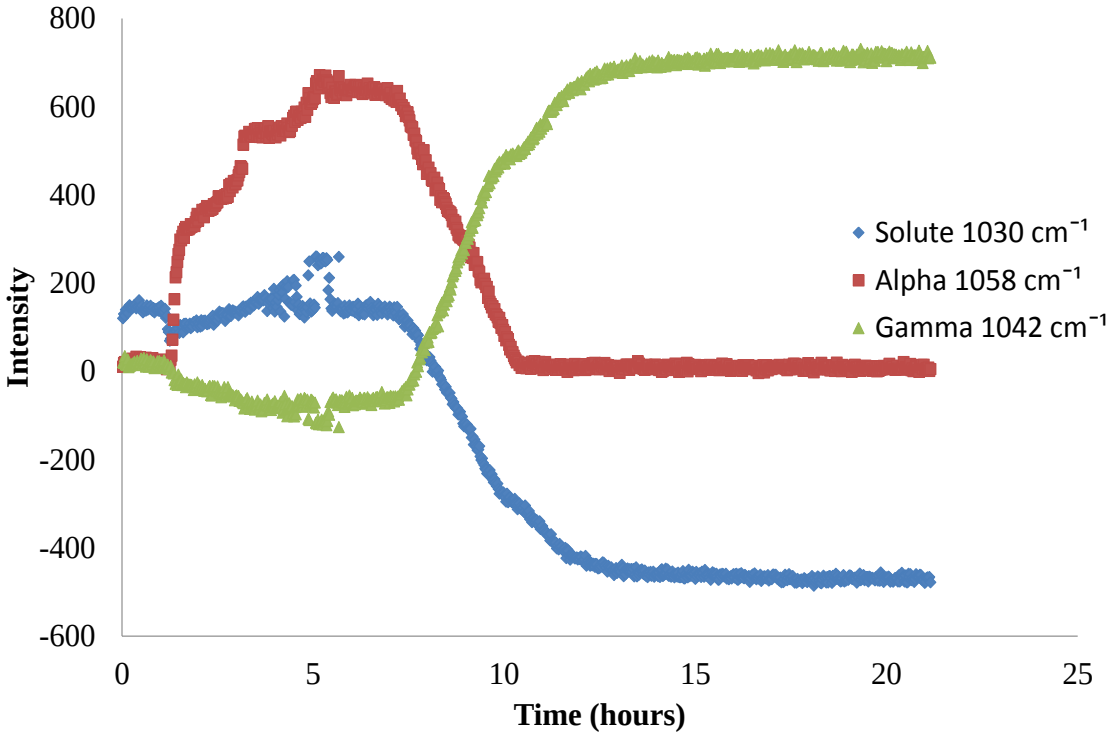

Figure 7-4: Crystallisation profiles of alpha (red), gamma (green) and D-mannitol solution (blue) for a batch STR experiment at 10°C in a 250 ml vessel with a solution concentration of 300 g/kg and 300 rpm, based on 1st derivative Raman intensity at 1058, 1042 and 1030 cm^{-1}, respectively

Additionally, the solute peak overlaps with the positive gamma peak at 1042 cm^{-1}, therefore, it was expected that this would affect the crystallisation profiles obtained for the gamma form. However, it was anticipated that the error introduced would be greater at the start of the measurements, just following nucleation and that this error would decrease as the crystallisation progressed due to the solid form becoming the greater influence on the Raman spectrum. The alpha peak selected to obtain crystallisation profiles at 1058 cm^{-1}, appears to be unaffected by the presence of the gamma polymorph and solute phase. The gamma form peak is overlapped slightly by the negative peak for the alpha polymorph so when a mixture of forms was present it was expected that the signal for the gamma form would be underestimated slightly due to the negative contribution from the alpha signal. Therefore, to correct for this, the effect was estimated using the unaffected alpha form peak at 1058 cm^{-1}. A ratio of the peak intensity of the

alpha peak at 1058 cm^{-1} and the negative region of the alpha peak at 1042 cm^{-1} was taken when only the pure alpha form was present. Therefore, once the ratio of these two wavenumbers deviated from the constant value when just the alpha form was present, it could be insinuated that this was due to the formation of the gamma polymorph and thus a correction was carried out to account for this and produce a more accurate crystallisation profile. Figure 7-5 shows the crystallisation profile for the gamma form before and after correcting for the negative effect of the alpha form peak.

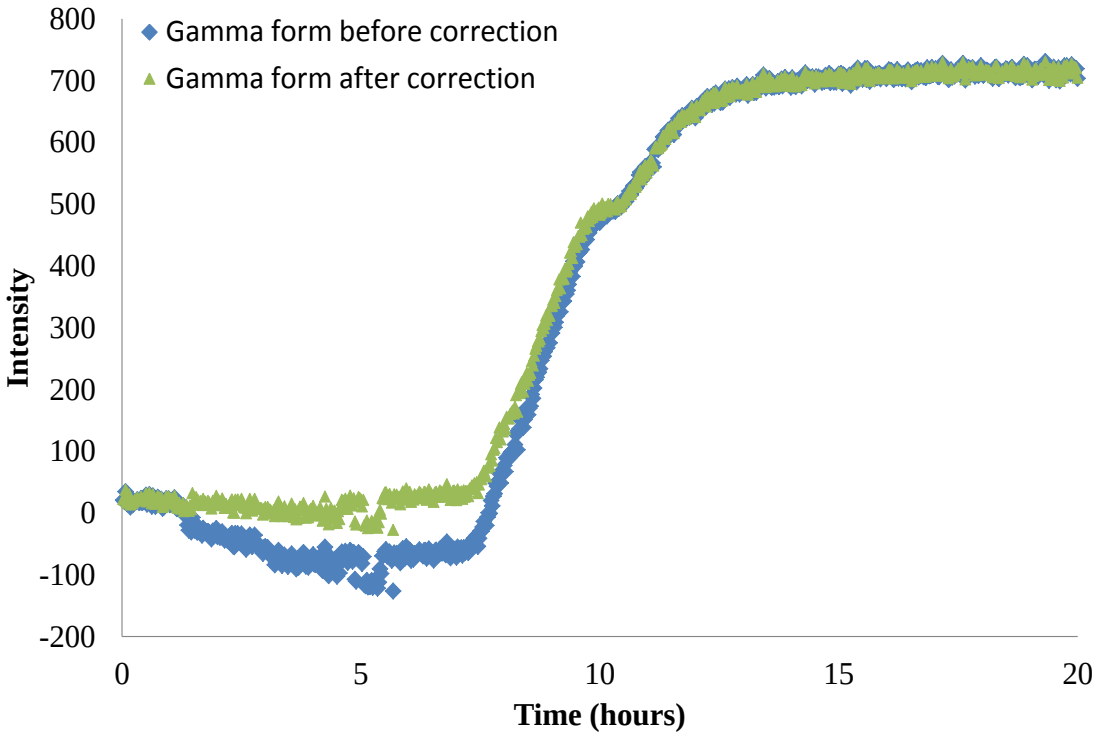

Figure 7-5: Crystallisation profile (1st derivative Raman intensity at 1042 cm^{-1}) for the gamma form using a solution concentration of 300 g/kg and 300 rpm agitation in a 250 ml batch STR vessel before and after correcting for the negative contribution of the alpha form using the ratio of the positive and negative alpha peaks to carry out the correction

As Figure 7-5 shows, in the uncorrected profile, the time period during which the alpha form causes the most error in the gamma crystallisation profile is during the period when the alpha form is the major polymorph present (as shown in Figure 7-7). As the transformation process begins, and the concentration of the gamma polymorph increases

in the vessel, the effect from the overlapping with the alpha form spectrum decreases and by the time the gamma polymorph becomes the dominant polymorph, the effect is minimal.

Figure 7-6, Figure 7-7 and Figure 7-8 show non-invasive Raman data collected for crystallisation in a 350 ml batch STR vessel containing a volume of 155 ml with an initial solution concentration of 200 g/kg, 300 g/kg or 350 g/kg, respectively.

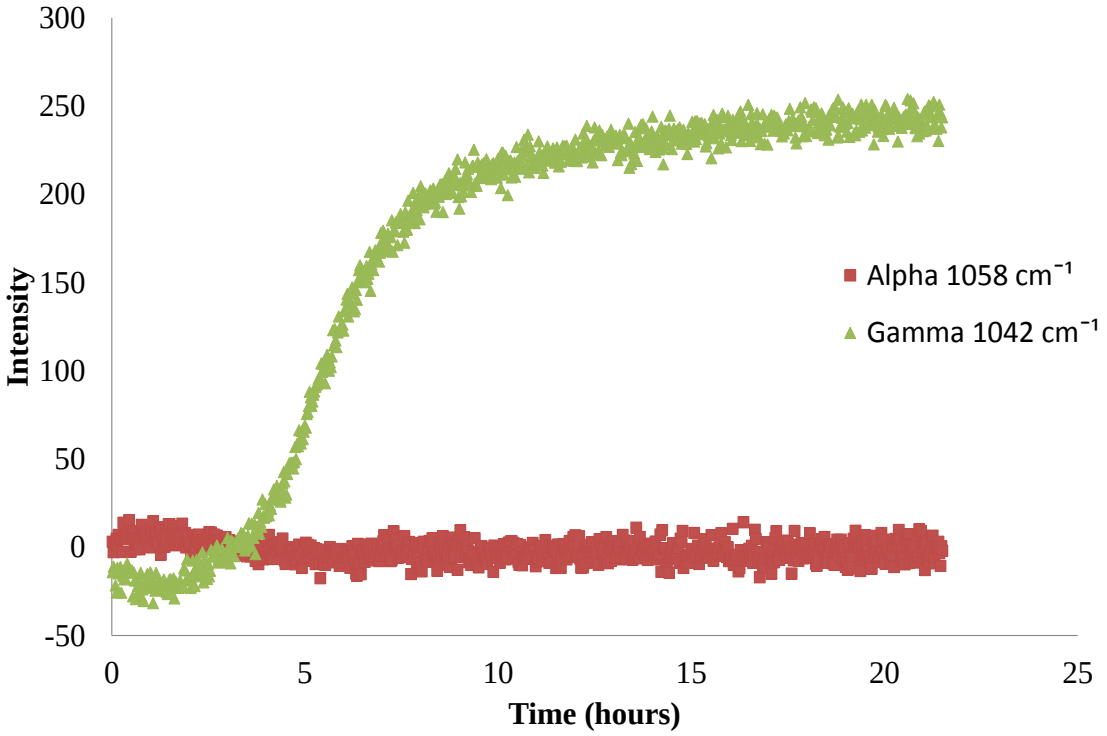

Figure 7-6: Crystallisation profile showing the formation of the stable gamma form of D-mannitol using a solution concentration of 200 g/kg in a batch STR at 10°C, based on 1st derivative Raman intensity at 1058 and 1042 cm^{-1}

Figure 7-6 shows that when the lowest solution concentration of 200 g/kg was used, there was no apparent nucleation was detected in the Raman measurements in the initial few hours. Nucleation of the stable gamma form began at approximately 3 hours and was followed by a rapid increase in the signal from 5 hours until the signal began to

level off after 15 hours suggesting the majority of crystal growth was complete. There appeared to be no nucleation of the metastable alpha form, or too little to be detected *in situ* using Raman spectrometry.

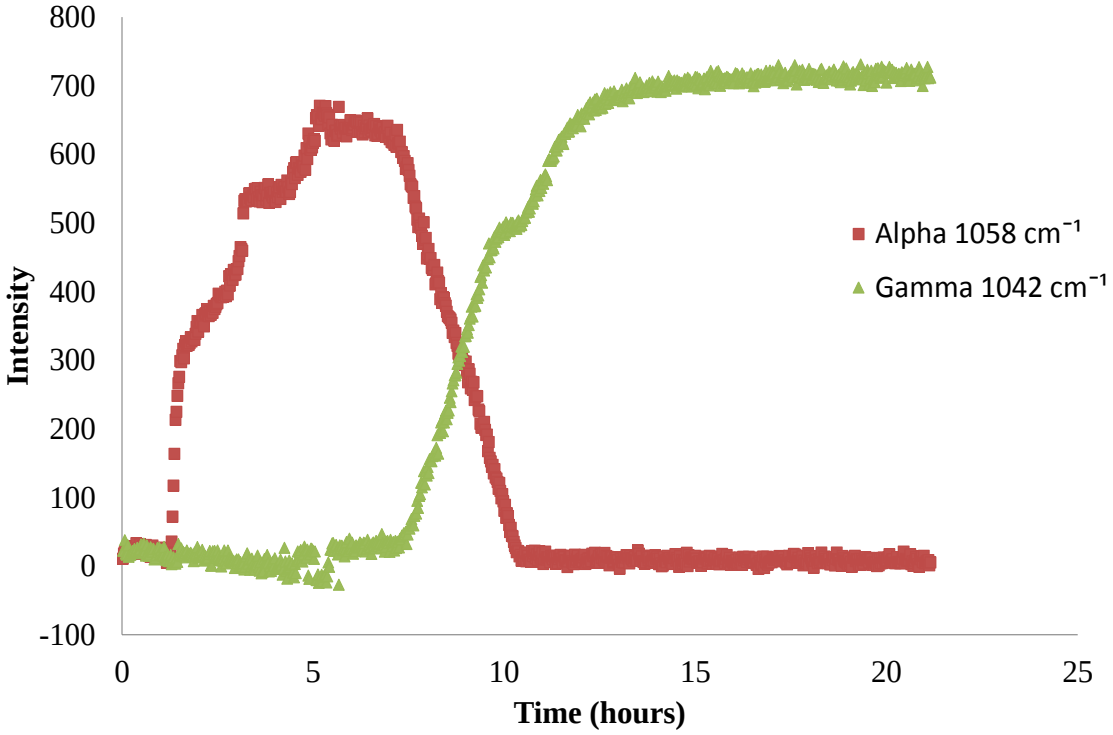

Figure 7-7: Crystallisation profile showing the transformation from alpha to gamma mannitol using a solution concentration of 300 g/kg in a batch STR at 10°C, based on 1st derivative Raman intensity at 1058 and 1042 cm^{-1}, respectively

When the initial solution concentration was increased to 300 g/kg, a significantly different crystallisation profile was obtained to that in Figure 7-6. Nucleation occurred much earlier (1.25 hours) than with 200 g/kg mannitol and the initial polymorph produced was the metastable alpha form. There was a rapid increase in the alpha form signal following nucleation which then increased more gradually over several hours before levelling off at around 5 hours. This period of steady state lasted for approximately 2 hours before the intensity of the alpha form decreased rapidly accompanied by a simultaneous increase in the signal for the gamma form. The signal for the alpha form became consistent at around 11 hours, while the gamma form signal

levelled off closer to 13 hours showing transformation to the thermodynamically stable polymorph was complete. The crystallisation profiles obtained in this experiment suggested that it would be possible to obtain both the alpha and gamma polymorphs if the material was isolated quickly and at the right point before any transformations commence (in the case of the metastable alpha form) or once the transformation was fully complete (in the case of the stable gamma form). The intensity of the signal for the gamma form once at steady state was significantly higher than that obtained in Figure 7-6 using a lower solution concentration which was expected as the Raman profile provides a good indication of the levels of solid material produced and it would be expected that a higher solution concentration would result in an increase in the concentration of particles.

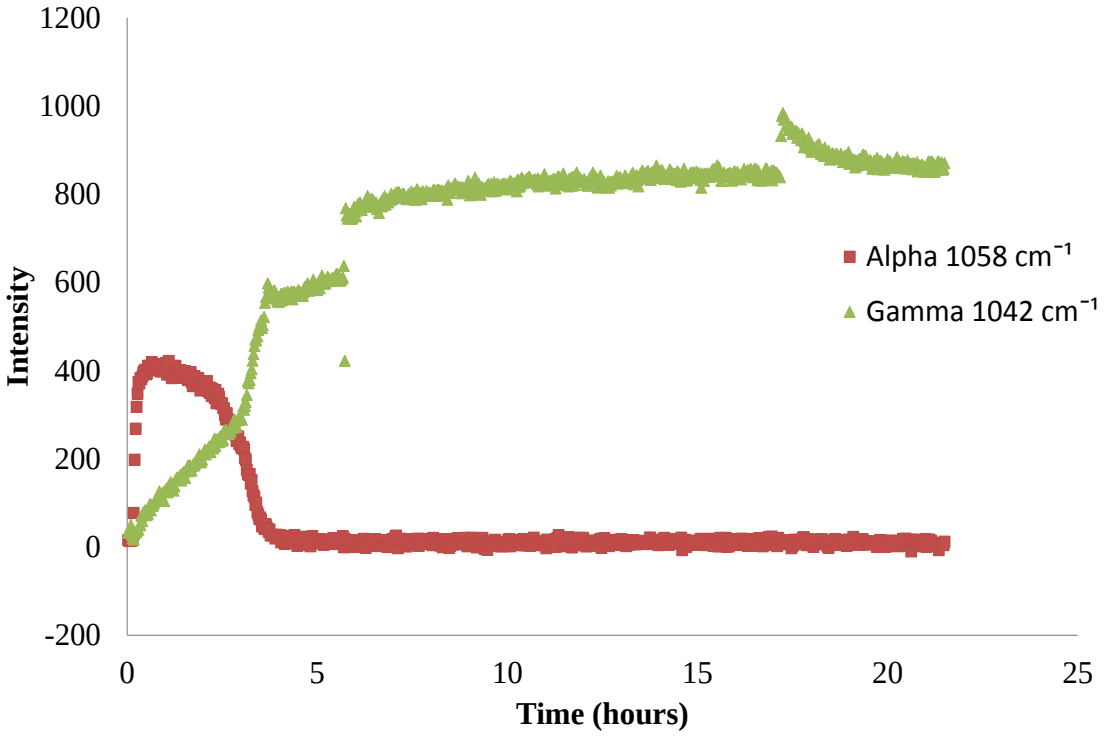

Figure 7-8: Crystallisation profile showing the transformation from alpha to gamma D-mannitol using a solution concentration of 350 g/kg in a batch STR at 10°C, based on 1st derivative Raman intensity at 1058 and 1042 cm^{-1}, respectively

Figure 7-8 shows that nucleation occurred rapidly (0.25 hours) when the highest solution concentration of 350 g/kg was used resulting in a rapid increase in the signal for the alpha polymorph during the crystal growth period with an almost immediate steady increase in the signal for the gamma form. This shows a mixture of forms nucleated using this concentration with the alpha form being the major form initially. However, once the signal for the alpha form had reached a maximum intensity shortly after the initial nucleation point, a steady decrease in the intensity was observed which reached a minimum value at approximately 4 hours and levelled off. The dissolution of this metastable form was accompanied with a steady increase in the signal for the gamma form as transformation was taking place, with the final stages of this transformation process (at the 4 hour time point) occurring more rapidly. This signal then reached steady state at around 6 hours. As well as the nucleation process occurring quicker when a higher solution concentration was used, the transformation process was also completed in a much shorter time period. This was due to a mixture of the alpha and gamma forms nucleating which accelerates the transformation to the thermodynamically stable polymorph. There was a slight increase in the intensity of the solid produced once the crystallisation was complete, however considering the solution concentration was increased by 50 g/kg; the relatively small increase observed does not appear to correlate with this. It is possible that at this high concentration, the agitation employed in the vessel was not sufficient enough to suspend all of the solid material produced and that the remaining solid material had sunk to the base of the vessel (which was observed at the end of the crystallisation once the foil had been removed from the vessel) and so was not detected in the Raman measurements obtained. The material collected at the end of the crystallisation confirmed that a higher solid concentration had been produced than at the lower concentrations.

The preliminary experiments agreed with the results reported by *Cornel et al*[5] in that an increase in the solution concentration (or initial supersaturation) resulted in increased levels of the alpha form nucleating followed by a transformation to the stable gamma form at some point during the crystallisation. However, it was also reported that it was

thought that the least stable alpha form transformed to the stable gamma form via a second metastable beta form (according to *Cornel et al*. a peak for this form could be observed between 1025-1035 cm^{-1}) which would make sense when the phase diagram of the three polymorphs of D-mannitol is consulted (Figure 3-3).[5] This was not observed in the results obtained using non-invasive Raman monitoring above. It is possible that the alpha polymorph transformed directly to the stable form or that the beta polymorph briefly nucleated in such small quantities that it could not be detected using Raman spectrometry. It was also suggested in the literature that there would be different induction times prior to the start of nucleation with differing solution concentrations; however, this was only reported using simulated process models and not demonstrated experimentally, as confirmed practically in these initial results. The effect of solution concentration on the polymorphic form is most likely due to the different solubility's of the polymorphs (Figure 3-3). With a higher solution concentration, at the same reactor temperature, the supersaturation will be in the metastable zone width for the metastable alpha form, therefore resulting in the initial nucleation of this form. As the solution concentration is decreased, the supersaturation will enter the metastable zone width of the stable gamma form and will therefore result in nucleation of the gamma form. Due to the fact the solution concentration had a major impact on the nucleation and transformation of the different polymorphs of D-mannitol, the next stage involved investigating the effect of scale on the outcome of the crystallisation.

7.3.1.1 Effect of Scale in the batch STR

As the initial experiments were carried out on a relatively small scale (350 ml vessel), an intermediate sized vessel of 500 ml and a larger vessel of 1 L were used to see if the scale at which the crystallisation was carried out would affect the polymorphs formed as this had not been previously reported. Figure 7-9 and Figure 7-10 show the Raman trend plots for experiments undertaken in the 500 ml vessel using an agitation of 300 rpm with a solution concentration of 300 or 350 g/kg, respectively.

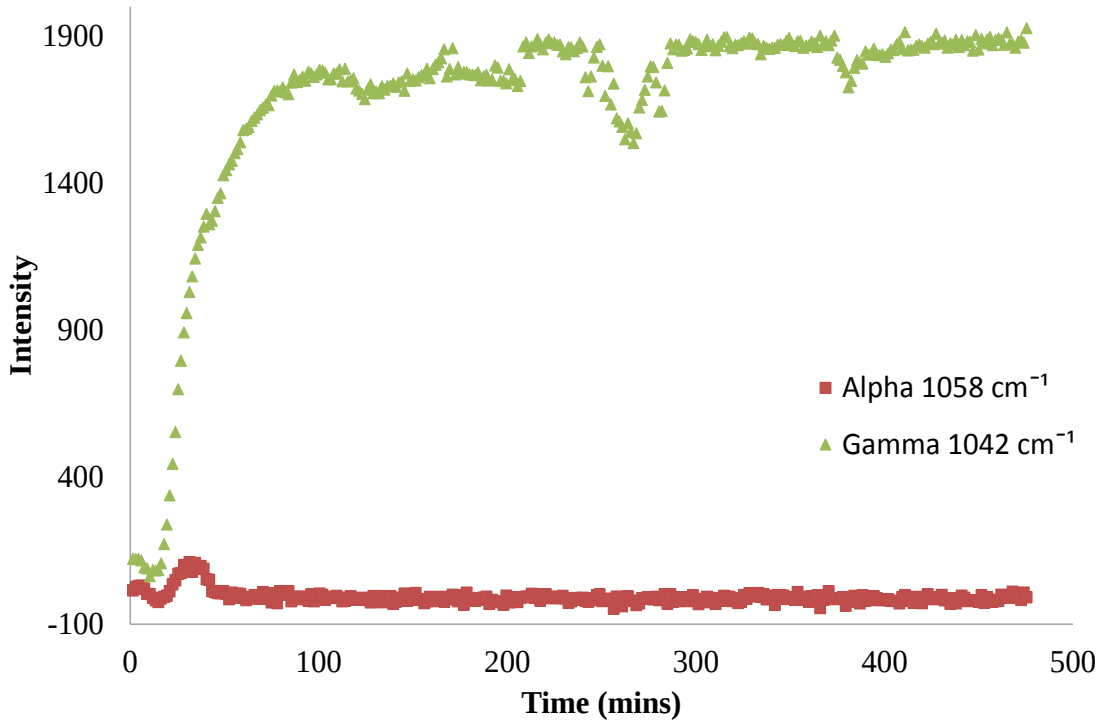

Figure 7-9: Crystallisation profile showing the formation of gamma mannitol using a solution concentration of 300 g/kg in a 500 ml batch STR at 10°C, based on 1st derivative Raman intensity at 1058 and 1042 cm-1

The crystallisation carried out at a 500 ml scale and 300 g/kg mannitol resulted in a nucleation time of approximately 25 minutes. The gamma polymorph appeared to be the only form which nucleated as detected by Raman and the majority of crystal growth was completed relatively quickly after around 40 minutes following nucleation suggesting a rapid crystal growth rate. The crystallisation profile obtained showed a similar polymorphic outcome as that observed at a lower solution concentration (200 g/kg) in the smaller scaled vessel (Figure 7-6). Additionally, nucleation occurred quicker than in the equivalent 300 g/kg experiment in Figure 7-7.

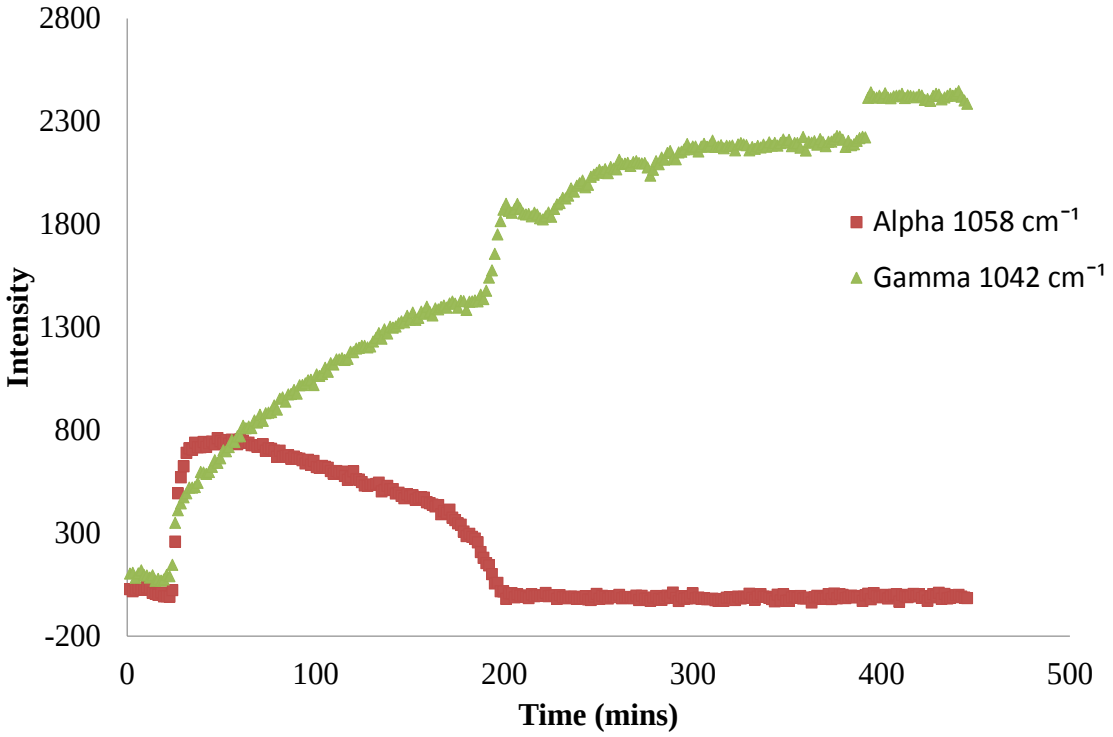

Figure 7-10: Crystallisation profile showing the formation of alpha and gamma mannitol using a solution concentration of 350 g/kg in a 500 ml batch STR at 10°C, based on 1st derivative Raman intensity at 1058 and 1042 cm^{-1}, respectively

Figure 7-10 shows that at the higher concentration of 350 g/kg, a mixture of polymorphs nucleated initially during the crystallisation in a 500 ml vessel. When comparing the results to those obtained at a smaller scale (155 ml) in Figure 7-8 it can be seen that a higher concentration of the alpha polymorph was formed at this smaller scale with the alpha polymorph being the major form in the initial stages. The transformation to the stable gamma form in Figure 7-10 was complete by approximately 3 hours compared to a 4 hour transformation period during the smaller scaled crystallisation. Due to there being less of the alpha form present in the 500 ml scale vessel, it was expected that the transformation process would occur quicker. However, the main observation in both the experiments conducted at the 500 ml scale was that the gamma polymorph was the predominant form and increasing the concentration did not have as great an effect as it did with the crystallisations at a smaller scale where an increase in the solution

concentration resulted in an appreciable increase in the levels of the alpha form. Therefore, the agitation rate within the vessel was increased to see if this had an impact on the polymorphic composition during nucleation. Figure 7-11 shows an overlay of the crystallisation profiles obtained during a 300 g/kg crystallisation at a 500 ml scale using an agitation of 300 and 400 rpm.

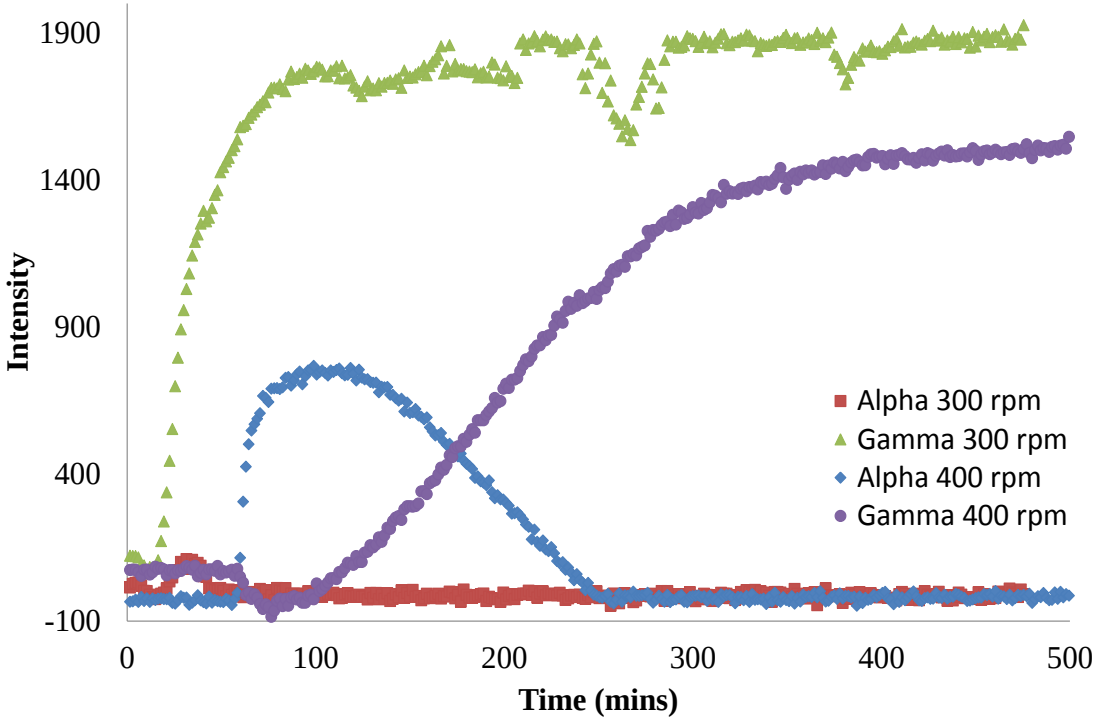

Figure 7-11: Crystallisation profiles showing the formation of alpha and gamma mannitol with increasing agitation using a solution concentration of 300 g/kg in a 500 ml batch STR at 10°C, based on 1st derivative Raman intensity at 1058 and 1042 cm^{-1}, respectively

Figure 7-11 shows that there was quite a significant difference in the crystallisation profiles obtained when the agitation in the vessel was increased from 300 to 400 rpm. There was significantly more alpha form produced initially when the agitation was increased and this remained in the vessel for a longer period of time before dissolution and transformation to the stable gamma form took place. Additionally, the induction period between reaching supersaturation and nucleation taking place was longer at a higher mixing intensity by around 40 minutes. This was unexpected as it was thought

that the conditions within the vessel would become more uniform more quickly with increased agitation and therefore nucleation would occur within a shorter time period. It is possible that at a lower mixing intensity of 300 rpm, areas of local high supersaturation existed (discussed previously in section 1.2.) which promoted nucleation at an earlier point than in the crystallisation carried out using a 400 rpm mixing intensity. The differences in the signal intensities when the crystallisations reached steady state also suggested that using the same solution concentration, there was a lower solid concentration of gamma mannitol obtained at a higher mixing intensity, which was confirmed with the solid recovery measurements. Similar results were obtained when the agitation was increased to 400 rpm using a solution concentration of 350 g/kg (figure not shown), in that increased levels of the alpha polymorph were formed during the crystallisation and remained in the vessel for a longer period of time.

Figure 7-12 shows the crystallisation of D-mannitol using a solution concentration of 300 g/kg and mixing intensity of 300 rpm carried out in a 1 L vessel, the largest scale reactor used in this study.

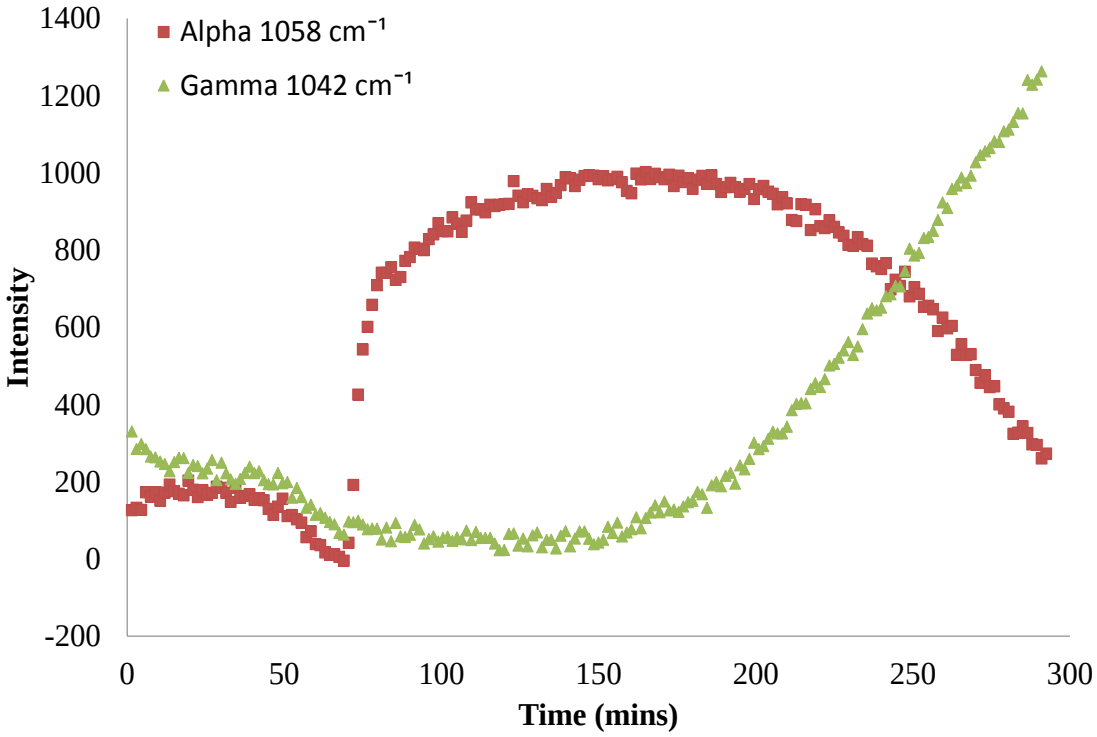

Figure 7-12: Crystallisation profile showing the formation of alpha and gamma mannitol using a solution concentration of 300 g/kg in a 1 L batch STR at 10°C, based on 1st derivative Raman intensity at 1058 and 1042 cm^{-1}, respectively

Figure 7-12 shows that nucleation occurred at approximately 1.25 hours which was similar to the induction time observed using the same solution concentration at the 350 ml scale (Figure 7-7). Additionally, the alpha polymorph nucleated as the major form, like the equivalent experiment in Figure 7-7, however in this case transformation to the stable gamma form began sooner (150 minutes onwards compared to 7.5 hours). This result was unexpected as it was thought the gamma polymorph would be obtained initially with a second increase in scale as with the 500 ml scale experiment at the same solution concentration in Figure 7-9. The only other difference apart from the volume, between the 250 and 500 ml vessel and the 1 L vessel was the impeller used to create agitation. A PTFE impeller was used in the 2 smaller vessels while a glass impeller was used in the 1 L vessel. Although the paddles of both impellers were of a similar overall size, the material appeared to impact the polymorphs produced. It is possible that the glass impeller produced more efficient mixing over the equivalent PTFE impeller as the

PTFE was found to be a more flexible material. It has also been reported that the impeller material can impact the polymorph produced and in the case of plastic impellers it has been found to absorb some of the energy on impact with a crystal(s) and result in a reduced secondary nucleation rate in comparison to alternative impeller materials.[31, 32] The signal intensity of the gamma form at the end of the Raman measurements in Figure 7-12 was at approximately 1200 and was still increasing which would result in a higher steady state signal intensity than that observed in both the 500 ml and 250 ml experiments. This also helped to confirm the theory that a glass impeller provided improved mixing and therefore created more efficient suspension of the particles preventing them sinking to the base of the vessel.

The crystallisation of D-mannitol appeared to be sensitive to many experimental factors and the polymorphic outcome was significantly different depending on changes in these variables. The solution concentration, vessel size, mixing intensity and impeller material were all found to impact which polymorph(s) nucleated and the timescale of full transformation to the thermodynamically stable polymorph. However, unlike similar experiments in a batch STR reported in the literature, the beta form was not detected as a polymorphic intermediate using Raman spectrometry. A selection of the experiments was repeated and the results found to be reproducible.

7.3.1.2 Acoustic emission monitoring of batch STR crystallisation of D-mannitol

Along with the non-invasive Raman measurements, a number of experiments were also monitored using acoustic emission spectrometry to determine if any complementary information could be obtained on the crystallisation process. It is known that the intensity of an acoustic signal is influenced by a number of factors including the solid concentration, particle size, shape and density of the material as well as the operating conditions, in particular the mixing intensity applied. These particle and operating parameters will impact the energy and number of collisions and therefore the frequency and intensity of the acoustic spectrum. Firstly, several preliminary experiments were

carried out to see if an increase in the overall number of particles resulted in an increase in the acoustic signal intensity. It was important to know which frequency ranges corresponded to the background noise (*e.g.* heater-chiller operation, impeller movement) and whether this could be separated from the signals generated when the particles collide with the vessel wall. These results obtained for experiments undertaken in a 500 ml vessel are shown in Figure 7-13 and Figure 7-14.

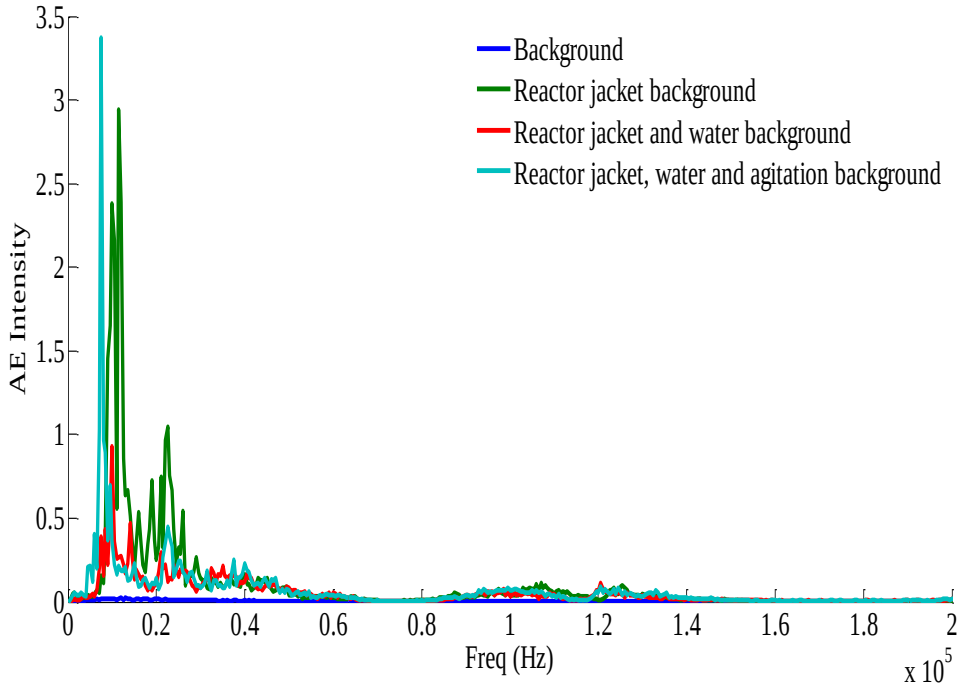

Figure 7-13: Acoustic emission spectra of background signals of the 500 ml batch stirred tank reactor including the signal obtained from the heater chiller (green), heater chiller and filled vessel (red) and heater chiller, filled vessel and 300 rpm agitation (turquoise)

Figure 7-13 shows that the majority of the background acoustic signal occurs at a frequency below 30 kHz and is caused by the heater-chiller and the movement of the fluid (in this case water) within the vessel due to the stirring of the impeller. There were some frequency ranges above this which showed acoustic signals (e.g. 80-140 kHz) which were extremely low in intensity therefore, the frequency region above 150 kHz was selected to study the effect of the particles on the acoustic emission spectrum

obtained. The change in the integrated region of the spectrum at 150-450 kHz with increasing solid concentration of D-mannitol suspended in diethyl ether is shown in Figure 7-14.

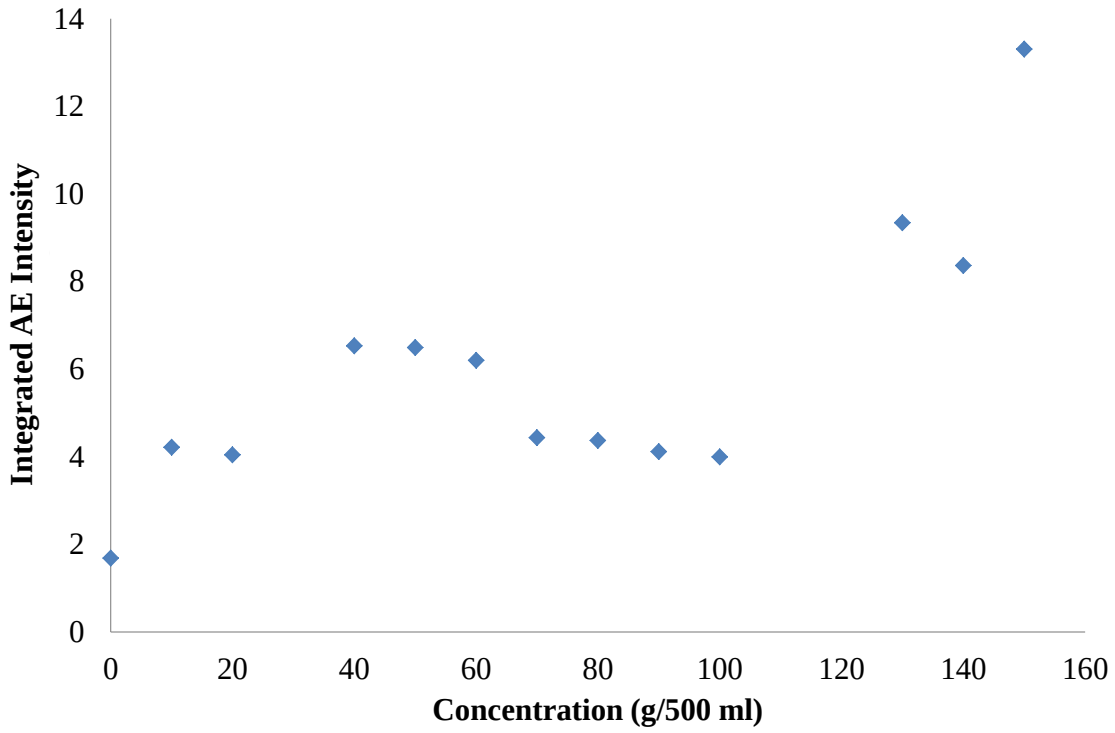

Figure 7-14: Graph showing the integrated area (150-450 kHz) of the acoustic emission spectra obtained as the solid concentration of D-mannitol was increased in a 500 ml batch STR

As can be seen in Figure 7-14, a linear increase of the acoustic signal intensity with an increase in the solid concentration was not observed. There was a slight increase in the intensity between 10 and 60 g however; the largest increase was seen at higher concentrations of particles above 120 g. Due to the concentration of particles produced in the crystallisations of D-mannitol in a 500 ml vessel previously, being in the region of 40-70 g it was not known whether a sufficient acoustic signal would be obtained. Figure 7-15 shows the acoustic spectra obtained during crystallisation monitoring in a 500 ml vessel using a solution concentration of 250 g/kg and mixing intensity of 300 rpm and the corresponding crystallisation profile obtained from integrating the area from 150-450 kHz (Figure 7-16).

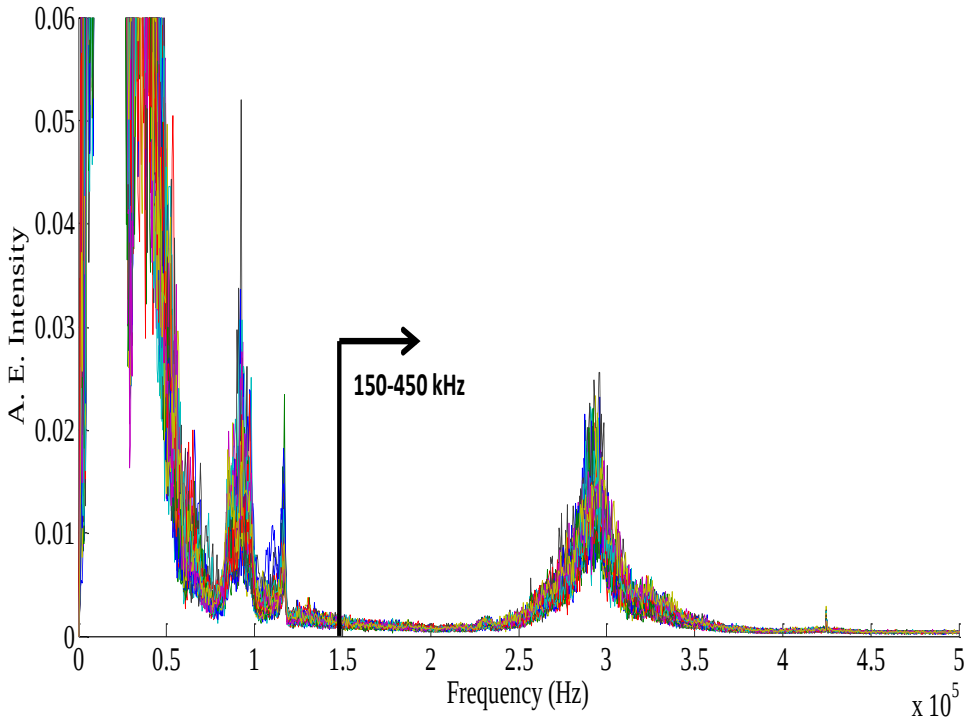

Figure 7-15: Acoustic emission spectra obtained during the crystallisation of D-mannitol using a solution concentration of 250 g/kg in a 500 ml vessel with a mixing intensity of 300 rpm

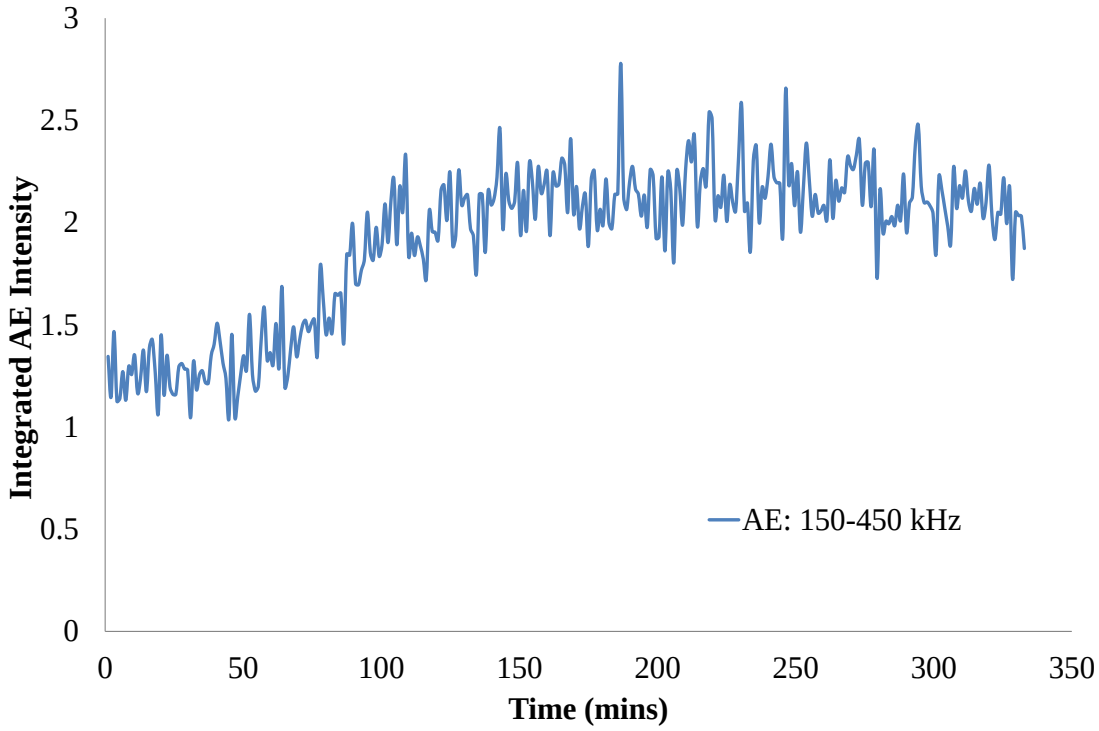

Figure 7-16: Crystallisation profile obtained from the integration of acoustic emission spectra using a solution concentration of 250 g/kg of D-mannitol in a 500 ml vessel with 300 rpm agitation

Figure 7-16 shows that the crystallisation profile obtained from the acoustic emission measurements fluctuates more than the Raman profiles obtained previously. This is most likely due to the nature of the measurements as for each 2 second measurement there will be a different number of particle collisions taking place during that short time period and the number of particles which make contact with the vessel wall will not be consistent. Additionally, the transducer is not just collecting data from the section of the vessel wall which it is in contact with but from particle collisions around the whole vessel owing to propagation of the ultrasonic waves through the glass. As the signals obtained will be stronger from the collisions taking place closer to the transducer, this will also cause the trend to fluctuate more. The signal intensity in Figure 7-16 remains stable from the start of the measurements until approximately 50 minutes suggesting there are few particles in the vessel. The intensity then increases steadily over a further period of 50 minutes suggesting nucleation has taken place followed by crystal growth

showing there are an increasing number of particle collisions. The signal then levels off at around 100 minutes for the remainder of the crystallisation suggesting the number of particles, and so particle collisions, in the vessel is relatively consistent. Figure 7-17 shows an overlay of the Raman and acoustic emission crystallisation profiles obtained during the same crystallisation experiment.

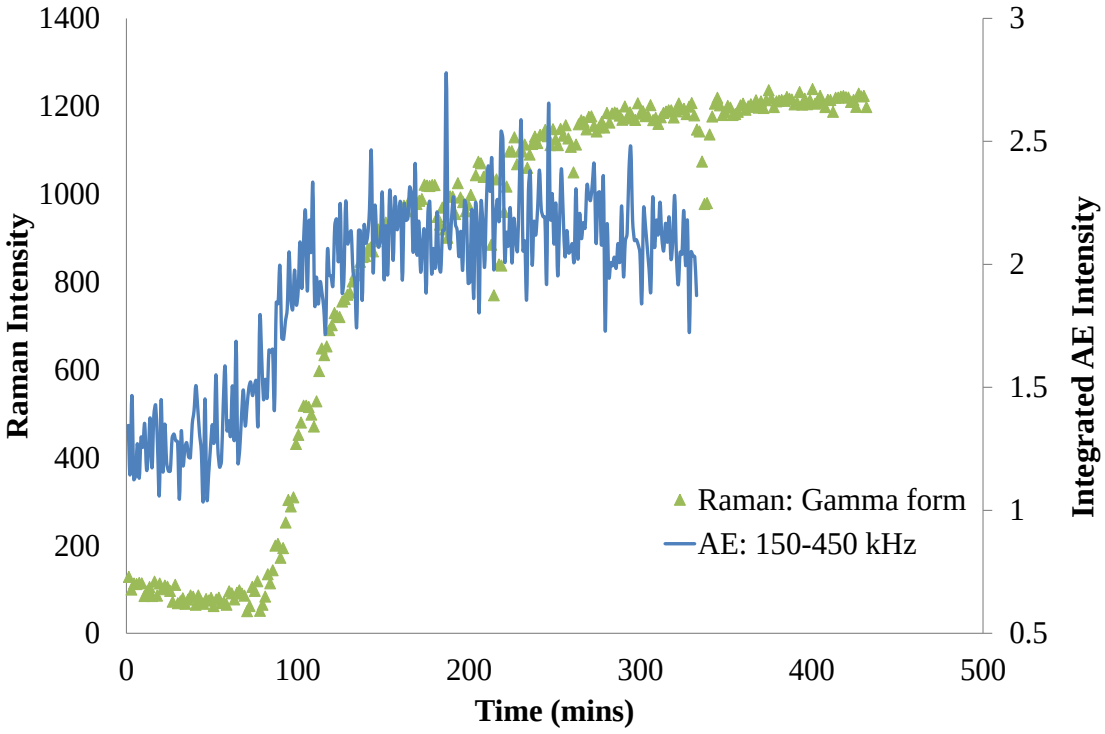

Figure 7-17: Crystallisation profiles obtained from Raman (intensity at 1042 cm^{-1}) and acoustic emission measurements using a solution concentration of 250 g/kg of D-mannitol in a 500 ml vessel with 300 rpm agitation

Figure 7-17 shows that the profiles obtained from the Raman and acoustic emission measurements show similar trends. The intensity of the acoustic signal starts to increase earlier than the Raman profile, suggesting that this measurement technique may be more sensitive to the nucleation event during crystallisation. The acoustic signal also levels off earlier than the Raman profile which could be due to particle size effects. As the frequency range being studied is at the higher frequency end, and this is thought to be dominated by smaller particles, it is possible that the number of particles in this smaller

size range became consistent at an earlier stage than the overall number of particles, as observed in the Raman measurements which were still increasing gradually until a later stage in the crystallisation. Figure 7-18 shows an overlay of the Raman and acoustic emission profiles obtained during a 250 g/kg crystallisation with a mixing intensity of 400 rpm.

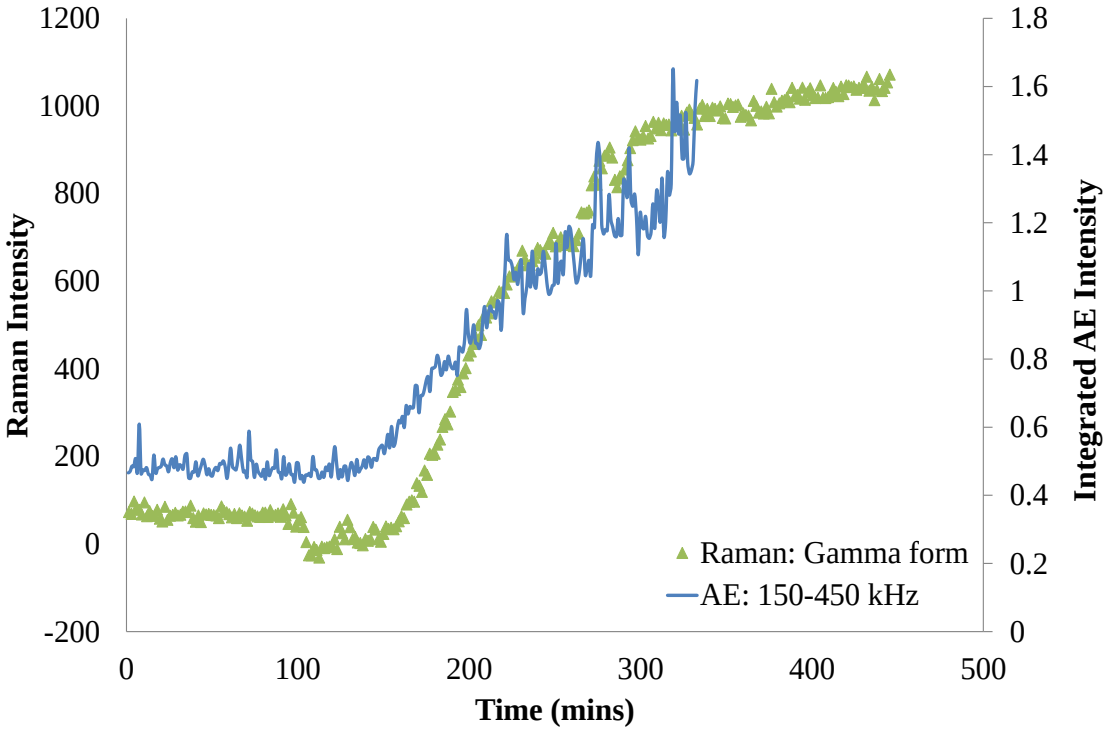

Figure 7-18: Crystallisation profiles obtained from Raman (intensity at 1042 cm^{-1}) and acoustic emission measurements using a solution concentration of 250 g/kg of D-mannitol in a 500 ml vessel with 400 rpm agitation

The crystallisation profiles in Figure 7-18 show that the intensity of the acoustics trend increases approximately 10 minutes earlier than the Raman signal. This suggests that the acoustic emission signal is sensitive to either a smaller numbers of particles or particles of a smaller size and could be used to detect nucleation earlier than Raman as shown in Figure 7-17. However, although the acoustics signal increases earlier during nucleation, the profiles then overlap during the crystal growth stage showing that the trends in this crystallisation are more agreeable.

Although useful crystallisation profiles were obtained in the batch STR with D-mannitol, it was found that useful acoustic emission results were only obtained with the lower solution concentration. It is possible that due to the inefficient mixing connected with batch STRs that at higher solution concentrations the agitation isn't sufficient enough to create adequate particle collisions with the vessel wall and other particles meaning an acoustics signal is not obtained. The increased number of particles (at higher solution concentrations) could therefore help to 'muffle' the collisions taking place. Therefore, acoustic emission monitoring was coupled with batch OBR reactors (section 7.3.3.) which claim to create more efficient mixing and it would be expected that an improved acoustic spectrum would be obtained so long as the method of mixing generates increased intensity and occurrence of collisions between the particles and the vessel wall compared to that in an STR.

7.3.2 Batch OBR: Non-invasive Raman monitoring

Since the scale at which the crystallisation experiments of D-mannitol were carried out in a batch STR had an impact on the outcome of the polymorphs obtained throughout the course of the crystallisation, this was included in the design of experiments conducted, along with the variables that had previously been studied in chapter 4 using L-glutamic acid. As the experiments were all completed using a fixed temperature of 10^{o}C, the effect of final temperature was redundant and therefore, removed from the previous design. Therefore, a 2 level, 4^{-1} factorial design was carried out initially to determine the factors, if any, which affected the crystallisation of D-mannitol in the batch OBR. There were four subsequent experiments carried out to form a full design for the 1 L scale. The conditions for the eight preliminary experiments and the four additional experiments are shown in Table 7-2. The polymorphs formed during nucleation and the mean particle size and span of the end product as determined by off-line FBRM measurements are shown in Table 7-3.

Table 7-2: Different operating conditions used in the twelve DoE experiments of D-mannitol in the batch OBR

Experiment	Concentration (g/kg) (A)	Frequency (Hz) (B)	Amplitude (mm) (C)	Volume (ml)
1	300	3	10	1000
2	350	1	10	1000
3	350	3	30	1000
4	300	1	30	1000
5	300	3	30	250
6	350	3	10	250
7	350	1	30	250
8	300	1	10	250
9	300	3	30	1000
10	350	3	10	1000
11	350	1	30	1000
12	300	1	10	1000

Table 7-3: Outcome of the 12 DoE experiments in the batch OBR showing the initial polymorphic composition obtained from Raman measurements, the final polymorph using XRD, the particle size measurements using FBRM and the solid recovery values

	Polymorph Obtained					
Experiment	**Raman**	**XRD**	**d (0,5) (µm)**	**span**	**Solid Recovery (g)**	**Yield (%)**
1	α/γ	γ	11.4	2.8	59.7	19.9
2	α/γ	γ	12.5	2.5	110.1	31.5
3	α/γ	γ	13.0	2.6	143.0	40.9
4	α/γ	γ	13.5	3.9	97.4	32.5
5	α	γ	24.2	4.5	29.5	39.3
6	α/γ	α/ γ	11.6	2.4	18.5	21.1
7	α/γ	γ	12.3	3.5	33.5	38.3
8	α/γ	γ	13.2	3.5	15.7	20.9
9	α/γ	γ	10.4	2.5	128.1	42.7
10	α	γ	17.8	4.1	74.1	21.2
11	α	α/γ	13.1	4.1	134.2	38.3
12	-	-	-	-	-	-

=major form

Table 7-3 shows that one of the crystallisations, experiment 12, produced no crystals at all. This was thought to be mainly due to the low oscillation frequency and amplitude used as all other experiments using a solution concentration of 300 g/kg resulted in particles being formed. Additionally, there is a difference in the polymorphic composition shown in Table 7-3 obtained by Raman and X-ray diffraction. This was due to the metastable alpha form being difficult to isolate and thus transforming to the stable form whilst drying in the oven. Table 7-4 shows the main effects and interactions for the results of the experiments from the full factorial design carried out (experiments 1-4 and 8-12) in Table 7-2.

Table 7-4: Main effects and strongest interactions of the factors used in the DoE experiments in the batch OBR

	Main Effects			Interaction Effects		
	A	**B**	**C**	**AB**	**AC**	**BC**
d (0,5)	**5.25**	3.38	2.11	-0.75	-4.17	**-4.98**
span	**1.03**	0.40	0.90	-0.35	-0.87	**-1.79**

Table 7-4 shows that of all the main effects (concentration (A), frequency (B) and amplitude (C)) investigated in the full factorial design, concentration appeared to have the biggest effect and was a dominant factor on the value of the d (0,5) and the span. As this is a positive value in all cases, the response increases when going from a low to a high concentration. This was the same result as was observed for a similar batch DoE study carried out using L-glutamic acid (section 4.3.1). The interaction between frequency and amplitude was larger than the effect of either factor alone for the d (0,5) and the span values. However, for both the d (0,5) and span response, the interaction values are negative. An increase in the amplitude with a fixed low frequency resulted in an increase in the response for both the average particle size and the span values which can be observed in experiments 2 and 11 where the average particle size increased from 12.45 at 1 Hz 10 mm to 13.09 µm at 1 Hz 30 mm and the span from 2.54 to 4.07. Conversely, an increase in the amplitude at a high fixed frequency resulted in a decrease in both responses, which can be seen in experiments 3 and 10 in Table 7-3. The average particle size decreased from 17.78 at 3 Hz 10 mm to 13.03 µm at 3 Hz 30 mm and the span decreased from 4.10 to 2.62. The DoE study of L-glutamic acid also found the main interaction to be between the frequency and amplitude, however, this value was negative for the d(0,5) value and positive for the span. The result of this design of experiments using D-mannitol and the previous DoE with L-glutamic acid in a batch OBR both showed very similar outcomes in that the concentration is the main effect on the particle size which would be expected as a higher solution concentration allows for larger overall growth of the crystals. Additionally, the fact that the frequency and

amplitude had the main combined effect on the particle size suggested that the experimental conditions could be altered in order to obtain particles of a certain size and distribution.

7.3.2.1 Effect of oscillation frequency and amplitude

As it was found the agitation intensity within a batch STR had a significant effect on the outcome of the crystallisation of D-mannitol (section 7.3.1.), it was expected that the equivalent OBR mixing parameters, oscillation frequency and amplitude, would also impact the particle properties. Figure 7-19 shows an overlay of the Raman profiles obtained during the OBR crystallisations in experiments 4 and 9 when the oscillation frequency was increased at the lower solution concentration of 300 g/kg.

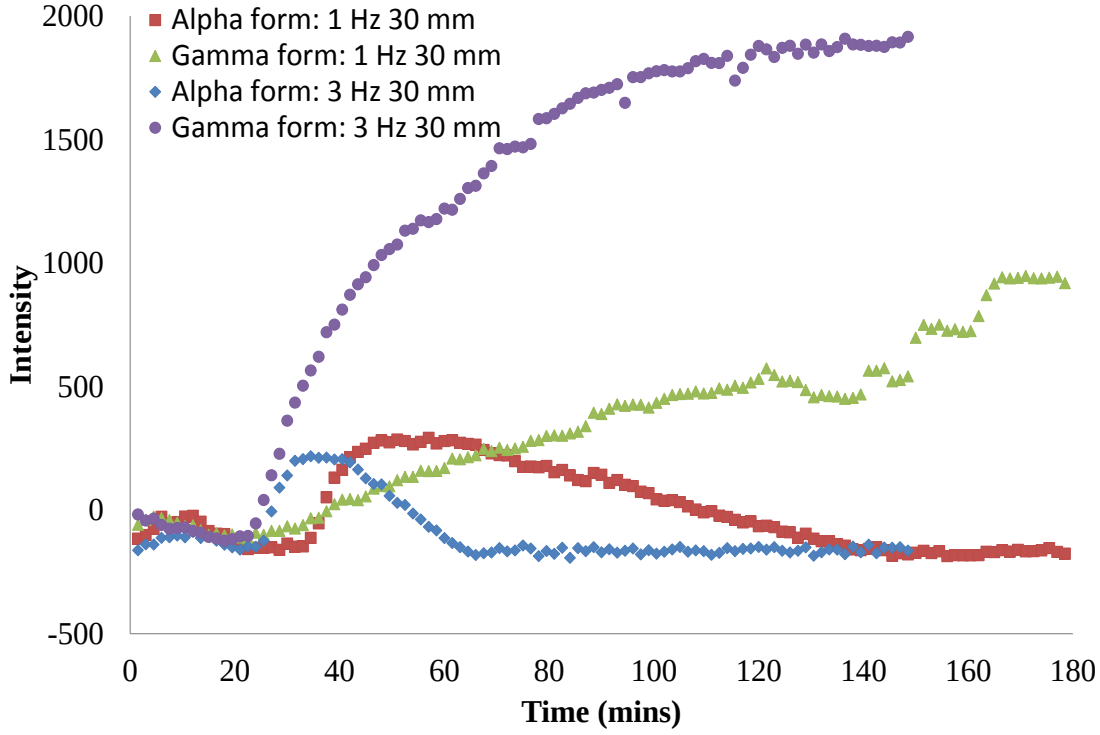

Figure 7-19: Crystallisation profiles of alpha and gamma D-mannitol from experiments 4 and 9 in table 7-2 when the oscillation frequency was increased with a fixed amplitude of 30 mm and solution concentration of 300 g/kg in a 1 L vessel, based on 1st derivative Raman intensity at 1058 and 1042 cm^{-1}, respectively

Figure 7-19 shows that when a low frequency of 1 Hz and amplitude of 30 mm is applied to a 300 g/kg crystallisation in a 1 L vessel, a mixture of the alpha and gamma polymorphs nucleates at approximately 35 minutes. The signal for the alpha form reaches a maximum intensity relatively quickly following nucleation (at around 45 minutes) and then starts to decrease gradually until it appears no more of this form is detected from around 130 minutes onwards. The signal for the gamma form increases at a steady rate immediately following nucleation and reaches a consistent value once complete transformation has taken place from 160 minutes onwards. When the frequency was increased to 3 Hz, keeping all other experimental conditions constant, a mixture of the alpha and gamma forms nucleated once more. However, increasing the oscillation frequency caused nucleation to occur at an earlier point in the crystallisation with the first signs of nucleation detected by Raman just after 20 minutes (15 minutes earlier than using the lower frequency). Additionally, the alpha polymorph remained in the vessel for a much shorter period of time (blue profile) with the intensity reaching a minimum value at 65 minutes. This indicated a much quicker transformation to the stable form resulted from a higher frequency of oscillation, however, the intensity of the gamma form did not level off quicker and was still increasing slowly towards the end of the measurements. The significantly higher signal intensity obtained following transformation at the higher oscillation frequency suggested that a higher concentration of particles had been produced also. This was confirmed with the solid recovery measurements in Table 7-3 which showed a higher concentration of particles was obtained at a higher frequency with a value of 128.1 g being obtained compared to 97.4 g at a lower frequency. It is also likely that the most intense oscillation conditions of 3 Hz and 30 mm resulted in increased levels of particles being suspended efficiently as it was observed that due to the high concentrations used for these experiments that a certain amount of material descended to the base of the vessel. Figure 7-20 shows the crystallisation profiles obtained when the oscillation frequency was increased in a 1 L vessel at the higher solution concentration of 350 g/kg.

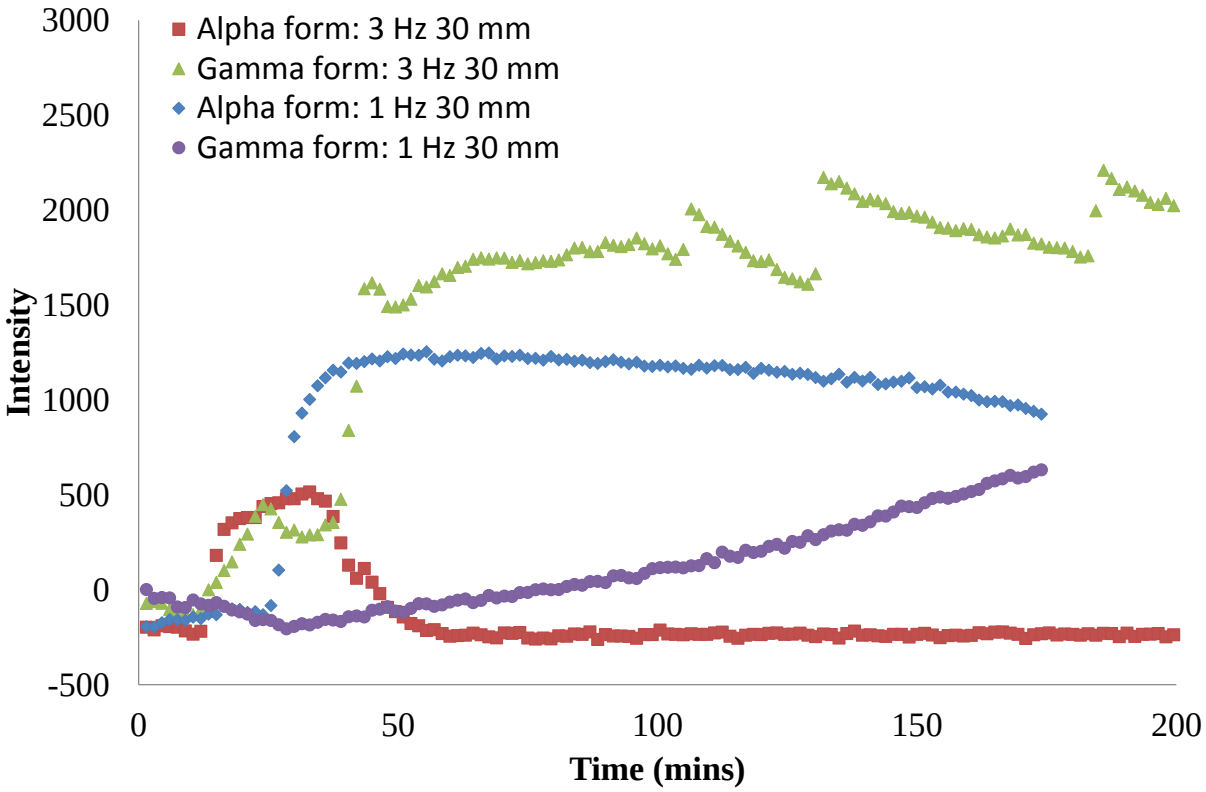

Figure 7-20: Crystallisation profiles of alpha and gamma Mannitol from experiments 3 and 11 in table 7-2 when the oscillation frequency was increased with a fixed amplitude of 30 mm and a solution concentration of 350 g/kg in a 1 L vessel, based on 1st derivative Raman intensity at 1058 and 1042 cm^{-1}, respectively

Figure 7-20 shows that as with increasing the oscillation frequency at a lower solution concentration (Figure 7-19), the induction time for nucleation was shorter at a higher frequency of 3 Hz by approximately 15 minutes. Similarly, the alpha polymorph remained in the vessel longer at a lower oscillation frequency; however, in this case the alpha polymorph nucleated as the major form rather than a mixture of forms being obtained, as with a solution concentration of 300 g/kg. Transformation to the stable form began relatively quickly, after approximately 25 minutes following nucleation (50 minutes onwards), however, the transformation was reasonably slow and transformation was not close to completion by the end of the measurements (after 3 hours). The higher oscillation frequency resulted in an apparent 50:50 mixture of the alpha and gamma

polymorphs following nucleation as the signal intensities were very similar. However, transformation of the metastable form to the gamma form began 25 minutes following nucleation (at 40 minutes) and at this higher frequency the transformation was rapid, and there was no alpha form detected by Raman after 50 minutes. At this time, the signal for the gamma form became relatively consistent suggesting the majority of crystal growth was complete, which occurred significantly quicker than at a lower frequency of 1 Hz. The effect of increasing oscillation amplitude on the outcome of crystallisations using a solution concentration of 350 g/kg in a 1 L vessel is shown in Figure 7-21.

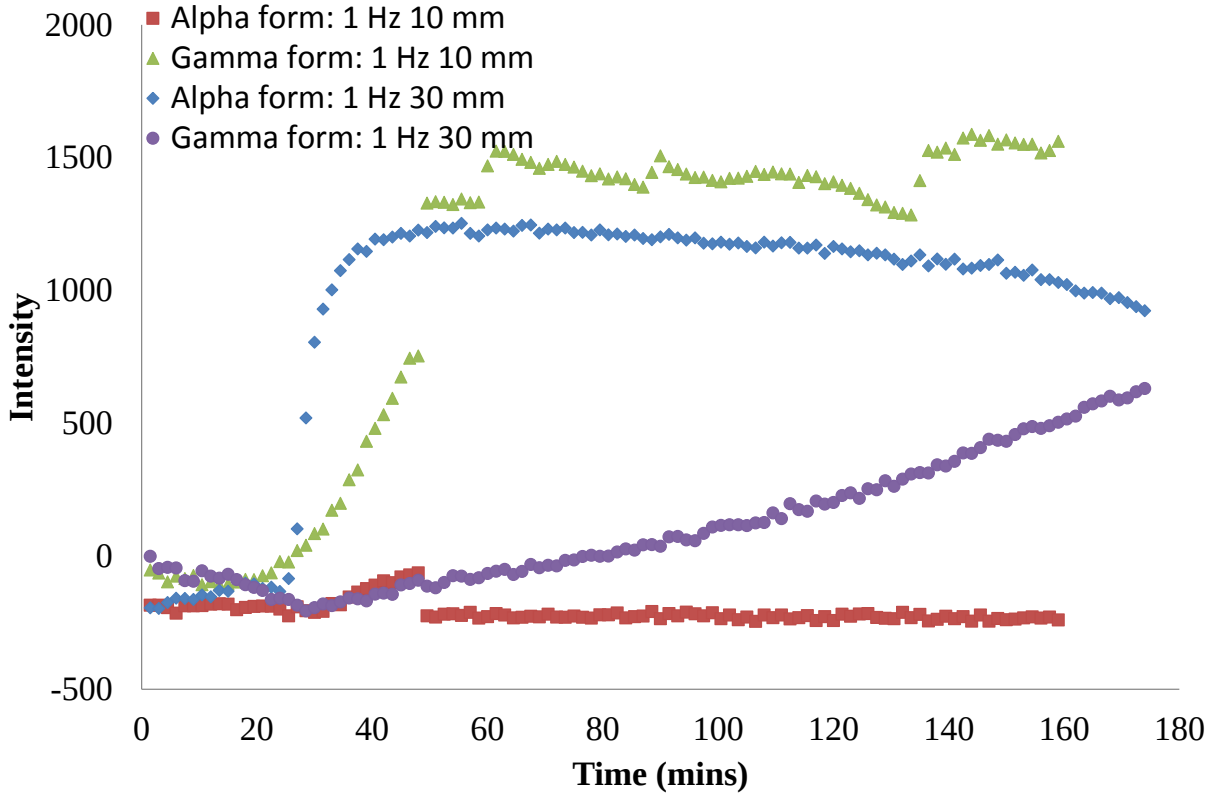

Figure 7-21: Crystallisation profiles of alpha and gamma Mannitol from experiments 2 and 10 in table 7-2 when the oscillation amplitude was increased with a fixed frequency of 1 Hz and a solution concentration of 350 g/kg in a 1 L vessel, based on 1st derivative Raman intensity at 1058 and 1042 cm^{-1}, respectively

When the oscillation amplitude was altered the nucleation time was not affected significantly with this event occurring at around 25 minutes in both cases. However, the

polymorphic composition of the nuclei was considerably different by just increasing the amplitude from 10 to 30 mm with all other operating conditions constant. The growth rate at the higher oscillation amplitude also appeared to be more rapid. At a low amplitude of 10 mm, the gamma form was the major form to nucleate along with a small level of the alpha form, however this only remained in the vessel for less than 20 minutes. In contrast, increasing the amplitude to 30 mm resulted in the alpha form nucleating as the sole polymorph as detected by Raman spectrometry. The growth rate of the alpha form also appeared to be more rapid than the gamma form in experiment 2 as the signal intensity increased faster and reached a maximum value in an extremely short time period following nucleation. The transformation of the alpha form to the thermodynamically stable gamma form was a gradual process using the oscillation conditions of 1 Hz and 30 mm and was not complete within 3 hours. As with the batch STR experiments (section 7.3.1.), an increase in the intensity of mixing, whether it be revolutions of an impeller or the amplitude of oscillation, resulted in increased levels of the alpha polymorph nucleating at the outset of the crystallisation. This suggests this polymorph requires relatively forceful conditions to nucleate (as well as a high solution concentration), as a mixing intensity of 400 rpm in a relatively small 500 ml vessel creates intense mixing. It is known that an increase in the mixing intensity results in a decrease in the metastable zone width for a given polymorph which means with an increase in the mixing intensity the metastable zone width for the stable form could decrease meaning the supersaturation ends up in the metastable zone for the alpha form instead. It has also been reported previously that the oscillation frequency and amplitude can affect the polymorphic composition of the particles obtained during a crystallisation in an OBR.[31]

7.3.2.2 Effect of solution concentration

The solution concentration was found to influence which polymorph(s) nucleated in the batch STR therefore, this was also investigated in the batch OBR experiments. Figure

7-22 shows the effect of increasing solution concentration on the crystallisation of D-mannitol with a fixed frequency and amplitude (1 Hz 30 mm) in a 1 L vessel.

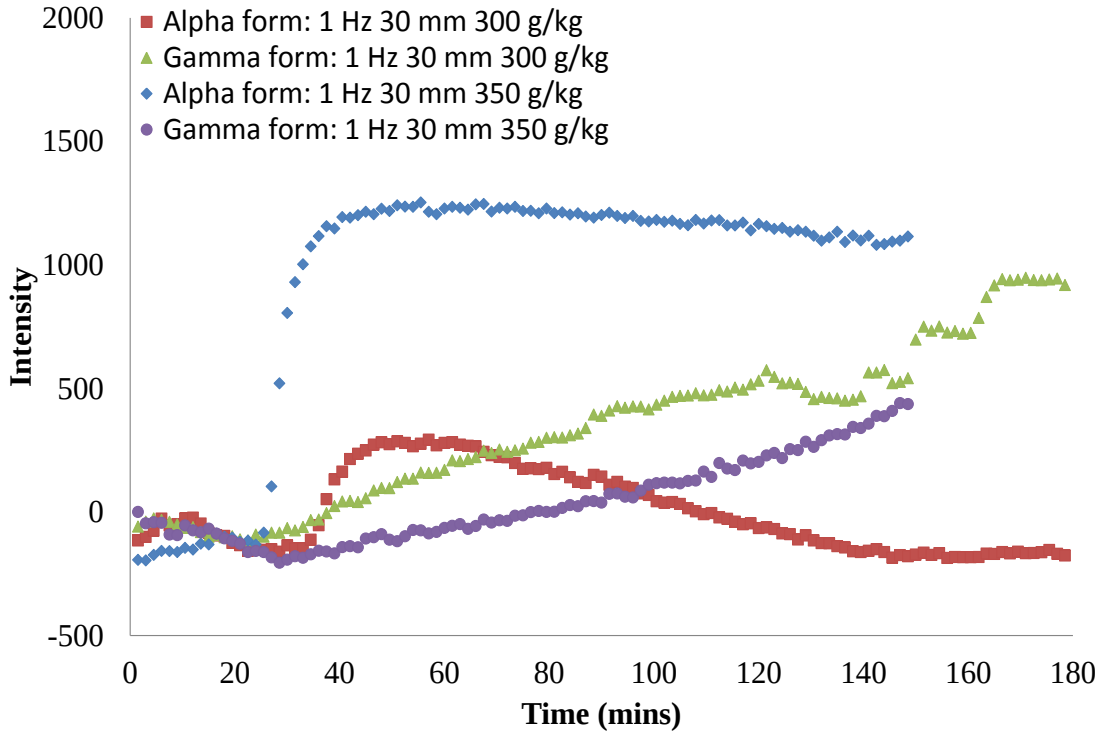

Figure 7-22: Crystallisation profiles of alpha and gamma Mannitol from experiments 4 and 11 in table 7-2 when the solution concentration was increased with a fixed frequency of 1 Hz and amplitude of 30 mm in a 1 L vessel, based on 1st derivative Raman intensity at 1058 and 1042 cm^{-1}, respectively

As with the batch STR experiments carried out, an increase in the solution concentration resulted in a shorter induction time for nucleation as shown in Figure 7-22. The high solution concentration experiment (350 g/kg) nucleated approximately 10 minutes earlier than the 300 g/kg crystallisation using the same oscillation conditions. Additionally, there were increased levels of the alpha polymorph following nucleation when a higher solution concentration was used and this remains in the vessel longer due to it nucleating as the major form (with no gamma form being detected by Raman immediately following nucleation), therefore, the transformation process was much slower and takes place over a number of hours. The lower solution concentration

crystallisation results in a mixture of forms nucleating, meaning the transformation process was accelerated and this was completed by ~140 minutes. This was the opposite trend to that observed in the batch STR experiments where a higher solution concentration resulted in a mixture of forms nucleating and a more rapid transformation to the stable form. This suggests that in the batch OBR, the mixing employed is also an important factor as well as the solution concentration on the preliminary stages of the crystallisation process (*i.e.* nucleation and any subsequent transformation). Figure 7-23 shows the effect of increasing solution concentration at the most intense oscillation conditions of 3 Hz and 30 mm.

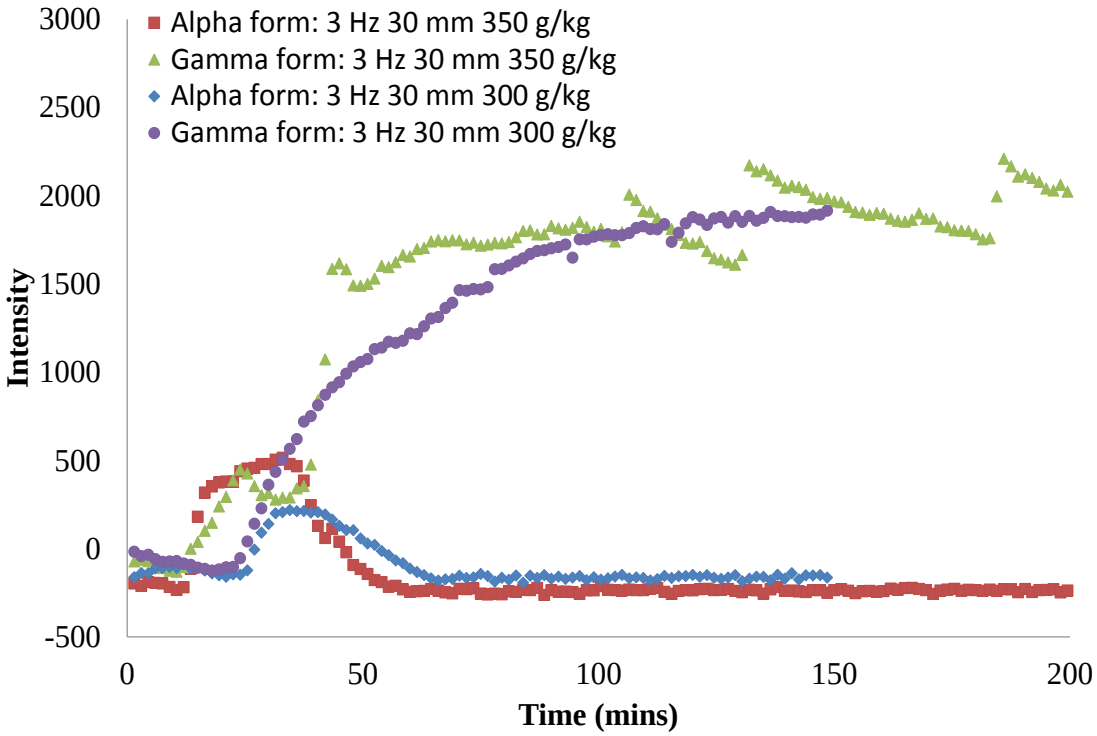

Figure 7-23: Crystallisation profiles of alpha and gamma Mannitol from experiments 3 and 9 in table 7-2 when the solution concentration was increased with a fixed frequency of 3 Hz and amplitude of 30 mm in a 1 L vessel, based on 1st derivative Raman intensity at 1058 and 1042 cm^{-1}, respectively

The effect of solution concentration on the nucleation outcome for the OBR is much less obvious in Figure 7-23. As with previous experiments, nucleation occurs at an earlier

time point using a higher initial solution concentration, however, when oscillation conditions of 3 Hz and 30 mm were used, a similar mixture of the alpha and gamma forms nucleates. The transformation process also takes place on a similar timescale of approximately 30-35 minutes at both solution concentrations. Additionally, the signal intensity of the gamma form following transformation remained at a similar level when the crystallisation had appeared to have reached steady state, with the profile for the higher solution concentration appearing to be slightly higher in intensity towards the end. This suggested that a similar solid concentration was produced at both initial solution concentrations, which was confirmed in table 3 with experiment 3 resulting in a slightly increased solid recovery value. This suggested that in this case the oscillation applied to the process had a much greater influence on the outcome of the crystallisation than the solution concentration, which had been shown to have the biggest impact on nucleation in the batch STR when the mixing intensity was kept constant.

7.3.2.3 Effect of scale of operation

As the crystallisation of D-mannitol was affected by the scale at which the crystallisation was carried out (even with a relatively small increase from 155 to 500 ml), this effect was also investigated with batch OBR reactors at two different scales; 250 ml and 1 L. Figure 7-24 shows the effect of increasing reactor volume using oscillation conditions of 3 Hz 10 mm and an initial solution concentration of 350 g/kg.

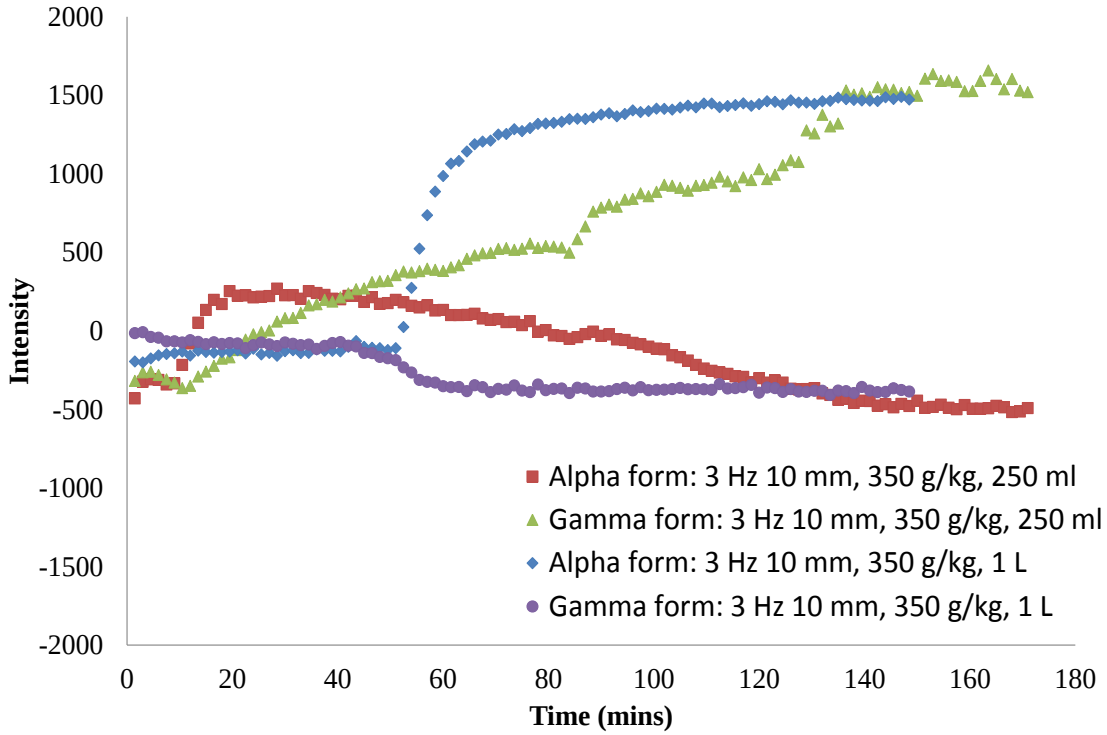

Figure 7-24: Crystallisation profiles of alpha and gamma Mannitol from experiments 6 and 10 in table 7-2 when the reactor volume was increased with a fixed frequency of 3 Hz and amplitude of 10 mm using a 350 g/kg solution concentration, based on 1st derivative Raman intensity at 1058 and 1042 cm^{-1}, respectively

Figure 7-24 shows nucleation occurred rapidly after the measurements were started when the crystallisation was carried out at the smaller volume of 250 ml and a mixture of the alpha and gamma forms was detected by Raman spectrometry from 15 minutes onwards. Nucleation occurred under the same conditions, 40 minutes later in the larger scale vessel. This suggested that the conditions may become increasingly uniform at a smaller scale within a shorter time period resulting in nucleation occurring earlier. However, during the larger scale experiment, the alpha polymorph was the only form detected during nucleation and remained in the vessel without transforming until the crystallisation was stopped. This was unexpected as it was thought that if nucleation occurred earlier at a smaller scale this meant there was improved mixing at this scale and therefore, from earlier results carried out in a batch STR, it would be anticipated that the

alpha polymorph would be more prevalent under conditions of improved mixing leading to increased levels of the alpha form at the smaller scale. However, this outcome was also found to be the case for a similar set of experiments using the same solution concentration of 350 g/kg but with oscillation conditions of 1 Hz and 30 mm (figure not shown). Figure 7-25 shows the effect of reactor scale on experiments carried out at a lower solution concentration of 300 g/kg and an oscillation frequency of 3 Hz and 30 mm amplitude.

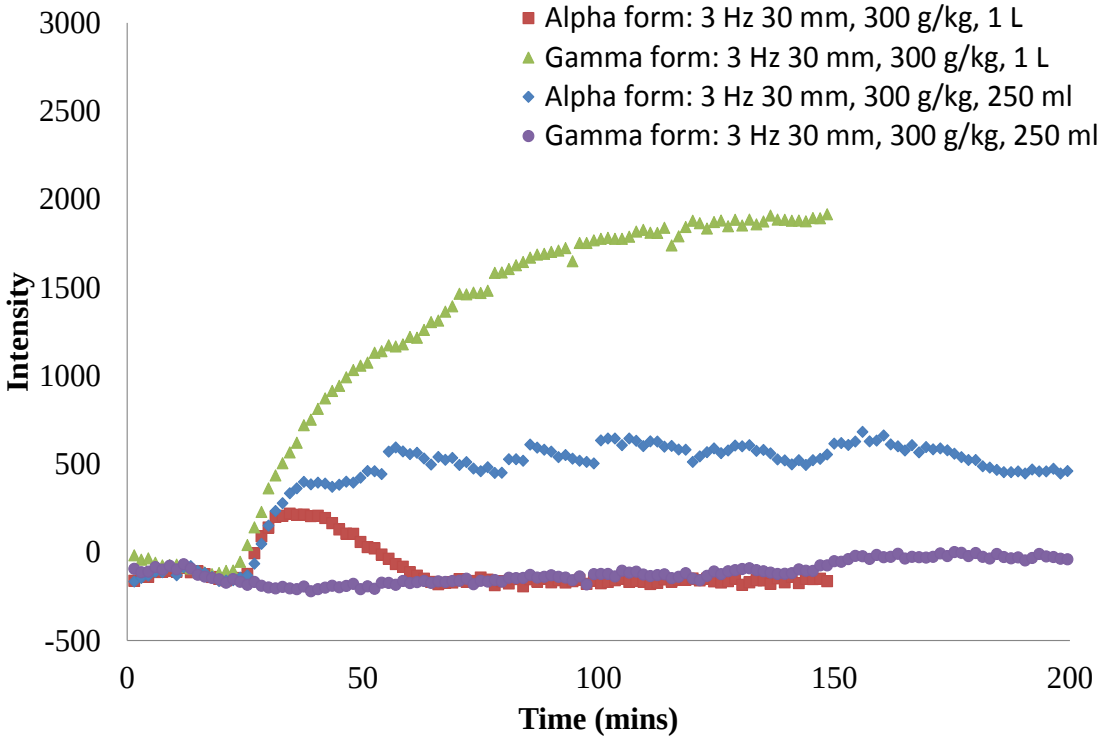

Figure 7-25: Crystallisation profiles of alpha and gamma Mannitol from experiments 5 and 9 in table 7-2 when the reactor volume was increased with a fixed frequency of 3 Hz and amplitude of 30 mm using a 300 g/kg solution concentration, based on 1st derivative Raman intensity at 1058 and 1042 cm^{-1}, respectively

Figure 7-25 shows that the scale at which the crystallisation was conducted did not affect the point of nucleation greatly when the most intense oscillation conditions were employed. However, although nucleation occurred at the same point in the crystallisation using both 250 ml and 1 L vessels, the polymorphs which nucleated

differed. The alpha polymorph was formed during the small scale experiment and remained in the vessel until the crystallisation was stopped after around 3 and a half hours. The signal appeared to be beginning to decrease towards the end of the measurements suggesting the transformation process may have been commencing. Conversely, the larger scale crystallisation resulted in a mixture of the alpha and gamma forms nucleating with complete transformation taking place within a comparatively shorter timescale (approximately 50 minutes). This outcome was more expected from the results obtained in the batch OBR where an increase in the scale using the same mixing conditions led to increasing amounts of the gamma form produced during nucleation. A second set of experiments carried out at different scales using the same solution concentration of 300 g/kg, but with the least intense oscillation conditions of 1 Hz and 10 mm, agreed with the results in Figure 7-25 in that improved mixing was observed at the smaller scale of 250 ml. In those experiments, the gamma polymorph was the major form obtained during nucleation, however, when the same experiment was carried out in a 1 L batch OBR, nucleation did not occur at all throughout 3 hours of operation. This suggests that even in batch OBRs, which are reported to produce more efficient mixing, as the scale is increased there is a loss in the efficiency of mixing obtained in the vessel.

7.3.3 Acoustic emission monitoring in the batch OBR

Many of the experiments conducted in Table 7-2 were monitored using non-invasive acoustic emission as well as Raman spectrometry. In some cases a FBRM probe was also integrated to provide particle size information during the crystallisation. As with the batch STR experiments in section 7.3.1.2.; preliminary measurements were carried out to determine if an acoustic signal could be obtained from particles in a batch OBR and also the effect of background noise on the spectra obtained. Figure 7-26 shows the background measurements obtained at the same three oscillation conditions with the heater chiller unit on and the vessel containing distilled water.

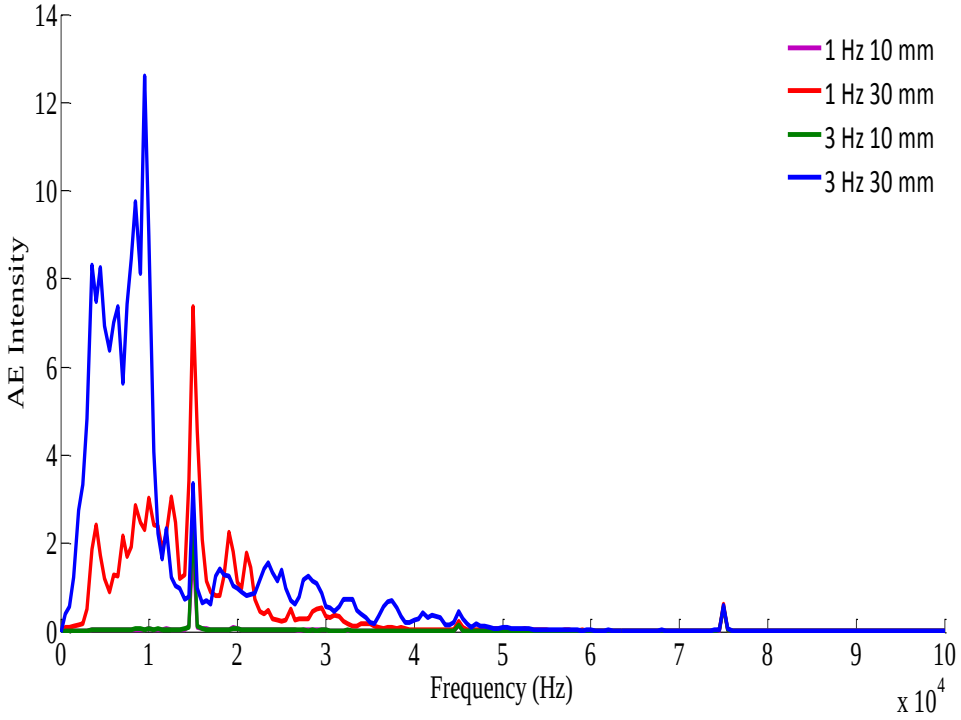

Figure 7-26: Acoustic emission spectra of background signals of 1 L batch OBR including the signal obtained from the heater chiller and filled vessel (with water) with applied oscillation of 1 Hz 10 mm, 1 Hz 30 mm, 3 Hz 10 mm and 3 Hz 30 mm

As can be seen in Figure 7-26, the majority of the acoustic signal from the background noise attributable to the heater chiller and movement of the baffles occurs below 50 kHz. However, there is also a spike that occurs at approximately 75 kHz; as this was not observed in the background spectra for the batch STR, it was likely that this spike was caused by the movement of the baffles. It was discussed in a previous chapter (4.3) that it was thought that the baffles actually made contact with the vessel wall and caused scraping to occur. It is possible that this caused the spike observed which was apparent at all oscillation conditions employed in Figure 7-26. As expected, the acoustic intensity was highest for the most intense frequency and amplitude (3 Hz, 30 mm), however the amplitude appears to have the greater effect on the intensity rather than the frequency as signal intensity was significantly higher for the background measurements for oscillation

at 1 Hz 30 mm than 3 Hz 10 mm. In fact, the spectra obtained for the lowest frequency oscillation conditions (1 Hz 10 mm and 1 Hz 30 mm) are very similar and of low intensity. It was found that when crystallisations were carried out using the lowest oscillation intensity of 1 Hz 10 mm, no significant acoustic emission signal was obtained showing that it is not enough to just have particles in the vessel and that a certain amount of force (mixing intensity) is required to provide higher energy collisions in order to obtain an acoustic crystallisation profile. Figure 7-27 and Figure 7-28 show the effect of increasing solid concentration of D-mannitol in a 1 L batch OBR using oscillation conditions of 1 Hz 30 mm, 3 Hz 10 mm and 3 Hz 30 mm, respectively. The weakest oscillation conditions of 1 Hz 10 mm were not investigated for acoustic monitoring due to it being observed during the crystallisation experiments that the material was not well suspended and many of the particles descended to the base of the vessel.

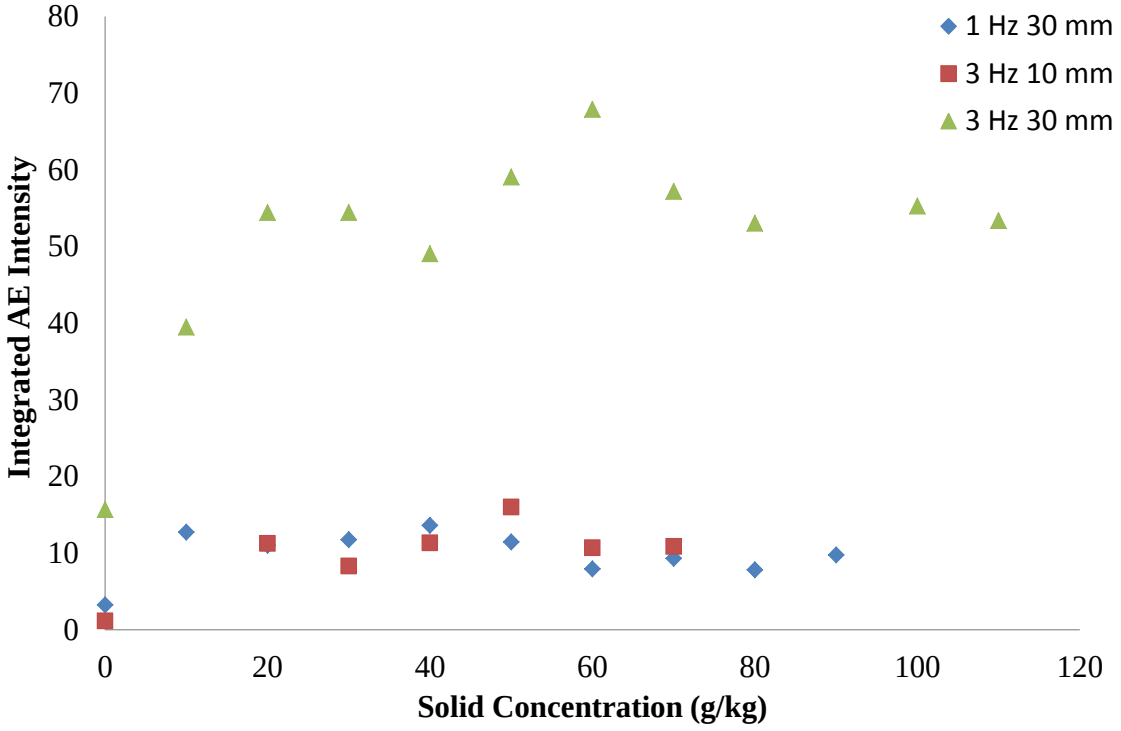

Figure 7-27: Graph showing the integrated area (150-450 kHz) of the acoustic emission spectra obtained as the solid concentration of D-mannitol was increased in diethyl ether in a 1 L batch OBR

Figure 7-27 shows that the acoustic emission intensity obtained using the most intense oscillation conditions of 3 Hz and 30 mm was significantly higher. This was expected as the mixing is relatively strong using this frequency and amplitude and therefore, the particles would most likely collide with other particles and the vessel wall more often and with greater impact causing the higher intensity signal observed. It was also noted that the intensity increased with increasing solid concentration until above 60 g/kg, where the signal decreased slightly and remained at a consistent value for the remainder of the concentration increments added to the vessel. It was observed during the experiment that above 60 g/kg the entire mass of the particles were no longer suspended efficiently and with each increment of particles added, increasing amounts of these sunk to the bottom of the reactor. This showed that there was only a certain concentration of particles which could be efficiently mixed in the vessel using the highest oscillation intensity and this value was found to decrease at lower oscillation conditions (Figure 7-28).

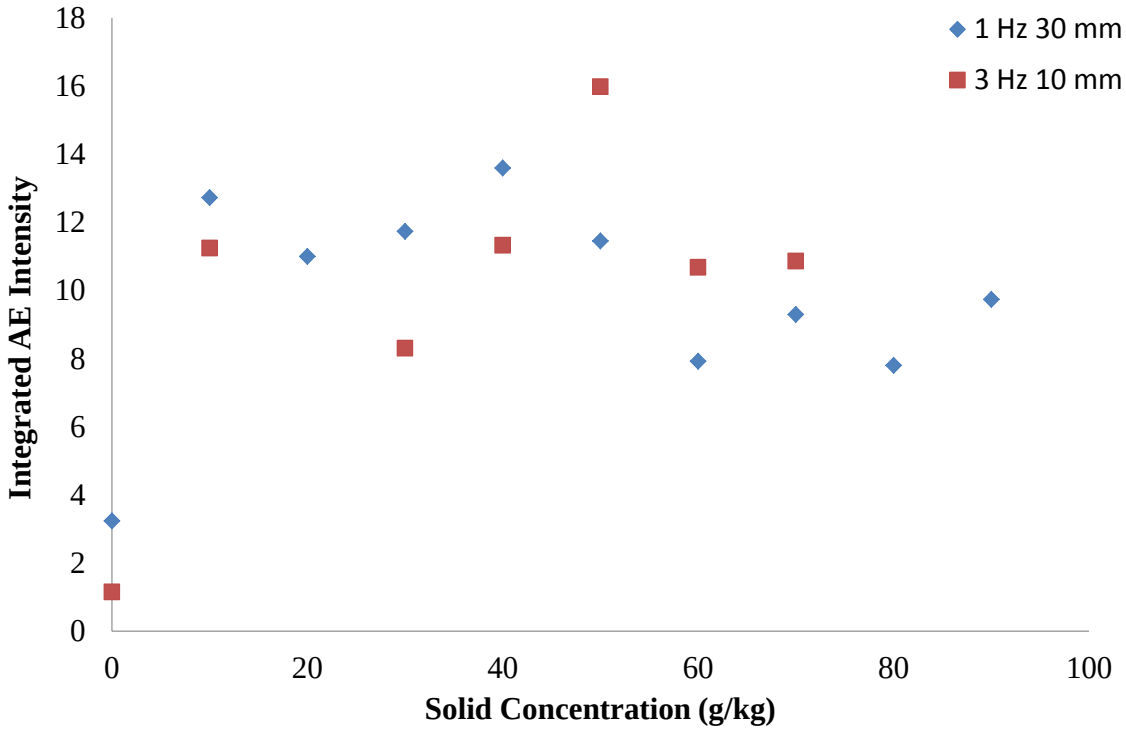

Figure 7-28: Graph showing the integrated area (150-450 kHz) of the acoustic emission spectra obtained as the solid concentration of D-mannitol was increased in diethyl ether in a 1 L batch OBR

Figure 7-28 shows that the acoustic intensity of the measurements was relatively similar using both 1 Hz 30 mm and 3 Hz 10 mm oscillations. In both of these experiments the same effect was observed as in Figure 7-27 where a maximum concentration was reached, above which mixing efficiency declined. For the lower intensity oscillation conditions studied in Figure 7-28 this value was found to be lower with concentrations above 40 g/kg (for 1 Hz 30 mm) and 50 g/kg (3 Hz 10 mm) not being suspended fully . Figure 7-29 shows an example of the acoustic spectra obtained during crystallisation monitoring of experiment 1 in Table 7-2.

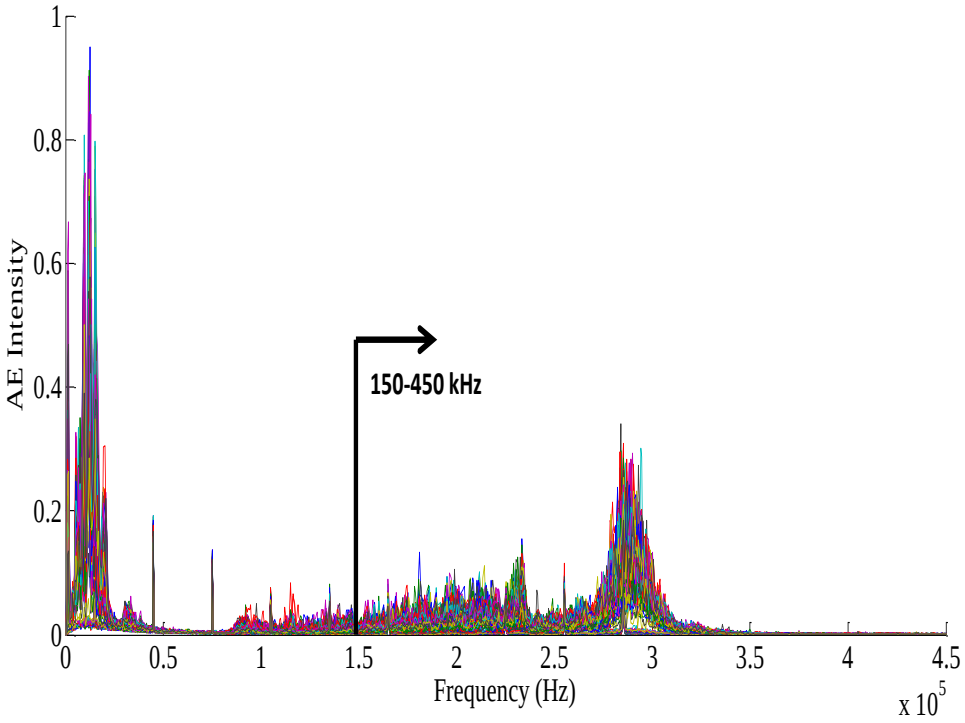

Figure 7-29: Acoustic emission spectra obtained during the crystallisation of D-mannitol in experiment 1 in table 7-2 using a solution concentration of 300 g/kg in a 1 L batch OBR vessel with a oscillation intensity of 3 Hz and 10 mm

Figure 7-29 shows the signals obtained from the particles collisions (above 50 kHz) are much more intense than those obtained in the batch STR (Figure 7-15) and cover a wider range of frequencies. As with the crystallisations monitored using AES in the batch STR experiments, the region 150-450 kHz was selected to study the evolution of particles

during the crystallisation process as this was known to be a region unaffected by background noise and contained the most intense signals likely to be associated with particle collisions. Figure 7-30 shows the crystallisation profile obtained from integrating the area 150-450 kHz from experiment 1 in Figure 7-29.

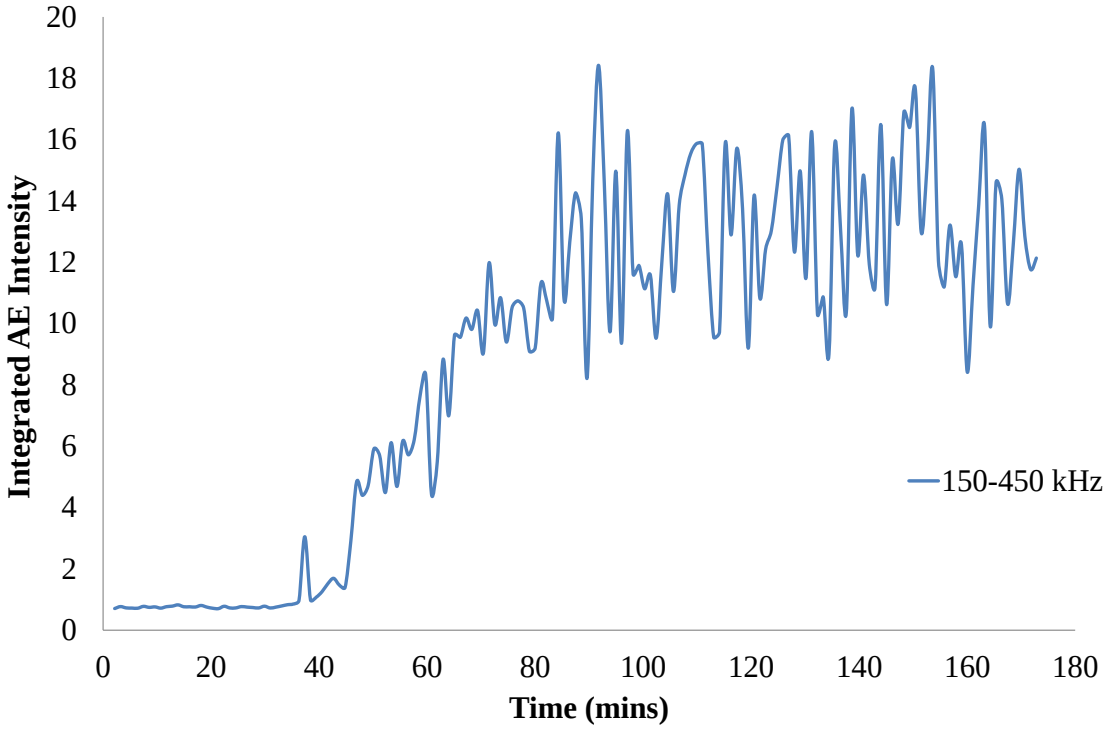

Figure 7-30: Crystallisation profile obtained from the integration of acoustic emission spectra D-mannitol from experiment 1 in table 7-2 using a solution concentration of 300 g/kg, an oscillation frequency of 3 Hz and amplitude of 10 mm

Figure 7-30 shows that during the initial 35-40 minutes of the acoustic measurements, the signal remained constant at close to zero intensity suggesting very few particles were present in the vessel. From 40 minutes onwards the intensity increased fairly rapidly over a period of around 40 minutes suggesting that nucleation had taken place followed by crystal growth causing an increase in the number of particle collisions with the vessel wall and baffles, and possibly also with other particles. The signal subsequently remained at a relatively constant intensity from approximately 90 minutes onwards suggesting the number of particles, and so collisions in the vessel, were more consistent.

Comparing the trend obtained in Figure 7-30 with that acquired using a batch STR in Figure 7-16, it can be seen that the overall intensity of the profile obtained from acoustic emission monitoring of a batch OBR crystallisation was much higher than in the batch STR. This suggests that the particles are colliding with more force and perhaps more often with oscillatory mixing compared with agitation achieved using an impeller. This could mean that the mixing achieved using baffles is in fact more efficient and creates more uniformity in the vessel than that possible in an OBR. Figure 7-31 shows the acoustic profile shown in Figure 7-30 overlaid with the Raman data for experiment 1 in Table 7-2.

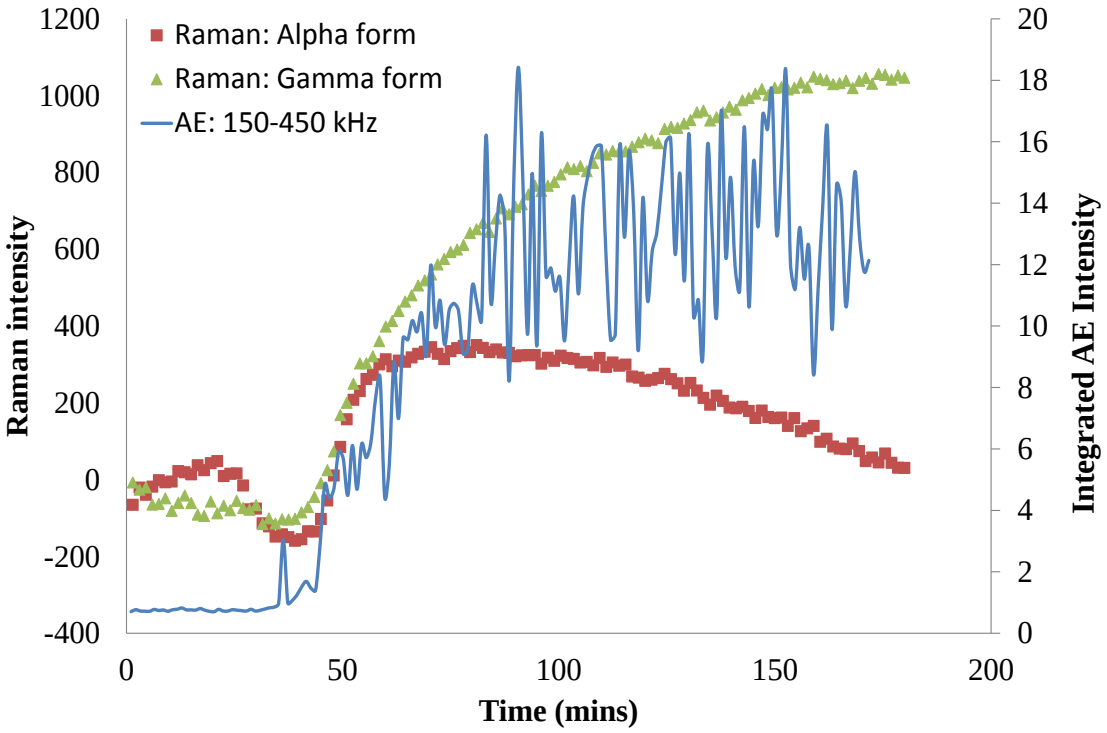

Figure 7-31: Crystallisation profiles obtained from Raman (intensity at 1058 and 1042 cm^{-1}) and acoustic emission measurements of D-mannitol from experiment 1 in table 7-2 using a solution concentration of 300 g/kg, an oscillation frequency of 3 Hz and amplitude of 10 mm

Figure 7-31 shows that nucleation was detected at similar points in the crystallisation using both acoustic emission and Raman monitoring. This is in comparison with the batch STR experiment in Figure 7-17 whereby nucleation appeared to be detected by

acoustic emission prior to the Raman measurements. It is possible that there was a higher nucleation rate (due to the higher solution concentration) in the batch OBR experiment due to the higher supersaturation, which would result in a larger number of smaller nuclei. This could mean there was not a delay in nucleation being detected by AES and Raman spectrometry due to there being a sufficient number of particles in a short space of time. It can be seen in Figure 7-31 that the acoustic signal levels of at around 90 minutes for the remainder of the crystallisation, whereas in the Raman profiles the alpha form signal decreases steadily, while the gamma signal increases simultaneously. Therefore, the acoustic profile shows the overall number of particles which appears to remain relatively constant even throughout the transformation process detected using Raman. Due to the fact it has been reported previously that particle size information can also be extracted from acoustic emission data of particulate processes, this was investigated further with the crystallisation data obtained.[14, 15] Figure 7-32 shows the regions of the acoustic emission spectrum which were thought to be associated with different particle sizes. It has been reported in the literature that an increase in the relative intensity of the acoustic signal is observed at lower frequency regions with an increase in the particle size.[14, 15, 33] This is due to the surface area and impact time associated with an increase in particle size resulting in an increase in emission amplitude and a corresponding decrease in frequency.[27]

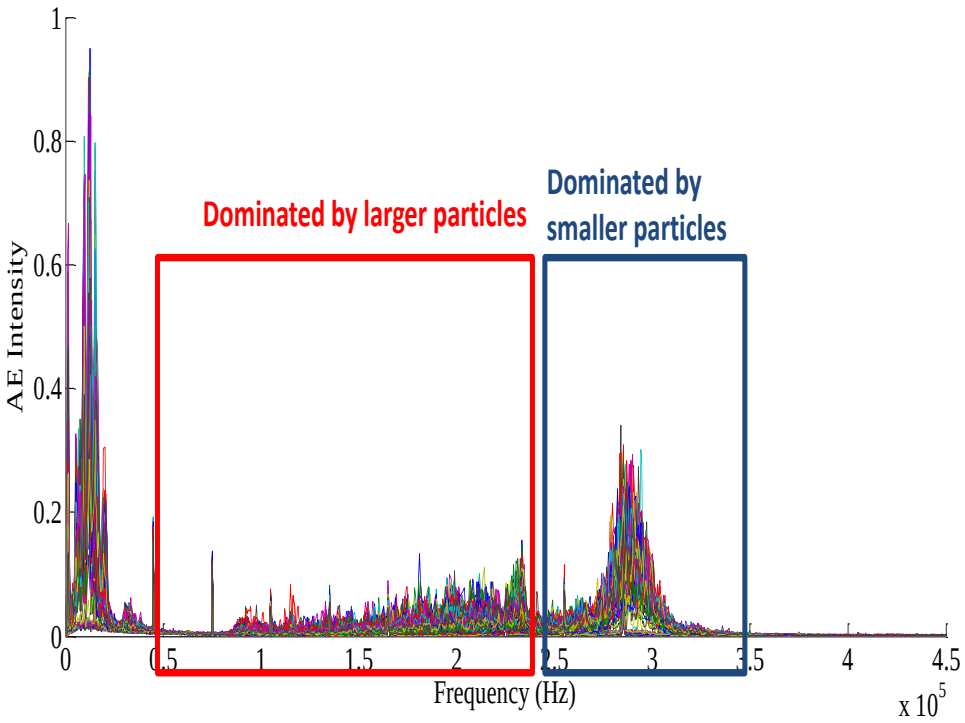

Figure 7-32: Acoustic emission spectra obtained during the crystallisation of D-mannitol in experiment 1 in table 7-2 using a solution concentration of 300 g/kg in a 1 L batch OBR vessel with a oscillation intensity of 3 Hz and 10 mm showing the frequency regions dominated by different particle sizes

When the acoustic emission spectra obtained during the crystallisation experiments were studied in more detail it was found that the intensity in both of the regions highlighted in Figure 7-32 increased at different points throughout the crystallisation, with an increase in the acoustic intensity in the region between 250 and 350 kHz appearing first. This agrees with acoustic data reported in the literature with respect to reaction monitoring whereby a ratio of the integration of the high (250-350 kHz) or low (50-250 kHz) frequency regions could be used to determine trends in particles of a smaller or larger size, respectively.[14] This suggested that this region could be attributed to particles of a smaller size which formed during nucleation causing the increase observed. The trends in particle size observed in the acoustic emission spectra were corroborated using *in-situ* FBRM data in subsequent experiments. Figure 7-33 shows the trend obtained from

plotting the ratio of acoustic emission frequency ranges showing the progression of particles of a smaller mean size with time.

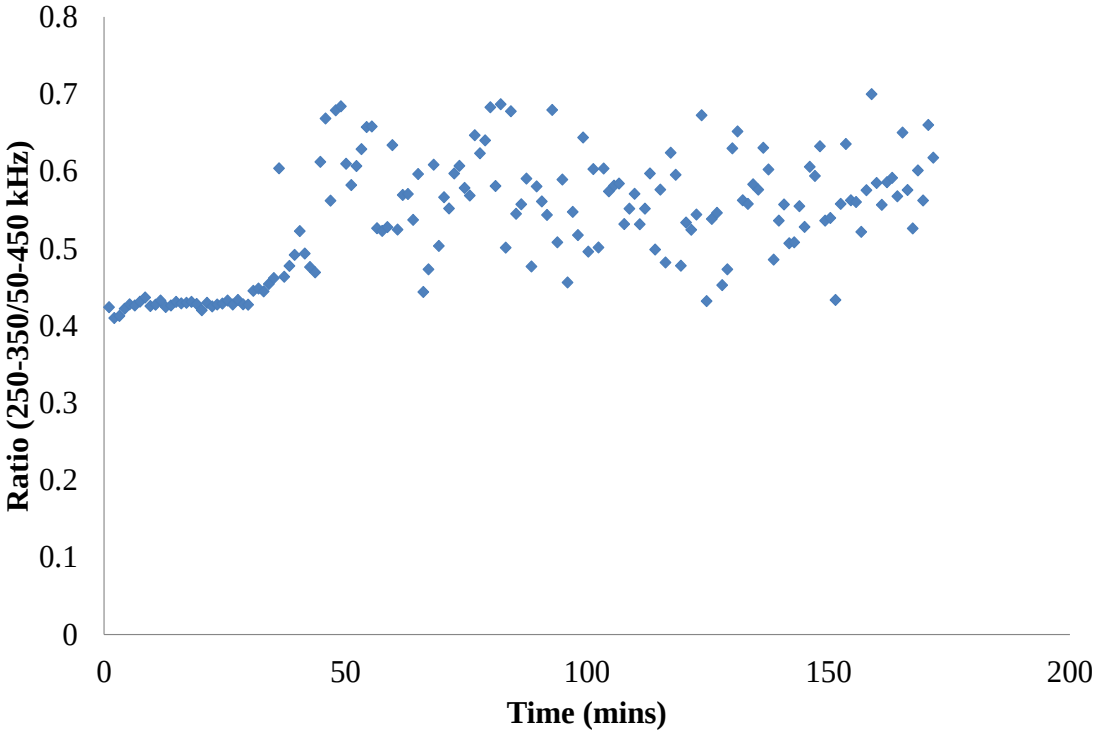

Figure 7-33: Graph of the ratio of acoustic emission frequency ranges (250-350/50-250 kHz) showing the progression of particles in the smaller size range during the crystallisation

Figure 7-33 shows that there is no trend of the ratio of frequency ranges dominated by small particles for the first 40 minutes due to no particles being present and then the intensity begins to increase during particle formation. This agreed with the Raman crystallisation profile which showed there were very few crystals in the vessel prior to 40 minutes and nucleation occurred thereafter. From 50 minutes onwards, the trend then became slightly erratic which could have been due to the associated noise with low intensity measurements. Alternatively this could have suggested that the amount of small particles in the vessel did not decrease as would be expected during the crystal growth period. This was most likely due to the transformation process which was known to be occurring from the Raman crystallisation profile in Figure 7-31. During the transformation process, there will be dissolution of alpha form crystals and subsequent

nucleation of gamma form crystals thereby increasing the number of particles in the smaller size range. As the transformation process was still progressing by 150 minutes, this was why the trend obtained from the acoustic measurements related to particles in the small size range remained at around a relatively constant level. An overlay of the Raman and acoustic emission profiles (integrated region of 150-450 kHz) is shown in Figure 7-34 for experiment 9 in table 7-2 for a solution concentration of 300 g/kg and oscillation conditions of 3 Hz and 30 mm.

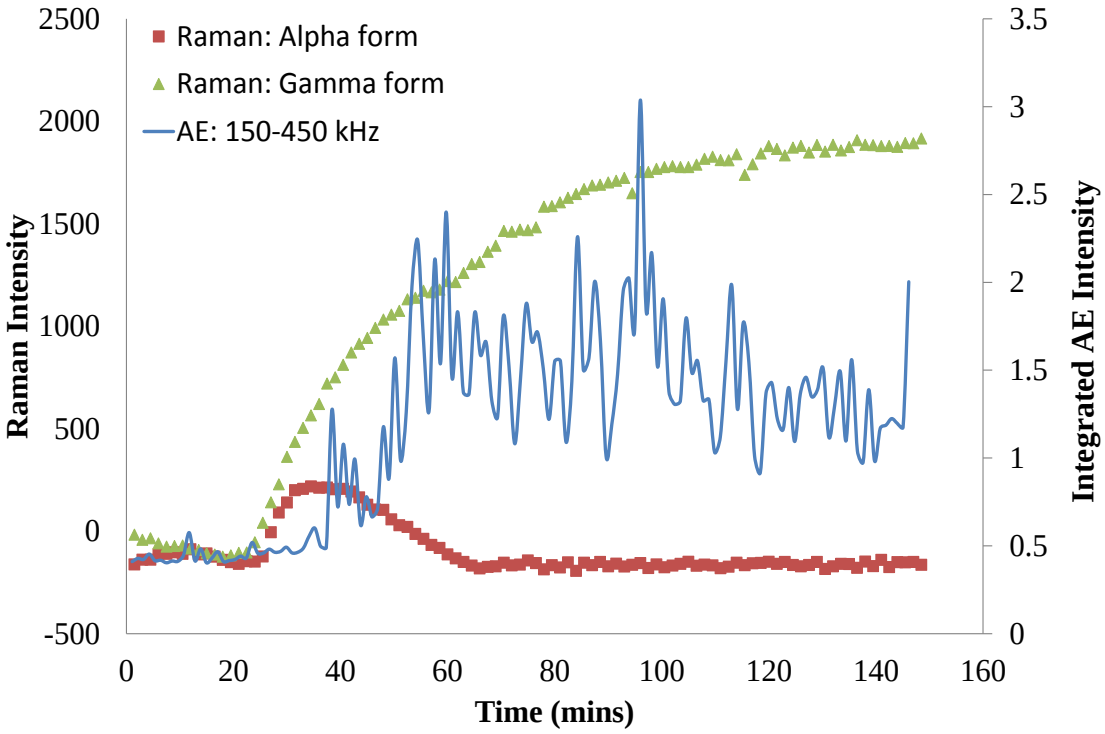

Figure 7-34: Crystallisation profiles obtained from Raman (intensity at 1058 and 1042 cm^{-1}) and acoustic emission measurements of D-mannitol from experiment 9 in table 7-2 using a solution concentration of 300 g/kg, an oscillation frequency of 3 Hz and amplitude of 30 mm

Figure 7-34 shows that nucleation was detected approximately 20 minutes earlier in the Raman measurements than in the acoustic crystallisation profile obtained. Due to the fact the range of frequencies studied was in the frequency region 150-450 kHz and it is known that higher frequencies correspond to smaller particles, it is possible that in the initial stages of the crystallisation the growth rate was higher than the nucleation rate

which meant that the particles grew to a larger size more quickly. This would have caused a larger signal in the frequency range below 150 kHz which was not included in the frequency region studied and may be why nucleation was not detected in the acoustic profile in Figure 7-34. It can also be observed that as the Raman signal levelled off towards the end of the crystallisation, the acoustic profile showed a slight decrease in comparison from 100 minutes onwards. It was thought that differences in particle size rather than solid concentration (the main influence on Raman spectra) would attribute to the decrease in the acoustic signal observed. Figure 7-35 and Figure 7-36 show the acoustic emission trends obtained from the ratio of frequency ranges attributable to small and large particle size ranges as well as the FBRM measurements collected during the crystallisation at smaller (1-10 µm) and larger (100-250 µm) particle size ranges, respectively.

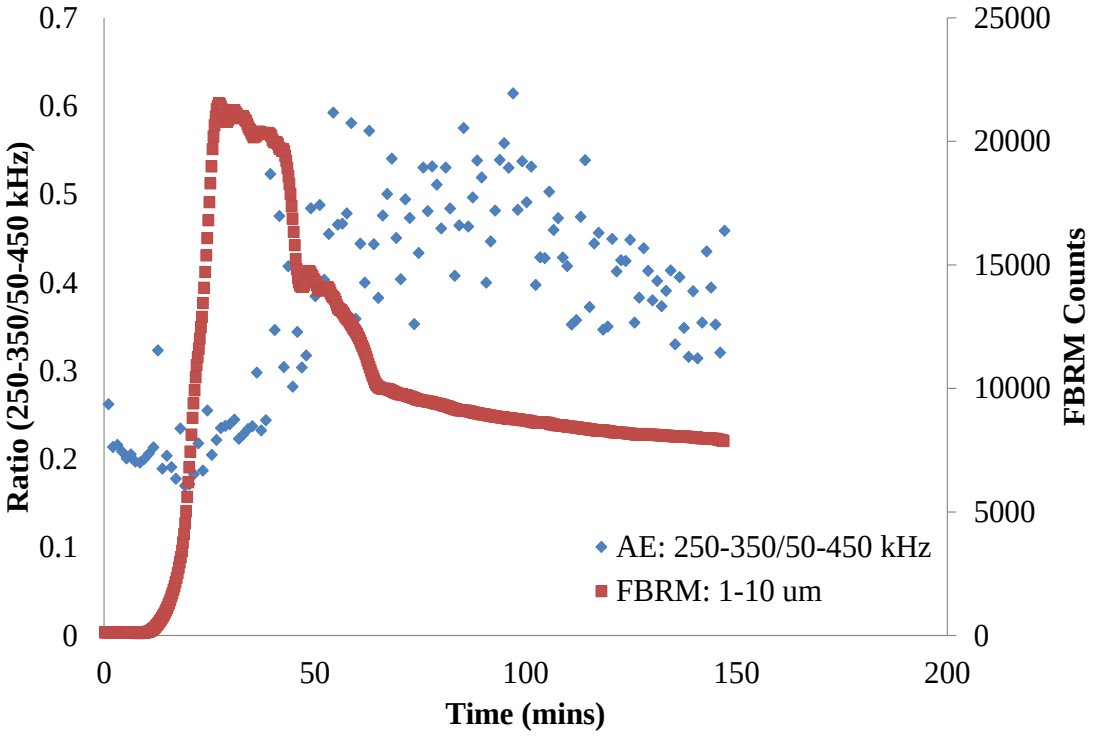

Figure 7-35: Crystallisation profiles obtained from FBRM and a ratio of frequency ranges from acoustic emission measurements of D-mannitol from experiment 9 in table 7-2 using a solution concentration of 300 g/kg, an oscillation frequency of 3 Hz and amplitude of 30 mm

Figure 7-35 shows there was a rapid increase in the counts in the FBRM profiles obtained for the smaller particle size ranges at approximately 15 minutes showing nucleation had taken place and this was detected around 10 minutes earlier than the Raman measurements in Figure 7-34 which was expected as it is known FBRM is a more sensitive technique for detecting nucleation. As can be seen in the acoustic emission profile describing the trend of particles in the smaller size range, the increase in intensity is delayed in comparison to the increase in counts in the FBRM signal and starts to increase approximately 5 minutes after the rapid increase observed by FBRM. The increase in the acoustic trend was also a steadier increase over a longer period of time in comparison with the FBRM profile, most likely due to the FBRM measurements determining the total number of particles in the vessel, whereas the acoustic emission measurements relate the number of collisions detected in the vessel so this value would be expected to increase less rapidly than the FBRM counts. As can be seen in Figure 7-35, the decrease in the signal observed in the acoustic emission profile was also delayed in comparison to the FBRM measurements. The acoustic emission profile began to decrease just after the transformation to the stable gamma form was complete as determined by the Raman crystallisation profile (Figure 7-34) suggesting that nucleation of the stable gamma form was complete and this caused the decrease in the acoustic signal observed. The FBRM profile decreased quicker as it is known that alpha form crystals are much finer than the coarser gamma form crystals and the decrease observed could be aligned with the decrease observed in the alpha form signal for the Raman measurements. Therefore, the trend of the larger size ranges was also studied, shown in Figure 7-36.

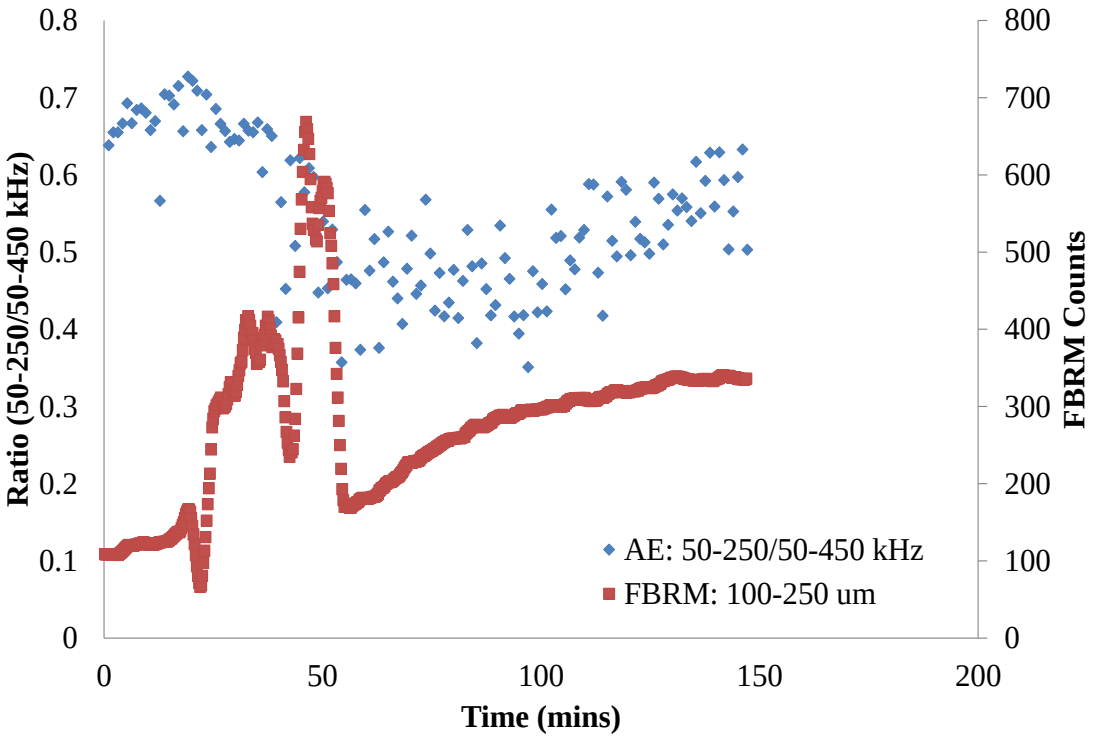

Figure 7-36: Crystallisation profiles obtained from FBRM and a ratio of frequency ranges from acoustic emission measurements of D-mannitol from experiment 9 in table 7-2 using a solution concentration of 300 g/kg, an oscillation frequency of 3 Hz and amplitude of 30 mm

It can be seen in Figure 7-36 that there was an increase in the counts of the larger particle size range from around 20 minutes (10 minutes after the increase in the small particle size range in Figure 7-35 indicating nucleation was taking place) however, the count value suggested that there was a much smaller number of large particles in the vessel. A sharp increase in the FBRM trend after 40 minutes seemed to have an impact on the acoustic signal in Figure 7-34 as this is the point at which the acoustic intensity begins to increase. It is likely that the increase in larger particles in the vessel resulted in an increase in particle collisions and also an increase in the force of these collisions therefore resulting in an overall increase in the acoustic signal observed. As the FBRM measurements showed, the number of larger particles in the vessel was increasing in Figure 7-36 during the transformation. The frequency range attributed to larger particles also showed an increase in intensity during this same time period. This confirmed why

the Raman signal remained steady during this period, as the overall solid concentration was most likely remaining relatively constant while the particle sizes were changing. The changes in the small and high particle size ranges in the FBRM measurements show the variations in the trends were relatively small and gradual. In addition, as the counts for the large particles increased, the counts for the small particles decreased suggesting this did not have a significant impact on the Raman profile. Figure 7-37 shows the crystallisation profiles obtained from the Raman and acoustic measurements of experiment 3 in Table 7-2 using a solution concentration of 350 g/kg and an oscillation intensity of 3 Hz and 30 mm.

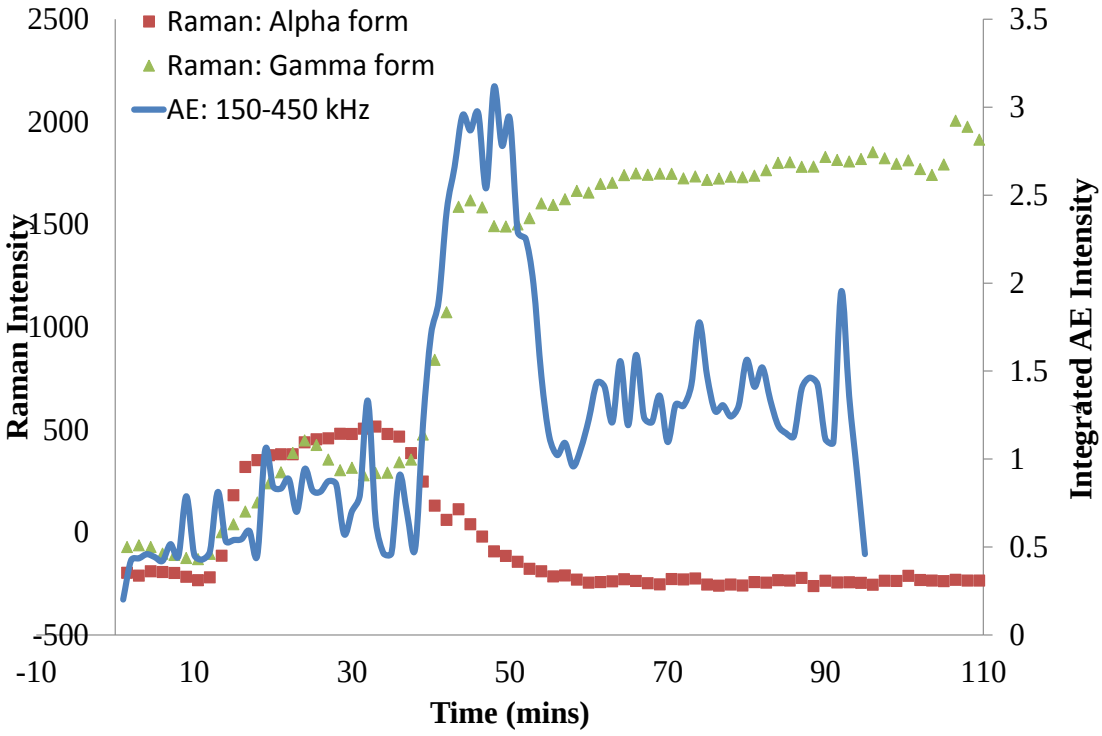

Figure 7-37: Crystallisation profiles obtained from Raman (intensity at 1058 and 1042 cm^{-1}) and acoustic emission measurements of D-mannitol from experiment 3 in table 7-2 using a solution concentration of 350 g/kg, an oscillation frequency of 3 Hz and amplitude of 30 mm

As Figure 7-37 shows there was a small increase in the acoustic intensity around the same time as nucleation was identified by the Raman measurements showing there were a small number of particle collisions being detected. This was followed by a larger

increase in the acoustic intensity which accompanies the rapid transformation process observed by Raman. The spike in the acoustic signal occurred at the same time that there was a significant increase in the gamma form and there was also a lesser amount of alpha form in the vessel. Therefore, at this point in the crystallisation there was the highest concentration of solid material leading to the spike in the acoustics signal. It is possible that the particle size of the gamma form during this rapid particle formation period also contributed to the significant rise in signal. Once the transformation process was complete and there was no longer any alpha form remaining in the vessel, according to the Raman measurements, the acoustics signal then decreased and levelled off along with the Raman gamma form profile showing the crystallisation had reached steady state. The relatively rapid decrease in the acoustic profile was possibly due to the majority of small particles growing to a larger size and therefore no longer having such an effect on the higher frequency region.

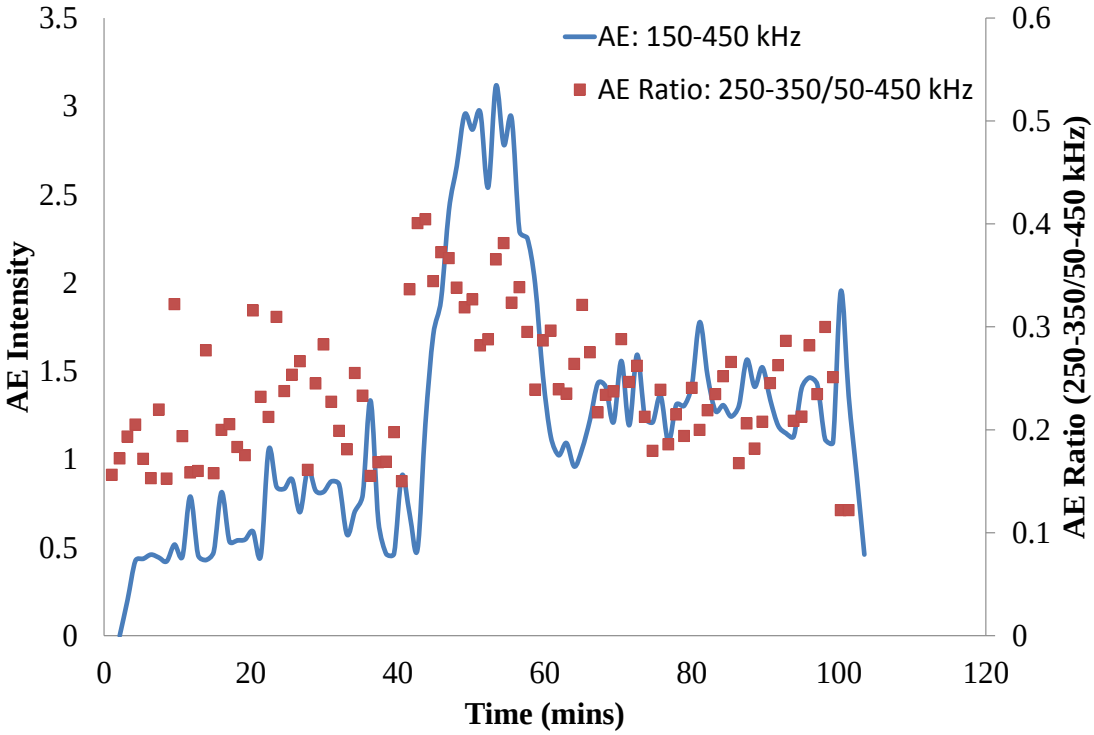

Figure 7-38: Crystallisation profiles obtained from integrating acoustic emission spectra (150-450 kHz) and a ratio of frequency ranges from acoustic emission measurements of D-mannitol from experiment 3 in table 7-2 using a solution concentration of 350 g/kg, an oscillation frequency of 3 Hz and amplitude of 30 mm

Figure 7-38 shows that at the same time point that a rapid increase in the acoustic intensity of the integrated region (150-450 kHz) was detected; an increase in the trend attributable to particles of a smaller size range was observed. This happened at the same point during the crystallisation that rapid transformation to the gamma form was detected from the Raman measurements shown in Figure 7-37. This suggested that during this swift transformation period, a large amount of nuclei of the gamma polymorph were present causing the trends seen in Figure 7-38 where an increased amount of particle collisions were occurring causing a greater effect on the higher frequency region of the acoustic emission spectrum (due to the relatively small size of the particles). Figure 7-39 shows a similar trend which was observed in the acoustics profile of experiment 11 in Table 7-2 using a solution concentration of 350 g/kg and oscillation conditions of 1 Hz and 30 mm which on this occasion was monitored using FBRM (see Figure 7-40) as well as Raman.

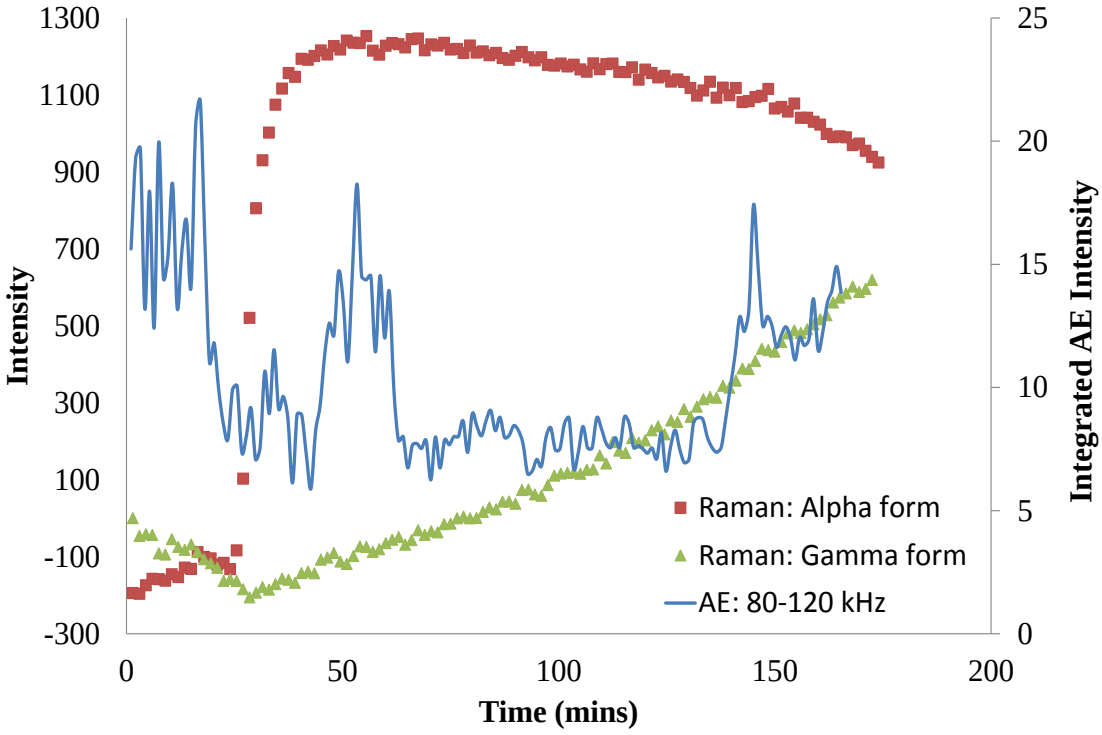

Figure 7-39: Crystallisation profiles obtained from Raman (intensity at 1058 and 1042 cm^{-1}) and acoustic emission measurements of D-mannitol from experiment 11 in table 7-2 using a solution concentration of 350 g/kg, an oscillation frequency of 1 Hz and amplitude of 30 mm

When the region from 150-450 kHz was integrated as with the previous acoustic spectra obtained, there was no obvious crystallisation profile. Therefore, lower frequency regions of the spectra (above 50 kHz) were investigated to see if there were any signals evident here. It was found that the acoustic signals obtained for the crystallisation of experiment 11 were prominent in the range 80-120 kHz and so this was the region selected for integration to produce the trend in Figure 7-39. A shown, there was a similar spike in the acoustic signal as observed during the crystallisation in Figure 7-37 which occurred approximately 10 minutes after the significant increase in the signal for the alpha form was detected using Raman. It was thought that as it was the alpha polymorph that formed in a relatively rapid nucleation event in this case, an adequate acoustic emission signal was not obtained at higher frequency regions. It is known that the alpha form crystals nucleate as much finer crystals than the gamma and so much weaker collisions would be expected which may cause further breakage of the already small crystals. Therefore, an acoustic signal may not be observed until a later stage in the crystallisation once sufficient crystal growth had taken place thus causing more of an effect on lower frequency regions in the acoustic spectra as shown in Figure 7-39. Figure 7-40 and Figure 7-41 show the FBRM data collected during experiment 11.

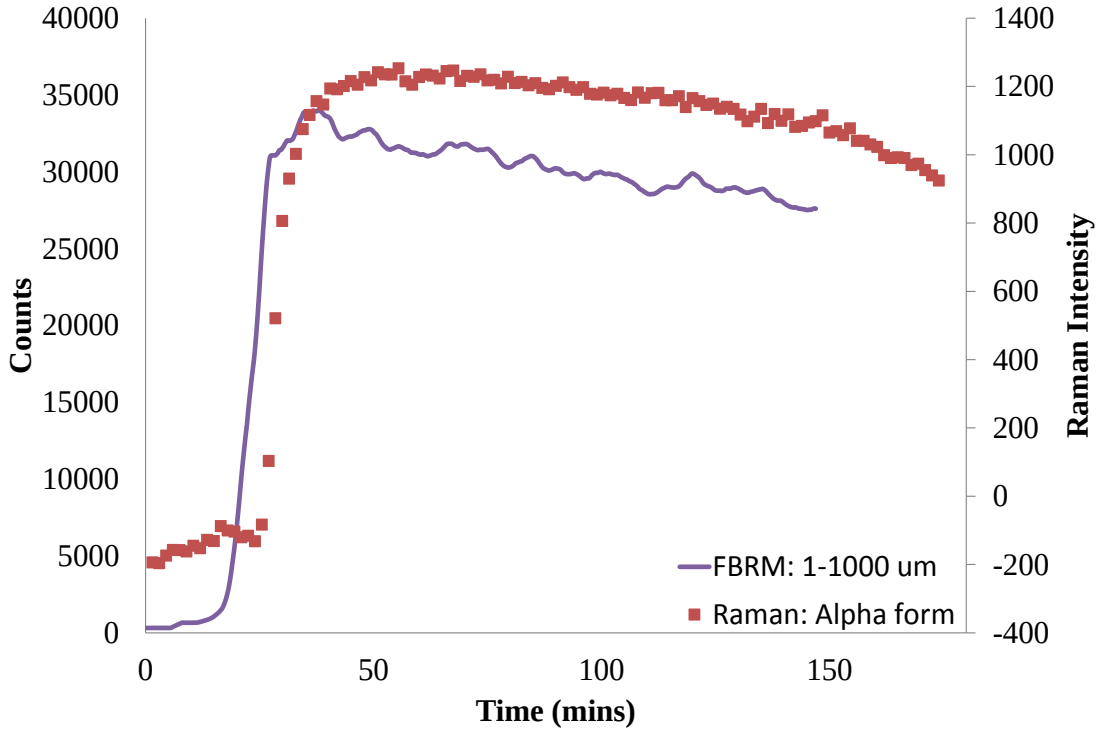

Figure 7-40: Crystallisation profiles obtained from FBRM and Raman measurements (intensity at 1058 cm^{-1}) of D-mannitol from experiment 11 in table 7-2 using a solution concentration of 350 g/kg, an oscillation frequency of 1 Hz and amplitude of 30 mm

Figure 7-40 shows the FBRM trends obtained from particles in the total size range being monitored (1-1000 µm) and the Raman profile for the alpha form. This shows that during the crystallisation the Raman profile obtained for the alpha polymorph follows a similar trend to that obtained by FBRM (1-1000 µm). Nucleation was detected slightly earlier by FBRM (less than 5 minutes), however, both the Raman and FBRM trends (1-1000 µm) then show a rapid increase in intensity (or counts for FBRM) which reaches a maximum value at approximately 40 minutes with a subsequent gradual decrease in intensity for the remainder of the crystallisation. This suggests that the Raman crystallisation profile describes what is occurring with all the particles in the vessel (*i.e.* it is influenced more by the total concentration of solid material rather than the particle size of this material).

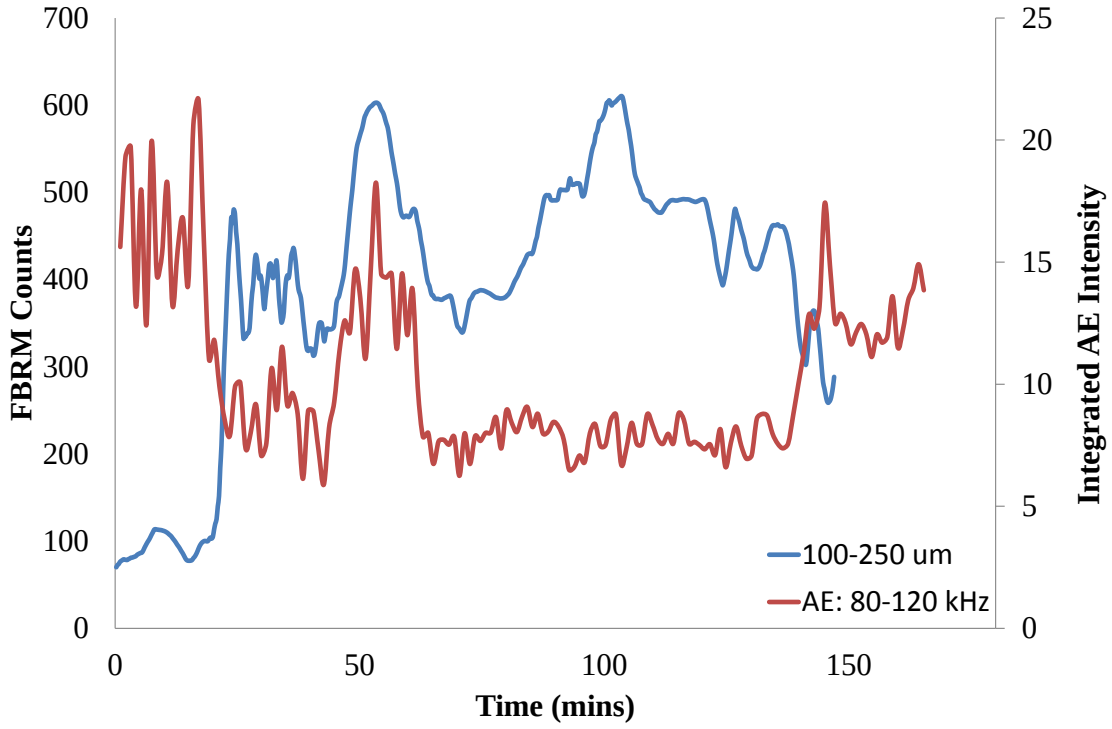

Figure 7-41: Crystallisation profiles obtained from FBRM and acoustic emission measurements of D-mannitol from experiment 11 in table 7-2 using a solution concentration of 350 g/kg, an oscillation frequency of 1 Hz and amplitude of 30 mm

Figure 7-41 shows the acoustics profile for the frequency range 80-120 kHz overlaid with the FBRM trend for particles in the size range 100-250 µm. The spike in intensity observed in the acoustic signal appeared to correlate with an increase in the number of particles in the size range shown, which occurred just after the rapid increase in the intensity of the alpha form signal in the Raman measurements. This suggested that a certain amount of crystal growth had taken place following nucleation and the presence of larger particles in the vessel had a short term effect on the acoustic signal. However, from 60 minutes onwards the acoustic signal then decreased back to its original value and did not begin to increase in intensity again until nearly 150 minutes when transformation to the gamma form was progressing. Figure 7-42 shows the profile for the FBRM measurements of particles below the 10 µm size range along with the ratio of

acoustic emission measurements showing the trend obtained at a higher frequency range (smaller particles).

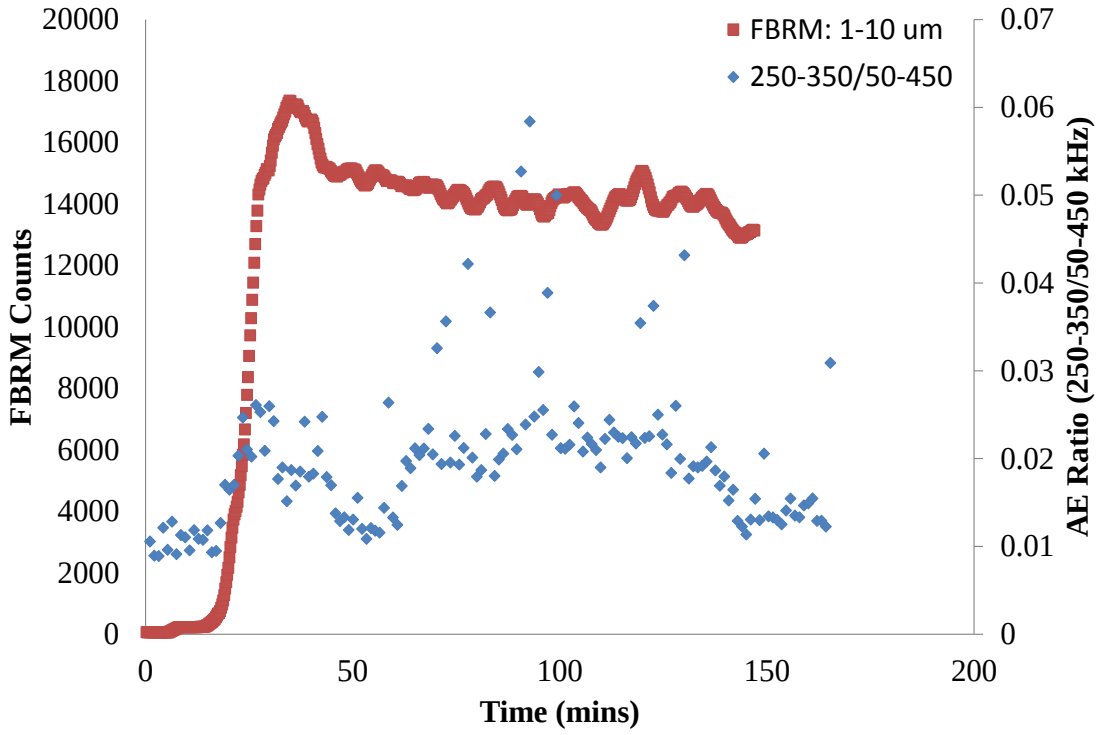

Figure 7-42: Crystallisation profiles obtained from FBRM and a ratio of frequency ranges from acoustic emission measurements of D-mannitol from experiment 11 in table 7-2 using a solution concentration of 350 g/kg, an oscillation frequency of 1 Hz and amplitude of 30 mm

Figure 7-42 shows that the trend obtained from the higher frequency range in the acoustic emission spectra shows an increase in the intensity at approximately the same time as that observed in the FBRM measurements of particles in the size range 1-10 µm. However, it can be seen that the acoustic emission profile is of a low intensity in comparison to trends observed with previous experiments despite the FBRM signal having a comparative high value of counts during nucleation. This suggests that the alpha form particles produced immediately following nucleation have a much reduced effect on the acoustic emission signal in comparison to the gamma form due to the gamma form crystals being larger, less fragile needles, as explained previously. However, it can be seen that the acoustic trend in Figure 7-42 still follows a similar trend

to that of the FBRM profile (1-10 µm) showing a steady decrease in the signal as the crystallisation progresses suggesting crystal growth is taking place causing a reduction in the number of particles in the small size range. Figure 7-43 shows similar profiles, but this time for the larger particle size range in the FBRM trend (100-250 µm) and the trend in the lower frequency range in the acoustic emission spectra.

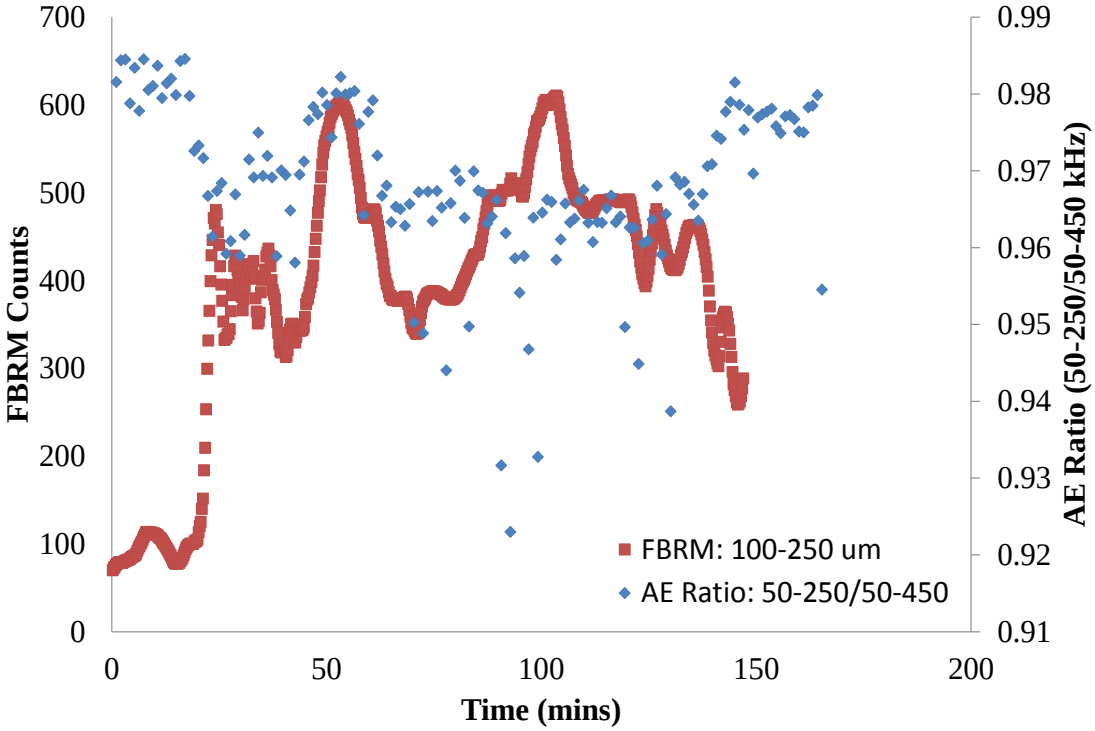

Figure 7-43: Crystallisation profiles obtained from FBRM and a ratio of frequency ranges from acoustic emission measurements of D-mannitol from experiment 11 in table 7-2 using a solution concentration of 350 g/kg, an oscillation frequency of 1 Hz and amplitude of 30 mm

The trend in the acoustic emission spectra at a lower frequency range shows that at around 50 minutes there was an increase in the signal which corresponds to an increase in the number of particles in a larger size range (100-250 µm) in the FBRM profile. This suggested that an increase in the number of particles caused an increase in the acoustic signal which was expected as these resulted in collisions of increased energy. However, in comparison with the FBRM trend in Figure 7-42, the count value was considerably lower for the larger particle size range showing there were much fewer of these sized

particles in the vessel. Additionally, the FBRM profile showed a decrease in the count value towards the end of the measurements while the acoustic profile continued to increase gradually. It was thought that particles may be continuing to grow and therefore, be included in the subsequent particle size range (>250 µm). However, this profile was studied and the particles did not seem to be included in the next larger size range trend. Therefore, it was thought that the particles may have sunk to the bottom of the vessel once a certain particle size was reached (above 250 µm). An experiment had been carried out to examine the effect of increasing particle size range on the acoustic signal, like that in Figure 7-27, however, it was observed that particles above the 250 µm sieve fraction size were not suspended efficiently and therefore sunk to the bottom of the vessel having little impact on the acoustic signal. Therefore, the next size range down in the FBRM measurements was compared with the acoustic trend in Figure 7-44Figure 7-43.

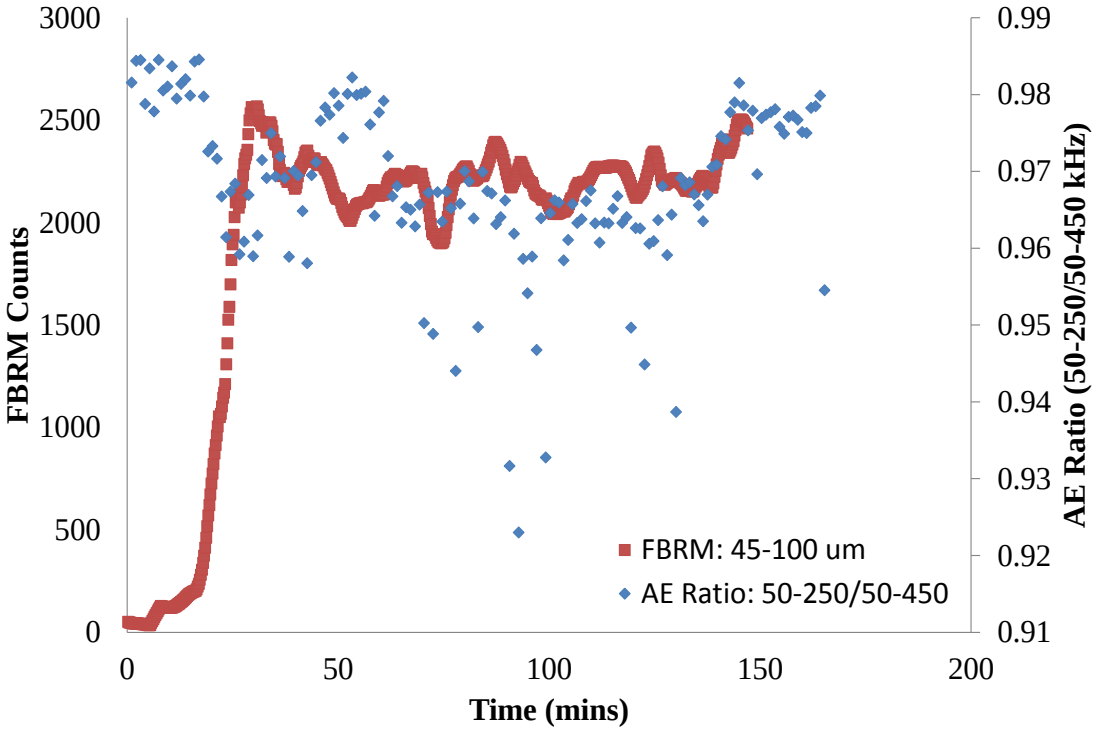

Figure 7-44: Crystallisation profiles obtained from FBRM and a ratio of frequency ranges from acoustic emission measurements of D-mannitol from experiment 11 in table 7-2 using a solution concentration of 350 g/kg, an oscillation frequency of 1 Hz and amplitude of 30 mm

Figure 7-44 shows that the acoustic trend from approximately 60 minutes onwards follows the FBRM trend for particles in the size range 45-100 µm. The increase towards the end of the crystallisation in both profiles shows an increase in the particle size is taking place corresponding to crystal growth. Therefore, from Figure 7-42-Figure 7-44 and the trends observed from the previous crystallisations monitored using acoustic emission spectrometry, it can be determined that higher frequency regions in the acoustic spectrum correspond to smaller particle sizes in the range below 10 µm. Lower frequency regions can be attributed to larger particles and in the case of D-mannitol, mainly particles in the range 50-250 µm due to the inefficient suspension of particles larger than 250 µm which was observed experimentally.

It was found that an acoustic signal could also be obtained from several of the experiments carried out at the smaller scale of 250 ml. However, these were only attained using more intense oscillation conditions and were lower in intensity due to the lower number of particles present in the vessel, therefore, the figures are not shown. Additional experiments were carried out in a continuous oscillatory baffled reactor like that undertaken with L-glutamic acid in chapter 5.3. However, despite the different experimental conditions adopted using a design of experiments approach, the relatively high solution concentration led quickly to blocking and so prevented the use of this reactor for the crystallisation of D-mannitol.

7.4 Conclusions

As shown in the previous chapters (4-6), non-invasive Raman spectrometry is an advantageous technique for monitoring crystallisation and is able to provide information on polymorphic form and solid concentration, as well as the effect of operating conditions on the process including nucleation and growth profiles. However, the main drawback of this technique is that particle size information is not obtained which is an important aspect of the crystallisation process and the particle size and distribution of the end product are key properties in industrial crystallisation. Therefore, Raman spectrometry would require to be used alongside a particle size technique in order to obtain all the necessary information on the process. As the information provided using Raman spectrometry can be obtained *in-situ* and potentially in real time, it would be counter-intuitive to then conduct time-consuming off-line particle size analysis in order to obtain the remaining necessary information. As this chapter demonstrates, acoustic emission spectrometry as a non-invasive measurement technique shows promise as a complementary procedure to Raman spectrometry. Information on the development of the crystallisation as a whole (*i.e.* the total solid concentration) could be determined which provided an indication of when nucleation occurred and trends in crystal growth. However, it was not evident that acoustic emission was any more sensitive than Raman for the detection of nucleation. As expected, FBRM appeared to be the most sensitive technique to detect this crystallisation event in contrast to results reported in the literature which suggested acoustic emission could be the most sensitive technique available for the detection of nucleation of a compound consisting of needle-shaped particles of a similar density.[25]

However, it was determined through crystallisation monitoring that information on changes in the particle size could be obtained from acoustic emission data without the need for extensive data analysis as reported previously.[30] By splitting the AE spectrum into different frequency ranges it was possible to extract information on particle size. A lower frequency range (50-250 kHz) was found to be dominated by particles of a larger

size and a higher frequency range of 250-350 kHz could be attributed to smaller particle sizes. Through comparisons with results from FBRM, it was shown that trends of particles in the size region of 50-250 µm could be followed during crystallisation by using the lower frequency range and trends for 1-50 µm particles by changes in the intensity at the higher frequency range. This demonstrated that important information on how the particle size changes throughout the crystallisation could be ascertained, as has been demonstrated in alternative particulate processes such as powder blending reported in the literature.[15]

Additionally, this section of work on a relatively under-studied compound with regards to crystallisation resulted in some increased knowledge on what factors impact the formation and growth of the polymorphs of D-mannitol. Firstly, it was confirmed that solution concentration played an important factor on which polymorph(s) nucleated, with a lower supersaturation resulting in formation of the thermodynamically stable gamma form, while increasing the solution concentration resulted in increased levels of the alpha polymorph with subsequent transformation to the gamma form.[5] As the stable form is also the least soluble, increasing the solution concentration at a fixed reactor temperature will make it more likely for the supersaturation value to be in the metastable form for the unstable alpha polymorph resulting in the initial nucleation of this form. Furthermore, it was found that the induction time between attaining supersaturation and nucleation taking place decreased as the solution concentration was increased. The induction time between reaching supersaturation and nucleation occurring is more obvious with certain compounds than others; however, an increase in the supersaturation is known to reduce the length of this induction period (chapter 2.1.1.2.). From the study carried out in the batch STR it was established that mixing was also an important parameter on the outcome of the crystallisation of D-mannitol. Increasing the reactor scale by a relatively small amount (from 155 to 500 ml) resulted in a completely different outcome under the same experimental conditions. It was discovered that the mixing intensity also needed to be increased in order to obtain similar results. This

suggested that nucleation of the alpha form was very much dependent on sufficient mixing being applied to the reactor contents. The effect of reactor scale on the crystallisation suggested that scaling up to industrial scale would be problematic with this compound and the optimum experimental conditions established at the laboratory scale most likely would result in a completely different outcome as the scale was increased.

The design of experiments study carried out in the batch OBR showed that like the study carried out using L-glutamic acid in chapter 4, solution concentration had the main effect on the particle properties of the end product, while the interaction between oscillation frequency and amplitude impacted the particles the most. This suggested oscillatory mixing within a batch OBR could have potential advantages over conventional batch stirred tank reactors in that mixing conditions could be altered to obtain different particle properties. The frequency and amplitude of oscillation was found to affect the nucleation outcome. It is known that the metastable zone width is affected by varying frequencies and amplitudes and therefore the supersaturation value may be located in the metastable zone width for the stable form under a certain set of oscillation conditions and the metastable form under an alternative set of conditions. However, a number of unsuccessful experiments carried out in the continuous OBR suggested that this reactor technology was limited to the compound type which could be effectively crystallised. Highly soluble compounds requiring a high solution concentration for crystallisation, like D-mannitol, may not be compatible with continuous oscillatory baffled reactors and an alternative continuous crystallizer like the mixed suspension, mixed product removal may prove to have a more positive outcome (chapter 6).

7.5 References

1. S. N. Campbell Roberts, A. C. Williams, I. M. Grimsey and S. W. Booth, Quantitative analysis of mannitol polymorphs. FT-Raman spectroscopy, Journal of Pharmaceutical and Biomedical Analysis, 2002, **28**, 1135-1147.
2. J. R. Beattie, L. J. Barrett, J. F. Malone, J. J. McGarvey, M. Nieuwenhuyzen and V. L. Kett, Investigation into the subambient behavior of aqueous mannitol solutions using temperature-controlled Raman microscopy, *European Journal of Pharmaceutics and Biopharmaceutics*, 2007, **67**, 569-578.
3. W. L. Hulse, R. T. Forbes, M. C. Bonner and M. Getrost, Influence of protein on mannitol polymorphic form produced during co-spray drying, *International Journal of Pharmaceutics*, 2009, **382**, 67-72.
4. Y.-Y. Lee, J. X. Wu, M. Yang, P. M. Young, F. van den Berg and J. Rantanen, Particle size dependence of polymorphism in spray-dried mannitol, *European Journal of Pharmaceutical Sciences*, 2011, **44**, 41-48.
5. J. Cornel, P. Kidambi and M. Mazzotti, Precipitation and Transformation of the Three Polymorphs of d-Mannitol, *Industrial & Engineering Chemistry Research*, 2010, **49**, 5854-5862.
6. A. S. Myerson, ed., Handbook of industrial crystallization, 2nd edn., Butterworth-Heinemann, Woburn, 2001.
7. H. Hao, W. Su, M. Barrett, V. Caron, A.-M. Healy and B. Glennon, A Calibration-Free Application of Raman Spectroscopy to the Monitoring of Mannitol Crystallization and Its Polymorphic Transformation, *Organic Process Research & Development*, 2010, **14**, 1209-1214.
8. W. Su, H. Hao, M. Barrett and B. Glennon, The Impact of Operating Parameters on the Polymorphic Transformation of d-Mannitol Characterized in Situ with Raman Spectroscopy, FBRM, and PVM, *Organic Process Research & Development*, 2010, **14**, 1432-1437.
9. H. Mühlenweg and E. D. Hirleman, Laser Diffraction Spectroscopy: Influence of Particle Shape and a Shape Adaptation Technique, *Particle & Particle Systems Characterization*, 1998, **15**, 163-169.
10. P. Hamilton, D. Littlejohn, A. Nordon, J. Sefcik and P. Slavin, Validity of particle size analysis techniques for measurement of the attrition that occurs during vacuum agitated powder drying of needle-shaped particles, *Analyst*, 2012, **137**, 118-125.
11. B. O'Sullivan and B. Glennon, Application of in Situ FBRM and ATR-FTIR to the Monitoring of the Polymorphic Transformation of d-Mannitol, *Organic Process Research & Development*, 2005, **9**, 884-889.
12. A. Vaccaro, J. Šefčík and M. Morbidelli, Modeling Focused Beam Reflectance Measurement and its Application to Sizing of Particles of Variable Shape, *Particle & Particle Systems Characterization*, 2006, **23**, 360-373.
13. N. K. Nere, D. Ramkrishna, B. E. Parker, W. V. Bell and P. Mohan, Transformation of the Chord-Length Distributions to Size Distributions for Nonspherical Particles with Orientation Bias†, *Industrial & Engineering Chemistry Research*, 2006, **46**, 3041-3047.

14. A. Nordon, Y. Carella, A. Gachagan, D. Littlejohn and G. Hayward, Factors affecting broadband acoustic emission measurements of a heterogeneous reaction, *Analyst*, 2006, **131**, 323-330.
15. P. Allan, L. J. Bellamy, A. Nordon and D. Littlejohn, Non-invasive monitoring of the mixing of pharmaceutical powders by broadband acoustic emission, *Analyst*, 2010, **135**, 518-524.
16. J. T. T. Leskinen, M.-A. H. Okkonen, M. M. Toiviainen, S. Poutiainen, M. Tenhunen, P. Teppola, R. Lappalainen, J. Ketolainen and K. Järvinen, Labscale fluidized bed granulator instrumented with non-invasive process monitoring devices, *Chemical Engineering Journal*, 2010, **164**, 268-274.
17. S. Poutiainen, S. Matero, T. Hämäläinen, J. Leskinen, J. Ketolainen and K. Järvinen, Predicting granule size distribution of a fluidized bed spray granulation process by regime based PLS modeling of acoustic emission data, *Powder Technology*, 2012, **228**, 149-157.
18. J. W.R. Boyd and J. Varley, The uses of passive measurement of acoustic emissions from chemical engineering processes, *Chemical Engineering Science*, 2001, **56**, 1749-1767.
19. T. Sawada, Y. Gohshi, C. Abe and K. Furuya, Acoustic emission from phase transition of some chemicals, *Analytical Chemistry*, 1985, **57**, 1743-1745.
20. H. N. G. Wadley and R. Mehrabian, Acoustic emission for materials processing: a review, *Materials Science and Engineering*, 1984, **65**, 245-263.
21. A. Nordon, R. J. H. Waddell, L. J. Bellamy, A. Gachagan, D. McNab, D. Littlejohn and G. Hayward, Monitoring of a heterogeneous reaction by acoustic emission, *Analyst*, 2004, **129**, 463-467.
22. M. Whitaker, G. R. Baker, J. Westrup, P. A. Goulding, D. R. Rudd, R. M. Belchamber and M. P. Collins, Application of acoustic emission to the monitoring and end point determination of a high shear granulation process, *International Journal of Pharmaceutics*, 2000, **205**, 79-91.
23. R. Hou, A. Hunt and R. A. Williams, *Acoustic monitoring of pipeline flows: particulate slurries*, *Powder Technology*, 1999, **106**, 30-36.
24. R. Hou, A. Hunt and R. A. Williams, Acoustic monitoring of hydrocyclones, *Powder Technology*, 2002, **124**, 176-187.
25. N. Gherras, E. Serris and G. Fevotte, Monitoring industrial pharmaceutical crystallization processes using acoustic emission in pure and impure media, *International Journal of Pharmaceutics*, 2012, **439**, 109-119.
26. P. D. Thorne, The measurement of acoustic noise generated by moving artificial sediments, *Journal of Acoustical society of America*, 1985, **78**, 1013-1023.
27. P. D. Thorne and D. J. Foden, Generation of underwater sound by colliding spheres, *Journal of Acoustical society of America*, 1988, **84**, 2144-2152.
28. S. B. Abebea, X. Z. Wang, R. Lia, K. J. Roberts and X. Lai, The information content in NIR spectral data for slurries of organic crystals, *Powder Technology*, 2008, **179**, 176-183.
29. D. Vervloet, J. Nijenhuis and J. R. van Ommen, Monitoring a lab-scale fluidized bed dryer: A comparison between pressure transducers, passive acoustic emissions and vibration measurements, *Powder Technology*, 2010, **197**, 36-48.

30. J. G. Bouchard, P. A. Payne and S. Szyszko, Non-invasive measurement of process states using acoustic emission techniques coupled with advanced signal processing, *Chemical Engineering Research and Design*, 1994, **72**, 20-25.
31. X. Ni and A. Liao, Effects of mixing, seeding, material of baffles and final temperature on solution crystallization of l-glutamic acid in an oscillatory baffled crystallizer, *Chemical Engineering Journal*, 2010, **156**, 226-233.
32. T. W. Evans, G. Margolis and A. F. Sarofim, Mechanisms of secondary nucleation in agitated crystallizers, *AIChE Journal*, 1974, **20**, 950-958.
33. M. F. Leach, G. A. Rubin and J. C. Williams, Particle size determination from acoustic emissions, *Powder Technology*, 1977, **16**, 153-158.

8 Conclusions and suggestions for future work

8.1 Conclusions

The main aims of this study were as follows:

- The evaluation and application of non-invasive measurement techniques to crystallisation processes in order to assess if increased knowledge and understanding of the process could be obtained which could potentially be applied to real-time monitoring and control.
- Assess the potential advantages and drawbacks of batch oscillatory baffled reactor (OBR) technology compared to conventional batch stirred tank reactors and determine the difficulties involved with transferring to continuous OBR operation. Additionally, the main two types of continuous reactor for crystallisation; plug flow (*e.g.* COBR) and mixed suspension, mixed product removal (MSMPR) were studied which allowed comparisons to be made on their potential benefits.
- Finally, with increased knowledge on the process being obtained through the use of non-invasive measurement techniques, it was anticipated additional knowledge of the crystallization of the two compounds selected for this study (L-glutamic acid and D-mannitol) would be acquired.

8.1.1 Evaluation of non-invasive measurement techniques

Although *in situ* measurement techniques have been widely applied to batch crystallisation processes including Raman spectrometry, which was one of the main techniques investigated in this study, this has been through the use of immersion probes.[1-3] These types of probes have several disadvantages including probe fouling, which is especially problematic with crystallisation where the probe crystal can often act as a centre for nucleation and once probe fouling occurs it is very difficult to counteract, therefore resulting in inaccurate or potentially useless data depending on the extent of fouling. Additionally, immersion probes employ a sampling spot size with a diameter of

around 100 µm which in some cases can be smaller than the actual particles produced during a crystallisation process. Therefore, it is possible that only a single particle may be analyzed during a single measurement which is an issue if more than one polymorph is present. The alternative probe used in this study was a wide-area illumination P^hAT probe which can be used to acquire measurements non-invasively; therefore, meaning issues with probe fouling are eliminated. Additionally, the 6 mm spot diameter size used in this study, allows for increasingly representative sampling of increased numbers of particles present inside the vessel. This non-invasive probe which has been applied more for off-line sampling; reduces many of the problems associated with conventional Raman monitoring of crystallisations. The ability to make measurements through the vessel was particularly advantageous in this study for crystallisation monitoring in the continuous reactors. In the COBR, probe ports were not in place which meant non-invasive or off-line measurements were the only options. In contrast, the small scale of the MSMPR vessel meant that once the inlet and outlet tubing had been added there were no probe ports available meaning either no *in situ* measurements could be made without increasing the scale of operation (drastically increasing the material usage), or only off-line sampling and analysis could be employed. The ability to make non-invasive measurements was, therefore, an advantage in both of these cases. The main drawback of non-invasive Raman is that in many cases there will be a background spectrum from the reactor material, in this case glass, however, in the example of L-glutamic acid and D-mannitol, sufficient peaks for the different polymorphs could be identified which were not hugely impacted by the glass background. It is also possible that if this was an issue, further data analysis such as a background subtraction could be undertaken to reduce the effects of this on the sample spectrum.

Raman spectrometry has commonly been used for polymorph identification and solid concentration monitoring, and polymorphic transformation monitoring including for the model compound, L-glutamic acid, used in this study.[4-6] However, it was found in this study that increased knowledge on the process could be obtained, especially when

investigating the impact of operating conditions on particle properties. By monitoring the different polymorphs and attaining crystallisation profiles for these it was possible to determine how the operating conditions including oscillation frequency and amplitude (in an OBR) affected the progression and outcome of the crystallisation. For instance, the nucleation time/temperature, crystal growth profiles and time to reach steady state were all affected by the operating conditions employed. The increased information obtained through these crystallisation profiles allowed for possible explanations to be drawn as to why the operating conditions affected the properties of the end product. For instance, it was observed that inefficient suspension of the particles (as determined by Raman) led to a wide particle size distribution. Additionally, for continuous operation, being able to determine when the system is operating at steady state means that the product can be recycled initially and collected for further processing when it is known that the properties are consistent. The additional information obtained from crystallisation profiles and the knowledge of varying operating conditions on particle properties shows the potential for feedback control. In batch operation, once nucleation occurs it is difficult to change the outcome (*e.g.* polymorph) by varying the operating conditions and most often recrystallisation is necessary. By monitoring the crystallisation, it is possible to save time and money by stopping a crystallisation which is not progressing optimally and begin the recrystallisation step prior to the pre-determined end point. However, in continuous operation, it may be more viable to monitor the crystallisation and if the crystallisation is not progressing as desired, alter the operating conditions to change the properties of the particles exiting the vessel. As the magnitude of product being produced with continuous operation is likely to be much higher than most batch processes, this would reduce the risk of obtaining out-of-specification product while waiting on the result of off-line analysis and thus once deviations are detected, corrective action could be taken immediately.

Acoustic emission spectrometry (AES) is a comparatively understudied technique with few examples of application to crystallisation monitoring.[7] Raman monitoring provides a

great deal of information on the process, however, there is little information available on particle size and, therefore, AES was investigated for its applicability to crystallisation monitoring with this in mind. It was found that like Raman monitoring, AES could be used to obtain crystallisation profiles which showed the nucleation time, crystal growth trends and steady state profile. As AES equipment is significantly cheaper than a typical Raman instrument this showed the potential for collecting similar information with lower cost instrumentation, which is often an important factor when a decision is made to purchase an instrument. However, no chemical information is obtained from AE measurements so it would be anticipated that this technique could be used for the monitoring of a well-established process whereby the polymorphic composition of the product is not expected to change. Additionally, particle size information could be extracted when separate frequency regions were studied more closely. Profiles showing trends in small or large particle size ranges during the crystallisation process could be obtained which were corroborated using *in situ* FBRM measurements. This meant the trend in small particles just following nucleation could be established showing the time period over which nucleation took place and also by looking at the decrease in the profile for small particles with the corresponding increase in the profile for particles in a larger size range, information on the crystal growth process could be observed. There are several different particle sizing technologies available, however, the two most widely used including laser diffraction and focused beam reflectance measurement are known to have issues with the measurement of needle-shaped particles which are commonplace in crystallisation processes.[8-10] Therefore, it is possible that acoustic emission spectrometry may be a potential alternative to these techniques, at least with regard to changes in particle size rather than absolute measurement of particle size distributions. Although, it is not possible to obtain an exact particle size using this technique, it may be possible to monitor the process to keep particles within a certain desired range and also determine when the particle size becomes consistent. This technique, like Raman, shows many potential advantages for the monitoring and control of continuous crystallisation processes as well as the monitoring of batch processing.

8.1.2 Evaluation of crystallisation reactor technology

8.1.2.1 Batch

Batch OBR technology was investigated for its potential advantages to crystallisation over conventional STR technology. The crystallisations undertaken in the batch OBR were found to produce particles of improved particle properties in the majority of cases (when sufficient oscillation was applied to create adequate suspension of the particles). Products comprising of narrower particle size distributions were obtained when comparable mixing intensity was used in both the OBR and STRs. Additionally, it was found that the crystallisations were repeatable in the batch OBR with particles of a similar polymorphic composition and particle size distribution being obtained. In comparison, when repeat experiments were carried out in the batch STR, although the polymorphic form remained the same, the particle size distribution varied between experiments. When a DoE was carried out to determine the effect of varying operating conditions on the outcome of crystallisations in the batch OBR using both L-glutamic acid and D-mannitol, it was found that the main effect on the particle properties was the solution concentration while the main interaction was between the oscillation frequency and amplitude. The solution concentration was the main factor in determining which polymorph was obtained. This was expected as the solution concentration affects the point on the solubility diagram (and which polymorph's metastable zone) that nucleation first occurs, so will help to determine the polymorphic composition of the end product. The fact that the combination of oscillation frequency and amplitude impacted the outcome of the crystallisation meant that this could provide potential benefits to the control of the particle properties over the batch STR, which uses conventional agitation created using an impellor. It was found that the mean particle size and PSD varied when different combinations of frequency and amplitude were applied meaning that a product with particles of a certain size and distribution could be obtained repeatedly using this technology. Additionally, the polymorphic composition of the final product was impacted by varying oscillation frequency and amplitude. It has been reported previously that the metastable zone width is affected by the oscillation frequency and

amplitude and so this affects where in the metastable zone nucleation takes place and correspondingly the polymorphic composition of the particles obtained.[11] Conversely, it was found that with batch STR technology, altering the mixing intensity within the range used in this study, did not greatly affect the particle size distribution obtained and this remained much wider and in some cases bimodal in comparison to the products obtained in the OBR. Therefore, it was found that increased control over the particle properties using the operating conditions, and increased consistency of the product were possible with batch OBR technology.

8.1.2.2 Continuous

It is claimed that the batch OBR can be used to determine optimum operating conditions at small scale which can then be transferred to continuous operation in the COBR.[12] However, during this study using L-glutamic acid, it was found that using the same operating conditions including oscillation frequency and amplitude resulted in different outcomes with respect to the physical properties of the particles. Under all conditions, only the metastable alpha polymorph was obtained in the COBR with a relatively narrow PSD which is advantageous in the case of L-glutamic acid as the alpha form is the desired form due to easier handling in downstream processing. However, if this is the case for all systems, that only the metastable form is produced, this could be a potential advantage or disadvantage depending on the compound in question. In the case of L-glutamic acid, this reactor was also found to be relatively restrictive with respect to the workable range of operating conditions, in particular solution concentration, which could limit the optimization of this reactor or potentially lead to damage of certain components (when blocking occurs). This was also particularly evident in the case of D-mannitol, where the high aqueous solubility of the compound, and so the high solution concentration required, was found to be incompatible with this reactor when unseeded crystallisation was undertaken. However, when the operating conditions were optimized with L-glutamic acid, it was observed that steady state was reached in the relatively short time period of 1.5-2 residence times. Therefore, this reactor may be a beneficial option for a single compatible compound which is produced continuously resulting in

large quantities of product. It may not be such a good option for a plant where flexibility is key and where smaller quantities of constantly changing products are manufactured. For this, batch may still be the best choice available or perhaps an alternative type of continuous technology such as the MSMPR. However, if batch operation is selected, the batch OBR offers many advantages over conventional STRs and could lead to significant improvements in product quality.

Continuous mixed suspension, mixed product removal reactors have been widely used in crystallisation to determine nucleation and growth kinetics at steady and unsteady state operation.[13-16] However, there has been little work carried out with polymorphic systems in this type of reactor which made L-glutamic acid an ideal candidate. Unexpectedly, like with the COBR, the metastable alpha form could be produced with relative ease in this vessel for extended periods of time. However, the thermodynamically stable polymorph could only be obtained in its pure form once a polymorphic transformation had taken place, even when seeding was employed. That being said, there were some obvious advantages of continuous crystallisation using a MSMPR reactor. Firstly, a much higher solution concentration could be accommodated which results in increased productivity and a wider possible working range of certain operating conditions. Blocking of the vessel tubing was an issue at higher concentrations, but measures could be taken to reduce this effect. It was also possible to operate crystallisations at relatively small scale which meant that optimum conditions could be established in the actual end reactor to be used and then if necessary, scaled up to meet product demand. However, as an MSMPR vessel is a modified batch stirred tank vessel, this means it has the same issues with scale up as a conventional batch STR resulting in reduced product quality and consistency with increased scale. Additionally, crystallisations in this type of reactor are known to take at least 10 residence times to reach steady state meaning a great deal of material would need to be discarded (or recycled) before product properties were consistent. Therefore, both continuous vessels have their different advantages and disadvantages so from the current choice of reactor types available there doesn’t appear

to be a ‘one size fits all’ option which is flexible and capable of being adapted to different compound types.

8.1.3 Additional knowledge of L-glutamic acid and D-mannitol

L-glutamic acid is a widely studied compound with respect to batch crystallisation and the kinetics, polymorphs and transformation processes have been well characterized.[6, 17-19] However, there has been less research into the effect of operating conditions on the crystallisation process and the particle properties especially in the batch OBR and continuous reactors. The polymorphic composition of the product was determined mainly by the solution concentration, however, the type of mixing employed (impeller agitation or baffle oscillation) also impacted the polymorphic form as the stable beta form was obtained in the batch STR while using similar conditions in the OBR, a mixture of forms was obtained. This was thought to be due to the narrower metastable zone width observed in an OBR due to the alternative, more efficient mixing, meaning nucleation begins in the metastable zone for the alpha rather than the beta form as in the STR. It was found that most of the operating conditions studied had an impact on the particle properties, especially the polymorphic form due to varying operating conditions impacting the metastable zone width which, therefore, affected nucleation and crystal growth.

D-mannitol is a relatively understudied compound in crystallisation in comparison to L-glutamic acid.[20, 21] As well as the solution concentration affecting the polymorphic form during the crystallisation, it was found that mixing played an important part in the nucleation event. As the mixing intensity was increased, the levels of the metastable form increased. Similarly as the scale was increased (so decreasing the mixing efficiency), the polymorphic composition following nucleation was also affected. However, the polymorphic transformation process from one of the metastable forms (alpha) to the stable form (delta) via a second metastable form (beta) reported previously

in similar batch STR experiments was not observed in this study.[20] Instead, direct transformation from the alpha to the stable delta form was observed in all cases. As with L-glutamic acid, changing the oscillation conditions in the batch OBR resulted in differing mixtures of the alpha and gamma polymorphs nucleating leading to differences in the transformation time to the stable form. Additionally, the induction time for nucleation was affected by the mixing intensity with increased intensity resulting in a shorter induction time. By monitoring the crystallisations of D-mannitol whilst varying the operating conditions it was possible to obtain a lot more information on the mechanisms of this compound and which factors affect the crystallisation the most. It was found that this compound appeared to be much more sensitive to operating conditions than L-glutamic acid.

8.2 Future work

This study demonstrated increased knowledge could be obtained from both batch and continuous crystallisation processes with the implementation of *in situ* measurement techniques. However, this was a relatively early study, especially with respect to oscillatory baffled reactor technology and the use of non-invasive monitoring for continuous crystallisation. Therefore, there is scope for continued research in this area and a number of suggestions are given below.

- Due to the limited number of compounds which have been applied to crystallisation in the COBR, it would be beneficial to widen this in order to obtain further knowledge on the processes taking place during crystallisation. For instance, will the metastable form always be obtained for every compound crystallised in this reactor? Secondly, attempting seeding experiments for more problematic compounds, such as high solubility compounds such as D-mannitol which were unable to be used with this reactor type, in an attempt to widen the possible uses of this reactor.

- In order for continuous crystallisation, and manufacturing as a whole to be adopted by the pharmaceutical industry, more development of the reactor technology is required. The main drawback of continuous OBR technology is the limitation of only being able to use low solubility compounds for unseeded crystallisations due to the issues of blocking. If a system was in place to reduce the effects of fouling/sedimentation and subsequent blocking of the reactor this would allow for a much wider application of this technology. A heating/cooling cycle could be employed during the crystallisation to re-dissolve particles when fouling becomes an issue or to dissolve particles which are likely to cause fouling such as particles in a smaller size range. An alternative solution to fouling could be the use of ultrasound to remove the particles from the reactor wall and therefore prevent the buildup and eventual blocking of the vessel.
- As acoustic emission spectrometry has not been widely applied to crystallisation monitoring there is increased research needed into this technique. For instance, this technique was only applied at a relatively small scale of below 1 L, where there were found to be sufficient particle collisions to be detected by the transducer. It would be important to determine at what point increasing the scale of batch operation would impact the signal obtained by a single transducer as it would be expected there would be a decrease in the signal with an increase in the scale. Therefore, there may be a need to incorporate an increasing number of transducers at different positions on the reactor vessel as the scale was increased in order to allow for a sufficient acoustic signal to be obtained which was representative of the entire reactor contents. Additionally, this technique was not applied to continuous reactors so this would be an important area to investigate further. As in a batch reactor, the transducer is detecting particle collisions which are taking place throughout the vessel and this results in an adequate signal, however, monitoring a certain point in the continuous OBR would be expected to contain at any given time a much lower concentration of particles which may not be able to be detected over the background noise from the reactor jacket.

- Finally, as it has often been reported that continuous manufacturing will only widely be adopted if a product can be manufactured from start to finish in a single continuous process, it would be necessary to firstly, investigate the separate unit operations separately, and then link these together in a fully integrated manufacturing operation. However, this will be relatively challenging and having the appropriate technology available for each individual unit operation in order to make a reliable and flexible process with not be easy. This also means that once a fully continuous process has been developed, real time monitoring using techniques including those described in this work, will be vital for the successful, long-term operation of the process.

8.3 References

1. H. Alatalo, J. Kohonen, H. Qu, H. Hatakka, S.-P. Reinikainen, M. Louhi-Kultanen and J. Kallas, In-line monitoring of reactive crystallization process based on ATR–FTIR and Raman spectroscopy, *Journal of Chemometrics*, 2008, **22**, 644-652.
2. A. Caillet, F. Puel and G. Fevotte, In-line monitoring of partial and overall solid concentration during solvent-mediated phase transition using Raman spectroscopy, *International Journal of Pharmaceutics*, 2006, **307**, 201-208.
3. J. Cornel, C. Lindenberg and M. Mazzotti, Quantitative Application of in Situ ATR-FTIR and Raman Spectroscopy in Crystallization Processes, *Industrial & Engineering Chemistry Research*, 2008, **47**, 4870-4882.
4. T. Ono, J. H. Horst and P. J. Jansens, Quantitative Measurement of the Polymorphic Transformation of l-Glutamic Acid Using In-Situ Raman Spectroscopy, *Crystal Growth & Design*, 2004, **4**, 465-469.
5. H. Qu, H. Alatalo, H. Hatakka, J. Kohonen, M. Louhi-Kultanen, S. Reinikainen and J. Kallas, Raman and ATR FTIR spectroscopy in reactive crystallization: Simultaneous monitoring of solute concentration and polymorphic state of the crystals, *Journal of Crystal Growth*, 2009, **311**, 3466-3475.
6. J. Schöll, D. Bonalumi, L. Vicum, M. Mazzotti and M. Müller, In Situ Monitoring and Modeling of the Solvent-Mediated Polymorphic Transformation of l-Glutamic Acid, *Crystal Growth & Design*, 2006, **6**, 881-891.
7. N. Gherras, E. Serris and G. Fevotte, Monitoring industrial pharmaceutical crystallization processes using acoustic emission in pure and impure media, *International Journal of Pharmaceutics*, 2012, **439**, 109-119.
8. P. Hamilton, D. Littlejohn, A. Nordon, J. Sefcik and P. Slavin, Validity of particle size analysis techniques for measurement of the attrition that occurs during vacuum agitated powder drying of needle-shaped particles, *Analyst*, 2012, **137**, 118-125.
9. H. Mühlenweg and E. D. Hirleman, Laser Diffraction Spectroscopy: Influence of Particle Shape and a Shape Adaptation Technique, *Particle & Particle Systems Characterization*, 1998, **15**, 163-169.
10. A. Vaccaro, J. Šefčík and M. Morbidelli, Modeling Focused Beam Reflectance Measurement and its Application to Sizing of Particles of Variable Shape, *Particle & Particle Systems Characterization*, 2006, **23**, 360-373.
11. X. Ni and A. Liao, Effects of mixing, seeding, material of baffles and final temperature on solution crystallization of l-glutamic acid in an oscillatory baffled crystallizer, *Chemical Engineering Journal*, 2010, **156**, 226-233.
12. S. Lawton, G. Steele, P. Shering, L. Zhao, I. Laird and X. Ni, Continuous Crystallization of Pharmaceuticals Using a Continuous Oscillatory Baffled Crystallizer, *Organic Process Research & Development*, 2009, **13**, 1357-1363.
13. K. A. Berglund and E. J. deJong, The calculation of growth and nucleation kinetics from MSMPR crystallizer data including growth rate dispersion, *Separations Technology*, 1990, **1**, 38-45.

14. M.-R. Chen and M. A. Larson, Crystallization kinetics of calcium nitrate tetrahydrate from MSMPR crystallizer, *Chemical Engineering Science*, 1985, **40**, 1287-1294.
15. E. Kougoulos, A. G. Jones and M. W. Wood-Kaczmar, Estimation of crystallization kinetics for an organic fine chemical using a modified continuous cooling mixed suspension mixed product removal (MSMPR) crystallizer, *Journal of Crystal Growth*, 2005, **273**, 520-528.
16. S. Ü. Tanrıkulu, İ. Eroğlu, A. N. Bulutcu and S. Özkar, Crystallization kinetics of ammonium perchlorate in MSMPR crystallizer, *Journal of Crystal Growth*, 2000, **208**, 533-540.
17. S. Khan, C. Y. Ma, T. Mahmud, R. Y. Penchev, K. J. Roberts, J. Morris, L. Özkan, G. White, B. Grieve, A. Hall, P. Buser, N. Gibson, P. Keller, P. Shuttleworth and C. J. Price, In-Process Monitoring and Control of Supersaturation in Seeded Batch Cooling Crystallisation of l-Glutamic Acid: From Laboratory to Industrial Pilot Plant, *Organic Process Research & Development*, 2011, **15**, 540-555.
18. M. Kitamura, Polymorphism in the crystallization of L-glutamic acid, *Journal of Crystal Growth*, 1989, **96**, 541-546.
19. M. Kitamura and T. Ishizu, Growth kinetics and morphological change of polymorphs of L-glutamic acid, *Journal of Crystal Growth*, 2000, **209**, 138-145.
20. J. Cornel, P. Kidambi and M. Mazzotti, Precipitation and Transformation of the Three Polymorphs of d-Mannitol, *Industrial & Engineering Chemistry Research*, 2010, **49**, 5854-5862.
21. H. Hao, W. Su, M. Barrett, V. Caron, A.-M. Healy and B. Glennon, A Calibration-Free Application of Raman Spectroscopy to the Monitoring of Mannitol Crystallization and Its Polymorphic Transformation, *Organic Process Research & Development*, 2010, **14**, 1209-1214.